Oxygen Tolerant Copper-mediated Reversible Deactivation Radical Polymerization

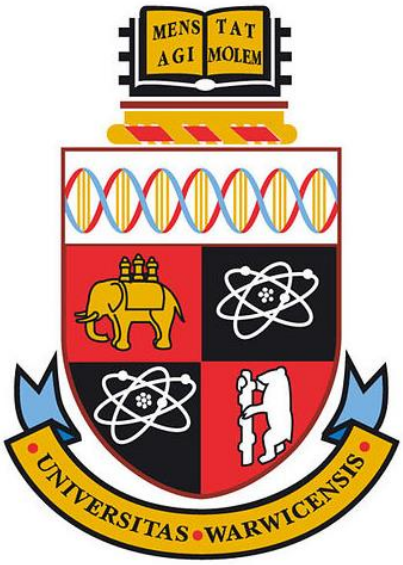

Evangelia-Eleni Liarou

A thesis submitted in partial fulfilment of the requirements of the degree of

Doctor of Philosophy in Chemistry

Department of Chemistry

University of Warwick

February 2020

This Ph.D. thesis is dedicated to my parents.

Στους γονείς μου,

για την υπομονή και τη στήριξή τους.

List of Contents

List of Schemes

List of Figures

List of Tables

Abbreviations

ADF-STEM	Annular dark field-scanning transmission electron microscopy
AIBN	Azobisisobutyronitrile
AGET	Activator Generated by Electron Transfer
AgCl	Silver chloride
ARGET	Activators regenerated by electron transfer
ATRP	Atom transfer radical polymerization
***n*-BA**	*n*-Butyl acrylate
BSA	Bovine serum albumin
$CDCl_3$	Deuterated chloroform
CHCA	α-cyano-4-hydroxycinnamic acid
Co	Cobalt
CRP	Controlled radical polymerization
CTA	Chain transfer agent
CV	Cyclic voltammetry
Cu	Copper
DCTB	*trans*-2-[3-(4-*tert*-butylphenyl)-2-methyl-2-propyldene] malononitrile
DMA	N,N Dimethylacrylamide
DMF	Dimethyl formamide
DMSO	Dimethyl sulfoxide
DNA	Deoxyribonucleic acid
DP_n	Degree of polymerization
$E_{1/2}$	Half-wave potential
***e*-ATRP**	Electrochemically mediated- atom transfer radical polymerization
EBiB	Ethyl-2-bromoisobutyrate
EDX	Energy-Dispersive X-ray spectroscopy
EELS	Electron energy loss spectroscopy
EGA	Ethylene glycol methyl ether acrylate
EM	Electron microscopy

ESI-ToF-MS	Electrospray ionization-time of flight-mass spectroscopy
f	Initiator efficiency
FRP	Free radical polymerization
GOx	Glucose oxidase
HA	Hexyl acrylate
HEAm	Hydroxyethyl acrylamide
HCl	Hydrochloric acid
HMTETA	1,1,4,7,10,10-hexamethyltriethylenetetramine
HR-TEM	High-resolution transmission electron microscopy
I	Initiator
ICAR	Initiators for continuous activator regeneration
IPA	Isopropyl alcohol
ISET	Inner sphere electron transfer
$\mathbf{k_i}$	Rate constant of initiation
$\mathbf{k_p}$	Rate constant of propagation
$\mathbf{k_t}$	Rate constant of termination
L	Ligand
LA	Lauryl acrylate
LMCT	Ligand-to-metal charge transfer
LRP	Living radical polymerization
$\mathbf{[M]_0}$	Monomer concentration at t = 0
[M]t	Monomer concentration at t = t
MA	Methyl acrylate
MALDI-ToF-MS	Matrix assisted laser desorption ionization- time of flight-mass spectroscopy
$\mathbf{Me_6Tren}$	tris[2-(dimethylamino)ethyl]amine
MeCN	Acetonitrile
MeOH	Methanol
MS	Mass spectroscopy
MMA	Methyl methacrylate
MW	Molecular weight

NaBr	Sodium bromide
NAM	N-Acryloylmorpholine
NiPAM	N-Isopropylacrylamide
NMR	Nuclear magnetic resonance
NMP	Nitroxide mediated polymerization
OSET	Outer sphere electron transfer
$PEGA_{480}$	Poly(ethylene glycol) methyl ether acrylate
PET-RAFT	Photoinduced electron transfer-reversible addition fragmentation chain transfer
PLP	Pulsed-laser polymerization
PMDETA	*N,N,N',N'',N''*-pentamethyldiethylenetriamine
PMMA	Poly(methyl methacrylate)
PRE	Persistent radical effect
PS	Poly(styrene)
RAFT	Reversible addition fragmentation chain transfer
RDRP	Reversible deactivation radical polymerization
Ru	Ruthenium
SARA-ATRP	Supplemental activator and reducing agent atom transfer radical polymerization
SEC	Size exclusion chromatography
SEM	Scanning electron microcopy
SET-LRP	Single electron transfer living radical polymerization
$Sn(EH)_2$	tin(II) 2-ethylhexanoate
***t*-BA**	*tert*-butyl acrylate
TEA	Triethylamine
TEAS	Transient electronic absorption spectroscopy
TEM	Transmission electron microscopy
TEMPO	2,2,6,6- tetramethylpiperidinyl-1-oxy
TFE	2,2,2-Trifluoroethanol
TFEA	2,2,2-Trifluoroethyl acrylate
TFEMA	2,2,2-Trifluoroethyl methacrylate
THF	Tetrahydrofuran

TMEDA	Tetramethylethylenediamine
Tol	Toluene
UV	Ultraviolet
UV-Vis	Ultraviolet-Visible
XPS	X-ray photoelectron spectroscopy
Zn	Zinc
ZnTPP	Zinc tetraphenylporphyrine

Acknowledgments

First and foremost, I thank my supervisor, Professor David Haddleton. I am grateful for working under his supervision since, apart from his constant guidance and support, he has created an environment of “scientific freedom” where creativity and new ideas are always supported. It should be noted that these 3,5 years, Professor Haddleton would always have a solution for any possible problem or difficulty, and this is because he is a supervisor that truly cares about his students’ happiness and development.

Next, I thank Dr Athina Anastasaki for her support, her general help throughout my studies, her guidance on project planning and scientific writing and all the constructive scientific discussions we had. I would also like to thank Dr Paul Wilson for valuable discussions and advice, as well as for always being willing to help with a range of scientific challenges.

I would like to thank the members of the Haddleton group (past and present) that have been part of these studies. Firstly, I want to thank Dr Alan Wemyss, James Town and Ellis Hancox who have been great friends and inspirational colleagues, always willing to help, discuss ideas and process scientific plans. Next, I would like to thank my good friends and past members of the group: Dr Glen Jones, Dr Nikolaos Engelis and Dr Vasiliki Nikolaou for their support and advice. Also, I thank Dr Richard Whitfield for his help and input in the productive collaboration we had.

I would also like to acknowledge Prof. Ana Sanchez for her constructive guidance in microscopy, Prof. Kelly Velonia for giving me the opportunity to participate in such an advantageous collaboration and Dr Daniel Lester for providing help and advice on SEC equipment.

I would like to express my sincere gratitude to Arkadios Marathianos for his unconditional support and encouragement, for his significant intellectual contribution, and for being the “voice of reason” during this challenging period.

Finally, words are not enough to thank my family (Mom, Dad, grandmothers and my little fella Ektoraki) without whom nothing would have been possible.

Declaration

Experimental work contained in this thesis is original research carried out by the author, unless otherwise stated, in the Department of Chemistry at the University of Warwick, from October 2016 until February 2020. No material contained herein has been submitted for any other degree, or at any other institution.

Results from other authors are referenced in the usual manner throughout the text.

Date: 28.08.2020

_____

Evangelia-Eleni Liarou

Abstract

The focus of this Ph.D. thesis is to develop Cu-RDRP and render it a more user-friendly and versatile platform. For this purpose, three different Cu-RDRP methodologies, Cu(0)-wire mediated RDRP (*Chapter 2*), photoinduced Cu-RDRP (*Chapter 3*) and aqueous Cu-RDRP with the pre-disproportionation of Cu(I) (*Chapter 4*), are studied in the absence of conventional deoxygenation. Without the use of extrinsic oxygen scavengers and reducing agents, a range of well-defined polymers (*i.e.* poly(acrylates), poly(methacrylates), poly(styrene) and poly(acrylamides)) are synthesized under various conditions (temperatures, solvents, reaction scale). In all the different oxygen tolerant approaches, high end-group fidelity is maintained, leading to well-defined block copolymers *in-situ*.

In each of the three different approaches, the concentration of oxygen in the polymerization reactions is monitored *in-situ* with the use of an oxygen probe, and the mechanism of oxygen consumption is investigated and discussed. Furthermore, the role of the polymerization reagents on the evolution of oxygen consumption is elucidated, highlighting the importance of each component.

Apart from the oxygen tolerant nature of these platforms, the effect of UV-irradiation on Cu-based complexes is investigated (*Chapter 5*), providing insights into the excited state dynamics and the photo-redox behaviour of Cu(II)-based complexes, and the effect of different aliphatic amines on photoinduced Cu-RDRP.

Chapter 1.

An Introduction into Radical Polymerization

1.1 Polymers: a brief introduction

The term "polymer" (originating from the Greek word "πολυμερές" (*polymerḗs*), designating a compound that consists of many repeating units) was initially coined by Berzelius in 1833, indicating identical chemical compounds owning the same empirical formula but with different chemical and physical properties; Although placing the existence of polymers throughout history is rather impossible, it was in 1920 when the term with its current etymology was employed by Staudinger in his *manifesto* "Über Polymerisation".[1] Thus, that landmark publication set the ground for polymer chemistry as we know it until today. Although it has been extensively stated that *polymers are found everywhere* in everyday life, the statement is rather difficult to fully quantify due to the numerous natural and synthetic examples.

1.2 Polymerization classification: a synopsis

The traditional classification of polymerization processes included two main categories based on the IUPAC Commission on Macromolecular Nomenclature (1974); condensation polymerization and addition polymerization. That classification was based on whether small molecules are evolved in the growth process, or not. However, increased advances in the field of polymer synthesis has led to the

replacement of this classification, with the "modern" distinction criteria being based on the polymerization mechanism and not on polymer structures. In this context, nowadays most of polymerizations can be classified as *step-growth* or *chain-growth* processes, as was first introduced by Flory in 1953.[2]

The *step-growth* polymerization process follows a one reaction mechanism for the formation of the polymer, with initiation, propagation and termination steps being largely absent.[2,3] Practically, the presence of two molecular species can react, and chain growth occurs at slow rates. There is a steady rise in the molecular weight of the polymer during polymerization, while high molecular weight polymers require high conversions. On the other hand, *chain-growth* polymerization has distinct steps (*i.e.* initiation, propagation and termination(s)) with different rates and mechanisms.[2,4] A distinctive feature of the chain-growth process is that the monomers react with active centres including free radicals, organometallic complexes or ions, with a common type of chain growth process being initiated by a free radical. The initiation is usually triggered by an external stimulus (*e.g.* energy (temperature, light), catalysts, highly reactive compounds). The most common chain-growth process is the widely employed Free-Radical Polymerization (FRP).

1.3 Free-Radical Polymerization (FRP)

Many commonly used polymers (*e.g.* polystyrene) are synthesized through FRP due to the high versatility and the low-cost of the technique.[5] Experimentally, the FRP process exhibits relative tolerance to impurities, moisture and air, as well as compatibility with various solvents and monomers.[6] Thus, FRP is considered as one of the least demanding polymerization processes. In this context, high molecular weight polymers with industrial interest and application can be produced in a facile

manner. The FRP process can be considered as following three distinctive steps : initiation, propagation and termination.[7]

The first step which includes the initiation, is considered to involve two events. The first event includes the production of free radicals (R·) (referred to as initiator, or primary, radical) usually from the dissociation of initiating species (I) either through heat or light, where k_d is the rate constant for the initiator dissociation (**Eq. 1.1**). The second part of the initiation includes the addition of one of these radicals to a monomer to produce a chain-initiating radical M· as depicted in **Eq. 1.2**, with k_i being the rate constant for the initiation step.

The initiation process is followed by propagation, where the free radical at the end of the polymer chain reacts with a monomer leading to the formation of a new, identical radical but larger by one monomer unit. This chain growth process which takes place at rapid rates is described by **Eq. 1.3** with k_p being the rate constant of propagation with values within the range 10^2 -10^4 L mol^{-1} s^{-1}.

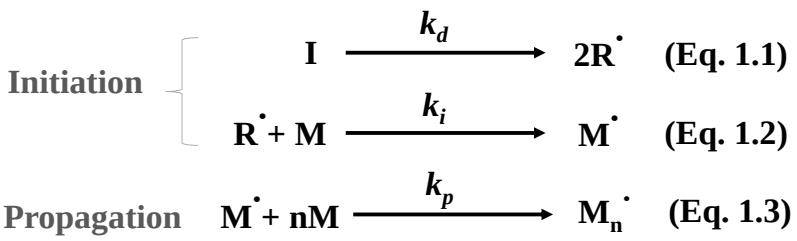

Eventually, the propagating polymer chain loses its radical activity and undergoes termination. The two possible mechanism that lead to termination events are combination and disproportionation.[8] Combination is the process in which two radical species react with each other, and this radical coupling leads to the formation of a "dead" polymer chain, with a total length equal to the sum of the two radical chains. The combination process is described by **Eq. 1.4** with k_{tc} being the rate constant of combination. Alternatively, cessation of the propagating radical growth can occur

through disproportionation, which includes the formation of two new radicals (one saturated and one unsaturated) through hydrogen abstraction, as depicted in **Eq. 1.5** (k_{td} is the rate constant of disproportionation). In general terms, the termination events can be described in **Eq. 1.6** with the term "dead polymer" indicating the propagating chain which underwent growth cessation, with k_t being the rate constant of termination.[9]

Combination	$M_n^{\cdot} + M_m^{\cdot} \xrightarrow{k_{tc}} M_{n+m}$		**(Eq. 1.4)**
Disproportionation	$M_n^{\cdot} + M_m^{\cdot} \xrightarrow{k_{td}} M_n + M_m$		**(Eq. 1.5)**
Termination (General)	$M_n^{\cdot} + M_m^{\cdot} \xrightarrow{k_t}$	**"dead polymer"**	**(Eq. 1.6)**

1.4 Living Polymerization

In a general description, living polymerization is a type of chain growth polymerization in which the propagating polymer chains are unable to terminate.[10] Although living polymerization was observed during 1920's by Ziegler and Bahr,[11] and early approaches had been made during 1940's with a notable one being by Waley and Watson with the polymerization of sarcosine carbonic anhydride,[12] the concept of living polymerization was pioneered by Szwarc in the 1950's with his work on the anionic polymerization of styrene.[13] The distinctive characteristic of living polymerization is that initiation is faster than propagation with each initiator molecule initiating only one polymer chain, with the polymer chains growing simultaneously and at the same rate. In this context, the degree of polymerization (DP) is linked to the concentration of initiator at time zero, as well as the amount of monomer consumed (**Figure 1-1**). Once there is full consumption of the monomer, the growth is complete resulting in polymer chains of a similar length, unless there is no extra supply of

monomer. The absence (or better the negligible presence) of chain transfer and chain termination are the main characteristics of the *livingness*, and they can be mainly observed in anionic systems where the anions at the ends of the polymer chains eliminate bimolecular termination.[14]

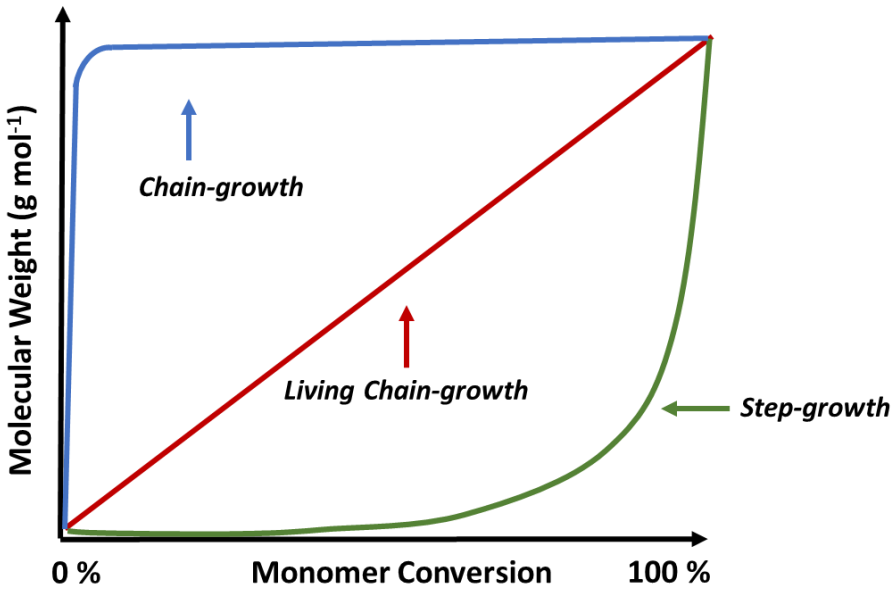

Figure 1-1. Molecular weight evolution *versus* increasing monomer conversion for chain-growth (blue), living chain-growth (red) and step-growth (green) polymerization.

However, living polymerizations are often highly vulnerable to impurities such as moisture (H_2O), O_2 and CO_2 (further discussion in section 1.7) thus, highly purified reagents and stringent anaerobic conditions are usually required. Furthermore, high temperatures and solvents able to undergo chain transfer often need to be avoided. As a result, although even nowadays the production of high-quality polymers (*i.e.* predetermined narrow molecular weight distributions, block copolymers, ease of functionalization of the terminated chain ends) is a distinctive feature of living polymerizations, the commercialization of these processes can be hindered by these highly-demanding experimental conditions.

1.5 Reversible Deactivation Radical Polymerization

The term Reversible Deactivation Radical Polymerization (RDRP) is being widely used to describe a family of polymerization techniques which, broadly speaking share a common characteristic, namely a dynamic equilibrium between active and dormant species.[15,16] This equilibrium can be accomplished either *via* the reversible deactivation of the propagating radical to form the dormant species, or *via* "degenerate transfer" between the propagating radicals and the dormant species. Although the term "Controlled/Living Radical Polymerization" has also been used to describe these polymerization processes, many controversies have arisen based on whether these systems are *living* or *controlled*. Based on the IUPAC, the term *living* should be avoided since RDRPs proceed *via* a radical intermediate and thus, radical-radical termination is inevitable to some extent.[17] Additionally, in these systems there is high possibility of side reactions related to chain transfer to solvent or monomer and as such, the RDRPs deviate from the definition of *livingness* as proposed by Szwarc. Hence, although these systems exhibit a proximity to living polymerizations in comparison to the free-radical process, they are commonly called RDRPs. The primary aim of this family of techniques is to eliminate chain breaking reactions, reserve the same probability of growth for each chain and obtain polymers with controlled molecular weights and narrow dispersity.[18] The three most viable techniques included in the RDRP family are nitroxide-mediated polymerization (NMP),[19] reversible addition-fragmentation chain transfer (RAFT)[20] polymerization and the transition metal-mediated approaches[21,22] (*e.g.* atom transfer radical polymerization (ATRP)).

1.5.1 Nitroxide-mediated polymerization (NMP)

Nitroxide-mediated polymerization is historically the first example of RDRP. It was discovered at CSIRO and early publications and patents by Solomon and Rizzardo in 1980's describe NMP as *a method for controlled-growth radical polymerization*.[23] In early efforts to stabilize radical polymerization, the development of methods for probing the chemistry of its initiation were included, with radical-trapping and the use of nitroxides being among those.[19] Nitroxides are able to selectively scavenge carbon-centred radicals and can efficiently act as inhibitors for radical polymerization.[19] In this context, 2,2,6,6- tetramethylpiperidinyl-1-oxy (TEMPO) in particular was used as a radical trap in order to study the initiation in methyl acrylate polymerization.[24] As a result of these studies, nitroxides were verified as selective scavengers of carbon-centred radicals to yield stable (under certain thermal conditions) alkoxyamines. Among the conclusions that followed these studies it was suggested that the alkoxyamines were thermally labile at higher temperatures and collectively, these observations led to the development of NMP.

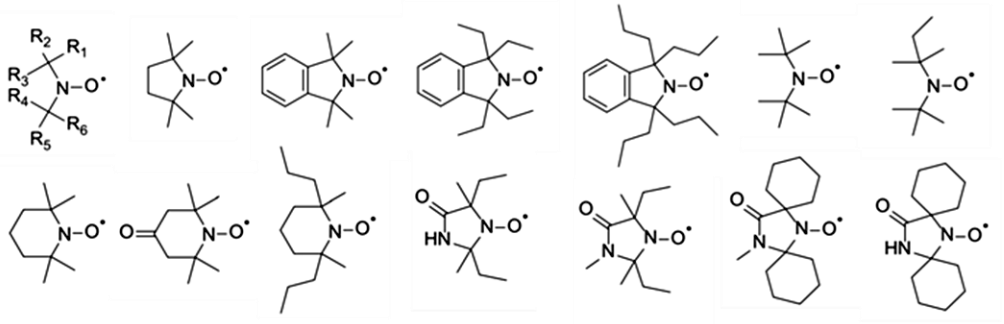

Scheme 1-1. Different nitroxides used in NMP.[25]

Although NMP was originally applicable only to styrenic monomers,[24] the last 15 years the development of nitroxides[26] and alkoxyamines[27,28] provided access to more monomer families including acrylates,[29] methacrylates (under certain

conditions)[30], acrylamides,[31] acrylonitrile[27] and 1,3-dienes.[32] In general terms, the control in NMP is dominated by the equilibrium between dormant species in which the nitroxide is covalently bound to the polymer chain-end, and active species $P_n^{\cdot}$ in which the nitroxide is homolytically cleaved to generate a propagating radical at the polymer chain-end, as shown in **Scheme 1-2**, with k_d and k_c determining the activation/deactivation equilibrium constant K ($K = k_d/k_c$).[33,34,35] In order to minimize side reactions, the concentration of $P_n^{\cdot}$ should be low. Moreover, a further factor that plays an important role over the control over the NMP process is that exchange between the dormant and active species needs to be much faster than propagation and termination,[36] so such that all of the polymer chains grow simultaneously. Broadly speaking, although NMP provides control over the macromolecular characteristics of the obtained polymers, termination events are possible to occur including transfer to monomer[37,38] or transfer to the nitroxide,[39,40] leading to the generation of P_nX species where X is the fragment of the transfer agent.[35]

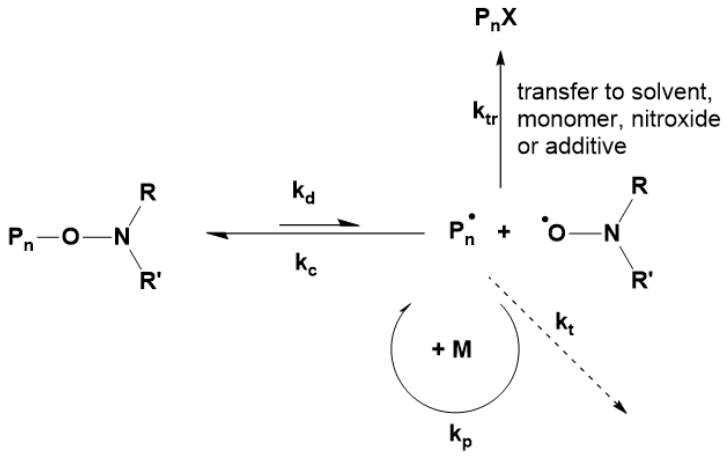

Scheme 1-2. Proposed mechanism of NMP.

1.5.2 Reversible addition-fragmentation chain transfer polymerization (RAFT)

RAFT was first reported in 1998 by Chiefari *et al*. at CSIRO,[20] and until now has been one of the most well-studied RDRP techniques. The RAFT mechanism, following the RDRP process, is based on the equilibrium between active and dormant chains, achieved by degenerative transfer.[36] For this process, a source of radicals such as a conventional radical initiator is required (*e.g.* AIBN), as well as a chain transfer agent (CTA) or as is also called, RAFT agent.[41–43] As depicted in **Scheme 1-3**, upon decomposition of the initiator that lead to the formation of propagating species ($P_n^{\cdot}$), the propagating radical is added to the CTA (thiocarbonylthio compounds (RSC(Z) = S) are the most commonly used) followed by fragmentation of the intermediate radical, finally leading to the formation of a thiocarbonylthio compound and a new radical ($R_n^{\cdot}$). In the next step, the new radical reacts with a monomer unit leading to the formation of a propagating radical ($P_m^{\cdot}$). The reversible transfer of the a thiocarbonylthio group (or any other functional chain-end group) between the dormant chains and the propagating radicals is a key characteristic for the RAFT process.

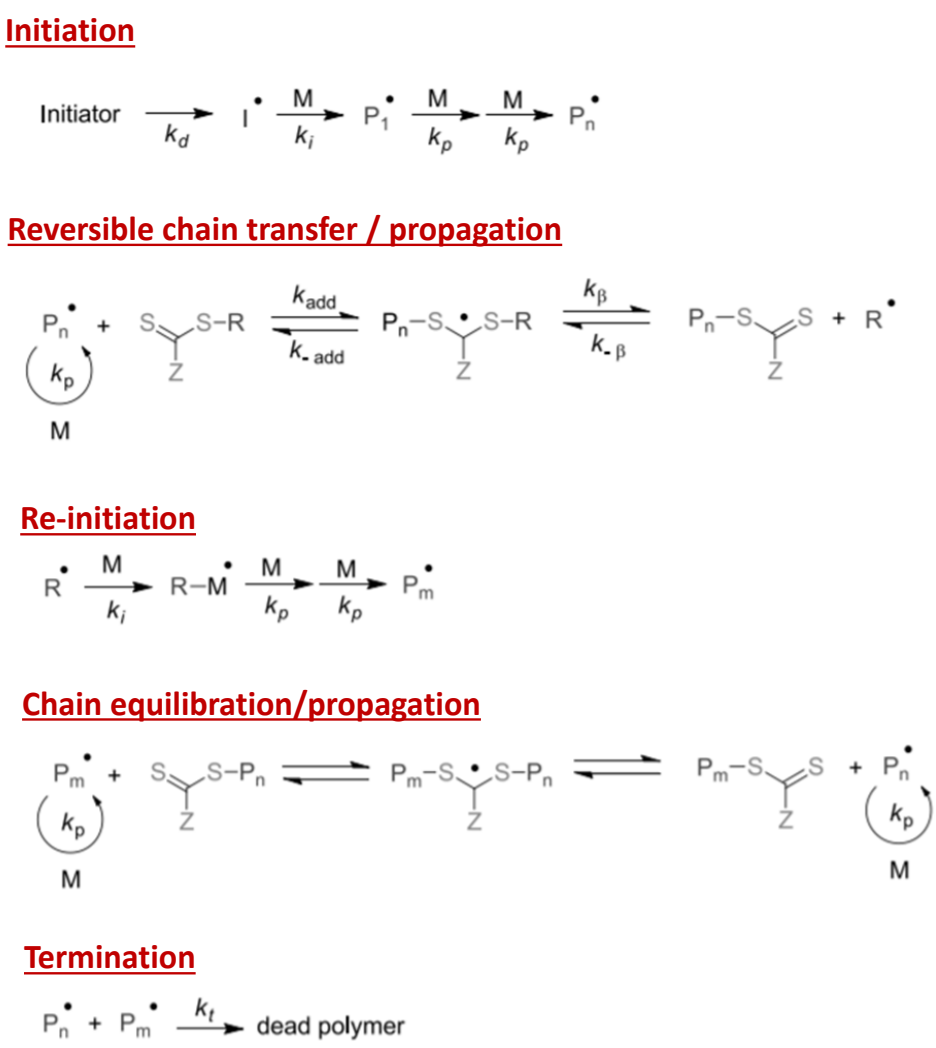

Scheme 1-3. Proposed mechanism of RAFT.

In a successful RAFT process, the rate of addition/fragmentation is higher than the rate of propagation leading to similar degree of polymerization for all the chains. One of the most distinct differences between RAFT and other RDRPs (*e.g.* ATRP or NMP) is that a bimolecular termination event does not lead to loss of the chain end, with the number of end-functionalized chains remaining the same even upon, conventional for other RDRPs, termination events.[44]

1.5.3 Copper-mediated Reversible Deactivation Radical Polymerization (Cu-RDRP)

1.5.3.1 Atom Transfer Radical Polymerization (ATRP)

Transition metal mediated/catalyzed methodologies were introduced in 1995 using low valent Ru(II)[21] and Cu(I)[45] complexes as catalysts in conjunction with alkyl halides as initiators. Up until this point, ionic and ionic-related polymerization were most successful living polymerizations requiring the use of very anhydrous conditions and pure (protic-free) reagents and solvents. The transition metal-based radical techniques such as ATRP[21,45] and Single Electron Transfer-Living Radical Polymerization (SET-LRP),[46–48] emerged as powerful tools for the synthesis of numerous materials, with different architectures and functionalities, in a variety of media and under different conditions without the requirement of rigorously removing water and other protic impurities or the need for protecting groups for monomers containing such functionality.[15,16,49,50] These methods depend on an activation-deactivation equilibrium between active and dormant species, related to the transition metal complex (Mt^m X/L) (with Mt being the metal at *m* oxidation state and L being the ligand) which activates (k_{act}) an alkyl halide (P_n-X) *via* reversible homolytic bond cleavage, leading to Mt^{m+1} X_2/L and a $P_n^{\cdot}$ radical which leads to chain growth (**Scheme 1-4**). The deactivator, namely the transition metal complex in the higher oxidation state, reversibly reacts (k_{deact}) with the propagating radical ($P_n^{\cdot}$) to regenerate the dormant species and the activator. [51–56]

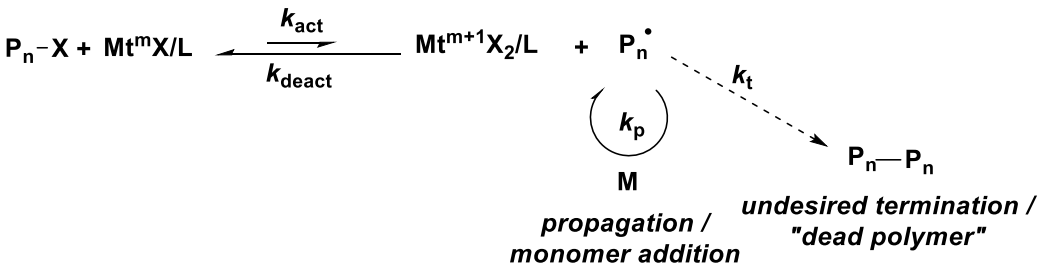

Scheme 1-4. Simplified ATRP activation/deactivation equilibrium.

All the RDRP methods are eventually followed by termination events, to some extent. However, at the initial stages of the polymerization there is a small presence termination which results in slight excess of deactivating species, shifting the equilibrium towards the dormant species, decreasing the rate of polymerization but supressing the rate of termination, ultimately resulting in better control over the molecular weight distributions. This self-regulating ability of the technique is known as persistent radical effect (PRE).[33,57,58] In general, there are many factors that synergistically contribute to a controlled ATRP process by shifting the equilibrium, including among others the structure of the ligand and thus the nature and stability of the catalyst, [56,59–64] the initiator[36,52,65–68] and the reaction medium.[15,50,69]

In general, for the RDRPs which are catalyzed by copper (Cu), there are two possible mechanistic pathways described in the literature, outer-sphere electron transfer (OSET) and inner-sphere electron transfer process (ISET).[70,71] The traditional ATRP is considered to follow the ISET process where a transition metal complex in the lower oxidation state (most often Cu^I/L), activates an alkyl halide, through an energetically favoured ISET process, to generate a radical and the transition metal complex in a higher oxidation state (*i.e.* Cu^{II}/L). Subsequently, the generated radical can propagate with monomer before reacting with the higher oxidation state complex to return to the alkyl halide.[72]

Alternative approaches to conventional ATRP have been introduced mainly by Matyjaszewski and colleagues, including Activator Regenerated by Electron Transfer (ARGET-ATRP)[73] and Initiators for Continuous Activator Regeneration (ICAR-ATRP),[74] in order to minimize the transition metal loadings. ARGET-ATRP has been considered a "greener" approach to conventional ATRP with the utilization of ppm of the catalyst and in the presence of a suitable reducing agent[75] (*i.e.* tin(II) 2-ethylhexanoate ($Sn(EH)_2$),[76] glucose,[73,77,78] ascorbic acid,[79] more). In the ARGET process, the reducing agent is employed to (re)generate the active catalyst from the, accumulated *via* termination events, deactivating species.[76] In the ICAR-ATRP, low loadings of the metal catalyst are as previously used and thus, in order to avoid the activator's consumption through termination evens, a free-radical source (e.g. AIBN) is employed to regenerate the activator.[73]

1.5.3.2 Single Electron Transfer-Living Radical Polymerization

The concept of SET-LRP was introduced in 2002 by Percec and colleagues who reported on the fast polymerization of acrylates, methacrylates and vinyl chloride at ambient temperature, generating polymers with "ultrahigh" molecular weight.[47] The process was conducted in polar media and, as previously in ATRP, in the presence of *N*-containing ligands and alkyl halide initiators. Although the "core idea" of RDRP remains the same for both ATRP and SET-LRP, the mechanistic differences between the latter and supplemental activator and reducing agent (SARA)-ATRP have been the focus of controversy in the literature.[71] Included in RDRPs, SET-LRP relies on the equilibrium between dormant and active species.

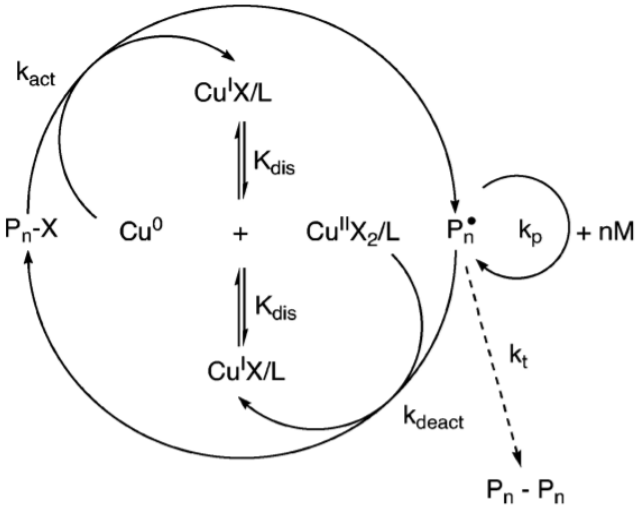

Scheme 1-5. The mechanism of SET-LRP as proposed by Percec and colleagues. Figure adapted from reference ***47***.

The main difference between SET-LRP and SARA-ATRP is that in the first, Cu(0) is considered as the activator that abstracts the halogen atom from the initiator *via* a heterolytic outer-sphere electron transfer (OSET) mechanism. Specifically, in polar solvents including H_2O, dimethyl sulfoxide (DMSO), alcohols and ionic liquids, Cu(I) undergoes rapid disproportionation towards "nascent", highly reactive Cu(0) particles and Cu(II)Br in the presence of *N*-containing ligands that promote disproportionation (*i.e.* tris[2-(dimethylamino)ethyl]amine (Me_6Tren)).[46,47] The proposed mechanism of SET-LRP (**Scheme 1-5)** suggests that the initiation step (or activation, k_{act}) includes a SET from Cu(0) which is the electron donor species, to the electron-acceptor alkyl halide.[80] During the formation of radicals, Cu(I) is generated and instantaneously disproportionates into Cu(0) atomic species and Cu(II), thus the Cu(I) species are spontaneously consumed while the Cu(0) species are continuously produced.[47,81] The "nascent" Cu(II) is considered to provide the reversible deactivation (k_{deact}), thus acting as the deactivator, the generated Cu(0) induces the reactivation of dormant species, whilst Cu(I) does not participate in the activation of alkyl halides but only supplies the activating and deactivating species through its disproportionation.

In 2013, Haddleton and colleagues demonstrated a novel method for conducting Cu(0)-mediated RDRP in water, by exploiting full disproportionation of Cu(I) in water and in the presence of the aliphatic tertiary amine Me_6Tren.[81] Specifically, the key-step for a controlled Cu(0)-RDRP in water was to allow for full disproportionation of Cu(I) prior to addition of monomer and initiator. Thus, upon completion of the pre-disproportionation reaction where nascent Cu(0) and Cu(II) are generated, the addition of monomer and initiator followed, and within 15 minutes well-defined polyacrylamides and hydrophilic polyacrylates were synthesized. The advantageous nature of this platform lies on the mild reaction conditions which include low or ambient temperature and the fast polymerization rates. Apart from the polymerization of acrylamides in water, other more complex aqueous media such as blood serum,[82] alcoholic beverages[83] and ionic liquids[4784] were employed for the Cu(0)-RDRP of NiPAm, resulting in successful disproportionation of Cu(I) (and thus, *in-situ* generation of highly active Cu(0)). Finally, even in complex media, control over the macromolecular characteristics of the obtained polymers was achieved, with low dispersities, high chain-end fidelity and high monomer conversions. It should be noted that although the Cu(0)-RDRP platform is considered as a robust and versatile system, exhibits some limitations which lie on the fact that less activated monomers such as vinyl pyrrolidone (VP) and vinyl acetate (VA) are incompatible with the technique, while further development is required for the polymerization of styrene, methacrylates and methacrylamides.[47]

1.5.3.3 Cu(0)-RDRP: Mechanistic aspects

The use of Cu(0) has provided many advantages in the implementation of Cu-RDRP including the simple removal of Cu-species when Cu(0)-wire is utilized, milder conditions (*i.e.* ambient temperature or below) and shorter reaction times.[16]

Nevertheless, significant interest has been focussed on the mechanistic profile of Cu-RDRP with the main debate up to date being between two models that the same polymerization components are used; the supplemental activator and reducing agent (SARA)-ATRP and SET-LRP.[71] The SARA-ATRP model follows the same rationale as conventional ATRP with the main species responsible for deactivation being Cu(II) and for activation Cu(I), while Cu(0) acts as a supplemental activator of alkyl halides and as a reducing agent for Cu(II). In the SARA-ATRP approach the kinetic contribution of disproportionation is very small, whilst comproportionation has a predominant role. In contrast, in the SET-LRP approach, the disproportionation of Cu(I) towards Cu(0) and Cu(II) has a predominant role with Cu(0) being the main active species (**Figure 1-2**).

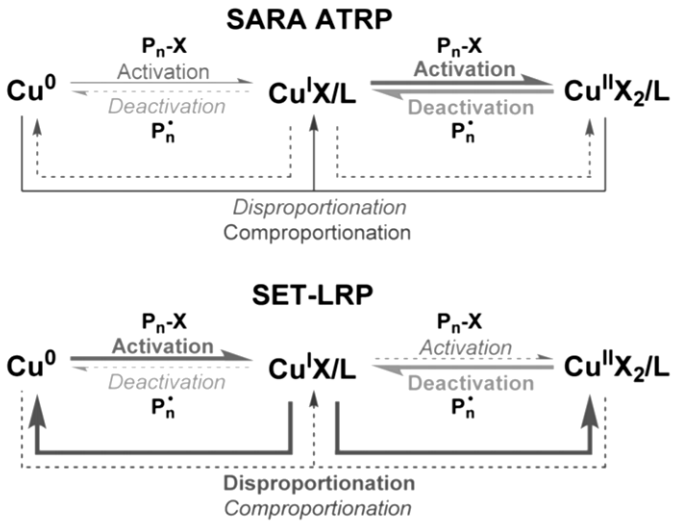

Figure 1-2. Simplified mechanistic illustration for SARA-ATRP (top) and SET-LRP (bottom) with bold arrows indicating major reactions, solid arrows indicating contributing reactions and dashed arrows representing minor reactions. Figure adapted from reference ***71*.**

1.5.4 Photoinduced Cu-mediated Reversible Deactivation Radical Polymerization

Unarguably, the development of RDRP techniques has proved to be a cornerstone for the field of polymer chemistry and materials science since their implementation leads to polymers with diverse properties, well-defined macromolecular characteristics and a wide range of functionality. [32,85–89] One of the most challenging tasks in the field, has been the "*on demand*" regulation of RDRP techniques, namely the achievement of spatiotemporal control over the polymerization. In this context, researchers developed the implementation of external stimuli including light, electrochemical processes with applied voltage or mechanical processes in order to render the equilibrium between active and dormant species tunable.[90,91]

In particular, the use of light has attracted considerable interest since it allows the polymerization to proceed under mild conditions, it is non-invasive, environmentally benign, and gives high potential for spatiotemporal control.[91,92] After the first report on the photopolymerization of vinyl monomers by Oster and Yang in 1968,[93] significant developments have been made in the field of photopolymerization, with the three main approaches being the use of light for activation of the catalyst,[56,94] monomer[95,96] or initiator.[97–100] In particular, the direct activation of the catalyst through light irradiation has been the focus of many investigations that are based on RDRP and Cu-RDRP. Hawker and colleagues, utilizing visible light and a photoactive iridium complex (fac-[Ir(ppy)$_3$](ppy = 2-pyridylphenyl), reported the synthesis of well-defined poly(methyl methacrylate) (PMMA) with spatiotemporal control.[94,101] Their investigation was based on the ability of the Ir-based catalyst to absorb light and form excited Ir^{III*} species that can reduce the alkyl bromide initiator, leading to the

generation of initiating radicals. The Ir^{IV} produced can subsequently oxidize the active radical chain-end leading to the formation of dormant species, and this process, upon addition of a photon can be repeated. The same Ir-catalyst was employed by Boyer and colleagues who pioneered on the development of photoinduced electron transfer (PET)-RAFT.[102–104] Apart from Ir-based catalysts, different metal-based catalysts have also been developed including Cu,[56,105–107] cobalt (Co),[108–110] zinc (Zn),[111–117] ruthenium (Ru),[102,118,119] iron (Fe)[120,121] and iodine (I),[122] and even metal-free systems have been reported to provide control over the produced polymers.[123,124]

Copper, particularly in the form of Cu(II) donor ligand complexes, has been known to participate in photoredox reactions upon UV-irradiation.[125] The concept of photoinduced Cu-mediated polymerization was first developed by Yagci and colleagues,[126] who reported on the photo(co)polymerization of methacrylates. They utilized Cu(II) in order to photo-generate Cu(I) *in-situ*, in the presence of *N,N,N′,N″,N″*-pentamethyldiethylenetriamine (PMDETA). The polymerization, although having been conducted in bulk, showed a linear increase of the molecular weight with increasing conversion, and the ability of the system to undergo copolymerization was illustrated by a chain extension. As proposed by Yagci and colleagues, the initial step included the *in-situ* generation of the Cu(I)X/L activator from the Cu(II) species which subsequently reacted with the initiator P_n-X to form an active radical $P_n^{\cdot}$, which in turn could propagate with monomer addition (M), terminate and undergo deactivation through reaction with Cu(II)X_2/L, leading to Cu(I)X/L and a halogen-terminated polymer chain (**Figure 1-3**).

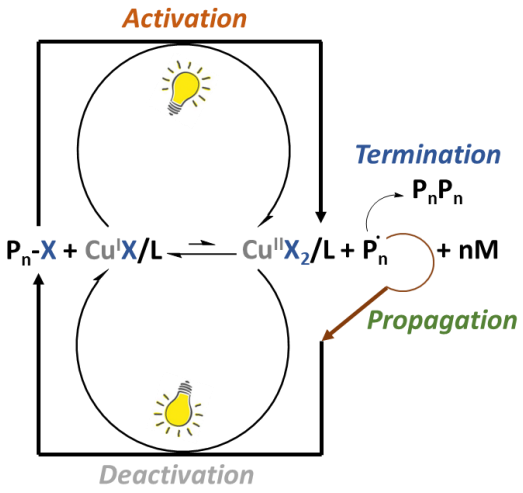

Figure 1-3. Graphical illustration of the mechanism of photoinduced controlled radical polymerization as reported by Yagci and colleagues. Figure adapted from reference ***126***.

The use of visible light and sunlight was reported by Konkolewicz, Matyjaszewski and colleagues for photoinduced ATRP of (meth)acrylic monomers.[127] The use of Cu(II)Br_2/TPMA complexes with low ppm of the Cu catalyst were used under mild light sources including blue and violet LEDs and sunlight, to generate well-defined polymers able to undergo chain extension. The proposed mechanism of photoinduced ATRP was based on the homolytic cleavage of the Cu(II)X/L complex in the excited state to form the Cu(I)/L activator and a halogen radical responsible for the initiation of the polymerization. The system exhibited "on demand" control by switching the light source "on" and "off".[127]

In 2014, Haddleton and co-workers reported on the photoinduced Cu-RDRP of acrylates utilizing Cu(II)Br_2 and the aliphatic tertiary amine Me_6Tren, with UV-irradiation (λ_{max} ~ 365 nm) as the light source.[105] The obtained polymers exhibited controlled molecular weights, low dispersity values and high end-group fidelity at near-quantitative (>99%) monomer conversions. With this approach, the polymerization rates were significantly faster (quantitative conversions were obtained

in less than 2 hours) compared to the previous approaches and, notably, temporal control was also demonstrated. In subsequent reports by the Haddleton group, the successful photoinduced Cu-RDRP of various acrylates (hydrophilic, hydrophobic and functionalized) in different organic media,[106] as well as the synthesis of one-pot multiblock copolymers was demonstrated.[128] Apart from the employment of organic media, the scope of this synthetic platform was greatly expanded in aqueous media.[129] The addition of sodium halides (NaBr) enhanced the control over the polymerization in water and as a result, water-soluble acrylates were successfully polymerized under UV-irradiation and in the presence of the Cu(II)Br_2/Me_6Tren complex. Notably, high end-group fidelity was maintained allowing for *in-situ* chain extensions in water. Furthermore, the polymerization exhibited high temporal control, as depicted by the "on-off" experiments.

1.5.4.1 Photoinduced Cu-RDRP: Mechanistic aspects

The increasing interest into photoinduced-RDRP systems has led researchers to begin to understand the mechanism behind this versatile synthetic platform, hence many approaches have been made to understand the dynamics of these systems. In their first study, Haddleton and co-workers reported that an excess of the aliphatic amine ligand Me_6TREN (relative to Cu(II)Br_2) is required to maintain excellent control over the polymerization of acrylates.[105] UV–Vis spectroscopy was applied to follow the polymerization and monitor the effect of UV-irradiation on the components of the polymerization over time. Based on their findings, they proposed that the photoexcitation of free Me_6Tren is responsible for the C-Br bond homolysis, which occurs through an outer-sphere single-electron transfer (OSET) when the alkyl halide initiator is present. This C-Br scission is followed by the formation of an initiating

radical, a Me_6Tren-based radical cation and its analogous Br-counterion, with the initiating radical mediating the propagation. When monomer is present, propagation occurs while the deactivating species Cu(II)Br_2/Me_6Tren reserves the control over the polymerization (**Figure 1-4**).

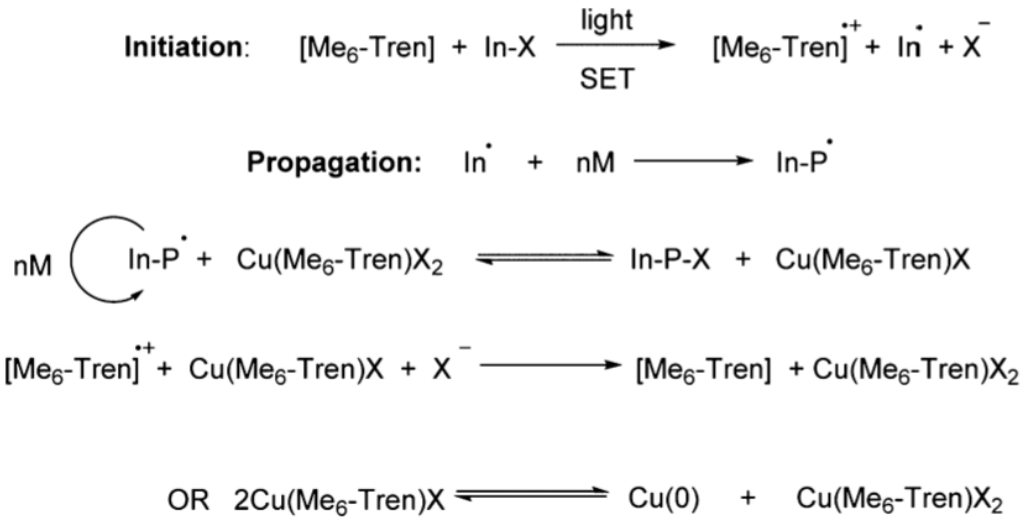

Figure 1-4. Proposed mechanism for the Cu(II)Br_2/Me_6Tren-mediated photoinduced RDRP. Figure reproduced by reference ***105***.

Barner-Kowollik and colleagues investigated the initiation mechanism of photoRDRP by utilizing pulsed-laser polymerization (PLP) and high-resolution mass spectrometry, highlighting the important role of the ligand which acts as a reducing agent.[130] They demonstrated that upon UV-irradiation, scission of the initiator's C-Br bond occurs which subsequently provides radicals that can propagate and also react with Cu(II) species **(Figure 1-5)**. Upon UV irradiation, an electron transfer reaction takes place between the photoexcited ligand and Cu(II) complexes leading to the generation of Cu(I) species, and apart from that, it was proposed that the Cu(II) complex gets excited and subsequently quenched by the free ligand, generating the analogous Cu(I) complex and the ligand radical cation.

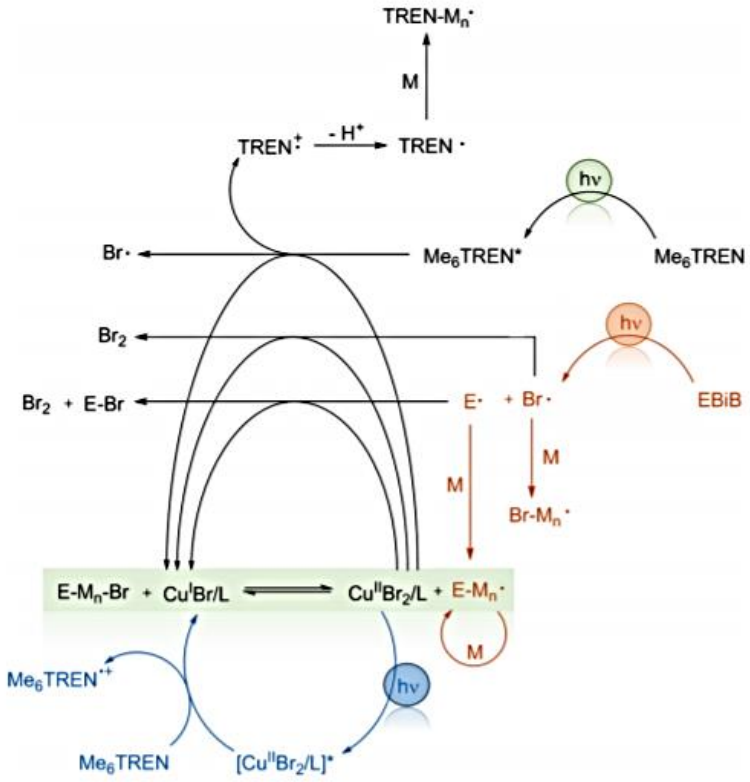

Figure 1-5. Proposed mechanism of photoRDRP as reported by Kowollik and colleagues. Figure reproduced from reference ***130***.

In a recent report, Haddleton and colleagues investigated the effect of UV-irradiation on Cu(II)-based complexes when different aliphatic amines are used as ligands.[56] Different characterization techniques such as transient electronic absorption spectroscopy (TEAS), UV-vis spectroscopy, electrospray ionization time of flight mass spectrometry (ESI-ToF-MS) and cyclic voltammetry (CV) were applied in order to provide insights into the catalyst behaviour upon photo-irradiation, namely the excited-state dynamics, the electrochemical behaviour of the Cu(II)/Cu(I) redox couples and the detection of different species upon complexation of the ligand to the metal centre (before and after UV-irradiation). It was found that, after the use of Me_6Tren, similarly good control over the polymerization was achieved when the tridentate PMDETA was used, while when the linear tetradentate 1,1,4,7,10,10-

hexamethyltriethylenetetramine (HMTETA) and the bidentate tetramethylethylenediamine (TMEDA) were used, poor control over the molecular weights and dispersity values was seen. These observations for the polymerizations where HMETA- and TMEDA-based complexes were used, were attributed to restricted mobility of those complexes which leads to inability of the complex to abstract the halogen atom from the alkyl halide initiator. Further insight was provided through the TEAS measurements which showed that the observed beat in the transient absorption spectra was due to the system oscillating between two different oxidation states of Cu, possibly caused by motion of the bromine between the copper and the ligand.

1.6 O_2-tolerant Controlled Radical Polymerizations

1.6.1 General aspects and common misconceptions

The increased interest in controlled radical polymerization techniques such as ATRP, RAFT and NMP has led to the development of these techniques as versatile platforms, tolerant to various conditions (*i.e.* high/low temperatures), different media and scales, and functional groups. However, since the early beginning of their development, stringent anaerobic conditions were required for their implementation in order to omit contamination from oxygen, air and moisture.

In 1991, Bhanu and Kishore in a review article reported that although the effect of oxygen in polymer degradation had been well-understood and documented, there was little knowledge on its effect on polymer synthesis.[131] Indeed, the role of oxygen in the polymerization's dynamics has remained, even until today, insufficiently investigated considering its longstanding, disadvantageous or not, presence. Although,

as commonly believed, oxygen acts as an inhibitor for radical polymerizations, it was as early as 1937 that aerial oxygen was used as initiator for the synthesis of low-density polyethylene, and as was finally demonstrated, it could act both as initiator and inhibitor for the polymerization, when high temperature (above 160-170 ^{o}C) and high pressure was applied.[132,133] Among other cases, oxygen has been shown to promote redox initiated polymerizations under specific conditions,[134–136] it can itself participate in redox reactions to generate initiating radicals as reported for the polymerization of vinyl monomers in the presence of O_2, ascorbic acid and transition metal salts,[136] has been essential for the production of hydrogen peroxides in photosensitized polymerizations.[137] However, even though there have been reports on the beneficial aspect of oxygen, the constant progress and pursuing of controlled macromolecular characteristics have rendered the presence of oxygen as problematic for controlled radical polymerization systems.

Indeed, oxygen is a well-known radical scavenger that reacts with carbon-centred free radicals produced thermally, photochemically or catalytically, and leads to the formation of peroxide radicals and hydroperoxides. The latter react very slowly (*i.e.* compared to alkyl radicals), leading to induction periods which last until all the oxygen in the polymerization solution gets consumed (or turns into peroxides) and in general, they are not efficient at reinitiating the polymerization. As early as 1948, Bovey and Kolthoff in their review article discussed the inhibition of vinyl polymerization.[138] As they reported, ideal inhibitors are substances that cause an induction period in the polymerization. During the induction period, the inhibitor gets consumed and subsequently the polymerization starts. Substances that act as inhibitors are often misconceived as retarders, with the latter having different effect on the polymerization than inhibitors. Typically, the retarders cause retardation throughout

the entire polymerization, without being related to an induction period. However, both inhibitors and retarders react with all the free radical produced, with retarders being less efficient and hindering the initiation of some polymer chains.

A report by Mayo *et al*. described that although the autooxidation of hydrocarbons that contain unreacted double bonds leads to the formation of hydroperoxides, hydrocarbons that contain reactive bonds (*i.e.* vinyl monomers) form polyperoxides (**Scheme 1-6**).[139,140] They hypothesized that a copolymerization-type reaction takes place between oxygen and the monomer, with the latter reacting thousand times faster with oxygen than with itself when the concentration of the two is equal in the reaction. In a study by Decker and Jenkins,[141] it was shown that the homopolymerization of acrylates in the presence of air does not begin until all of the dissolved oxygen gets consumed into peroxide since $k_4[O_2] >> k_5[M]$ (**see Scheme 1-6**). The peroxide radical reacts very slowly and thus, an induction (τ) period is observed.

Although the effect of oxygen on a radical polymerization, an thus the observed induction period, are dependent on many factors including temperature and pressure, as well as the diffusion coefficient of oxygen in different media,[142] early reports tried to corelate τ with experimental variables (*i.e*. monomer (M), initiator (A) and O_2 concentration).[143–145] As a result of these studies, the general expression $\boldsymbol{\tau = K[O_2]^a[M]^b[A]^c}$ was generated, with a, b and c values indicating the type of termination for $R^{\cdot}$, as described in **Scheme 1-6**.

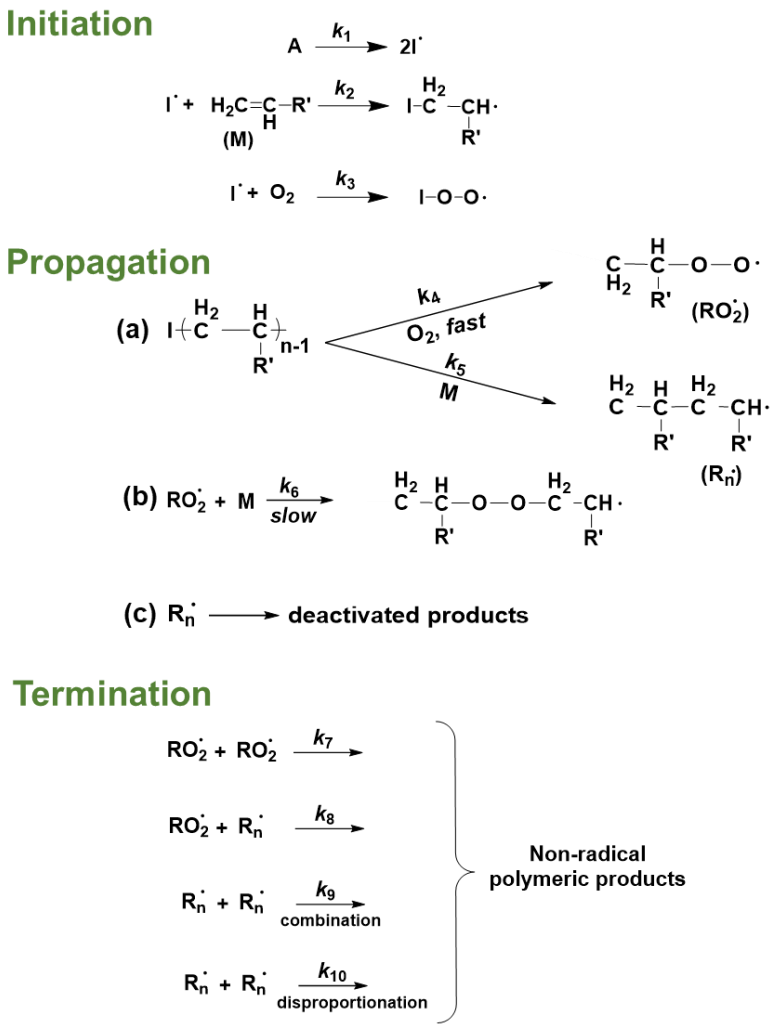

Scheme 1-6. The generation of peroxides during the radical polymerization of vinyl monomers, upon reaction of the generated radical with oxygen.

Since the induction period of the polymerization is dependent on the oxygen concentration, Schultz *et al.* defined this induction period as :

$$\tau = [O_2]_0/(-d[O_2]/dt)$$

with $[O_2]_0$ being the oxygen concentration present at the beginning of the polymerization and $(-d[O_2]/dt)$ representing the rate of oxygen consumption upon reaction with the monomer. In another investigation by Garton and George in 1973,[145] the effect of oxygen on the initiator was investigated. Based on the model of **Scheme 1-6**, the investigation was based on the assumptions that the contribution of the side

reaction c in the propagation step is small and that each reaction that leads to the generation of radicals, reaches a steady state which results in an equal rate of free radical generation and consumption. As a result, the correlation between the initiator and the peroxide formation (with f representing the initiator efficiency) can be described as :

$$f k_1[A] = (k_9 + k_{10})[R^\bullet]^2 + k_8[RO_2^\bullet][R^\bullet] + k_7[RO_2^\bullet]^2$$

It should be noted that although the above-mentioned investigations have been reported by many researchers and exhibit reproducibility, the proposed reaction models are expected to exhibit alterations from the existing systems, since different and more sophisticated mechanistic pathways have proposed for the various radical polymerization platforms.

Since oxygen sensitivity has been an obstacle for the implementation of RDRPs, investigations have been made to pogress oxygen tolerant radical polymerizations,[146,147] with (PET-)RAFT and (photo-)ATRP being the most well-studied techniques. In 2014, Liska and co-workers described in their review article several approaches and strategies for the elimination of the oxygen effects on photoinduced radical polymerization.[146] They classified these strategies as either chemical or physical. Recently, Boyer and colleagues highlighted some of the most common deoxygenation approaches up to date, including the ‘‘polymerising through’’ oxygen approach, the enzyme mediated deoxygenation and the continuous regeneration of a redox-active catalyst (**Scheme 1-7**).[147]

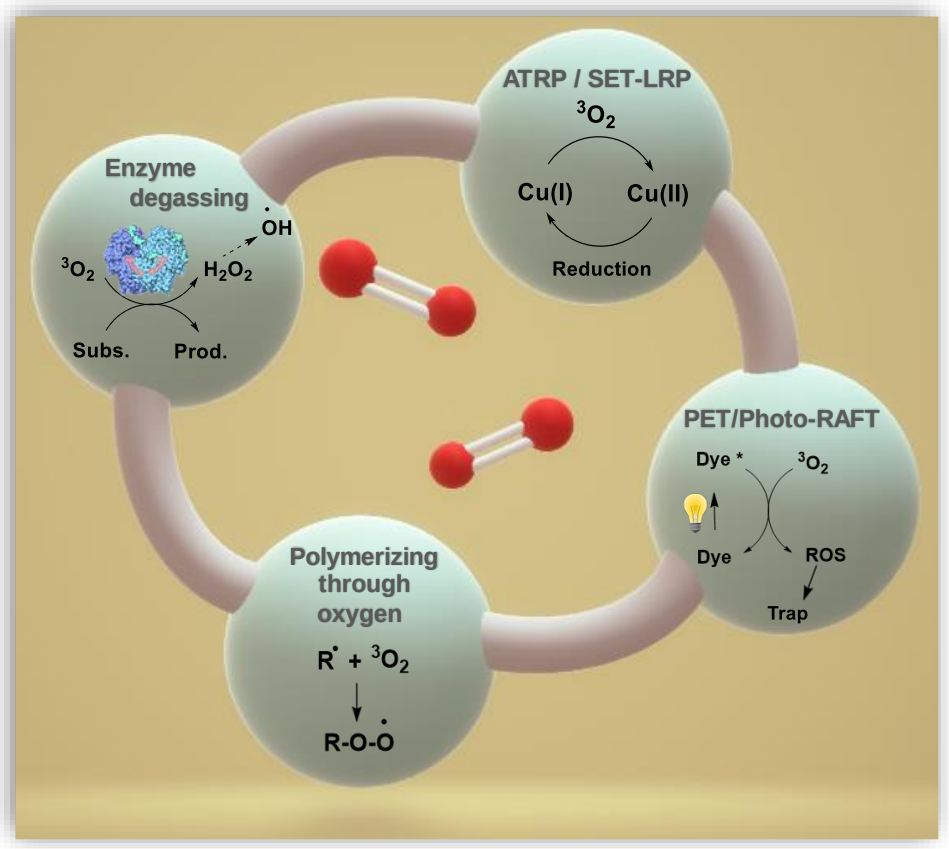

Scheme 1-7. Commonly applied oxygen tolerance approaches.

1.6.2 O_2-tolerant RAFT & PET-RAFT

The "polymerizing through" approach

As described by Boyer and colleagues, RAFT does not depend on a catalytic redox initiation process, hence it is possible to use initiating radicals to consume oxygen prior to the initiation of the polymerization.[147] This can be achieved without compromising control over the polymerization, when the initial concentration of oxygen in the solution is lower than the initiating radical concentration (this can also be observed in deoxygenated RAFT). Ergo, the polymerization can, under specific conditions, proceed without external deoxygenation. This approach was coined as "*polymerizing through*" oxygen (**Figure 1-6**). Although it is considered as a simplified

approach which does not require externally added reagents, it does lack a broad applicability and it is more compatible with low DPs, high monomer concentrations and high temperatures.[147]

As early as 2003, Sanderson and colleagues reported that styrene could undergo RAFT polymerization at high temperature (90 °C) without exhibiting high oxygen sensitivity.[148] Later, Zhang *et al*. demonstrated that the controlled presence of oxygen increased the rate of RAFT polymerization for styrene[149] and MMA,[150] without the need of an externally added radical initiator. This observation was attributed to the copolymerization of oxygen with the monomers which led to the generation of oligo-peroxides, which in turn decomposed to form additional radical species.[151]

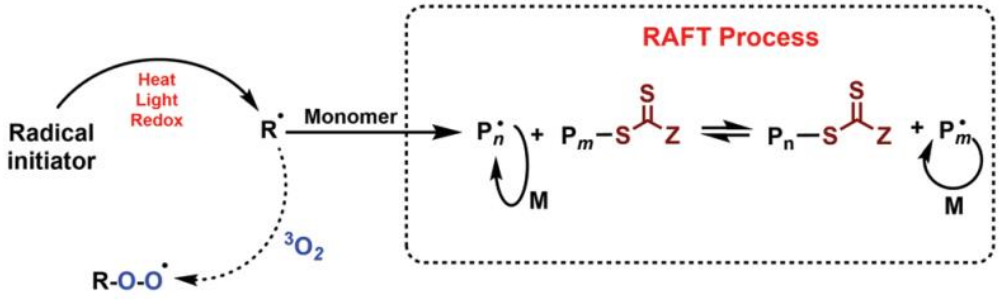

Figure 1-6. *Oxygen tolerant* RAFT polymerization *via* the "*polymerizing through*" oxygen approach. Figure reproduced from reference ***147***.

More recently (2015), Perrier and colleagues reported on the fast synthesis of multiblock copolymers in the presence of air.[152] The application of 100 °C led to high flux of radicals generated by the thermal initiator which was employed. Furthermore, the use of acrylamide monomers which have high rates of propagation, as well as the high monomer and initiator concentrations, facilitated the non-deoxygenated polymerization which led to quantitative monomer conversions within 3 minutes for each low DP block. A range of acrylamides and acrylates were also polymerized through non-deoxygenated RAFT polymerization by Cooper-White and colleagues,[153]

who demonstrated higher DPs (20-100) and mikto-arm star polymers, again by applying 100 ^{o}C. As a "polymerizing through" oxygen approach was considered the investigation by Junkers and co-workers who, at ambient and low temperature (0 ^{o}C) they employed an acid induced cyclohexanone/*tert*-butyl hydroperoxide initiation system for the RAFT polymerization of vinyl monomers in air.[154]

The "enzyme deoxygenation" approach (in RAFT)

Enzyme deoxygenation includes the addition of an enzyme (most commonly glucose oxidase (GOx)) in the non-deoxygenated polymerization, for the reduction of molecular oxygen into a non-radical quenching species such as hydrogen peroxide. Although this concept has been inspired by biochemical processes and exists in the field of polymer chemistry since the 90's, it has recently gained particular interest in the field of polymers. After the formative report by Iwata *et al.* in 1991,[155] who used GOx for the deoxygenation and initiation of the free-radical polymerization of hydroxyethyl methacrylamide, Yagci and colleagues reported the use of this enzyme in order to avoid O_2-derived inhibition in photoinitiated free-radical polymerization.[156] In 2014, Chapman *et al.* utilized the same enzyme for the non-deoxygenated RAFT polymerization of 2-hydroxyethyl acrylate.[157] With the addition of low GOx concentrations and at relatively mild reaction conditions (45^{o}C), the polymerization was performed without significant inhibition, even in open vessels, allowing for a subsequent study on high throughput synthesis of polymethacrylates and polymethacrylamides in open well plates.[158]

The use of photocatalysts in PET-RAFT

PET-RAFT polymerization, as developed by Boyer and colleagues, is a photocatalytic method which involves a photoinduced electron (or energy) transfer process to initiate RAFT polymerization.[159] The use of highly reducing photocatalysts

has rendered the PET-RAFT process an oxygen tolerant platform for the polymerization of various monomers under mild conditions (*i.e*. blue light irradiation). In their first study, Boyer and co-workers demonstrated the synthesis of high molecular weight polymers, with narrow molecular weight distributions and versatility over chain extensions, even in the presence of air, by exploiting the reducing ability of the $Ir(ppy)_3$ photocatalyst.[159] Subsequently, similar results were obtained when the $[Ru(bpy)_3]Cl_2$ catalyst was employed for the synthesis of multiblock copolymers, [160] with Hawker and colleagues also leveraging the catalyst's reducing ability for the online monitoring of polymerization kinetics in air.[161]

In subsequent studies, the Boyer group developed the concept of oxygen tolerant PET-RAFT with the use of 5,10,15,20-tetraphenyl-21*H*,23*H*-porphine (ZnTPP) as a photocatalyst, with the latter being more compatible with lower energy wavelengths of light in the visible spectrum, while in parallel maintaining control over the polymerization and even showing less inhibition compared to when $Ir(ppy)_3$ or $[Ru(bpy)_3]Cl_2$ were used.[111] When the reducing ability of ZnTPP was investigated in DMSO, it was found that the photocatalyst had the ability to photosensitize triplet oxygen into singlet oxygen (**Figure 1-7**), with the latter reacting with DMSO to form the analogous sulfone ($DMSO_2$).[162] Studies conducted in other solvents, showed that the efficiency of a photocatalyst for oxygen scrubbing is dependent on its ability to transform triplet oxygen into singlet.[117] Apart from metalloporphyrines, dyes such as Eosin Y (EY) have also shown to provide oxygen tolerance along with their photocatalytic activity.[163,164]

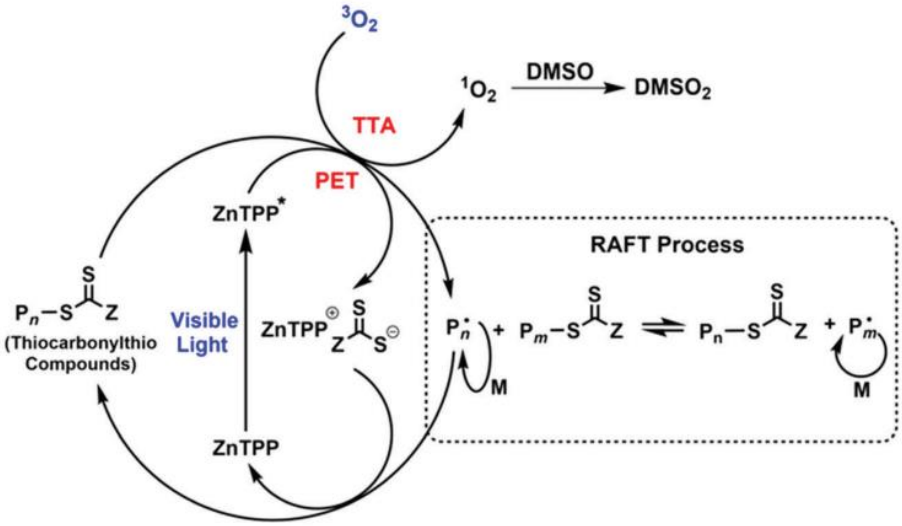

Figure 1-7. Oxygen tolerant PET-RAFT with the use of metalloporphirines. ZnTPP photosensitizes triplet oxygen into singlet oxygen which is subsequently quenched by DMSO to form $DMSO_2$. Figure reproduced from reference **147.**

Apart from PET-RAFT which involves initiation by a RAFT agent, other photoRAFT platforms that proceed without RAFT agents have also exhibited oxygen tolerant behaviour.[165] Photoiniferter systems have also shown good tolerance over oxygen, as described by Zhu's,[166] Qiao's,[167] and Johnson's[168] groups who employed the "polymerizing through" oxygen approach. Furthermore, in recent reports, the employment of more "bio-friendly" reagents such as organic dyes, ascorbic acid and vitamin B_2 or vitamin B_{12} have shown to facilitate the reduction of oxygen, leading to oxygen tolerant systems with controlled macromolecular characteristics.[169–171]

1.6.3 O_2-tolerant Cu-RDRP

As a transition metal-mediated polymerization, Cu-RDRP involves a Cu-based complex with *N*-containing ligands (*i.e.* amines), which is responsible for the regulation of the equilibrium between dormant and active species. Apart from the conventional ATRP which utilizes Cu(I), Cu(II)- and Cu(0)-mediated approaches have

also been developed which, broadly speaking, rely on the same redox concept for the regulation of the reversible deactivation process.

The implementation of (SARA/ARGET) ATRP in the presence of oxygen was first reported by Matyjaszewski in 1998 who demonstrated that the oxygen present in a sealed vessel could be scrubbed *via* oxidation of Cu(I) into Cu(II).[172] This process led to accumulation of the Cu(II) deactivator, necessitating the addition of a reducing agent (Cu(0) powder in this case) in order to regenerate the active Cu(I) species. Although for the sealed reactions an induction period and slower polymerization rate were observed, the obtained polymers exhibited controlled molecular weight and dispersity at high conversions, as well as high end-group fidelity which allowed for block copolymerizations.[173] Notably, the open-to-air reactions did not result in polymerization.

O_2-tolerance through extrinsic reducing agents

In a so-called oxygen tolerant Cu-RDRP system, the removal of oxygen is synergistically dependent on all the components including the initiator, the catalyst system which involves the copper species and the ligand, even the monomer and the solvent.[147,174,175] However, in some Cu-RDRP platforms the need for external reducing agents is necessary for a successful polymerization when no deoxygenation is applied. There have been reports about the ability of oxygen to initiate the polymerization in the presence of a suitable Cu-complex, yielding polymers with low dispersity values but uncontrolled molecular weights.[176] Hence, reducing agents that could regenerate the deactivator leading to control over the molecular weights were employed, with these approaches being known as either Activator Generated by Electron Transfer

(AGET-) ATRP, or Activator **Re**Generated by Electron Transfer (ARGET-) ATRP (when low ppm of the catalyst are used).[76,78]

Following this approach, Gnanou and Hizal employed phenolic compounds in the presence of Cu(II)/PMDETA for the AGET-ATRP of vinyl monomers, in the presence of air.[177] The aim of the phenol addition was the reduction of the catalyst complex, or Cu(II) which occurs from the oxidation of the catalyst Cu(I). As a result, molecular weights higher than the theoretical values were obtained, along with the presence of induction periods. In the same context, Matyjaszewski's group employed ascorbic acid as reducing agent for the mini-emulsion AGET-ATRP of *n*-butyl acrylate in the presence of air, resulting in negligible induction periods, whilst high concentration of the reducing agent was needed in order to achieve efficient polymerization rates.[178] The same concept was followed by the same and other groups, for the A(R)GET-ATRP and SET-LRP (from Percec's group) of vinyl monomers, with the use of various compounds which act as extrinsic reducing agents including ascorbic acid,[179–183] hydrazine,[80,184–186] glucose[179,187] and tin(II) 2-ethylhexanoate ($Sn(EH)_2$).[188–191]

O_2-tolerance through enzyme deoxygenation

The concept of enzyme deoxygenation was, as mentioned earlier, initially used in order to avoid O_2-inhibition in free radical polymerization.[155,156] The successful implementation of GOx inspired researchers to introduce the same concept in RAFT and subsequently in Cu-RDRP, in order to replace conventional deoxygenation and expand the scope of Cu-RDRP towards lower volumes which would facilitate the implementation of these systems on bio-approaches. Matyjaszewski and colleagues, recently (2018) utilized GOx along with sodium pyruvate for the ICAR-ATRP of

ligo(ethyleneoxide)methylethermethacrylate ($OEOMA_{500}$).[192] In this system, GOx catalyzed the oxidation of glucose into d-glucono-1,5-lactone and hydrogen peroxide (H_2O_2), with the latter being removed by the sacrificial substrate sodium pyruvate, in order to avoid the generation of new chains by H_2O_2. Their initial study was subsequently followed by the application of GOx for the deoxygenation of ARGET, ICAR, photo- and electrochemically mediated (eATRP) ATRP, in miniemulsion and emulsion, with low ppm of catalyst.[193] Furthermore, the same group reported on the synthesis of (DNA- and BSA-) bioconjugates through ICAR-ATRP, in which continuous air supply was applied.[194] In this case, GOx was used for the conversion of β-D-glucose and oxygen into gluconate and H_2O_2, with the latter being used along with acetylacetonate as substrate for horseradish peroxidase which, in turn, supplies the system with radicals. The reaction of the generated radicals with the monomer, led to carbon-based radicals which could reduce Cu(II) into Cu(I), providing the active catalyst species for ICAR-ATRP following the described biocatalytic cascade. (**Figure 1-8**).

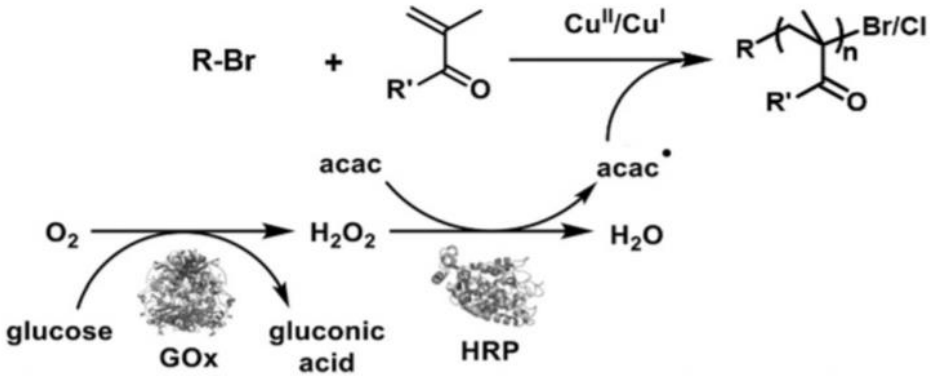

Figure 1-8. The biocatalytic cascade which starts from the GOx-catalyzed oxidation of glucose and ultimately leads to the generation of polymers in the presence of constant air supply. Figure reproduced from reference ***194***.

Achieving O_2-tolerance through headspace elimination

In 2018, Liarou, Haddleton *et al*., reported on the Cu(0)-RDRP of (meth)acrylates, styrene and acrylamides in organic and aqueous media, without any type of external deoxygenation or addition of extrinsic reducing agents.[175] By eliminating the headspace and upfilling the vessel with the reaction solution, the concentration of gaseous oxygen was significantly reduced, whilst the solution reaction still containing the dissolved oxygen included in the polymerization components. The application of an oxygen probe for the *in-situ* monitoring oxygen concentration in the polymerization solution showed that the all the components synergistically contributed to full oxygen consumption after 4 minutes of the start of the reaction. Furthermore, the O_2-reducing ability of each component was examined individually, leading to the conclusion that the initiator (ethyl α-bromoisobutyrate, EBiB), the Cu(0)-wire and the complex (Cu(II)Br_2/Me_6Tren) could individually lead to oxygen consumption when combined with the monomer (methyl acrylate, MA) and the solvent (DMSO), but the combination of all was the key-step to fast and full oxygen consumption (**Figure 1-9**). Although polymerization without headspace had very small induction period, the reactions conducted in bigger vessels had longer induction periods, analogous to the extent of headspace. Finally, the no-headspace polymerization exhibited controlled molecular weights and low dispersity values at quantitative conversions, for a range of monomers. Even in vessels with small headspace, the end-group fidelity was high, leading to *in-situ* chain extensions.

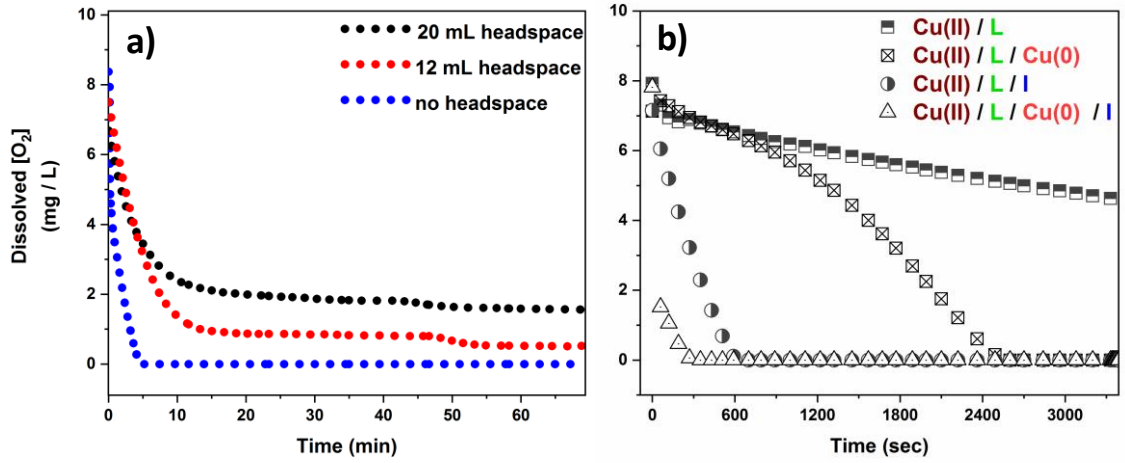

Figure 1-9. Line graphs illustrating a) the effect of the headspace and b) the effects of Cu(0) wire, EBiB (I), and Me_6Tren (L) on the evolution of the dissolved oxygen concentration during polymerization.

O_2-tolerance in photoinduced Cu-RDRP

External control over the Cu-RDRP dynamic equilibrium can be achieved through many stimuli including electrochemical and light. Light in particular has proved to be highly advantageous since it offers excellent regulation of the active/dormant species ratio and apart from that, it is a benign and versatile stimulus. The non-deoxygenated photoATRP was studied by Mosnacek and colleagues. In their studies, irradiation at λ > 350 nm and Cu(II)Br_2/TPMA as the catalyst complex were employed for the photoATRP of methyl methacrylate (MMA). It was shown that the photopolymerization exhibited and induction period which was only shortened when 4-fold excess of TPMA with respect to copper was used.[195] in the mechanistic pathway that was proposed, the Cu(II)Br_2/ligand complex undergoes photochemical reduction upon photoirradiation, leading to the active Cu(I)Br/ligand species. The latter can either undergo oxidation in the presence of oxygen to for Cu(II)Br(O_2), or activate the alkyl halide initiator, leading to the formation of radicals. Furthermore, it was

speculated that the free amine ligand could also participate in oxygen consumption. The photoATRP equilibrium is reached when full oxygen consumption has occurred (**Figure 1-10**). In a subsequent report by the same group, the effect of light intensity, ligand and the oxygen concentration were also investigated, showing that the evolution of a non-deoxygenated photoATRP is dependent on many parameters in order to reach good control over the macromolecular characteristics of the synthesized polymers. [196]

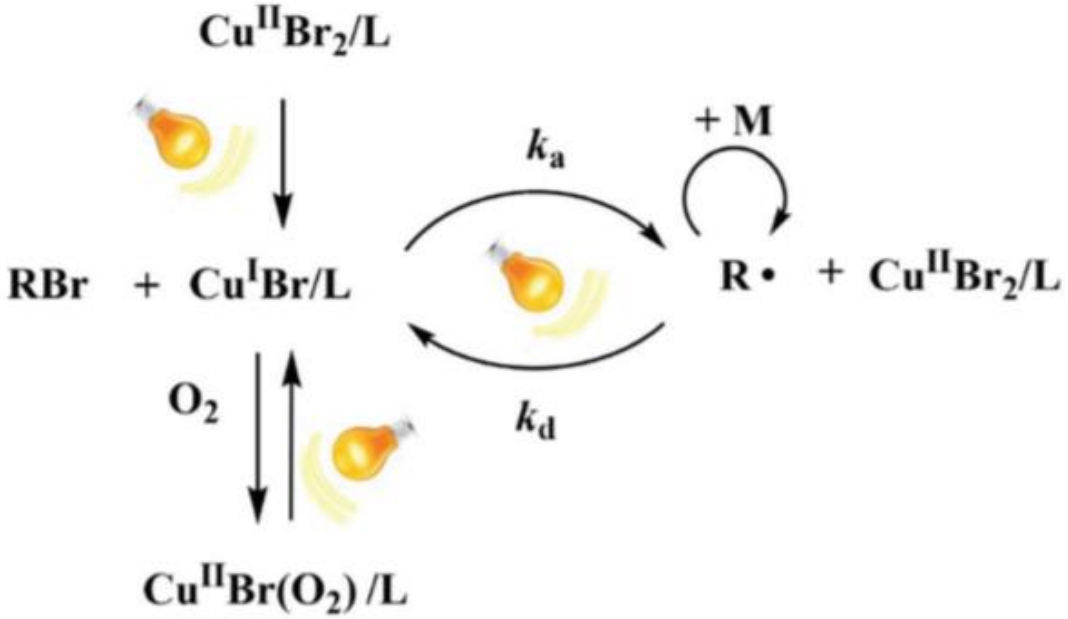

Figure 1-10. Simplified mechanism of photoATRP in the presence of oxygen, as proposed by Mosnacek and colleagues. Figure reproduced from reference ***195***.

The addition of triethylamine as reducing agent was used by Poly and colleagues for the non-deoxygenated photoATRP of MMA with Cu(II)/1,10-phenanthroline as the catalyst complex and upon irradiation with high intensity blue LED light. Their findings, although involved long induction periods and higher than expected molecular weights, verified the versatility of the approach when mild irradiation is applied.[197]

In 2019, Liarou, Haddleton and co-workers demonstrated the photoinduced Cu-RDRP of various hydrophobic, hydrophilic and semi-fluorinated (meth)acrylates in ultralow volumes (as low as 5 μL), without applying any type of extrinsic deoxygenation.[174] The online monitoring of the dissolved O_2 concentration, which was conducted through an oxygen probe, showed that the generation of sufficient amounts of active copper species was the requirement for efficient O_2-consumption, with the synergy of all the components leading to oxygen-free solutions as fast as 4 minutes. This approach was compatible with very low volumes (5-200 μL), as well as higher scales (*i.e.* 0.5 L).

This dissertation aims to introduce the next generation of RDRPs, by developing a series of *oxygen tolerant* Cu-RDRP platforms. Due to its simplicity, the work included in this thesis can possibly establish Cu-RDRP as a fully oxygen tolerant, versatile synthetic platform even for non-experts. Focusing on expanding the scope and applicability of Cu-RDRP, three different approaches are presented and discussed, including Cu(0)-wire mediated RDRP without external deoxygenation, *ultra-low volume* photoinduced Cu-RDRP and self-deoxygenating aqueous Cu-RDRP *via* pre-disproportionation of Cu(I). In contrast to existing approaches which add complexity to the several CRP approaches by relying on externally added reducing agents, the simplicity of this work lies on the circumvention of externally added reducing agents, oxygen scavengers and radical sources, along with the absence of any type of conventional deoxygenation (*i.e.* freeze-pump-thaw cycles or gas sparging). The oxygen-free environment is achieved through the reducing activity of the polymerization components which if not present, the polymerization would not commence in a controlled manner. Additionally, an important aspect of these platforms is that four different polymer families can be synthesized (*e.g.* acrylates,

methacrylates, styrene, acrylamides), in various media (organic and aqueous) and at different temperatures and scales, rendering these platforms flexile toolkits for the synthesis of different materials. Although the synthetic pathways which are developed in this current work are contacted in the presence of air/oxygen, these approaches exhibit excellent control over the polymerization which is depicted in the controlled macromolecular characteristics (controlled molecular weights, low *Đ*, near-quantitative monomer conversions) of the synthesized polymers. Apart from the development of Cu-RDRP as a robust, oxygen-tolerant platform, the mechanistic pathways of oxygen consumption are investigated in each approach, not only with the use of state-of-the-art analytical tools, but also by employing for the first time a fibre-optic oxygen probe, for the *in-situ* online monitoring of the dissolved oxygen.

1.7 References

1 H. Staudinger, *Berichte der Dtsch. Chem. Gesellschaft (A B Ser.*, 1920, **53**, 1073–1085.

2 P. J. Flory, *Principles of Polymer Chemistry*, Cornell Univ. Press, Ithaca, N. Y., 1953.

3 J. K. Stille, *J. Chem. Educ.*, 1981, **58**, 862.

4 S. Penczek, G. Moad, M. Barón, K. Hatada, M. Hess, A. D. Jenkins, R. G. Jones, J. Kahovec, P. Kratochvíl, P. Kubisa, E. Maréchal, R. F. T. Stepto, J. P. Vairon, J. Vohlídal and E. S. Wilks, in *Pure and Applied Chemistry*, 2008, **80**, 2163–2193.

5 M. F. Cunningham and R. Hutchinson, in *Handbook of Radical Polymerization*, John Wiley & Sons, Inc., 2003, 333–359.

6 K. Matyjaszewski and T. P. Davis, Eds., *Handbook of Radical Polymerization*, John Wiley & Sons, Inc., Hoboken, NJ, USA, 2002.

7 C. Barner-Kowollik, P. Vana and T. P. Davis, in *Handbook of Radical Polymerization*, John Wiley & Sons, Inc., 2003, 187–261.

8 G. Odian, *Principles of Polymerisation*, 4th Edition, Wiley, 2004

9 J. W. Nicholson, in *The Chemistry of Polymers*, Royal Society of Chemistry, Cambridge, 2006, 1–22.

10 B. Klumperman, in *Encyclopedia of Polymer Science and Technology*, Wiley, 2003.

11 K. Ziegler and K. Bähr, *Berichte der Dtsch. Chem. Gesellschaft (A B Ser.*, 1928, **61**, 253–263.

12 S.G. Waley and J. Watson, *Proc. R. Soc. London. Ser. A.*, 1949, **199**, 499–517.

13 M. Szwarc, *Nature*, 1956, **178**, 1168–1169.

14 M. Szwarc, *J. Polym. Sci. Part A Polym. Chem.*, 1998, **36**, IX–XV.

15 K. Matyjaszewski, *Macromolecules*, 2012, **45**, 4015–4039.

16 A. Anastasaki, V. Nikolaou, G. Nurumbetov, P. Wilson, K. Kempe, J. F. Quinn, T. P. Davis, M. R. Whittaker and D. M. Haddleton, *Chem. Rev.*, 2016, **116**, 835–877.

17 IUPAC Recommendations 1994, *Pure Appl. Chem.*, 1994, **66**, 2483-2486.

18 R. P. Quirk and B. Lee, *Polym. Int.*, 1992, **27**, 359–367.

19 G. Moad and E. Rizzardo, in *RSC Polymer Chemistry Series*, Royal Society of

Chemistry, 2016, 1–44.

20 J. Chiefari, Y. K. Chong, F. Ercole, J. Krstina, J. Jeffery, T. P. T. Le, R. T. A. Mayadunne, G. F. Meijs, C. L. Moad and G. Moad, *Macromolecules*, 1998, **31**, 5559-5562.

21 M. Kato, M. Kamigaito, M. Sawamoto and T. Higashimura, *Macromolecules*, 1995, **28**, 1721–1723.

22 J. Xia and K. Matyjaszewski, *Macromolecules*, 1997, **30**, 7697–7700.

23 D. H. Solomon and G. Waverley, *11 Patent Number: 4*, 1984, vol. 581.

24 M. K. Georges, R. P. N. Veregin, P. M. Kazmaier and G. K. Hamer, *Macromolecules*, 1993, **26**, 2987–2988.

25 D. H. Solomon and G. Waverley, *11 Patent Number: 4*, vol. 581.

26 K. Matyjaszewski, Ed., *Controlled Radical Polymerization*, American Chemical Society, Washington, DC, 1998, vol. 685.

27 D. Benoit, V. Chaplinski, R. Braslau and C. J. Hawker, *J. Am. Chem. Soc.*, 1999, **121**, 3904–3920.

28 J. Nicolas, B. Charleux, O. Guerret and S. Magnet, *Macromolecules*, 2004, **37**, 4453–4463.

29 L. Hlalele and B. Klumperman, *Macromolecules*, 2011, **44**, 7100–7108.

30 B. Charleux, J. Nicolas and O. Guerret, *Macromolecules*, 2005, **38**, 5485–5492.

31 B. Grassl, G. Clisson, A. Khoukh and L. Billon, *Eur. Polym. J.*, 2008, **44**, 50–58.

32 D. Benoit, E. Harth, P. Fox, R. M. Waymouth and C. J. Hawker, *Macromolecules*, 2000, **33**, 363–370.

33 H. Fischer, *Chem. Rev.*, 2001, **101**, 3581–3610.

34 T. Fukuda, T. Terauchi, A. Goto, K. Ohno, Y. Tsujii, T. Miyamoto, S. Kobatake and B. Yamada, *Macromolecules*, 1996, **29**, 6393–6398.

35 L. Petton, A. E. Ciolino, B. Dervaux and F. E. Du Prez, *Polym. Chem.*, 2012, **3**, 1867–1878.

36 A. Goto and T. Fukuda, *Prog. Polym. Sci.*, 2004, 29, 329–385.

37 P. B. Zetterlund, Y. Saka, R. McHale, T. Nakamura, F. Aldabbagh and M. Okubo, *Polymer*, 2006, **47**, 7900–7908.

38 B. Lessard, C. Tervo and M. Marić, *Macromol. React. Eng.*, 2009, **3**, 245–256.

39 J. He, Li and Y. Yang, *Macromolecules*, 2000, **33**, 2286–2289.

40 M. Souaille and H. Fischer, *Macromolecules*, 2001, **34**, 2830–2838.

41 G. Moad, E. Rizzardo and S. H. Thang, *Aust. J. Chem.*, 2009, **62**, 1402–1472.

42 M. R. Hill, R. N. Carmean and B. S. Sumerlin, *Macromolecules*, 2015, **48**, 5459–5469.

43 D. J. Keddie, *Chem. Soc. Rev.*, 2014, 43, 496–505.

44 S. Perrier, *Macromolecules*, 2017, 50, 7433–7447.

45 J.-S. Wang and K. Matyjaszewski, *J. Am. Chem. Soc.*, 1995, **117**, 5614–5615.

46 A. Moreno, S. Grama, T. Liu, M. Galià, G. Lligadas and V. Percec, *Polym. Chem.*, 2017, **8**, 7559–7574.

47 V. Percec, T. Guliashvili, J. S. Ladislaw, A. Wistrand, A. Stjerndahl, M. J. Sienkowska, M. J. Monteiro and S. Sahoo, *J. Am. Chem. Soc.*, 2006, **128**, 14156–14165.

48 B. M. Rosen and V. Percec, *Chem. Rev.*, 2009, **109**, 5069–5119.

49 G. R. Jones, A. Anastasaki, R. Whitfield, N. Engelis, E. Liarou and D. M. Haddleton, *Angew. Chemie Int. Ed.*, 2018, **57**, 10468–10482.

50 A. Anastasaki, V. Nikolaou and D. M. Haddleton, *Polym. Chem.*, 2016, 7, 1002–1026.

51 H. Tang, N. Arulsamy, M. Radosz, Y. Shen, N. V. Tsarevsky, W. A. Braunecker, W. Tang and K. Matyjaszewski, *J. Am. Chem. Soc.*, 2006, **128**, 16277–16285.

52 W. Tang, Y. Kwak, W. Braunecker, N. V. Tsarevsky, M. L. Coote and K. Matyjaszewski, *J. Am. Chem. Soc.*, 2008, **130**, 10702–10713.

53 A. Simula, V. Nikolaou, F. Alsubaie, A. Anastasaki and D. M. Haddleton, *Polym. Chem.*, 2015, **6**, 5940–5950.

54 F. Alsubaie, A. Anastasaki, V. Nikolaou, A. Simula, G. Nurumbetov, P. Wilson, K. Kempe and D. M. Haddleton, *Macromolecules*, 2015, **48**, 6421–6432.

55 F. Alsubaie, A. Anastasaki, V. Nikolaou, A. Simula, G. Nurumbetov, P. Wilson, K. Kempe and D. M. Haddleton, *Macromolecules*, 2015, **48**, 5517–5525.

56 E. Liarou, M. Staniforth, J. S. Town, A. Marathianos, M. Grypioti, Y. Li, Y. Chang, S. Efstathiou, E. Hancox, A. M. Wemyss, P. Wilson, B. A. Jones, M. Aljuaid, V. G. Stavros and D. M. Haddleton, *Eur. Polym. J.*, 2020, 109388.

57 H. Fischer, *Macromolecules*, 1997, **30**, 5666–5672.

58 H. Fischer, *J. Polym. Sci. Part A Polym. Chem.*, 1999, **37**, 1885–1901.

59 J. Foley, S. Tyagi and B. J. Hathaway, *J. Chem. Soc. Dalt. Trans.*, 1984, 1–5.

60 G. Kickelbick, T. Pintauer and K. Matyjaszewski, *New J. Chem.*, 2002, **26**, 462–468.

61 A. V. Malkov, I. R. Baxendale, M. Bella, V. Langer, J. Fawcett, D. R. Russell, D. J. Mansfield, M. Valko and P. Kočovský, *Organometallics*, 2001, **20**, 673–690.

62 J. Xia and K. Matyjaszewski, *Macromolecules*, 1997, **30**, 7697–7700.

63 P. V. Bernhardt, *J. Am. Chem. Soc.*, 1997, **119**, 771–774.

64 D. M. Haddleton, C. B. Jasieczek, M. J. Hannon and A. J. Shooter, *Macromolecules*, 1997, **30**, 2190–2193.

65 Y. Kwak and K. Matyjaszewski, *Macromolecules*, 2008, **41**, 6627–6635.

66 W. Tang and K. Matyjaszewski, *Macromolecules*, 2007, **40**, 1858–1863.

67 A. Goto and T. Fukuda, *Macromol. Rapid Commun.*, 1999, **20**, 633–636.

68 Y. Shen, S. Zhu, F. Zeng and R. Pelton, *Macromolecules*, 2000, **33**, 5399–5404.

69 T. G. Ribelli, F. Lorandi, M. Fantin and K. Matyjaszewski, *Macromol. Rapid Commun.*, 2019, **40**, 1800616.

70 C. Y. Lin, M. L. Coote, A. Gennaro and K. Matyjaszewski, *J. Am. Chem. Soc.*, 2008, **130**, 12762–12774.

71 D. Konkolewicz, Y. Wang, P. Krys, M. Zhong, A. A. Isse, A. Gennaro and K. Matyjaszewski, *Polym. Chem.*, 2014, **5**, 4396-4417.

72 D. Konkolewicz, Y. Wang, M. Zhong, P. Krys, A. A. Isse, A. Gennaro and K. Matyjaszewski, *Macromolecules*, 2013, **46**, 8749-8772.

73 K. Matyjaszewski, W. Jakubowski, K. Min, W. Tang, J. Huang, W. A. Braunecker and N. V. Tsarevsky, *Proc. Natl. Acad. Sci. U. S. A.*, 2006, **103**, 15309–15314.

74 H. Dong, W. Tang and K. Matyjaszewski, *Macromolecules*, 2007, **40**, 2974–2977.

75 Y. Kwak and K. Matyjaszewski, *Polym. Int.*, 2009, **58**, 242–247.

76 W. Jakubowski and K. Matyjaszewski, *Macromolecules*, 2005, **38**, 4139–4146.

77 A. de Vries, B. Klumperman, D. de Wet-Roos and R. D. Sanderson, *Macromol. Chem. Phys.*, 2001, **202**, 1645–1648.

78 W. Jakubowski and K. Matyjaszewski, *Angew. Chemie Int. Ed.*, 2006, **45**, 4482–4486.

79 K. Min, H. Gao and K. Matyjaszewski, *Macromolecules*, 2007, **40**, 1789–1791.

80 X. Jiang, B. M. Rosen and V. Percec, *J. Polym. Sci. Part A Polym. Chem.*, 2010, **48**, 2716–2721.

81 Q. Zhang, P. Wilson, Z. Li, R. McHale, J. Godfrey, A. Anastasaki, C. Waldron and D. M. Haddleton, *J. Am. Chem. Soc.*, 2013, **135**, 7355–7363.

82 Q. Zhang, Z. Li, P. Wilson and D. M. Haddleton, *Chem. Commun.*, 2013, **49**, 6608–6610.

83 C. Waldron, Q. Zhang, Z. Li, V. Nikolaou, G. Nurumbetov, J. Godfrey, R. McHale, G. Yilmaz, R. K. Randev, M. Girault, K. McEwan, D. M. Haddleton, M. Droesbeke, A. J. Haddleton, P. Wilson, A. Simula, J. Collins, D. J. Lloyd, J. A. Burns, C. Summers, C. Houben, A. Anastasaki, M. Li, C. R. Becer, J. K. Kiviaho and N. Risangud, *Polym. Chem.*, 2014, **5**, 57–61.

84 J. Ma, H. Chen, M. Zhang and M. Yu, *J. Polym. Sci. Part A Polym. Chem.*, 2012, **50**, 609–613.

85 A. H. Soeriyadi, C. Boyer, F. Nyström, P. B. Zetterlund and M. R. Whittaker, *J. Am. Chem. Soc.*, 2011, **133**, 11128–11131.

86 F. Alsubaie, A. Anastasaki, P. Wilson and D. M. Haddleton, *Polym. Chem.*, 2015, **6**, 406–417.

87 V. Beyer, J. Kim and C. R. Becer, *Polym. Chem.*, 2020, **11**, 1271-1291.

88 V. P. Beyer, B. Cattoz, A. Strong, D. J. Phillips, A. Schwarz and C. Remzi Becer, *Polym. Chem.*, 2019, **10**, 4259–4270.

89 R. Aksakal, M. Resmini and C. R. Becer, *Polym. Chem.*, 2016, **7**, 171–175.

90 F. A. Leibfarth, K. M. Mattson, B. P. Fors, H. A. Collins and C. J. Hawker, *Angew. Chemie Int. Ed.*, 2013, **52**, 199–210.

91 M. Chen, M. Zhong and J. A. Johnson, *Chem. Rev.*, 2016, **116**, 10167–10211.

92 Y. Yagci, S. Jockusch and N. J. Turro, *Macromolecules*, 2010, **43**, 6245–6260.

93 G. Oster and N.-L. Yang, *Chem. Rev.*, 1968, **68**, 125–151.

94 B. P. Fors and C. J. Hawker, *Angew. Chemie Int. Ed.*, 2012, **51**, 8850–8853.

95 M. Tanabe, G. W. M. Vandermeulen, W. Y. Chan, P. W. Cyr, L. Vanderark, D. A. Rider and I. Manners, *Nat. Mater.*, 2006, **5**, 467–470.

96 M. Tanabe and I. Manners, *J. Am. Chem. Soc.*, 2004, **126**, 11434–11435.

97 X. Zheng, M. Yue, P. Yang, Q. Li and W. Yang, *Polym. Chem.*, 2012, **3**, 1982–1986.

98 S. Dadashi-Silab, C. Aydogan and Y. Yagci, *Polym. Chem.*, 2015, **6**, 6595–6615.

99 T. Gong, B. J. Adzima and C. N. Bowman, *Chem. Commun.*, 2013, **49**, 7950–7952.

100 N. Zaquen, W. A. A. W. Azizi, J. Yeow, R. P. Kuchel, T. Junkers, P. B. Zetterlund and C. Boyer, *Polym. Chem.*, 2019, **10**, 2406–2414.

101 J. E. Poelma, B. P. Fors, G. F. Meyers, J. W. Kramer and C. J. Hawker, *Angew. Chemie Int. Ed.*, 2013, **52**, 6844–6848.

102 S. Shanmugam and C. Boyer, *J. Am. Chem. Soc.*, 2015, **137**, 9988–9999.

103 S. Shanmugam, J. Xu and C. Boyer, *Macromolecules*, 2014, **47**, 4930–4942.

104 N. Corrigan, J. Xu, C. Boyer and X. Allonas, *ChemPhotoChem*, 2019, **3**, 1193–1199.

105 A. Anastasaki, V. Nikolaou, Q. Zhang, J. Burns, S. R. Samanta, C. Waldron, A. J. Haddleton, R. McHale, D. Fox, V. Percec, P. Wilson and D. M. Haddleton, *J. Am. Chem. Soc.*, 2014, **136**, 1141–1149.

106 A. Anastasaki, V. Nikolaou, A. Simula, J. Godfrey, M. Li, G. Nurumbetov, P. Wilson and D. M. Haddleton, *Macromolecules*, 2014, **47**, 3852–3859.

107 M. A. Tasdelen, M. Uygun and Y. Yagci, *Macromol. Chem. Phys.*, 2011, **212**, 2036–2042.

108 A. Kermagoret, B. Wenn, A. Debuigne, C. Jérôme, T. Junkers and C. Detrembleur, *Polym. Chem.*, 2015, **6**, 3847–3857.

109 X. Miao, W. Zhu, Z. Zhang, W. Zhang, X. Zhu and J. Zhu, *Polym. Chem.*, 2014, **5**, 551–557.

110 Y. Zhao, M. Yu, S. Zhang, Y. Liu and X. Fu, *Macromolecules*, 2014, **47**, 6238–6245.

111 S. Shanmugam, J. Xu and C. Boyer, *J. Am. Chem. Soc.*, 2015, **137**, 9174–9185.

112 Y. Chu, Z. Huang, K. Liang, J. Guo, C. Boyer and J. Xu, *Polym. Chem.*, 2018, **9**, 1666–1673.

113 A. Bagheri, J. Yeow, H. Arandiyan, J. Xu, C. Boyer and M. Lim, *Macromol. Rapid Commun.*, 2016, **37**, 905–910.

114 N. Corrigan, A. Almasri, W. Taillades, J. Xu and C. Boyer, *Macromolecules*, 2017, **50**, 8438–8448.

115 A. J. Gormley, J. Yeow, G. Ng, Ó. Conway, C. Boyer and R. Chapman, *Angew. Chemie Int. Ed.*, 2018, **57**, 1557–1562.

116 G. Ng, J. Yeow, J. Xu and C. Boyer, *Polym. Chem.*, 2017, **8**, 2841–2851.

117 J. Yeow, S. Shanmugam, N. Corrigan, R. P. Kuchel, J. Xu and C. Boyer, *Macromolecules*, 2016, **49**, 7277–7285.

118 T. Chen, Y. Xu, Z. Peng, A. Li and J. Liu, *Polym. Chem.*, 2016, **7**, 5880–5887.

119 J. Yeow, J. Xu and C. Boyer, *ACS Macro Lett.*, 2015, **4**, 984–990.

120 C. Bian, Y. N. Zhou, J. K. Guo and Z. H. Luo, *Polym. Chem.*, 2017, **8**, 7360–7368.

121 X. Pan, N. Malhotra, S. Dadashi-Silab and K. Matyjaszewski, *Macromol. Rapid Commun.*, 2017, **38**, 1600651.

122 S. Dadashi-Silab, G. Szczepaniak, S. Lathwal and K. Matyjaszewski, *Polym. Chem.*, 2020, **11**, 843–848.

123 G. Yilmaz and Y. Yagci, *Polym. Chem.*, 2018, 9, 1757–1762.

124 N. J. Treat, H. Sprafke, J. W. Kramer, P. G. Clark, B. E. Barton, J. Read de Alaniz, B. P. Fors and C. J. Hawker, *J. Am. Chem. Soc.*, 2014, **136**, 16096–16101.

125 P. Natarajan and G. Ferraudi, *Inorg. Chem.*, 1981, **20**, 3708–3712.

126 M. A. Tasdelen, M. Uygun and Y. Yagci, *Macromol. Rapid Commun.*, 2011, **32**, 58–62.

127 D. Konkolewicz, K. Schrö, J. Buback, S. Bernhard and K. Matyjaszewski, *ACS Macro Lett.*, 2012, 1 (**10**), 1219-1223.

128 A. Anastasaki, V. Nikolaou, G. S. Pappas, Q. Zhang, C. Wan, P. Wilson, T. P. Davis, M. R. Whittaker and D. M. Haddleton, *Chem. Sci.*, 2014, **5**, 3536–3542.

129 G. R. Jones, R. Whitfield, A. Anastasaki and D. M. Haddleton, *J. Am. Chem. Soc.*, 2016, **138**, 7346–7352.

130 E. Frick, A. Anastasaki, D. M. Haddleton and C. Barner-Kowollik, *J. Am. Chem. Soc.*, 2015, **137**, 6889–6896.

131 V. A. Bhanu and K. Kishore, *Chem. Rev.*, 1991, **91** , 99 —117

132 Y. Tatsukami, T. Takahashi and H. Yoshioka, *Die Makromol. Chemie*, 1980, **181**, 1107–1114.

133 H. Grunig, P. C. Lim, G. Luft, H. Seidl and P. C. GmbH, *J. Macromol. Sci. Part A - Chem.*, 1983, **19**, 723–738.

134 J. S. Shukla, S. K. Shukla, R. K. Tiwari and G. K. Sharma, *J. Macromol. Sci. Part A - Chem.*, 1983, **20**, 13–22.

135 H. Narain, S. M. Jagadale and N. D. Ghatge, *J. Polym. Sci. Polym. Chem. Ed.*, 1981, **19**, 1225–1238.

136 G. G. Reddy, T. Nagabhushanam, K. Venkata Rao and M. Santappa, *Polymer*, 1981, **22**, 1692–1698.

137 G. Delzenne, S. Toppet and G. Smets, *J. Polym. Sci.*, 1960, **48**, 347–355.

138 F. A. Bovey and I. M. Kolthoff, *Chem. Rev.*, 1948, **42**, 3, 491-525

139 A. A. Miller and F. R. Mayo, *J. Am. Chem. Soc.*, 1956, **78**, 1017–1023.

140 F. R. Mayo and A. A. Miller, *J. Am. Chem. Soc.*, 1956, **78**, 1023–1034.

141 C. Decker and A. D. Jenkins, *Macromolecules*, 1985, 18, 6, 1241-1244.

142 W. Xing, M. Yin, Q. Lv, Y. Hu, C. Liu and J. Zhang, in *Rotating Electrode Methods and Oxygen Reduction Electrocatalysts*, Elsevier B.V., 2014, pp. 1–31.

143 V. G. V. Schulz and G. Henrici, *Die Makromol. Chemie*, 1956, **18**, 437–454.

144 G. Henrici-Olivé and S. Olivé, *Die Makromol. Chemie*, 1957, **24**, 64–75.

145 A. Garton and M. H. George, *J. Polym. Sci. Polym. Chem. Ed.*, 1973, **11**, 2153–2167.

146 S. C. Ligon, B. Husár, H. Wutzel, R. Holman and R. Liska, *Chem. Rev.*, 2014, 114, 577–589.

147 J. Yeow, R. Chapman, A. J. Gormley and C. Boyer, *Chem. Soc. Rev.*, 2018.

148 F. M. Calitz, M. P. Tonge and R. D. Sanderson, *Macromolecules*, 2003.

149 Z. Zhang, J. Zhu, Z. Cheng and X. Zhu, *Polymer*, 2007, **48**, 4393–4400.

150 Z. Zhang, X. Zhu, J. Zhu, Z. Cheng and S. Zhu, *J. Polym. Sci. Part A Polym. Chem.*, 2006, **44**, 3343–3354.

151 C. E. Barnes, R. M. Elofson and G. D. Tones, *J. Am. Chem. Soc.*, 1950, **72**, 210–215.

152 G. Gody, R. Barbey, M. Danial and S. Perrier, *Polym. Chem.*, 2015, **6**, 1502–1511.

153 S. Cosson, M. Danial, J. R. Saint-Amans and J. J. Cooper-White, *Macromol. Rapid Commun.*, 2017, **38**, 1600780.

154 J. Vandenbergh, B. Schweitzer-Chaput, M. Klussmann and T. Junkers, *Macromolecules*, 2016, **49**, 4124–4135.

155 H. Iwata, Y. Hata, T. Matsuda and Y. Ikada, *J. Polym. Sci. Part A Polym. Chem.*, 1991, **29**, 1217–1218.

156 F. Oytun, M. U. Kahveci and Y. Yagci, *J. Polym. Sci. Part A Polym. Chem.*, 2013, **51**, 1685–1689.

157 R. Chapman, A. J. Gormley, K.-L. L. Herpoldt and M. M. Stevens, *Macromolecules*, 2014, **47**, 8541–8547.

158 R. Chapman, A. J. Gormley, M. H. Stenzel and M. M. Stevens, *Angew. Chemie - Int. Ed.*, 2016, **128**, 4576–4579.

159 J. Xu, K. Jung, A. Atme, S. Shanmugam and C. Boyer, *J. Am. Chem. Soc.*, 2014, **136**, 5508–5519.

160 J. Xu, K. Jung and C. Boyer, *Macromolecules*, 2014, **47**, 4217–4229.

161 J. Niu, Z. A. Page, N. D. Dolinski, A. Anastasaki, A. T. Hsueh, H. T. Soh and C. J. Hawker, *ACS Macro Lett.*, 2017, 6, 10, 1109-1113.

162 N. Corrigan, D. Rosli, J. W. J. Jones, J. Xu and C. Boyer, *Macromolecules*, 2016, **49**, 6779–6789.

163 I. H. Lee, E. H. Discekici, A. Anastasaki, J. R. De Alaniz and C. J. Hawker, *Polym. Chem.*, 2017, **8**, 3351–3356.

164 J. Xu, S. Shanmugam, H. T. Duong and C. Boyer, *Polym. Chem.*, 2015, **6**, 5615–5624.

165 N. Corrigan, J. Xu and C. Boyer, *Macromolecules*, 2016, **49**, 3274–3285.

166 J. Li, C. Ding, Z. Zhang, X. Pan, N. Li, J. Zhu and X. Zhu, *Macromol. Rapid Commun.*, 2017, **38**, 1600482.

167 Q. Fu, K. Xie, T. G. McKenzie and G. G. Qiao, *Polym. Chem.*, 2017, **8**, 1519–1526.

168 J. R. Lamb, K. P. Qin and J. A. Johnson, *Polym. Chem.*, 2019, **10**, 1585–1590.

169 T. Zhang, J. Yeow and C. Boyer, *Polym. Chem.*, 2019, **10**, 4643–4654.

170 J. Yeow, R. Chapman, J. Xu and C. Boyer, *Polym. Chem.*, 2017, **8**, 5012–5022.

171 S. Shanmugam, J. Xu and C. Boyer, *Macromolecules*, 2017, **50**, 1832–1846..

172 K. Matyjaszewski, S. Coca, S. G. Gaynor, M. Wei and B. E. Woodworth, *Macromolecules*, 1998, **31**, 5967–5969.

173 K. Matyjaszewski, K. L. Beers, Z. Metzner and B. Woodworth, *J. Chem. Educ.*, 2001, **78**, 547.

174 E. Liarou, A. Anastasaki, R. Whitfield, C. E. Iacono, G. Patias, N. G. Engelis, A. Marathianos, G. R. Jones and D. M. Haddleton, *Polym. Chem.*, 2019, **10**, 963–971.

175 E. Liarou, R. Whitfield, A. Anastasaki, N. G. Engelis, G. R. Jones, K. Velonia and D. M. Haddleton, *Angew. Chemie*, 2018, **57**, 8998–9002.

176 A. E. Acar, M. B. Yağci and L. J. Mathias, *Macromolecules*, 2000, **33**, 7700–7706.

177 Y. Gnanou and G. Hizal, *J. Polym. Sci. Part A Polym. Chem.*, 2004, **42**, 351–

359.

178 K. Min, W. Jakubowski and K. Matyjaszewski, *Macromol. Rapid Commun.*, 2006, **27**, 594–598.

179 H. Dong and K. Matyjaszewski, *Macromolecules*, 2008, **41**, 6868–6870.

180 L. Bai, L. Zhang, J. Pan, J. Zhu, Z. Cheng and X. Zhu, *Macromolecules*, 2013, **46**, 2060–2066.

181 L. Zhang, Z. Cheng, S. Shi, Q. Li and X. Zhu, *Polymer*, 2008, **49**, 3054–3059.

182 B. Zhu, D. Lu, J. Ge and Z. Liu, *Acta Biomater.*, 2011, **7**, 2131–2138.

183 G. Wang, M. Lu and H. Wu, *Polym. Bull.*, 2012, **69**, 417–427.

184 S. Fleischmann, B. M. Rosen and V. Percec, *J. Polym. Sci. Part A Polym. Chem.*, 2010, **48**, 1190–1196.

185 N. H. Nguyen and V. Percec, *J. Polym. Sci. Part A Polym. Chem.*, 2011, **49**, 4756–4765.

186 N. H. Nguyen, X. Leng, H.-J. Sun and V. Percec, *J. Polym. Sci. Part A Polym. Chem.*, 2013, **51**, 3110–3122.

187 T. Guo, L. Zhang, H. Jiang, Z. Zhang, J. Zhu, Z. Cheng and X. Zhu, *Polym. Chem.*, 2011, **2**, 2385–2390.

188 P. Shivapooja, L. K. Ista, H. E. Canavan and G. P. Lopez, *Biointerphases*, 2012, **7**, 1–9.

189 K. Matyjaszewski, H. Dong, W. Jakubowski, J. Pietrasik and A. Kusumo, *Langmuir*, 2007, **23**, 4528–4531.

190 D. J. Siegwart, M. Leiendecker, R. Langer and D. G. Anderson, *Macromolecules*, 2012, **45**, 1254–1261.

191 H. Chen, L. Chen, C. Wang and R. Qu, *J. Polym. Sci. Part A Polym. Chem.*, 2011, **49**, 1046–1049.

192 A. E. Enciso, L. Fu, A. J. Russell and K. Matyjaszewski, *Angew. Chemie Int. Ed.*, 2018, **57**, 933–936.

193 Y. Wang, L. Fu and K. Matyjaszewski, *ACS Macro Lett.*, 2018, **7**, 1317–1321.

194 A. E. Enciso, L. Fu, S. Lathwal, M. Olszewski, Z. Wang, S. R. Das, A. J. Russell and K. Matyjaszewski, *Angew. Chemie Int. Ed.*, 2018, **57**, 16157–16161.

195 J. Mosnáček and M. Ilčíková, *Macromolecules*, 2012, **45**, 5859–5865.

196 K. Borská, D. Moravčíková and J. Mosnáček, *Macromol. Rapid Commun.*, 2017, **38**, 1600639.

197 Q. Yang, J. Lalevée and J. Poly, *Macromolecules*, 2016, **49**, 7653–7666.

Chapter 2.

Copper mediated polymerization without external deoxygenation or oxygen scavengers

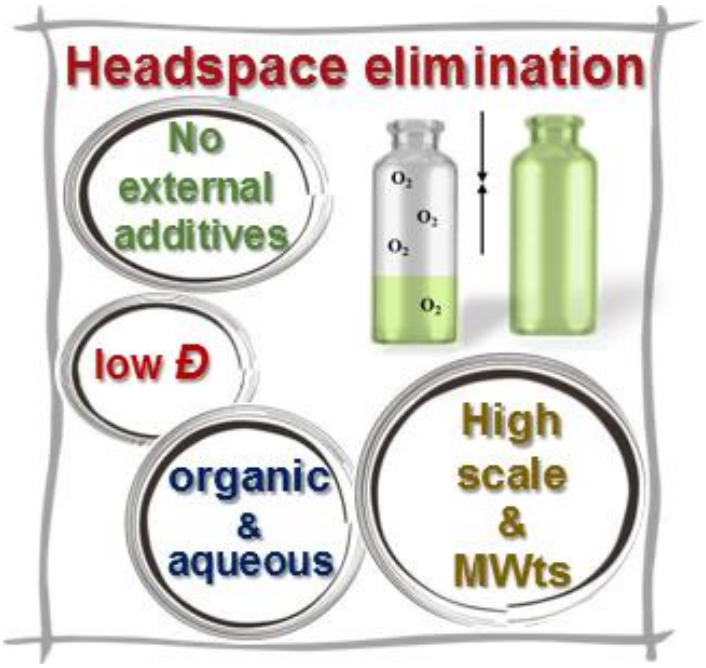

Overcoming the challenge of rigorous deoxygenation in copper mediated controlled radical polymerization processes (*e.g.* ATRP), a simple Cu(0)-RDRP system in the absence of external additives (*e.g.* reducing agents, enzymes etc.) is investigated. By simply adjusting the headspace of the reaction vessel, a wide range of monomers, namely (meth)acrylates, acrylamides and styrene was be polymerized in a controlled manner yielding polymers with low dispersity value, near-quantitative conversions and high end-group fidelity. Significantly, this approach is scalable (~ 125 g), tolerant

to elevated temperatures, compatible with both organic and aqueous media and does not rely on external stimuli which may limit the monomer pool. The robustness and versatility of this methodology was further demonstrated by the applicability to a number of other copper mediated techniques including conventional ATRP and photoinduced Cu-RDRP.

2.1 Introduction

The employment of RDRP systems has provided numerous advantages to the field of polymer science, since it has given access to polymeric materials with functionality, controlled dispersity and molecular weights, as well as designed architecture.[1–10] Among the various reversible deactivation radical polymerization (RDRP) methods, reversible-deactivation chain-transfer polymerization (RAFT),[4,11,12] single electron transfer-living radical polymerization (SET-LRP),[13,14] and atom transfer radical polymerization (ATRP)[15,16] are the most popular since their implementation provides a big range of materials which are excellent candidates for diverse applications.

Despite the numerous advantages provided by these techniques, a commonly known obstacle for their successful implementation is their sensitivity to oxygen. The integrity and precision of the generated materials is considered to be compromised by potential oxygen contamination during the polymerization which can react with carbon-centred radicals (as well as metal complexes) and irreversibly alter the reaction components (*e.g.* initiator/macroinitiator, catalyst etc.).[17–19] In this context, the polymerization is leaded to cessation, with terminated polymer chains and/or inefficient catalysts. To avoid these undesired events and eliminate oxygen from the polymerization mixture, stringent anaerobic conditions are traditionally applied, such as freeze pump thaw and inert gas sparging (nitrogen and argon most commonly).[20–22] Although these methods provide efficient oxygen removal, they are not always advantageous for a polymerization.

The majority of RDRP polymerizations involve volatile components such as the monomer and the solvent. Thus, gas sparging can lead to evaporation of these

components, eventually resulting in deviations between the theoretical and experimental yields (deviations commonly related to the molecular weights).[22,23] On the other hand, the freeze-pump-thaw approach can be incompatible with biomolecules such as enzymes and proteins, leading to their aggregation/denaturation.[24,25] Thus, the stringent anaerobic conditions required for most RDRP methods, apart from being costly and time-consuming, also limit their potential applications.

On account of this, considerable interest has been directed towards oxygen tolerant polymerization methods aiming to simplify the polymerization protocol and eliminate the above-mentioned deoxygenation techniques (**Scheme 2-1**).[26,27] In 1998, Matyjaszewski and colleagues reported on the ATRP of MMA and styrene in the presence of oxygen.[28] By adding excess of the catalyst complex Cu(I)Br/dNbpy and Cu(0) powder as reducing agent for the accumulated Cu(II), control over the polymerization was achieved, whilst slow polymerization rates were evident. Percec and co-workers reported on the SET-LRP of acrylates in the presence of oxygen. In their system, Cu(0) could reduce oxygen, leading to the generation of Cu_2O. For this reason, hydrazine hydrate was added as a reducing agent for Cu_2O into Cu(0).[29] In earlier reports, Chapman *et al*. employed the enzyme glucose oxidase (GOx) to effectively deoxygenate traditional RAFT polymerizations.[30,31] Boyer and co-workers exploited photoinduced electron transfer (PET)-RAFT to produce polymeric materials in open reaction vessels by either increasing the concentration of the photo-catalyst or employing a reducing agent (*e.g.* ascorbic acid).[32–35] Matyjaszewski's group also employed GOx in order to continuously convert oxygen to carbon dioxide, along with the addition of sacrificial substrates, for ICAR-ATRP in air.[36,37]

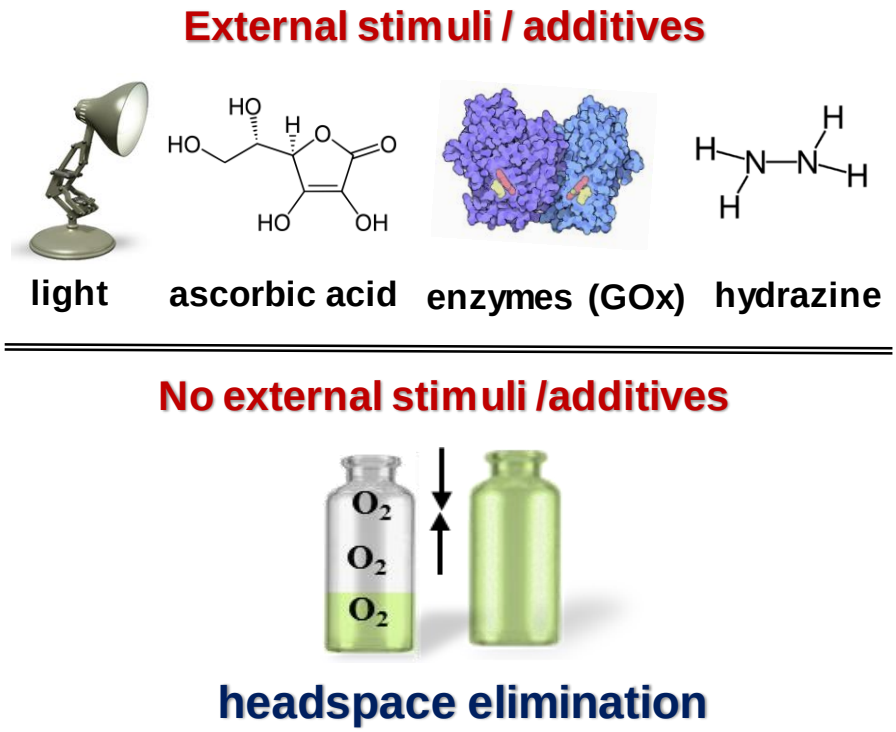

Scheme 2-1. Oxygen tolerant approaches for RDRPs

Despite these great developments, the vast majority of the current approaches rely on either light activation or the use of extrinsic oxygen scavengers such as reducing agents (*i.e.* ascorbic acid, hydrazine, phenols) and enzymes which although efficient, require the addition of sacrificial reagents for their successful application. The utilization of light as an external stimulus may limit the monomer pool as strongly absorbing monomers, including chromophores, would be incompatible with these techniques. Apart from that, the oxygen tolerant photo-mediated methods can be incompatible with specific enzymes and proteins as the secondary structure can be disrupted through irradiation.[38,39] Additionally, external reducing agents and enzymes can be costly, interfere with the monomer structure, be temperature dependent or alter the pH of the polymerization mixture,[40] thus significantly increasing the complexity of a given system.[41] Further limitations of the reported methods include the risk of

generating additional chains through side products,[36] as well as the incompatibility with a wide range of monomers, temperatures and solvents.

In this chapter, an alternative system to the existing oxygen tolerant approaches, less complex and independent of extrinsic reducing agents, is investigated and discussed. The Cu(0) wire-mediated RDRP of various acrylates and styrene was conducted in controlled manner by simply eliminating the headspace in the polymerization reaction. With this approach, control over the polymerization was achieved, with low dispersity values ($Đ$ < 1.2*)* and good agreement between experimental and theoretical M_n values being observed at quantitative conversions. Furthermore, high end-group fidelity was maintained, allowing for *in-situ* chain extensions and block-copolymerizations in the presence of oxygen. This approach was also scalable (~ 125 g), tolerant to elevated temperatures and compatible with both organic and aqueous media. Apart from Cu(0)-wire mediated RDRP, this methodology was compatible with conventional ATRP.

2.2 Results and Discussion

Initially, an 8 mL volume Cu(0)-wire catalyzed polymerization reaction was conducted in a 28 ml unsealed vial, with methyl acrylate (targeting DP_n = 50) as the monomer, ethyl α-bromoisobutyrate (EBiB) as the initiator, tris-(2-(dimethylamino)ethyl)amine (Me_6Tren) as the ligand and dimethyl sulfoxide (DMSO) as the solvent, in the *absence* of any commonly employed deoxygenation procedures (*i.e.* nitrogen sparging or freeze-pump-thaw). Although the reaction was left to proceed for >48 hours, no polymerization was evidenced, an observation which was attributed to the constant diffusion of oxygen in the polymerization reaction. Upon sealing the vial with a septum (or a screw lid, **Figure 2-1a**, **Table 2-1**) the polymerization reached near-quantitative conversion within 11 h, achieving dispersities as low as 1.10. Although a narrow molecular weight distribution was observed, the experimental molecular weight (6600 g mol^{-1}) deviated significantly from the theoretical value (4500 g mol^{-1}), an observation indicative of low initiator efficiency (***f***), which was subsequently verified through ^{1}H NMR (**Table 2-1, Figure 2-11**). In order to further clarify this, an identical experiment was conducted where freeze-pump-thaw cycles were used to thoroughly deoxygenate the reaction mixture prior to polymerization (**Figure 2-1d, Table 2-1**), leading to much lower molecular weights (5300 g mol^{-1}). This observation suggests that part of the initiator is consumed during the early stages of the non-deoxygenated polymerization, leading to higher than expected molecular weights. Based on these results, it was hypothesized that under these conditions, the initiator is somehow acting as an oxygen scavenger prior to the polymerization.

Since the presence of oxygen, both dissolved and in the gaseous was significant, it was speculated that reduction of the headspace within the vial would

lead to lower concentration of oxygen, thus contributing to improved initiator efficiencies. Indeed, by maintaining the reaction volume constant at 8 ml and altering the size of the vial from 28 ml (20 ml of headspace) to 20 ml (12 ml of headspace) and 8 ml (zero headspace), the initiator efficiency was significantly improved (**Table 2-1, Figures 2-11&12**), yielding polymers with 6200 g mol^{-1} and 5200 g mol^{-1} respectively (**Figure 2-1**).

Table 2-1: ^{1}H NMR and SEC analyses for PMA (targeted DP_n = 50) with different headspace volumes.[a]

Vessel	**Headspace (mL)**	**Time (h)**	**Conv. (%)**	**$M_{n,\,th.}$ (g/mol)**	**$M_{n,\,SEC}$[b] (g/mol)**	***Đ***	***f*** [d] **(%)**
Schlenk tube [c]	-	4	98	4400	5300	1.08	>99
8 mL vial	0	4	96	4300	5200	1.07	>99
20mL vial	12	6	96	4300	6200	1.07	84
28 mL vial	20	11	96	4300	6600	1.10	78

[a][MA]:[EBiB]:[Cu(II)Br2]:[Me6Tren] = 50:1:0.05:0.18 in DMSO (50%, *v/v*) solvent. [b] Determined by THF-SEC analysis based on DRI [c] 3x Freeze-Pump-Thaw cycles applied. [d] f : initiator efficiency based on ^{1}H NMR.

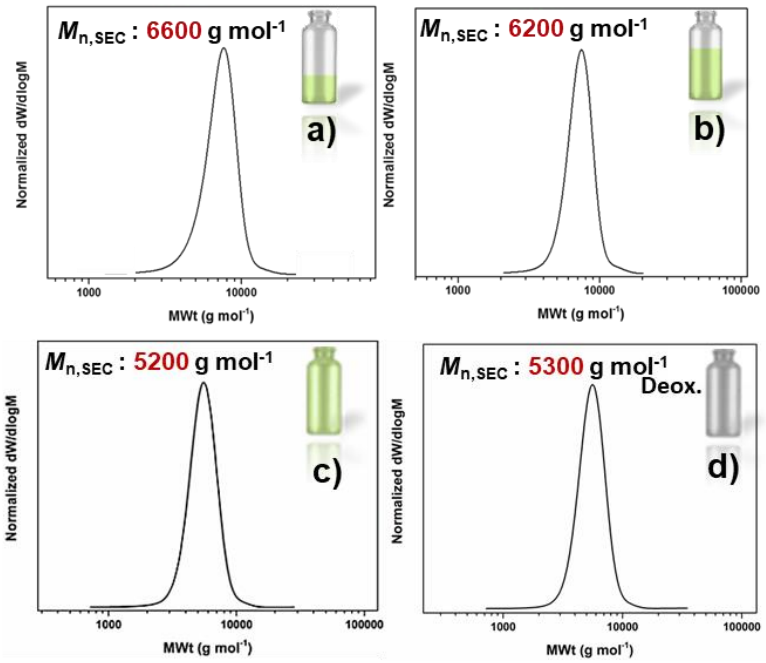

Figure 2-1. SEC traces for PMA with targeted DP_n = 50 in different vial sizes (**a-c**) and **d**) upon freeze-pump-thaw deoxygenation with [MA]:[EBiB]:[$CuBr_2$]:[Me_6Tren] = [50]:[1]:[0.05]:[0.18] and DMSO as solvent (50% v/v).

Thus, in the absence of any deoxygenation procedures and by simply eliminating the headspace within the vessel, similar initiator efficiencies, rates of reaction and control over the polymerization in comparison to the externally degassed system were achieved (**Table 2-1**, **Figure 2-1**, **Figure 2-10**). Kinetic experiments showed that the reaction without headspace followed fast polymerization rates in comparison to the other two cases where headspace was present, yielding 95 % monomer conversion after 2.5 h (**Table 2-2, Figure 2-2**). Noteworthy is that for the polymerizations in the presence of headspace which exhibited lower polymerization rates, accumulation of the deactivator Cu(II) is visually evident, as suggested by the characteristic deep green colour (**Figure 2-20**). The synthetic facility of this approach was further demonstrated by performing the polymerization in a multi-gram scale (~ 125 g) with well-defined poly(MA) obtained ($Đ$ ~ 1.10) at high yields (>90% conversion) (**Figure 2-12**).

Table 2-2. ^{1}H NMR and SEC analysis for the kinetics of PMA with targeted DP_n = 50 synthesized via Cu(0)-mediated RDRP (in the absence of any external deoxygenation).[a]

Time (hrs)	Conversion (%)	$M_{n,\ th.}$ (g/mol)	$M_{n,\ SEC}$[b] (g/mol)	$Đ$
0.5	47	2100	2500	1.09
1	86	3900	4700	1.07
1.5	91	4100	5100	1.07
2	93	4200	5100	1.08
2.5	95	4300	5300	1.08
3	96	4300	5300	1.08
3.5	96	4300	5300	1.08
4	97	4400	5500	1.08

[a][MA]:[EBiB]:[Cu(II)Br_2]:[Me_6Tren] = 50:1:0.05:0.18 in DMSO (50%, *v/v*) solvent. [b] Determined by THF-SEC analysis based on DRI.

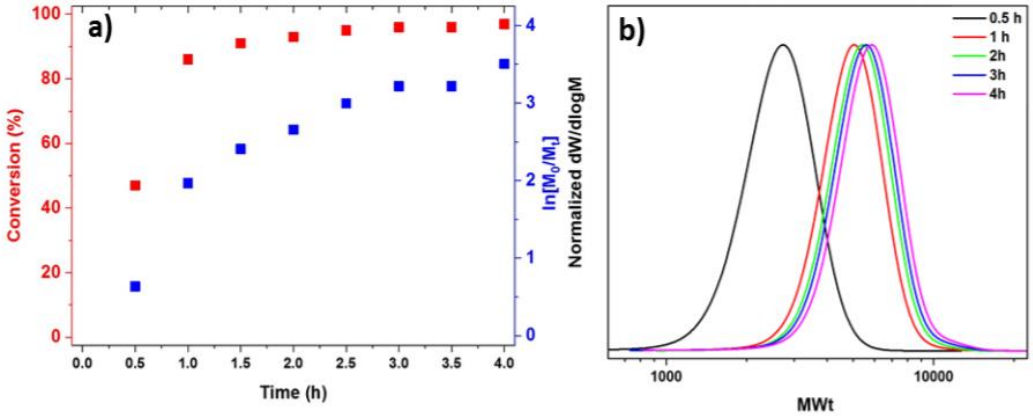

Figure 2-2. Deoxygenation-free polymerization kinetics for PMA with targeted DP_n = 50 in the absence of headspace with **a**) conversion and $\ln[M_0/M_t]$ versus time and **b**) SEC traces illustrated.

To explore the utility of this system across a wide range of molar masses, the ability of targeting higher degrees of polymerization was investigated. Under

otherwise identical conditions, targeting DP_n = 100-1000 resulted in high conversions (89-97%), low $Đ$ (1.06 - 1.13) and good agreement between theoretical and experimental molecular weights (**Table 2-3, Figure 2-3**). It should be noted that overall, for higher targeted molecular weights, longer reaction times were required, as expected.[42] Although the Cu(0)-RDRP of PMA with targeted DP_n = 50 reached near-quantitative conversion after ~ 2.5 h, the synthesis of PMA with targeted DP_n = 1000 lasted for ~ 20 h. This can be attributed to the lower initiator efficiency, especially in the presence of oxygen, where the initiator participates in oxygen consumption, thus less initiator is available for the polymerization. The role of the initiator in oxygen consumption will be described later in this chapter, in the oxygen consumption mechanism section.

Table 2-3. ^{1}H NMR and SEC analysis for the Cu(0)-mediated RDRP kinetics of MA with DP_n = 50 (in the absence of external deoxygenation, without headspace).[a]

DP_n	Conversion (%) ^{1}H NMR	$M_{n,\ th.}$ (g/mol)	$M_{n,\ SEC}$[b] (g/mol)	$Đ$
100	97	8500	11700	1.09
200	95	16500	20000	1.16
400	91	31500	35000	1.09
600	90	46700	48200	1.11
1000	89	79400	87000	1.13

[a] [MA]:[EBiB]:[Cu(II)Br_2]:[Me_6Tren] = 50:1:0.05:0.18 in DMSO (50%, *v/v*) solvent. [b] Determined by THF-SEC analysis based on DRI.

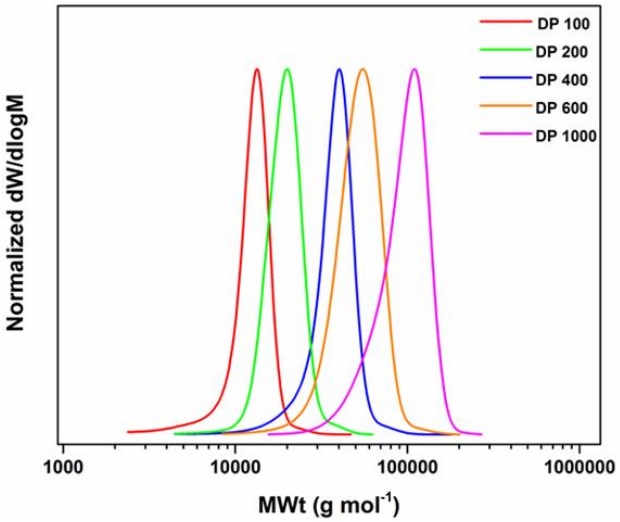

Figure 2-3. THF-SEC traces for PMA with DPs 100-1000 synthesized via Cu(0)-RDRP in the absence of deoxygenation.

Apart from DMSO which is a commonly used solvent for Cu-RDRP, under these optimized conditions (headspace elimination) the polymerization was screened in a selection of organic solvents including acetonitrile, toluene, methanol, isopropanol and trifluoroethanol. In all cases, well-defined polymers with low dispersity values and high yields were obtained (**Figure 2-13**, **Table 2-4**), expanding the scope of this approach to polymerizations that require different media other that DMSO. This approach is effective in both homogeneous (*e.g.* hexyl acrylate in TFE, **Figure 2-4b**) and heterogeneous/biphasic systems (*e.g.* *n*-butyl acrylate in DMSO,[43] **Figure 2-4a**) with the same level of control, highlighting the robustness of this system. Finally, when water was employed as the solvent for the non-deoxygenated Cu(0)-RDRP of the hydrophilic $PEGA_{480}$ with targeted DP_n = 10 (**Figure 2-14**, **Table 2-4**), well-defined $poly(PEGA)_{10}$ was obtained with low final dispersity ($Đ$ ~ 1.2), thus expanding the applicability of the methodology to both organic and aqueous media, as well as hydrophobic and hydrophilic monomer families. The compatibility of this approach was verified to a greater extent when additional monomer families apart from acrylates

were investigated. Using previously established polymerization protocols,[42,44] methacrylates (*i.e.* PMMA, **Table 2-4**, **Figure 2-4c & 2-15, Scheme 2-2**) and styrene (**Table 2-4**, **Figure 2-4d & 2-16, Scheme 2-3**) were successfully polymerized yielding well-controlled polymers with narrow molecular weight distributions in the *absence* of any standard deoxygenation. It should be noted that for the polymerization of MMA and styrene, methyl-α-bromophenylacetate (MBPA) was used as initiator, and PMDETA was used as ligand for PSt, based on previous literature.[44]

Table 2-4. ^{1}H NMR and SEC analysis for the Cu(0)-mediated RDRP kinetics of MA with DP_n = 50 (in the absence of external deoxygenation, without headspace).[a]

Polymer	Conv. (%)	$M_{n,\ th.}$ (g/mol)	$M_{n,\ SEC}$[b] (g/mol)	$Đ$	Solvent	Initiator
PMA_{50}	>99	4500	5600	1.11	MeCN	EBiB
PMA_{50}	95	4300	4900	1.09	IPA	EBiB
PMA_{50}	98	4400	4900	1.10	Tol-MeOH	EBiB
PMA_{50}	>99	4500	5200	1.07	TFE	EBiB
$P(n\text{-}BA)_{50}$	99	6500	8800	1.16	DMSO	EBiB
$P(HA)_{50}$	99	8000	9000	1.07	TFE	EBiB
$P(PEGA_{480})_{10}$	82	4100	3700	1.18	H_2O	EBiB
$PMMA_{50}$[c]	77	4100	7800	1.15	DMSO	MBPA
PSt_{50}[d]	91	5000	5400	1.20	IPA	MBPA

[a] [Monomer]:[Initiator]:[Cu(II)Br_2]:[Me_6Tren] = 50:1:0.05:0.18 in 50%, *v/v* solvent. [b] Determined by THF-SEC analysis based on DRI. [c] Polymerization conducted at ambient temperature with Me_6Tren as ligand [d] Polymerization conducted at 60 °C with PMDETA as ligand.

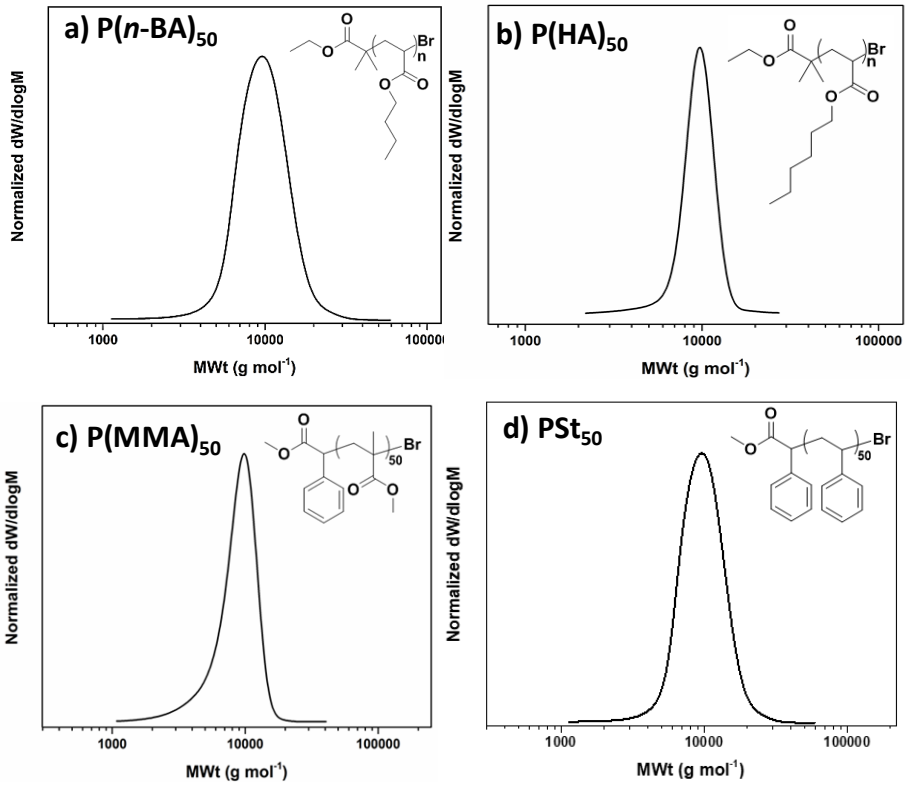

Figure 2-4. THF-SEC derived molecular weight distributions for **a**) P(n-BA)$_{50}$, **b**) P(HA)$_{50}$, c) PMMA$_{50}$ (at ambient temperature) and **d**) PSt$_{50}$ synthesized via Cu(0)-RDRP (at 60 ^{o}C) in the absence of deoxygenation.

A fundamental requirement of a controlled polymerization is the retention of active chain-ends, since it allows for production of diverse materials with combined properties.[45,46] The chain-end fidelity for PMA was determined by analysis of a low molecular weight sample (DP_n = 25). Matrix assisted laser desorption-ionization time-of-flight mass spectrometry (MALDI-ToF-MS) revealed a single peak distribution corresponding to *m/z* values for polymer chains comprising of the expected chain-ends, initiated with EBiB and capped by bromine (**Figure 2-5**). Furthermore, it was shown that the obtained DP_n (= 27) slightly deviated from the targeted (DP_n = 25).

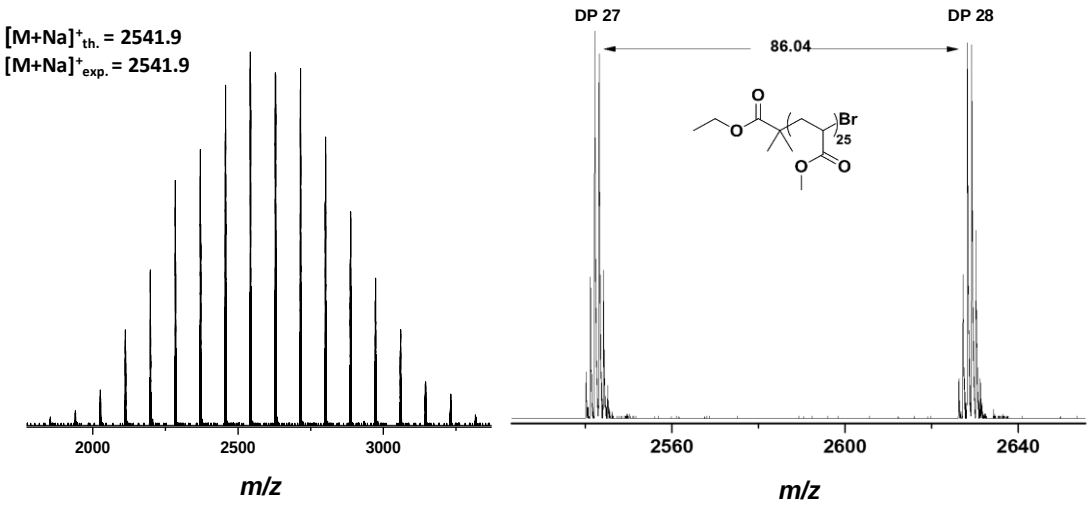

Figure 2-5. MALDI-ToF-MS spectra of PMA with targeted DP_n = 25 and actual DP_n = 27, synthesized via Cu(0)-RDRP in the absence of deoxygenation. The single peak distribution indicates that the majority of the polymer chains are Br-capped.

Characterization by ^{1}H-NMR also confirmed the bromine ω-functionality to be close to 100% when comparing signals corresponding to the ω-terminal methine signal with the CH_3 groups of the isobutyrate group of EBiB. The synthetic utility of these chain ends was then explored by *in-situ* re-initiation of the macroinitiator with a second aliquot of MA (**Figure 2-6a**), as well as with the synthesis of the PMA_{50}-*b*-PHA_{50} diblock copolymer (**Figure 2-6b)**. Although a clear shift to higher molecular weights was observed, a small low molecular weight shoulder was evident by SEC in both cases, indicating some termination events (**Figure 2-6a&b, Table 2-5**). This was attributed to the introduction of additional dissolved oxygen with the second monomer aliquot which was then responsible for the termination of propagating radicals. To verify this, the synthesis of the first poly(MA) block was repeated as previously, in the absence of any freeze pump-thaw or nitrogen sparging. Upon reaching near-quantitative conversion (> 97%), a second aliquot of deoxygenated MA was then added (**Figure 2-17, Table 2-5**). In this case, very good control was observed with the molecular weight distribution completely shifting to higher molecular weights and a

final dispersity as low as 1.06. This data suggests that the end group fidelity of the initial block was indeed close to 100% prior to the addition of the second monomer and that it is the dissolved oxygen that is responsible for the observed small amount of termination.

Table 2- 5. ^{1}H NMR and SEC analysis for the in-situ chain extensions synthesized *via* Cu(0)-RDRP in the absence of deoxygenation.[a]

Polymer	Deoxygenation process	Conversion ^{1}H NMR %	$M_{n,SEC}$ [b] (g mol^{-1})	$Đ$
PMA_{50} [c]	None	97	6200	1.05
PMA_{50}-PMA_{50} [d]		76	12900	1.06
PMA_{50} [c]	2nd monomer aliquot deoxygenated	97	6300	1.06
PMA_{50}-PMA_{50} [d]		95	12600	1.08
PMA_{50} [c]	None	99	6500	1.08
PMA_{50}-PHA_{50} [d]		76	14800	1.10

[a] [MA]:[EBiB]:[Cu(II)Br$_2$]:[Me$_6$Tren] = 50:1:0.05:0.18 in DMSO (50%, *v/v*) solvent for the 1st block. For the 2nd block / chain extension 50 eq. of the second monomer were added with respect to macroinitiator.

[b] Determined by THF-SEC analysis based on DRI. [c] Initial polymer / macroinitiator. [d] Final polymer after chain extension.

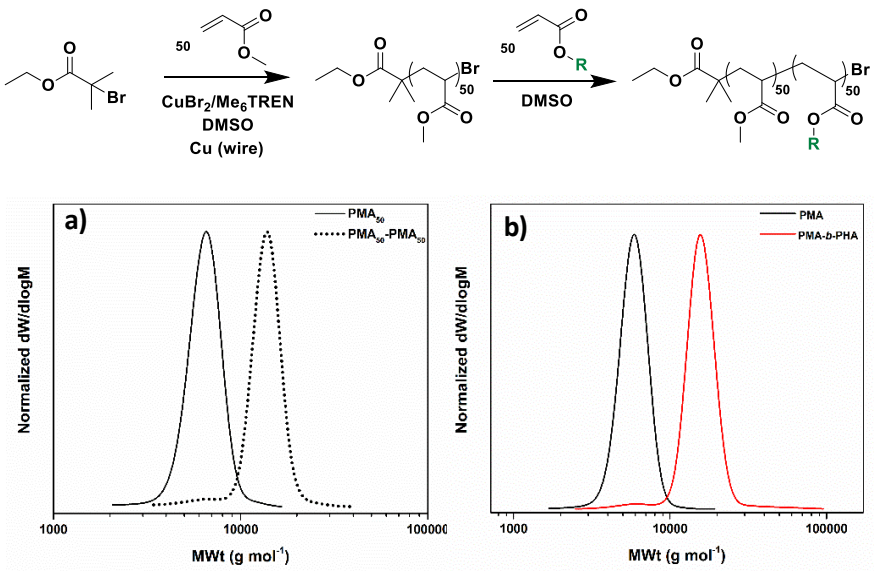

Figure 2-6. Reaction scheme (top) and SEC traces (bottom) for **a**) the *in-situ* chain extension of PMA_{50} with MA (50 eq.) and **b**) the block copolymer PMA_{50}-b-PHA_{50}.

Since the concentration of oxygen significantly affects the fate of the polymerization and the macromolecular characteristics of the obtained polymers, a fibre-optic oxygen probe was employed for the online monitoring of the dissolved O_2 concentration present in the polymerization solution over time (**Figure 2-7**). The online O_2 monitoring measurements showed that in the presence of bigger headspaces (*i.e*. 20 and 12 ml), the oxygen consumption was slow, requiring one hour to reach ~ 2 mg/ L and ~ 0.8 mg/ L, respectively (typical initial dissolved oxygen concentration is ~ 7 mg/L). On the contrary, upon eliminating the headspace, the oxygen was rapidly consumed within 5 min (~ 0 mg/L) explaining the shorter reaction times observed for this system (~ 2 h for the polymerization to reach completion) in comparison to the increased headspace (6-11 h to reach completion) (**Figure 2-8**).

Figure 2-7. Setup of the *in-situ* monitoring of the dissolved O_2 concentration in a typical, not externally deoxygenated, Cu(0)-mediated RDRP.

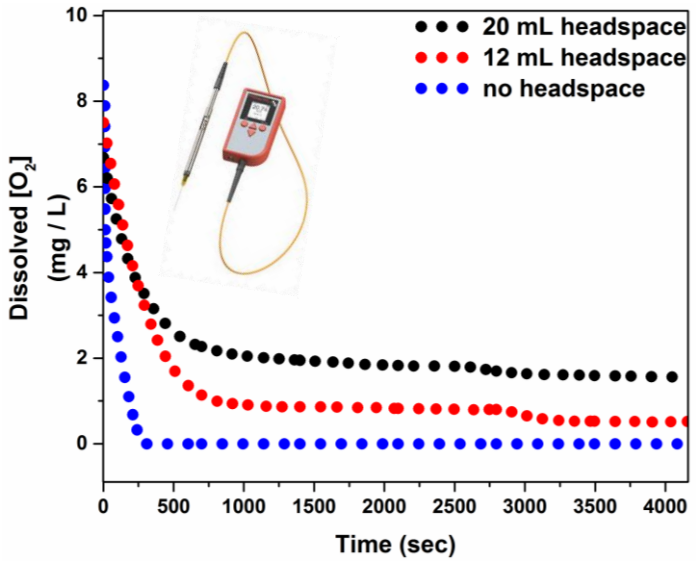

Figure 2-8. Line graphs illustrating the dissolved O_2 concentration over time for the reactions with a) 20 mL headspace (**black**), **b**) 12 mL headspace (**red**) and **c**) no headspace (**blue**).

These findings come in agreement with the polymerization results in the three different vessels, indicating that the prolonged reaction times observed for the cases where headspace was present, can be attributed to the high concentration of oxygen. As has already been reported, the presence of oxygen leads to induction periods which

are related to the time needed for oxygen consumption. When all the amount of oxygen reacts with either carbon-centred radical (mainly initiating radicals) or the metal catalyst species, then initiation of the polymerization starts.[28,47] Although the graphs in **Figure 2-8** illustrate the evolution of dissolved [O_2] in the polymerization solution over time, the role of the individual components on the oxygen consumption mechanism is not provided. In order to provide insights on which component is responsible for the oxygen consumption, each component of the polymerization was measured individually.

Initially, the solvent (DMSO) and the monomer, as well as a solution with both, were measured showing no oxygen consumption even after 1 h. Lack of oxygen consumption within 1 h was also evident for the solutions which included DMSO, MA and either only initiator or Cu(0)-wire (**Figure 2-18**). Subsequently, a standard solution of MA, DMSO, Cu(II)Br_2 and Me_6Tren was prepared. In the absence of Cu(0)-wire and initiator very little, if any, oxygen consumption was observed within 1 h, suggesting that the ligand had very limited reactivity with oxygen. It should be noted that the presence of free ligand is considered to play important role on the oxygen consumption in photoinduced polymerizations (*i.e.* photoinduced Cu-RDRP, photoATRP), where ligand-derived radical cations are generated.[27,48–50]

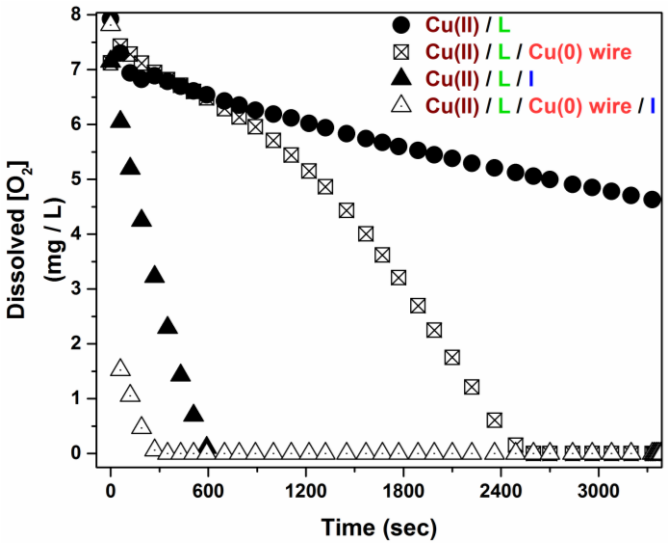

Figure 2-9. Line graphs illustrating the effects of Cu(0)-wire, EBiB (I), and Me_6Tren (L) on the evolution of the dissolved O_2 concentration during polymerization.

In the absence of initiator (when only Cu(0)-wire was present) a complete oxygen consumption took place in 42 min, highlighting the capability of Cu(0)-wire to act as a reducing agent (**Figure 2-9**). In this context, since the Cu(0)-wire alone in a MA/DMSO solution showed no oxygen consumption, it is hypothesized that its presence facilitates the reduction of Cu(II) into lower oxidation state species which are capable of oxidation, hence leading to oxygen consumption. Furthermore, these experiments suggest that the initiator is also responsible for the oxygen consumption, since upon addition of EBiB (in the absence of Cu(0)-wire), fast rates of oxygen consumption were observed (**Figure 2-9**). However, it should be noted that when the initiator was examined in the absence of copper species and ligand (only with M and DMSO), no oxygen consumption took place (**Figure 2-18**). This is further supported by the lower initiator efficiency observed in the presence of bigger headspaces, the longer reaction times when targeting polymers of higher molecular weights (lower concentration of initiator would lead to slower oxygen consumption) and by the

incapability of the system to afford "perfect" *in-situ* block copolymers. As such, the initiator can only participate in oxygen consumption when the complex is present, and this observation might be correlated with ability of the initiator to react with the Cu-complex, participating in the coordination sphere of the latter, and thus also leading to the formation of primary radicals which can react with oxygen.[48] Nevertheless, when both Cu(0)-wire and initiator were present, the oxygen was consumed within 5 min (twice as fast as when only initiator was present). It is concluded that fast oxygen consumption occurs when all the components of the polymerization are present (**Figure 2-9**) and thus, synergistically contribute to the oxygen-tolerant behavior of this methodology. Subsequently, the compatibility of this methodology with other copper mediated protocols was investigated. For this reason, the conventional (or normal) ATRP (when only CuBr is employed) of MMA with targeted DP_n = 100 was conducted in toluene as the solvent and at 90 ^{o}C,[51] by eliminating the headspace and in the absence of any external deoxygenation methods. As a result, PMMA with low dispersity and high yields was obtained (**Figure 2-19)**.

As a result, the proposed methodology which is based on the elimination of headspace in order to avoid conventional deoxygenation approaches, is compatible with both Cu(0)-RDRP conducted at ambient temperature (~ 25 ^{o}C) and above (60 ^{o}C for the polymerization of styrene), as well as conventional (Cu(I)-mediated) ATRP where temperature of 90 ^{o}C is applied.

2.3 Conclusion

In this chapter, a simple and versatile oxygen tolerant Cu(0)-RDRP methodology without the addition of extrinsic oxygen scavengers or reducing agents, is presented and discussed. In the absence of conventional deoxygenation techniques, including freeze-pump-thaw and gas sparging, the key-step for the successful implementation of Cu(0)-RDRP is the elimination of the vessel's headspace. Upon optimization of the reaction scale in order to avoid the presence of gaseous oxygen, well-defined poly(acrylates) in a range of molar masses were obtained. The robustness of the proposed methodology was verified with the controlled polymerization of a range of monomer families, including hydrophobic and hydrophilic acrylates, biphasic systems (P-*n*BA in DMSO), methacrylates and styrene. The versatility of this approach was further expanded to various temperatures (*i.e.* from ambient up to 90 ^{o}C) and solvents, including both organic and aqueous media. The high end-group fidelity maintained, provided access to *in-situ* chain extensions and block copolymers, without applying any type of extrinsic deoxygenation. The profile of oxygen consumption in the polymerization was examined through an oxygen probe, and the role of the polymerization components was individually examined and discussed. Conclusively, the user-friendly and in parallel versatile nature of this approach expands the current scope of oxygen tolerant polymerization strategies.

2.4 Experimental section

2.4.1 Materials

All materials were purchased from Sigma-Aldrich or Fischer Scientific and used as received unless otherwise stated. Copper(I) bromide (CuBr, 98%, Sigma-Aldrich) was washed with acetic acid and ethanol and dried under vacuum prior to use. Metallic copper (Cu^0) in the form of wire (gauge 0.25 mm) was purchased from Comax Engineered wires and purified by immersion in concentrated 37 % HCl for 15 minutes, subsequently rinsed with distilled water and acetone, and dried with compressed air prior to use. Tris-(2-(dimethylamino)ethyl)amine (Me_6Tren) was synthesized according to the literature and stored in the fridge.[52] *N,N,N′,N″,N″*-pentamethyldiethylenetriamine (PMDETA) was distilled prior to use. *N*-(*n*-Propyl)-2-pyridylmethanimine was synthesized according to literature procedure and stored under a nitrogen atmosphere prior to use.[51]

2.4.2 Instrumentation and Characterization techniques

Proton Nuclear Magnetic Resonance (^{1}H NMR)

^{1}H NMR spectra were recorded on Bruker DPX-300 or DPX-400 spectrometers in deuterated chloroform ($CDCl_3$) or deuterium oxide (D_2O) obtained from Sigma-Aldrich. Chemical shifts are given in ppm downfield from the internal standard tetramethylsilane. Monomer conversions were determined *via* ^{1}H NMR spectroscopy by comparing the integrals of monomeric vinyl protons to polymer signals.

Size Exclusion Chromatography (SEC)

THF. SEC measurements were carried out with an Agilent 390-LC MDS instrument equipped with differential refractive index (DRI), viscometry (VS), dual

angle light scatter (LS) and dual wavelength UV detectors. The system was equipped with 2 x PLgel Mixed C columns (300 x 7.5 mm) and a PLgel 5 µm guard column. The eluent was THF with 2 % TEA (triethylamine) and 0.01 % BHT (butylated hydroxytoluene) additives. Samples were run at 1 mL / min at 30 ºC. Poly(methyl methacrylate) and polystyrene standards (Agilent EasyVials) were used to create a third order calibration between 550 $gmol^{-1}$ and 1,568,000 $gmol^{-1}$. Analyte samples were filtered through a GVHP membrane with 0.22 μm pore size before injection. Respectively, experimental molar mass ($M_{n,SEC}$) and dispersity ($Đ$) values of synthesized polymers were determined by conventional calibration using Agilent GPC/SEC software (version A.02.01).

Matrix assisted laser desorption-ionization time-of-flight mass spectrometry (MALDI-ToF-MS).

MALDI-ToF-MS measurements were conducted using a Bruker Daltonics Ultraflex II MALDI-ToF mass spectrometer, equipped with a nitrogen laser delivering 2 ns laser pulses at 337 nm with positive ion ToF detection performed using an accelerating voltage of 25 kV. Solutions in tetrahydrofuran (THF) (50 µL) of *trans*-2-[3-(4-*tert*-butylphenyl)-2-methyl-2-propyldene] malononitrile (DCTB) as a matrix (saturated solution), sodium iodide as the cationization agent (1.0 mg mL^{-1}) and sample (1.0 mg mL^{-1}) were mixed, and 0.7 µL of the mixture was applied to the target plate. Spectra were recorded in reflectron mode calibrated with Poly(ethylene glycol) monomethyl ether (PEG-Me) 1900 kDa.

Oxygen Probe. Pocket Oxygen Meter - FireStingGO2 (Pyro Science)**:** The solvent-resistant oxygen probe OXSOLV measures oxygen partial pressure in most polar and nonpolar solvents. It is based on optical detection principles (REDFLASH

technology) and can be used both in pure and complex organic solvents. The fibre-optic oxygen sensor tip is covered with a stainless-steel tube 1.5 mm in diameter and 150 (or 40) mm in length. The analysis of the data was conducted with the FireStingGO2 Manager software.

2.4.3 Experimental procedures

Cu(0)-wire mediated RDRP of acrylates

General procedure for the Cu(0)-mediated RDRP of methyl acrylate (MA) with targeted DP_n = 50 (PMA_{50}) in the absence of any external deoxygenation.

MA (4 mL, 50 eq.), Me_6Tren (42.5 μL, 0.18 eq.), EBiB (129 μL, 1 eq.), $Cu(II)Br_2$ (9.86 mg, 0.05 eq.), DMSO (4 mL) and pre-activated copper wire (5 cm) wrapped around a stirring bar were added to septum sealed vials of 8 mL (no headspace left), 20 mL (12 mL headspace) and 28 mL (20 mL headspace). The polymerization was allowed to commence at ambient temperature. Kinetic studies were conducted to determine the time needed for near quantitative conversion to be reached. Once this conversion had been achieved, a sample was taken and passed through a short column of neutral alumina to remove dissolved copper salts prior to analysis by ^1H NMR in $CDCl_3$ and SEC in THF.

General procedure for the Cu(0)-mediated RDRP of *n*-butyl acrylate (BA) with targeted DP_n = 50 (PBA_{50}) in the absence of any external deoxygenation.

BA (4 mL, 50 eq.), Me_6Tren (26.8 μL, 0.18 eq.), EBiB (81.9 μL, 1 eq.), $Cu(II)Br_2$ (6.25 mg, 0.05 eq.), DMSO (4 mL) and pre-activated copper wire (5 cm) wrapped around a stirring bar were added to a septum sealed vial. The polymerization was

allowed to commence at RT. Kinetic studies were conducted to determine the time needed for quantitative conversion (typically >96%) and after the completion of the polymerization, a sample was taken and passed through a short column of neutral alumina to remove dissolved copper salts prior to analysis by ^{1}H NMR in $CDCl_3$ and SEC in THF.

General procedure for the Cu(0)-mediated RDRP of $PEGA_{480}$ with targeted DP_n = 10 in the absence of any external deoxygenation.

HPLC grade H_2O (4 mL), Me_6Tren (212 μL, 0.792 mmol, 0.18 eq.) and $Cu(II)Br_2$ (49 mg, 0.22 mmol, 0.05 eq.) were charged to a 8 mL vial and vortexed until complete dissolution of $Cu(II)Br_2$. EBiB (645 μL, 4.4 mmol, 1 eq.), poly(ethylene glycol) methyl ether acrylate (average M_n 480) ($PEGA_{480}$) (4 mL, 44 mmol, 10 eq.) and pre-activated copper wire (5 cm) wrapped around a stirring bar were added to the vial. The vial sealed with a septum and the polymerization left to commence. Samples were taken periodically and conversions were measured using ^{1}H NMR in D_2O and SEC analysis in THF, after having been passed through neutral alumina.

General procedure for the Cu(0)-mediated RDRP of hexyl acrylate (HA) with DP_n = 50 (PHA_{50}) in the absence of any external deoxygenation.

HA (4 mL, 50 eq.), Me_6Tren (22 μL, 0.18 eq.), EBiB (67 μL, 1 eq.), $Cu(II)Br_2$ (5.10 mg, 0.05 eq.), TFE (4 mL) and pre-activated copper wire (5 cm) wrapped around a stirring bar were added to an 8 mL septum sealed vial. The polymerization was allowed to commence at RT. Kinetic studies were conducted to determine the time needed for quantitative conversion (tyrically >96%) and after the completion of the polymerization, a sample was taken and passed through a short column of neutral alumina to remove dissolved copper salts prior to analysis by ^{1}H NMR in $CDCl_3$ and SEC in THF.

Cu(0)-wire mediated RDRP of methacrylates and styrene

General procedure for the Cu(0)-mediated RDRP of methyl methacrylate (MMA) with DP_n = 50 ($PMMA_{50}$) in the absence of external deoxygenation.

MMA (4 mL, 50 eq.), methyl-*α*-bromophenylacetate (MBPA) (119 μL, 1 eq.), Cu(II)Br_2 (8.35 mg, 0.05 eq.), DMSO (4 mL), Me_6Tren 36 μL, 0.18 eq.) and pre-activated copper wire (5 cm) wrapped around a stirring bar were added to an 8 mL septum sealed vial. The polymerization was allowed to commence at ambient temperature for 18 h without employing any deoxygenation procedure. After 18h, a sample dissolved in THF, passed through a short column of neutral alumina to remove dissolved copper salts prior to analysis by ^{1}H NMR in $CDCl_3$ and SEC in THF.

General procedure for the Cu(0)-mediated RDRP of styrene (St) with targeted DP_n = 50 in the absence of any external deoxygenation.

Styrene (4 mL, 50 eq.), MBPA (0.111 mL, 1 eq.), $CuBr_2$ (7.80 mg, 0.05 eq.), IPA (4 mL), PMDETA (0.052 mL, 0.36 eq.) and pre-activated copper wire (5 cm) wrapped around a stirring bar were added to a septum sealed vial. The polymerization was allowed to commence at 60 ˚C for 36 h. After 36 h, a sample was taken and passed through a short column of neutral alumina to remove dissolved copper salts prior to analysis by ^{1}H NMR in $CDCl_3$ and SEC in THF.

Chain Extensions and block copolymers

General procedure for the *in-situ* chain extension reaction for the synthesis of PMA_{50}-PMA_{50}.

MA (4 mL, 50 eq), DMSO (4 mL), EBiB (129 μL, 1 eq), Cu(II)Br_2 (9.86 mg, 0.05 eq), Me_6Tren (42.5 μL, 0.18 eq.) and pre-activated copper wire (5 cm) were added to a 20

mL septum sealed vial and the polymerization was allowed to commence. Upon reaching high conversion (>96%) for the first block of the homopolymer, a 1 : 1 (v/v) mixture of MA (4 mL) and DMSO (4 mL) was added to the reaction mixture and the polymerization was left to commence. Samples were taken periodically and conversions were measured using ^{1}H NMR in $CDCl_3$ and SEC analysis in THF, after having been being passed through neutral alumina.

General procedure for the synthesis of the block copolymer PMA_{50}-*b*-PHA_{50}.

The general procedure for Cu(0)-RDRP of MA was followed. Upon detection of >96% conversion a 1 : 1 (v/v) mixture of HA (4 mL) and DMSO (4 mL) was added to the reaction mixture without employing any deoxygenation process or nitrogen blanket. Utilizing a degassed syringe, samples were taken periodically for the measurement of conversion through ^{1}H NMR in $CDCl_3$ and SEC analysis in THF.

Conventional (Cu(I)-mediated) ATRP

General procedure for the ATRP of poly(methyl methacrylate) with targeted DP_n = 100 in the absence of external deoxygenation.

For PMMA with a targeted DP_n = 100, CuBr (0.134 g, 0.935 mmol), 9 mL toluene, *N*-(*n*-Propyl)-2-pyridylmethanimine (2 mol eq. to CuBr) and MMA (10 mL, 93.5 mmol) were added in a 20 mL vial immersed in a thermostated oil bath at 90 °C. When the contents reached reaction temperature, EBiB (0.137 mL, 0.935 mmol) was added. The polymerization was left to commence and samples were taken periodically for the measurement of conversion through ^{1}H NMR in $CDCl_3$ and SEC analysis in THF, after having been passed through neutral alumina for the removal of dissolved copper salts.

2.4.4 Supplementary Figures & Characterization

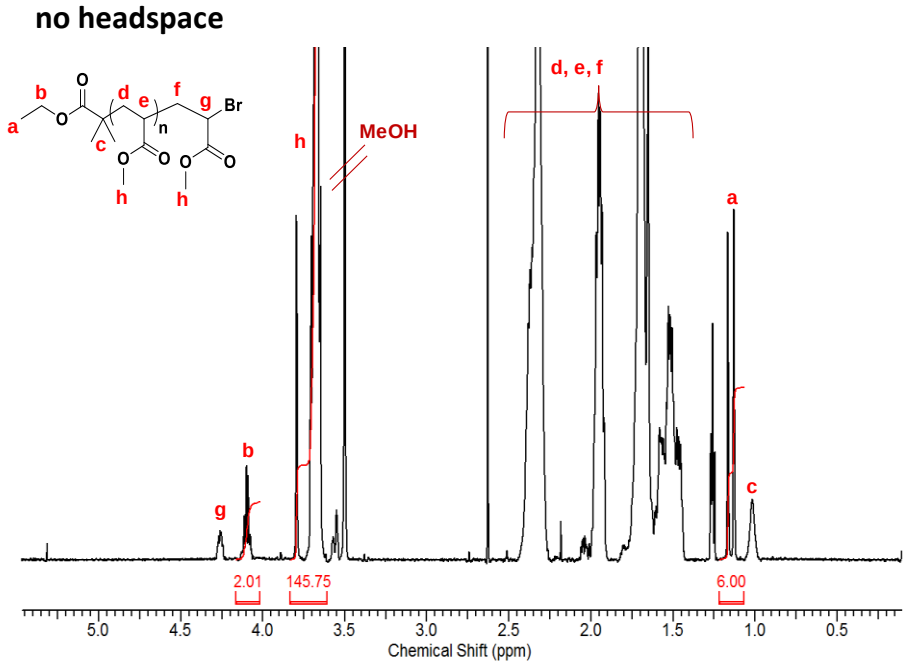

Figure 2-10. ^{1}H NMR in $CDCl_3$ of purified PMA_{50} synthesized *via* Cu(0)-RDRP in the absence of external deoxygenation, without headspace. Conversion (92%) was determined by comparing the integrals of monomeric vinyl protons (~ 5.7 - 6.5 ppm) to polymer signal.

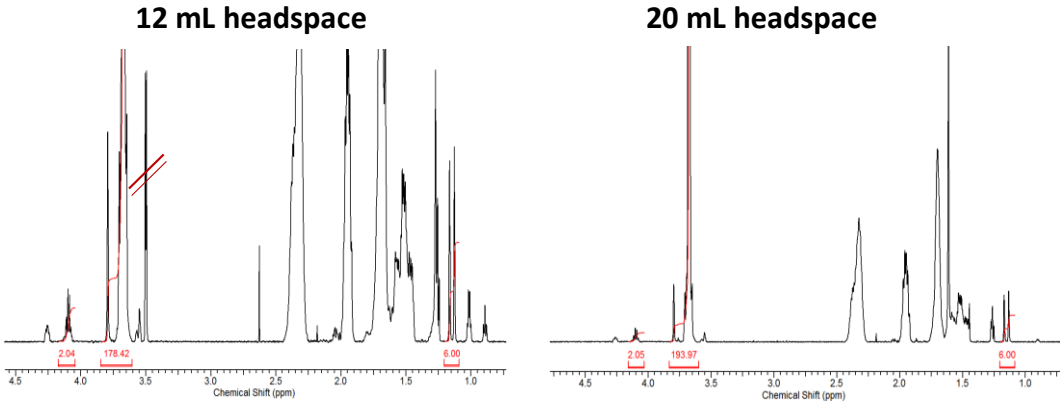

Figure 2-11. ^{1}H NMR in $CDCl_3$ of purified PMA_{50} synthesized via Cu(0)-RDRP in the absence of external deoxygenation with 12 mL (left) and 20 mL (right) headspace.

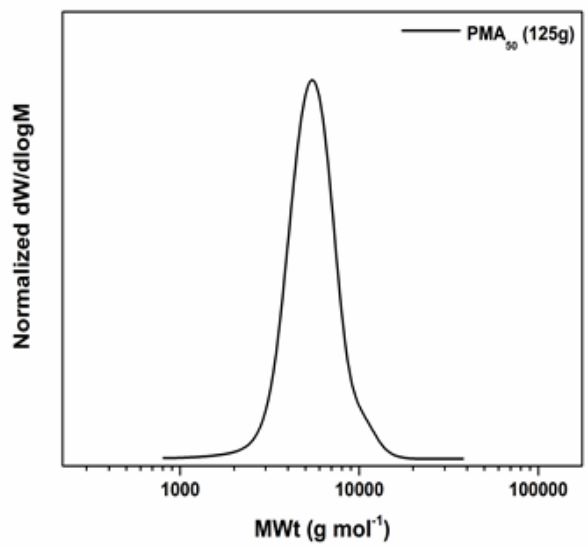

Figure 2-12. SEC trace of the higher scale (125 g) PMA_{50} (synthesis performed at RT) with $M_{n,SEC}$ = 5200 g/mol, $Đ$ = 1.10, conversion 92%, [MA]:[EBiB]:[$CuBr_2$]:[Me_6Tren] = [50]:[1]:[0.05]:[0.18]. DMSO as solvent 50% *v/v*.

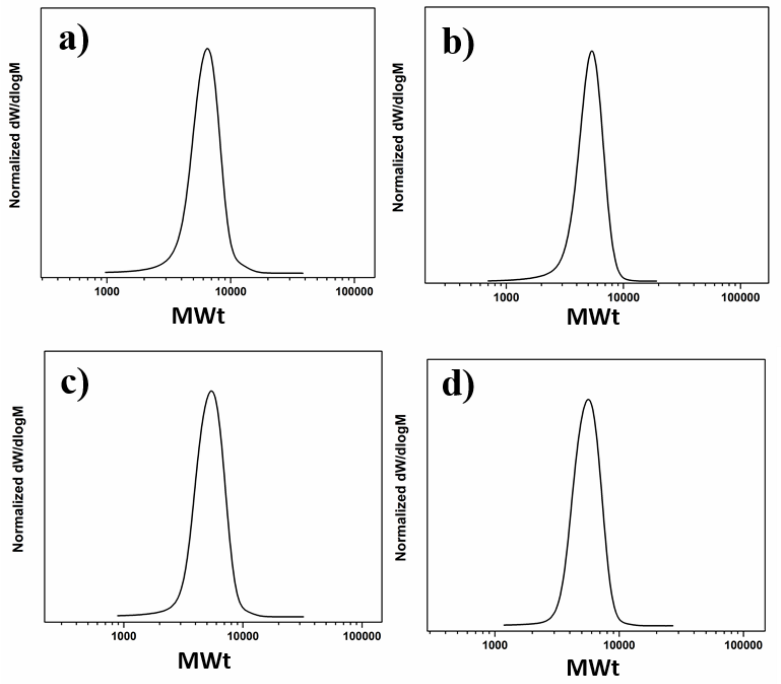

Figure 2-13. SEC traces of PMA_{50} synthesized *via* Cu(0)-RDRP in the absence of deoxygenation in **a**) MeCN, **b**) IPA, **c**) 80% Toluene - 20% Methanol and **d**) TFE.

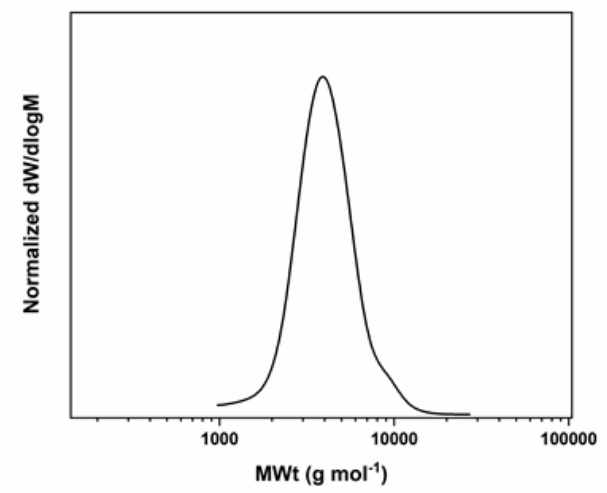

Figure 2-14. SEC trace of poly($PEGA_{480}$)$_{10}$ with $M_{n,SEC}$ = 3700 g/mol, $Đ$ = 1.18, 82% conversion. [$PEGA_{480}$]:[EBiB]:[$CuBr_2$]:[Me_6Tren] = [50]:[1]:[0.05]:[0.18]. H_2O as reaction solvent 50% *v/v.*

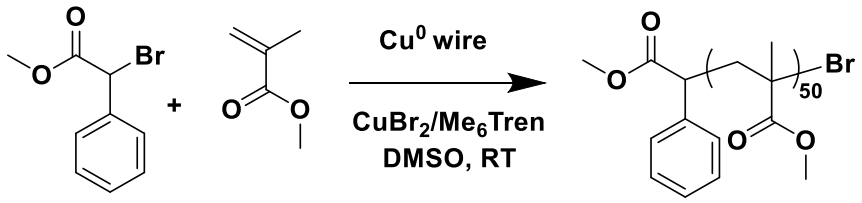

Scheme 2-2. Reaction scheme for the Cu(0)-mediated RDRP of $PMMA_{50}$. *Conditions:* [MMA]:[MBPA]:[$CuBr_2$]:[Me_6Tren] = [50]:[1]:[0.05]:[0.18]. DMSO solvent 50% *v/v,* ambient temperature (~ 25^{o}C).

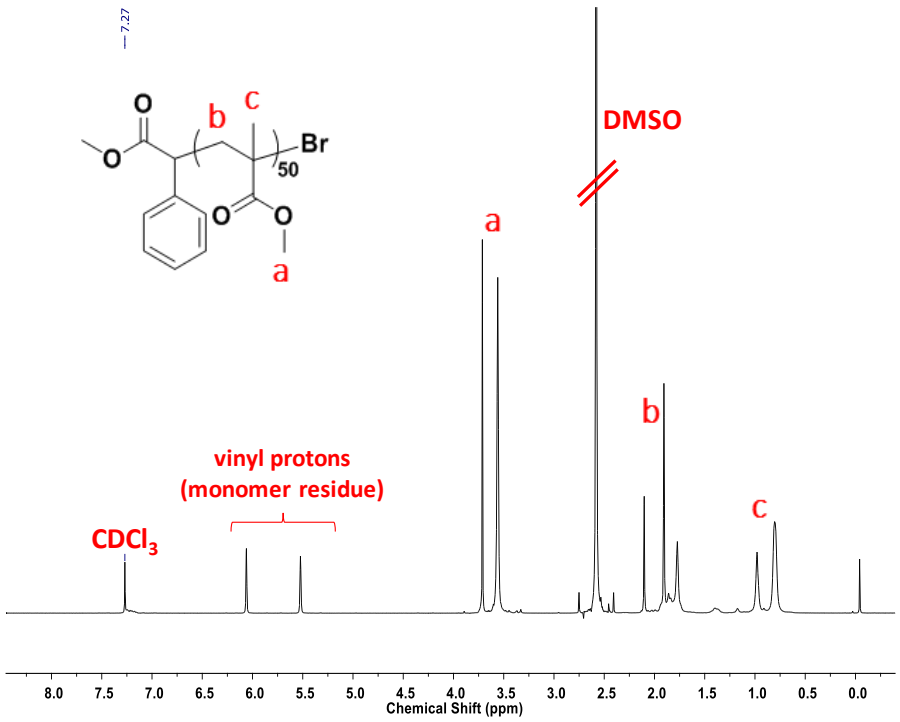

Figure 2-15. ^{1}H NMR of PMMA in $CDCl_3$. Conversion calculated by integration of methyl protons (a) with vinyl protons at ~ 6 ppm (77% conversion).

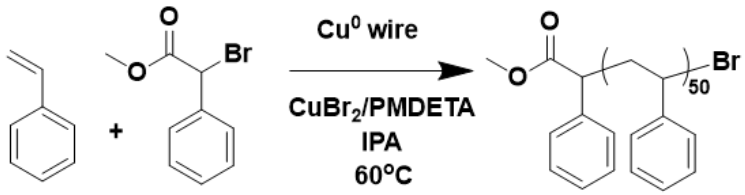

Scheme 2-3. Reaction scheme for the Cu(0)-mediated RDRP of PSt_{50}. Conditions: [PSt]:[MBPA]:[$CuBr_2$]:[PMDETA] = [50]:[1]:[0.05]:[0.36]. IPA solvent 50% v/v, temperature 60 ^{o}C.

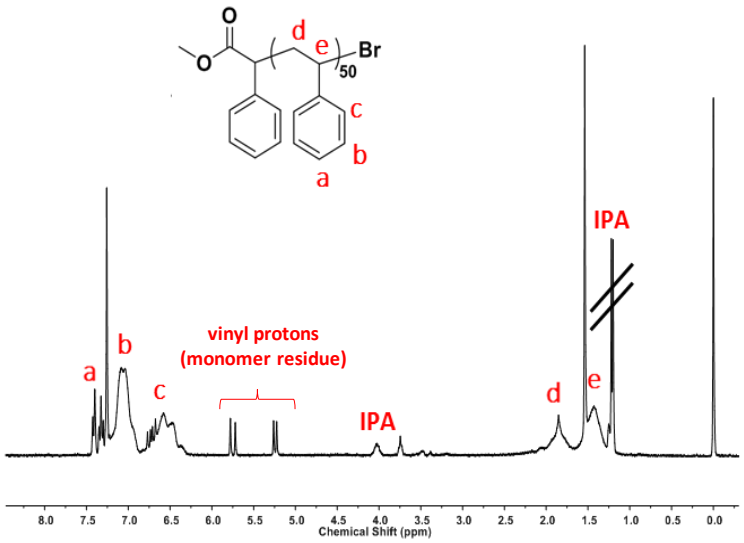

Figure 2-16. ^{1}H NMR of PS_{50} in $CDCl_3$ with conversion 91%.

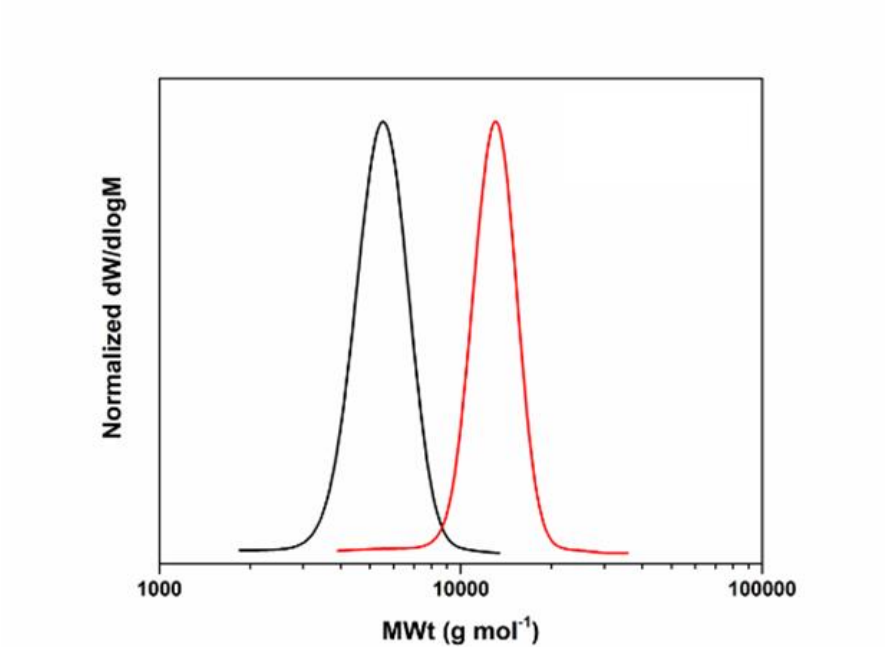

Figure 2-17. THF-SEC traces of the in-situ chain extension of PMA_{50}-PMA_{50} in DMSO with the second aliquot of MA deoxygenated via nitrogen sparging.

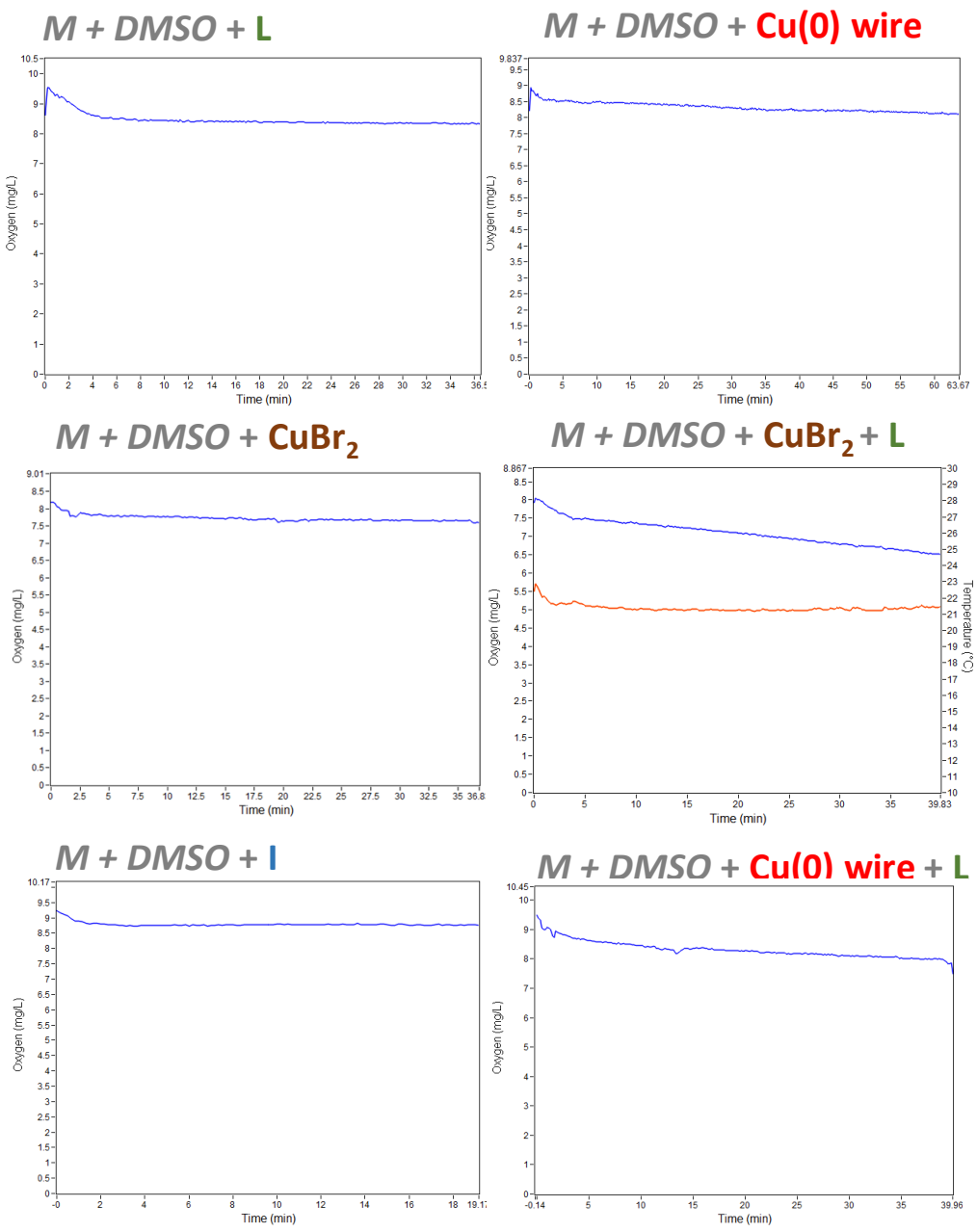

Figure 2-18. Line graphs illustrating the effect of the polymerization components (individually and combinations thereof) in the evolution of oxygen consumption.

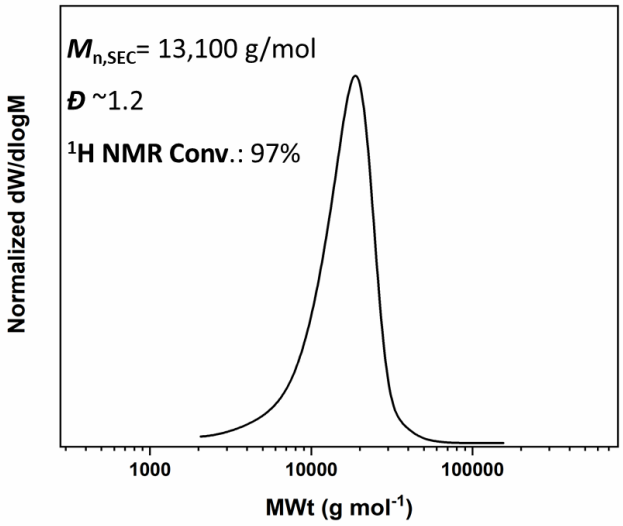

Figure 2-19. THF-SEC trace of PMMA with targeted DP_n = 100 synthesized *via* normal ATRP without applying any type of external deoxygenation.

Figure 2-20. Colour differences of the PMA_{50} polymerization solutions attributed to the generation of higher amounts of Cu(II) possibly after oxidation of the Cu(0)-wire when bigger headspace was present. Left: 20 mL headspace, middle: 12 mL headspace and right: no headspace.

2.5 References

1 A. Anastasaki, V. Nikolaou and D. M. Haddleton, *Polym. Chem.*, 2016, 7, 1002–1026.

2 K. Matyjaszewski, *Adv. Mater.*, 2018, **30**, 1706441.

3 K. Matyjaszewski, *Macromolecules*, 2012, **45**, 4015–4039.

4 S. Perrier, *Macromolecules*, 2017, 50, 7433–7447.

5 E. Baeten, J. J. Haven and T. Junkers, *Polym. Chem.*, 2017, **8**, 3815–3824.

6 J. De Neve, J. J. Haven, L. Maes and T. Junkers, *Polym. Chem.*, 2018, **9**, 4692–4705.

7 R. Aksakal, M. Resmini and C. R. Becer, *Polym. Chem.*, 2016, **7**, 171–175.

8 Y. Abdouni, G. Yilmaz and C. R. Becer, *Macromol. Rapid Commun.*, 2017, **38**, 1700212.

9 A. Anastasaki, V. Nikolaou, G. Nurumbetov, P. Wilson, K. Kempe, J. F. Quinn, T. P. Davis, M. R. Whittaker and D. M. Haddleton, *Chem. Rev.*, 2016, **116**, 835–877.

10 G. R. Jones, A. Anastasaki, R. Whitfield, N. Engelis, E. Liarou and D. M. Haddleton, *Angew. Chemie Int. Ed.*, 2018, **57**, 10468–10482.

11 J. Chiefari, Y. K. Chong, F. Ercole, J. Krstina, J. Jeffery, T. P. T. Le, R. T. A. Mayadunne, G. F. Meijs, C. L. Moad, G. Moad, E. Rizzardo and S. H. Thang, *Macromolecules*, 1998, **31**, 5559–5562.

12 G. Moad, E. Rizzardo and S. H. Thang, *Aust. J. Chem.*, 2009, **62**, 1402–1472.

13 V. Percec, T. Guliashvili, J. S. Ladislaw, A. Wistrand, A. Stjerndahl, M. J. Sienkowska, M. J. Monteiro and S. Sahoo, *J. Am. Chem. Soc.*, 2006, **128**, 14156–14165.

14 B. M. Rosen and V. Percec, *Chem. Rev.*, 2009, **109**, 5069–5119.

15 J.-S. Wang and K. Matyjaszewski, *J. Am. Chem. Soc.*, 1995, **117**, 5614–5615.

16 M. Kato, M. Kamigaito, M. Sawamoto and T. Higashimura, *Macromolecules*, 1995, **28**, 1721–1723.

17 V. A. Bhanu and K. Kishore, *Chem. Rev.*, 1991, **91**, 99–117.

18 S. C. Ligon, B. Husár, H. Wutzel, R. Holman and R. Liska, *Chem. Rev.*, 2014, 114, 577–589.

19 J. Yeow, R. Chapman, A. J. Gormley and C. Boyer, *Chem. Soc. Rev.*, 2018.

20 JoVE, *Science education database. Essentials of organic chemistry.*, 2019.

21 R. E. Rondeau, *J. Chem. Educ.*, 1967, **44**, 530.

22 G. Luyckx and J. Ceulemans, *Bull. des Sociétés Chim. Belges*, 2010, **96**, 151–163.

23 J. Homer and A. Coupland, *Analyst*, 1975, **100**, 865–872.

24 Y. Xiao and L. Konermann, *Protein Sci.*, 2015, **24**, 1247–1256.

25 T. Arakawa, S. J. Prestrelski, W. C. Kenney and J. F. Carpenter, *Adv. Drug Deliv. Rev.*, 2001, **46**, 307–326.

26 E. Liarou, R. Whitfield, A. Anastasaki, N. G. Engelis, G. R. Jones, K. Velonia and D. M. Haddleton, *Angew. Chemie*, 2018, **57**, 8998–9002.

27 E. Liarou, A. Anastasaki, R. Whitfield, C. E. Iacono, G. Patias, N. G. Engelis, A. Marathianos, G. R. Jones and D. M. Haddleton, *Polym. Chem.*, 2019, **10**, 963–971.

28 K. Matyjaszewski, S. Coca, S. G. Gaynor, M. Wei and B. E. Woodworth, *Macromolecules*, 1998, **31**, 5967–5969.

29 S. Fleischmann, B. M. Rosen and V. Percec, *J. Polym. Sci. Part A Polym. Chem.*, 2010, **48**, 1190–1196.

30 R. Chapman, A. J. Gormley, K.-L. L. Herpoldt and M. M. Stevens, *Macromolecules*, 2014, **47**, 8541–8547.

31 R. Chapman, A. J. Gormley, M. H. Stenzel and M. M. Stevens, *Angew. Chemie - Int. Ed.*, 2016, **128**, 4576–4579.

32 J. Yeow, R. Chapman, J. Xu and C. Boyer, *Polym. Chem.*, 2017, **8**, 5012–5022.

33 J. Yeow, S. Shanmugam, N. Corrigan, R. P. Kuchel, J. Xu and C. Boyer, *Macromolecules*, 2016, **49**, 7277–7285.

34 S. Shanmugam, J. Xu and C. Boyer, *Macromolecules*, 2016, **49**, 9345–9357.

35 T. Zhang, J. Yeow and C. Boyer, *Polym. Chem.*, 2019, **10**, 4643–4654.

36 A. E. Enciso, L. Fu, A. J. Russell and K. Matyjaszewski, *Angew. Chemie Int. Ed.*, 2018, **57**, 933–936.

37 A. E. Enciso, L. Fu, S. Lathwal, M. Olszewski, Z. Wang, S. R. Das, A. J. Russell and K. Matyjaszewski, *Angew. Chemie Int. Ed.*, 2018, **57**, 16157–16161.

38 C. M. Tseng, M. F. Lin, Y. L. Yang, Y. C. Ho, C. K. Ni and J. L. Chang, *Phys. Chem. Chem. Phys.*, 2010, **12**, 4989–4995.

39 M. F. Lin, Y. A. Dyakov, Y. T. Lee, S. H. Lin, A. M. Mebel and C. K. Ni, *J. Chem. Phys.*, 2017, **127**, 064308.

40 G. Zoldák, A. Zubrik, A. Musatov, M. Stupák and E. Sedlák, *J. Biol. Chem.*, 2004, **279**, 47601–47609.

41 F. Hollmann and I. W. C. E. Arends, *Polymers (Basel).*, 2012, **4**, 759–793.

42 G. R. Jones, R. Whitfield, A. Anastasaki, N. Risangud, A. Simula, D. J. Keddie and D. M. Haddleton, *Polym. Chem.*, 2018, **9**, 2382–2388.

43 C. Boyer, A. Atme, C. Waldron, A. Anastasaki, P. Wilson, P. B. Zetterlund, D. Haddleton and M. R. Whittaker, *Polym. Chem.*, 2013, **4**, 106–112.

44 R. Whitfield, A. Anastasaki, V. Nikolaou, G. R. Jones, N. G. Engelis, E. H.

Discekici, C. Fleischmann, J. Willenbacher, C. J. Hawker and D. M. Haddleton, *J. Am. Chem. Soc.*, 2017, **139**, 1003–1010.

45 J. S. Town, G. R. Jones and D. M. Haddleton, *Polym. Chem.*, 2018, **9**, 4631–4641.

46 J. S. Town, Y. Gao, E. Hancox, E. Liarou, A. Shegiwal, C. J. Atkins and D. Haddleton, *Rapid Commun. Mass Spectrom.*, 2019, rcm.8654.

47 V. A. Bhanu and K. Kishore, *Chem. Rev.*, 1991, **91**, 99– 117.

48 E. Liarou, M. Staniforth, J. S. Town, A. Marathianos, M. Grypioti, Y. Li, Y. Chang, S. Efstathiou, E. Hancox, A. M. Wemyss, P. Wilson, B. A. Jones, M. Aljuaid, V. G. Stavros and D. M. Haddleton, *Eur. Polym. J.*, 2020, 109388.

49 J. Mosnáček and M. Ilčíková, *Macromolecules*, 2012, **45**, 5859–5865.

50 J. Mosnáček, A. Eckstein-Andicsová and K. Borská, *Polym. Chem.*, 2015, **6**, 2523–2530.

51 D. M. Haddleton, M. C. Crossman, B. H. Dana, D. J. Duncalf, A. M. Heming, D. Kukulj and A. J. Shooter, *Macromolecules*, 1999, **32**, 2110–2119.

52 M. Ciampolini and N. Nardi, *Inorg. Chem.*, 1966, **5**, 41–44.

Chapter 3.

Ultra-low volume oxygen tolerant photoinduced Cu-RDRP

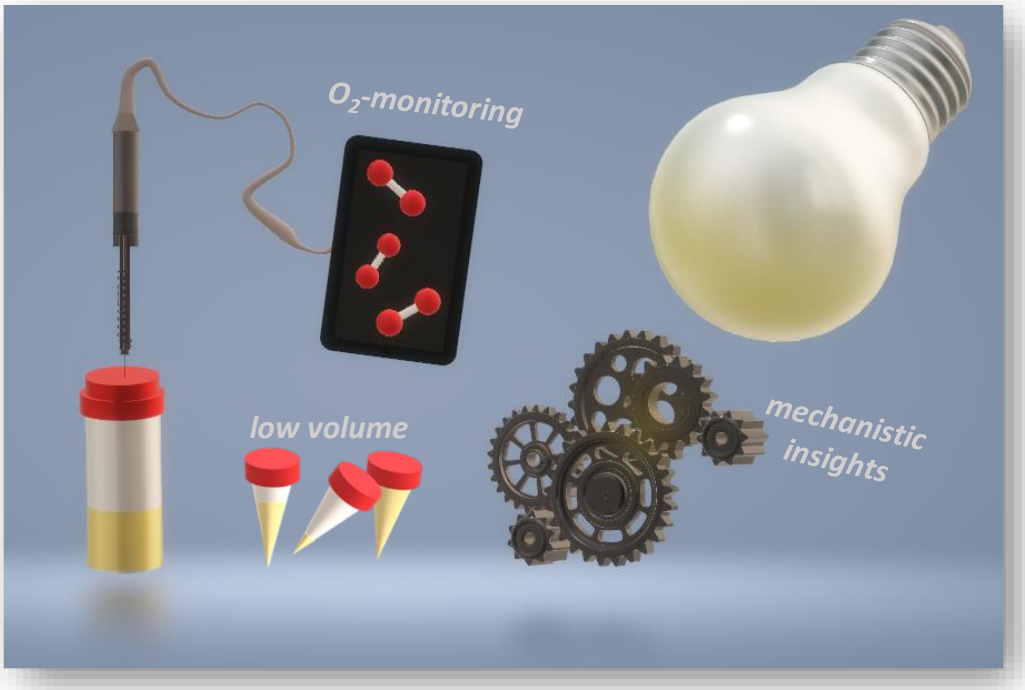

This chapter focuses on the development of oxygen tolerant ultra-low volume (as low as 5 μL total reaction volume) photoinduced Cu-mediated RDRP of a wide range of hydrophobic, hydrophilic and semi-fluorinated (meth)acrylates. In the absence of extrinsic deoxygenation, well-defined homopolymers can be obtained with low dispersity values, high end-group fidelity and near-quantitative conversions. Block copolymers can be efficiently synthesized in a facile manner and the compatibility of the system to larger scale polymerizations (up to 0.5 L) is demonstrated upon judicious optimization of the reaction conditions. An insight into the oxygen consumption

mechanism upon photo-irradiation is provided through an oxygen probe, and the role of each component is identified and discussed.

3.1 Introduction

The Reversible-deactivation radical polymerization (RDRP) systems have attracted significant interest during the last decades, due to their facile, versatile and robust nature.[1–10] Typically, all RDRP techniques (*e.g.* atom-transfer radical polymerization (ATRP),[11,12] single electron transfer-living radical polymerization (SET-LRP),[7,13] reversible addition-fragmentation chain-transfer polymerization (RAFT),[6,14,15] nitroxide-mediated polymerization (NMP)[16–18]) rely on intensive deoxygenation techniques including the use of glove box equipment, freeze-pump-thaw cycles or inert gas sparging to reduce (and ideally eliminate) the presence of oxygen. Oxygen is reported to be detrimental for radical polymerizations since it acts as an efficacious radical scavenger, rapidly reacting with carbon-centred radicals, and eventually leading to peroxy radicals and hydroperoxides which are inefficient at reinitiating the polymerization.[19–22]

Although traditional deoxygenation techniques are efficacious for the successful removal of oxygen, they can also be disadvantageous in some cases. For instance, the use of glove box equipment is a sophisticated, albeit expensive and time-consuming approach which also requires extensive training prior to use. Freeze-pump-thaw is another costly and time-consuming deoxygenation method which can also be problematic when proteins or enzymes are involved, leading to denaturation and loss of their secondary structure.[23–25] Finally, inert gas sparging with either argon or nitrogen (so-called “bubbling”) is perhaps the most popular and convenient method to remove oxygen from polymerization solutions. However, sparging can lack

reproducibility as it may alter the concentration of volatiles and precludes the use of low sample volumes. In addition, all the existing deoxygenation methods may not be available in all laboratories and/or add complexity to the set-up, thus restricting the accessibility to non-experts.

To mitigate this arduous task of conventional deoxygenation, many groups have exploited the use of enzymes to deoxygenate controlled radical polymerization.[21,26–29] For example, Yagci and colleagues, based on photoinitiated free radical polymerization developed an enzyme-based oxygen tolerant UV curing system, utilizing glucose oxidase (GOx) which in the presence of oxygen catalyzes the oxidation of *β*-D-glucose (G) to D-glucono-*δ*-lactone leading to oxygen consumption.[29] Chapman *et al.* were the first to use glucose oxidase (GOx) to remove oxygen in a RAFT polymerization where narrow molecular weight distributions were achieved even when the experiments were performed in open vessels.[27,28] In the case of ATRP, Matyjaszewski and co-workers subsequently reported the first controlled aqueous ATRP in an open vessel which was coined as "breathing ATRP". In their systems, GOx was employed to continuously remove oxygen from the polymerization solution.[26,30,31]

Among the various oxygen tolerant polymerization platforms, the approaches that use light as external stimulus have attracted considerable interest due to the polymerizations proceeding under conditions milder than conventional thermal approaches, it is non-invasive and environmentally benign, and gives the potential for spatiotemporal control.[32–34] Boyer and co-workers first reported the oxygen tolerance of PET-RAFT in which the oxygen can be consumed by either a photocatalyst or a reducing agent.[35] Examples of photocatalysts include (fac-[Ir(ppy)$_3$]),[36,37] zinc tetraphenylporphine (ZnTPP)[38,39] and Eosin Y,[40–42] while ascorbic acid[43,44] and

triethylamine[40,45] are the most commonly employed reducing agents. Considerable contributions but limited in number, have also been made in the field of photo-ATRP with Huang and co-workers,[46,47] utilizing a photoredox catalyst and without a tedious deoxygenation procedure, introducing a photoredox-mediated ATRP method for methacrylate-based polymers. Matyjaszewski's group presented a photoinduced Fe-catalyzed ATRP system for the synthesis of methacrylate polymers in non-deoxygenated solutions, employing $FeBr_3$ as catalyst.[48] The non-deoxygenated photoATRP was also extensively studied by Mosnáček and co-workers, who conducted extensive kinetic measurements in order to investigate the effect of ligand, light intensity and oxygen concentration for the photoATRP of MA and MMA.[49,50] Poly and co-workers, reported the synthesis of PMMA through photocatalyzed ATRP in the presence of air, utilizing copper (II) bromine/phenanthroline in the presence of triethylamine as reducing agent.[51]

The strong reducing ability of the photocatalysts facilitates the oxygen removal prior to polymerization.[21,49,52] This is particularly important for low-scale polymerizations and combinatorial synthesis. The ability to conduct polymerizations in extremely low volumes (typically from 20 μL to 500 μL) is an area of growing academic interest as it allows for the inexpensive, fast and high throughput screening of a wide range polymeric materials.[53–55] All the approaches that have been made by the above-mentioned groups strengthen the need for a comprehensively versatile oxygen tolerant photoinduced-RDRP methodology, capable for the facile synthesis of a range of materials, without compromising control over the molecular characteristics of the synthesized polymers. Moreover, although the above-mentioned contributions expand the oxygen tolerance scope, there is still the need for a further simplified strategy, independent of adjunctive reducing agents that add complexity to the system.

To date, PET-RAFT is the main controlled radical polymerization method that has been utilized for the high throughput synthesis of a range of polymeric materials.[46,56] However, examples of oxygen tolerant photoinduced ATRP are limited.[48–51,57] This is an oversight given the high efficiency of Cu-RDRP to synthesize a wide range of complex polymeric materials with controlled functionality, dispersity and architecture (*e.g.* stars,[10] multiblocks[58,59]). In addition, the key role of each component in oxygen consumption during photoinduced copper mediated radical polymerization has not been clarified.

In this chapter, the first *ultra-low* scale and fully oxygen tolerant photoinduced RDRP system, independent of any externally added oxygen quenchers, reducing agents or deoxygenation methods is developed and discussed.[57] In 8 mL scale, the efficient elimination of headspace gives access to a range of monomer families, including hydrophobic (*i.e.* as *n*-butyl acrylate, *n*-BA, and hexyl acrylate, HA), hydrophilic (poly(ethylene glycol methyl ether acrylate), $PEGA_{480}$) and semi-fluorinated (poly(2,2,2-trifluoroethyl acrylate), PTFEA and poly(2,2,2-trifluoroethyl methacrylate), PTFEMA) (meth)acrylates, with the utilization of various solvents. The versatility of the proposed oxygen-tolerance methodology is verified by achieving high control over the molecular weights and end-group fidelity in near-quantitative polymerizations, enabling *in-situ* chain extensions and block copolymerizations. This approach is efficiently scalable from extremely low volumes such as 5 μL, to high scale reactions of 0.5 L. Importantly, the polymerizations which were conducted at low volumes (up to 200 μL) were independent of the headspace presence, due to the homogeneous light diffusion (UV-irradiation) in the reaction solution, which is facilitated by the low reaction scale and the narrow shape of the reaction vessel. Additionally, an oxygen probe is employed for the online monitoring of oxygen

consumption in a photoinduced polymerization. The experimental data generating from the oxygen probe demonstrate preliminary insights into the oxygen consumption mechanism and the role of the different components that comprise a deoxygenation-free polymerization. This approach is the first example of such a low scale oxygen-tolerant Cu-RDRP, which can serve as a simple and in parallel robust platform, for the benchtop synthesis of polymer libraries at short reaction times and without the need of time-consuming deoxygenation methods.

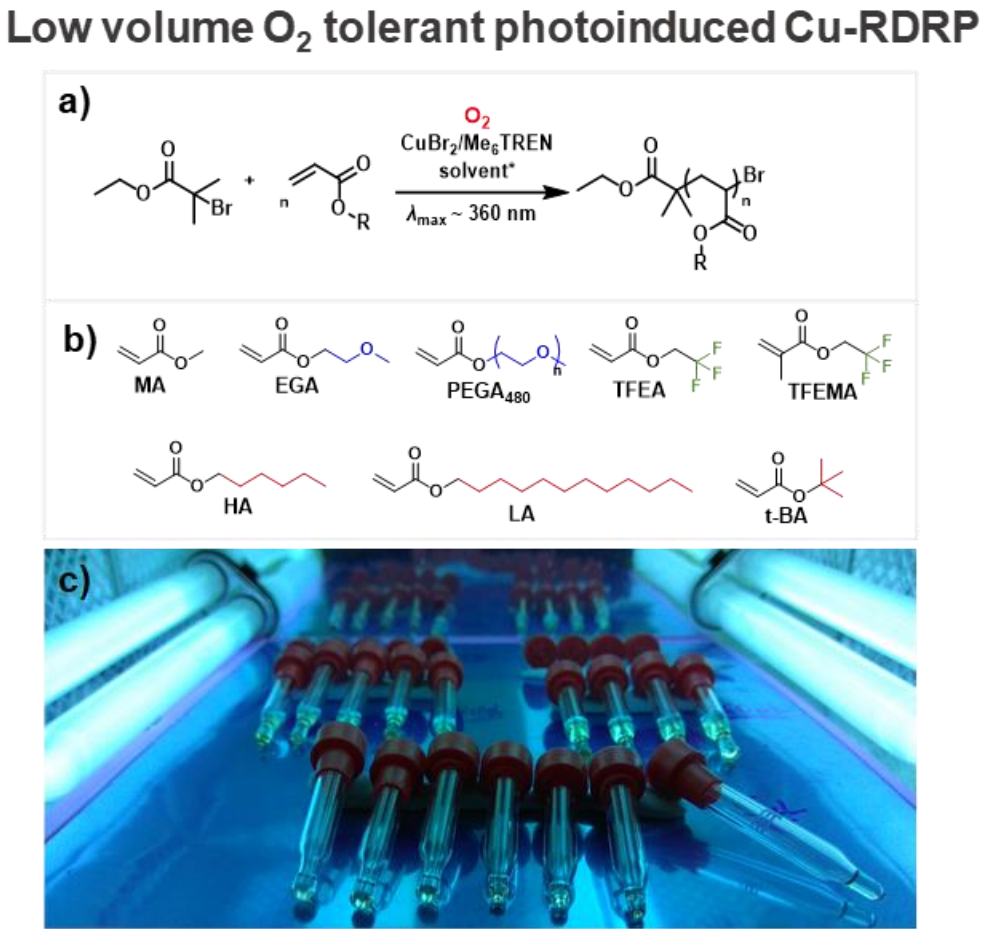

Scheme 3-1. a) Typical reaction scheme for the low volume oxygen tolerant photoinduced-RDRP, **b**) different hydrophobic, hydrophilic and semi-fluorinated monomers employed and **c**) low volume reaction setup utilizing commercially available glass inserts and a UV nail lamp with broad band emission and λ_{max} ~ 360 nm.

3.2 Results and Discussion

3.2.1 Oxygen tolerance studies in 8 mL scale

Initially, in order to explore the ability of the technique to perform in the presence of oxygen, the photoinduced Cu-RDRP of MA with targeted DP_n = 50 was conducted without any type of extrinsic deoxygenation. For this purpose, methyl acrylate (MA) was used as monomer, dimethyl sulfoxide (DMSO) as the solvent, tris(2-(dimethylamino)ethyl)-amine (Me_6Tren) as the ligand, ethyl α-bromoisobutyrate (EBiB) as the initiator and $Cu(II)Br_2$ as copper source, following the conditions [MA]:[I]:[$CuBr_2$]:[Me_6Tren] = [50]:[1]:[0.02]:[0.12] under a UV "nail lamp" with broad band emission and λ_{max} ~ 360 nm (**Scheme 3-3**). Based on the previous investigation on Cu(0) wire-mediated RDRP where the elimination of headspace was the crucial step to achieve an oxygen tolerant system, free of externally added reducing agents, the polymerization was left to commence in a fully filled (septum or lid capped) vial, without any type of commonly applied deoxygenation, yielding PMA_{50} in quantitative conversion (98%) with $M_{n,SEC}$ = 4,900 g mol^{-1} and $Đ$ ~ 1.08. In order to verify that headspace elimination can be efficiently applied to the photoinduced system, an identical reaction (from the same stock solution) was performed, with N_2-sparging applied prior to polymerization. The deoxygenated PMA_{50} yielded $M_{n,SEC}$ = 4,500 g mol^{-1} (expressed as molecular weight equivalents to PMMA narrow molecular weight standards) in quantitative conversion (98%) and Đ ~ 1.08, exhibiting negligible differences, if any, to the proposed non-deoxygenated system (**Figure 3-1**).

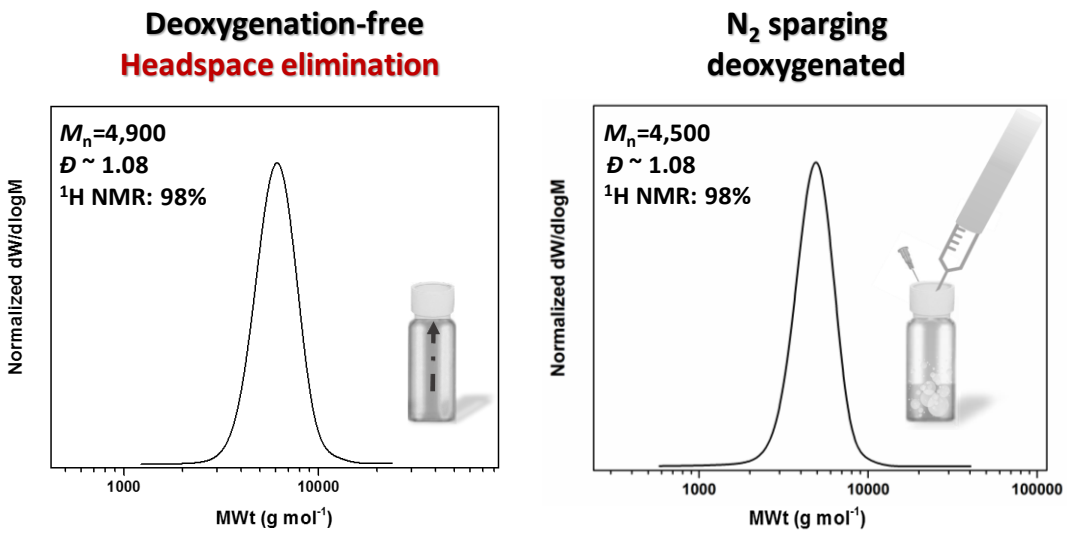

Figure 3-1. SEC traces of **a)** the non-deoxygenated PMA_{50} and **b)** the N_2 sparging-deoxygenated PMA_{50} both synthesized *via* photoinduced Cu-RDRP with [MA]:[EBiB]:[$CuBr_2$]:[Me_6Tren] = [50]:[1]:[0.02]:[0.12] and λ_{max} ~ 360 nm.

The importance of headspace was further investigated when three identical photoinduced Cu-RDRP reactions with different headspace volume (20, 12 and 3 mL of headspace) were conducted for the synthesis of PMA with targeted DP_n = 50. The reaction with 20 mL headspace led to no polymerization even after 8 hours of UV-irradiation, while the reaction with 12 mL headspace exhibited slow polymerization rates, reaching only ~ 65 % conversion. However, higher conversions, along with controlled molecular weights and low dispersity values, were observed for the polymerization with 3 mL headspace after 6 hours (**Figure 3-35**). These observations come in agreement with previous findings on Cu(0)-RDRP, where the extent of headspace played significant role on the evolution of the non-deoxygenated polymerizations. Nevertheless, it is hypothesized that the photoinduced Cu-RDRP approach is less oxygen tolerant in comparison to the Cu(0)-wire mediated approach discussed in Chapter 2 (*vide infra*), hence rendering the elimination of headspace

necessary for the successful implementation of this technique in the presence of oxygen.

In this context, the extent of control over high molecular weights was investigated with a range of different DPs (100-600) being targeted for PMA. For all the different DPs, the concentrations of Cu(II)Br_2 and ligand were maintained the same as for the case of DP_n = 50, with the ratio 1:6. For all the higher molecular weight polymerizations, no deoxygenation method was applied, with the only strategy followed being the total absence of headspace. Consequently, high molecular weights (~ 53,000 g mol^{-1}) were obtained, with narrow molecular weight distributions (1.08-1.12), in high conversions (90-98 %) (**Table 3-1, Figure 3-2**).

Table 3- 1. ^{1}H NMR and SEC analysis for PMA with different DPs synthesized *via* oxygen tolerant photoinduced Cu-RDRP. [a]

DP_n	Conversion ^{1}H NMR (%)	$M_{n,\,theory}$ (g mol^{-1})	$M_{n,SEC}$ [b] (g mol^{-1})	$Đ$
50	98	4500	4900	1.08
100	97	8600	10100	1.09
200	95	16000	17800	1.09
400	90	31500	31800	1.08
600	94	48800	53000	1.12

[a] In all polymerizations, the volume ratio of monomer to solvent was maintained 1:1 and conversion was calculated *via* ^{1}H NMR. [b] Determined by THF-SEC analysis based on DRI and expressed as molecular weight equivalents to PMMA narrow molecular weight standards.

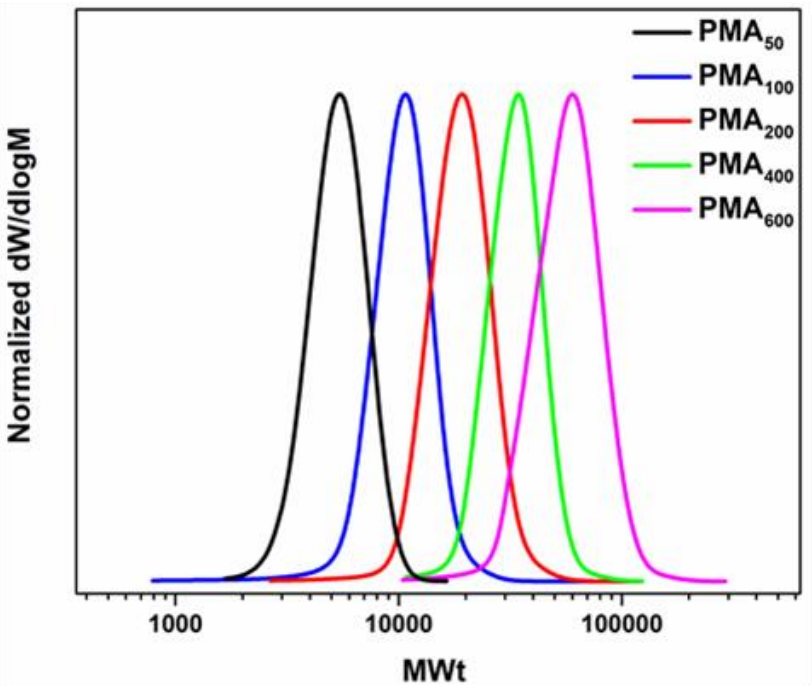

Figure 3-2. THF-SEC traces of PMA with targeted DPs = 50-600 synthesized *via* oxygen-tolerant photoinduced Cu-RDRP Scale: 8 mL.

Subsequently, in order to explore the applicability of the proposed methodology to the synthesis of different materials, photoinduced Cu-RDRP with headspace elimination was applied for a series of different monomer types and families including hydrophobic, hydrophilic and semi-fluorinated, acrylates and methacrylates in different solvents. Apart from MA, ethylene glycol methyl ether acrylate (EGA) was polymerized in DMSO, yielding poly(EGA)$_{50}$ with M_n = 6,500 g mol^{-1} and $Đ$ ~ 1.09 in 96% conversion (**Table 3-2, Figure 3-3, Scheme 3-4**). From the scope of more hydrophobic monomers which can be challenging due to solubility issues,[60] initially *n*-butyl acrylate was polymerized in DMSO, exhibiting controlled macromolecular characteristics at high monomer conversion, although generating a biphasic system (^{1}H NMR conversion: 97%, M_n = 7,500 g mol^{-1} and $Đ$ ~ 1.2, **Table 3-2, Figure 3-3**). The span of hydrophobic monomers reached a greater extent with the polymerization of hexyl acrylate (HA) in trifluoroethanol (TFE) (**Scheme 3-7**), a solvent which

facilitates the combined solubilization of monomer, polymer and Cu(II)Br_2, reifying the photoinduced RDRP of hydrophobic monomers.[43,44] Consequently, well-defined poly(hexyl acrylate) was obtained with M_n = 7,700 g mol^{-1} and $Đ$ ~ 1.13 in near-quantitative conversion (98%) (**Figure 3-3, Table 3-2**). Apart from the hydrophobic monomers, the polymerization of the hydrophilic poly(ethylene glycol methyl ether acrylate)$_{480}$ (PEGA$_{480}$) in DMSO also yielded well-defined P(PEGA$_{480}$)$_{20}$ with M_n = 9,500 g mol^{-1} and $Đ$ ~ 1.16, in near-quantitative conversion (97%) (**Table 3-2, Scheme 3-5, Figure 3-3**).

Subsequently, since the intermolecular interactions that occur from their C-F bonds exhibit properties of great interest, the oxygen tolerant photopolymerization of the semi-fluorinated trifluoroethyl acrylate (TFEA) and trifluoroethyl methacrylate (TFEMA) was explored, utilizing TFE as solvent (**Table 3-2**, **Figure 3-3, Schemes 3-8 & 3-9**). The obtained polymers showed low dispersity values and good agreement between theoretical and experimental M_n values, highlighting the compatibility of this non-deoxygenated system with fluorine-rich monomers (further discussion in the 3.2.1 section of this chapter "*The transition to ultra-low volumes*"). Subsequently, with dimethylformamide (DMF) as the solvent, *tert*-butyl acrylate which can undergo deprotection to produce acidic functional materials was polymerized in DMF (**Scheme 3-6**),[61,62] yielding experimental M_n close to the theoretical value ($M_{n,SEC}$ = 7,000 g mol^{-1}) and $Đ$ ~ 1.13 in high conversion (^{1}H NMR ~ 95%) (**Figure 3-3**, **Table 3-2**).

Table 3-2. ^{1}H NMR and SEC analysis for all the different polymers obtained through photoinduced RDRP without any type of deoxygenation. [a]

Polymer	Solvent	DP_n	Conv. ^{1}H NMR %	$M_{n,\,theory}$ (g mol^{-1})	$M_{n,SEC}$ [b]	$Đ$
P(*n*-BA)	**DMSO**	50	97	6400	7500	1.2
P(*t*-BA)	**DMF**	50	95	6300	7000	1.13
P(HA)	**TFE**	50	98	7800	7700	1.13
P(TFEA)	**TFE**	50	93	7400	9200	1.09
P(TFEMA)	**TFE**	50	88	7900	7700	1.14
P(EGA)	**DMSO**	50	96	6400	6500	1.09
P(PEGA$_{480}$)	**DMSO**	20	97	9500	9500	1.16

[a] In all polymerizations, the volume ratio of monomer to solvent was maintained at 1:1 throughout and conversion was calculated *via* ^{1}H NMR. [b] Determined by THF SEC analysis based on DRI and expressed as molecular weight equivalents to PMMA standards.

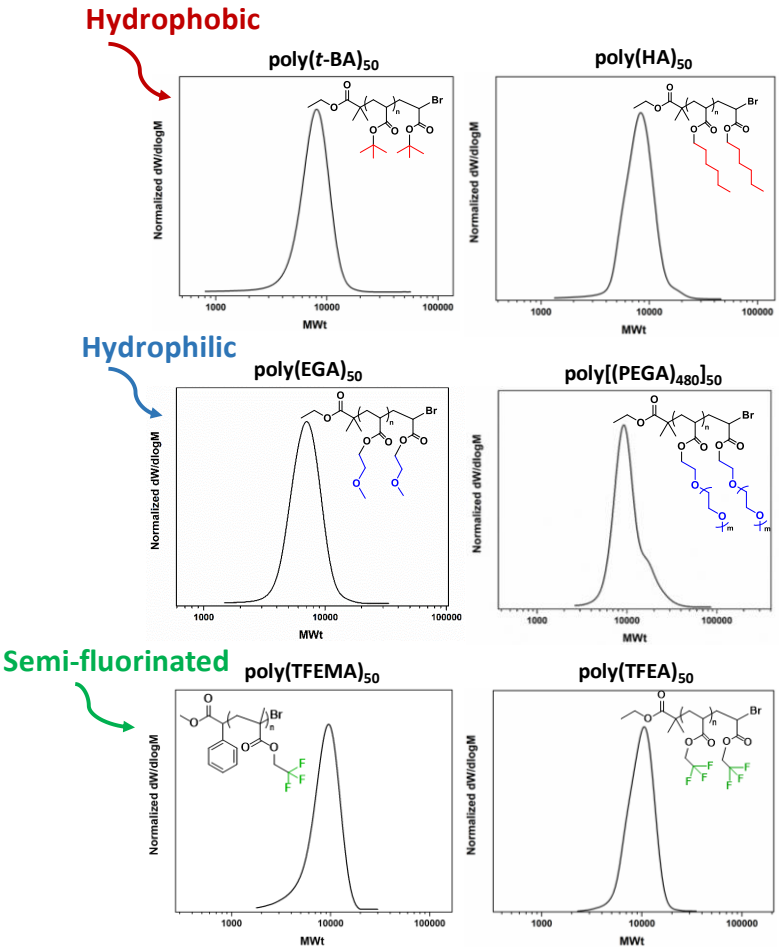

Figure 3-3. THF-SEC traces for the various hydrophobic, hydrophilic and semi-fluorinated polymers obtained *via* oxygen tolerant photoinduced Cu-RDRP.

The high chain end fidelity was subsequently exemplified by the *in-situ* re-initiation of the PMA_{50} macroinitiator with a second aliquot of MA (50 eq.), yielding PMA_{50}-PMA_{50} ($M_{n,SEC}$ = 10,500 g mol^{-1}, $Đ$ ~ 1.12) (**Figure 3-4a**). The conditions for the synthesis of the macroinitiator were [MA] : [EBiB] : [Cu(II)Br_2] : [Me_6Tren] = 50 : 1 : 0.02 : 0.12 in DMSO and were followed by the addition of 50 eq. MA without applying deoxygenation. The utility of the system's high end group fidelity was expanded to a greater degree when the addition of a non-deoxygenated *t*-BA aliquot (50 eq.) re-initiated the PMA_{50} macroinitiator, yielding the PMA_{50}-*b*-P(*t*-BA)$_{50}$ diblock copolymer ($M_{n,SEC}$ = 14,600 g mol^{-1}, $Đ$ ~ 1.11) through an one-pot process,

without intermediate purification of the macroinitiator (**Figure 3-4b**). Interestingly, while the utilization of DMSO exhibits excellent results for the synthesis of PMA, and DMF is a good solvent for P(*t*-BA), none of them proved efficient for the synthesis of a PMA_{50}-*b*-$P(t\text{-}BA)_{50}$ diblock copolymer. It should be noted that the solvent for a polymerization is particularly important since, apart from being able to complex with the metal centre in different ways,[63–65] it is necessary to facilitate the stabilization of Cu(II), especially when very low copper concentration is used. After utilizing different solvents, TFE exhibited excellent behaviour on the synthesis of PMA_{50}-*b*-$P(t\text{-}BA)_{50}$ since, apart from the efficient synthesis of the PMA_{50} macroinitiator, it also contains a fluorinated hydrophobic site which induces the solubilisation of the hydrophobic *t*-BA, thus homogenizing the reaction solution.[60,66] Both for PMA_{50}-PMA_{50} and PMA_{50}-*b*-$P(t\text{-}BA)_{50}$ a clear shift into higher molecular weights was evidenced, notwithstanding the presence of a small low molecular weight shoulder, indicative of some termination. Since the second monomer aliquot did not undertake any type of deoxygenation, its addition into the polymerization reaction introduced (mainly dissolved) oxygen, capable of reacting with propagating radicals and thus leading to some termination events. However, the low dispersity values ($Đ < 1.15$) for the *in-situ* chain extension and block copolymerization, as well as the good agreement between theoretical and experimental M_n values at high conversions, corroborate the robustness of the proposed methodology and render it a useful tool not only for the synthesis of homopolymers but also for *in-situ* block copolymerizations.

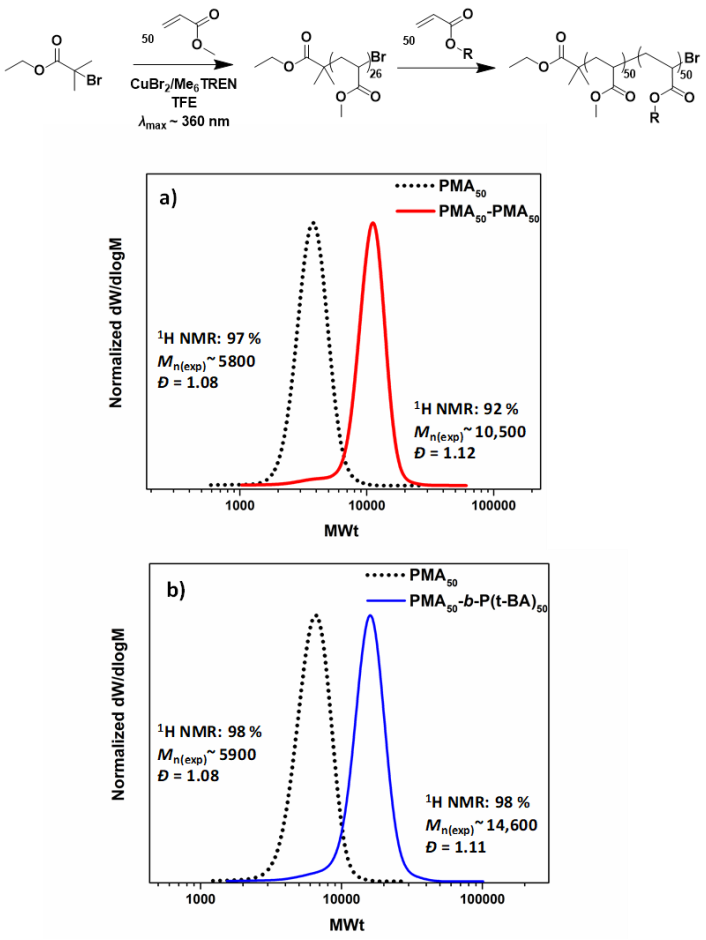

Figure 3-4. Reaction scheme (top) and THF-SEC traces of the *in-situ* chain extensions and block copolymerizations from PMA_{50} macroinitiator with initial conditions of [MA] : [EBiB] : [$Cu(II)Br_2$] : [Me_6Tren] = 50 : 1 : 0.02 : 0.12 with **a**) the chain extension PMA_{50}-PMA_{50} obtained after addition of a second aliquot of MA (50 eq.) and **b)** the block copolymer PMA_{50}-*b*-P(*t*-BA)$_{50}$ after the addition of *t*-BA (50 eq.). R = -C-$(CH_3)_3$.

3.2.2 The transition to ultra-low volumes

The ability to conduct controlled polymerizations in the presence of oxygen can potentially enable the high throughput synthesis of a wide range of polymers at low reaction volumes. In order to test this hypothesis, commercially available vial inserts with a full capacity of 200 μL were utilized and all the reactions were sealed with lids (**Figure 3-5**). To eliminate the headspace, the vial insert was initially fully filled with

the reaction solution (200 µL / 200 µL). Under these conditions, the photoinduced Cu-RDRP of MA with targeted DP_n = 50 was performed without deoxygenation, yielding well-defined PMA, with near-quantitative monomer conversion (96%, **Figure 3-19**), low dispersity and symmetric SEC trace ($Đ$ ~ 1.07, $M_{n,exp}$ ~ 5,200 g mol^{-1}) (**Figure 3-6a**).

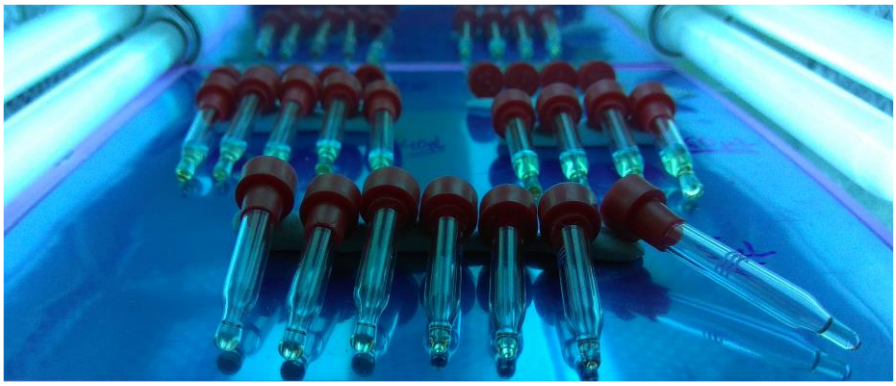

Figure 3-5. UV nail lamp reaction setup for the ultra-low volume polymerizations conducted in commercially available vial inserts (λ_{max} ~ 360 nm).

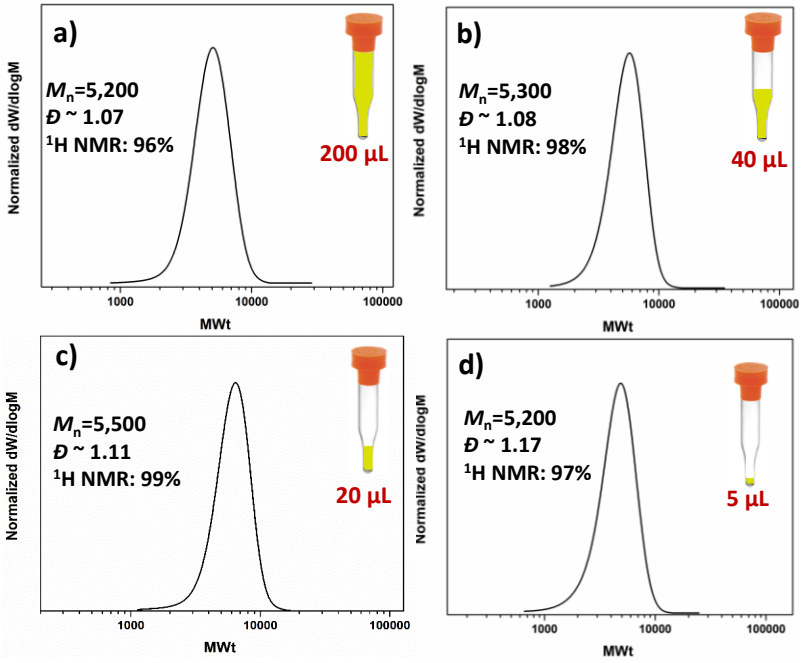

Figure 3-6. THF-SEC traces for PMA_{50} with **a**) 200 µL **b**) 40 µL, **c**) 20 µL and **d**) 5 µL reaction volume synthesized *via* oxygen tolerant photoinduced Cu-RDRP with [MA]:[EBiB]:[Cu(II)Br_2]:[Me_6Tren] = [50]:[1]:[0.02]:[0.12] using a UV lamp with broad band λ_{max} ~ 360 nm.

Encouraged by these initial findings, lower reaction volumes were applied, from 200 μL to 60, 40, 20, 10 and 5 μL (**Figure 3-6**, **Figures 3-20 & 3-21**). For these experiments, 200 μL commercially available vial inserts were used as previously, in which the headspace was increased from zero to 140, 160, 180, 190 and 195 μL, respectively. Despite the increase of the headspace, all polymerizations reached near-quantitative conversions (>96%) without compromising the control over the molecular weight and the molecular weight distributions ($Đ$ ~ 1.1). In all cases, comparable initiator efficiencies were observed ($M_{n,SEC}$ ~ 5,000-5,500 g mol^{-1}) indicating that for the low volume reactions in DMSO, the headspace has only negligible effects, if any, on the targeted molecular weight (**Table 3-3**). This was attributed to the absence of stirring in this system which limits the diffusion of oxygen into the polymerization solution. It should also be highlighted that even at ultra-low volumes (*i.e.* 5 μL), the polymerization proceeds efficiently, although with slightly higher dispersity values ($Đ$ ~ 1.17).

Table 3-3. ^{1}H NMR and SEC analysis for the low volume PMA_{50} obtained with different headspaces in the absence of deoxygenation [a]

Scale (μL)	Headspace (μL)	Conversion ^{1}H NMR (%)	M_n, theory (g mol^{-1})	M_n,SEC[b] (g mol^{-1})	$Đ$
200	0	96	4,300	5,200	1.07
60	140	98	4,400	5,400	1.08
40	160	98	4,400	5,300	1.08
20	180	99	4,500	5,500	1.11
10	190	99	4,500	5,000	1.11
5	195	97	4,400	5,200	1.17

[a] In all polymerizations, the volume ratio of monomer to solvent was maintained 1:1 and conversion was calculated *via* ^{1}H NMR. [b] Determined by THF SEC analysis based on DRI and expressed as molecular weight equivalents to PMMA narrow molecular weight standards.

The low volume experiments were also compatible with lower catalyst loadings, namely 150, 75, and 37 ppm of Cu-catalyst, while 300 ppm of catalyst is used in the standard system. The obtained results showed that low copper loadings can be used without significantly compromising the control over the molecular weight distributions **(Figure 3-7, Table 3-4).** However, the dispersity values were increased when as low as 37 ppm were used, due to less efficient deactivation of the polymer chains, as has been previously reported.[67,68] In agreement with the literature, when low Cu(II)Br_2 concentration is used, the rate of deactivation is lower than the rate of propagation, leading to higher dispersity values. This can be particularly evident in oxygen tolerant Cu-RDRP systems where the concentration of the Cu species is significantly important for the evolution of both the polymerization and the oxygen consumption (see section 3.2.3 "*Insights into the oxygen tolerance mechanism*").

Table 3-4. ^{1}H NMR and SEC analysis for the low volume (10 μL) PMA_{50} synthesized with different Cu(II)Br_2 concentrations and in the absence of deoxygenation [a]

Cu(II)Br_2 (ppm)	**Conversion ^{1}H NMR (%)**	**M_n, theory (g mol^{-1})**	**M_n,SEC[b] (g mol^{-1})**	***Đ***
300 (std) [c]	99	4,500	5,200	1.07
150	99	4,500	5,700	1.17
75	97	4,400	5,600	1.20
37	97	4,400	5,600	1.26

[a] In all polymerizations, the volume ratio of monomer to solvent was maintained 1:1, the total volume of the reaction was 10 μL and conversion was calculated *via* ^{1}H NMR. [b] Determined by THF SEC analysis based on DRI and expressed as molecular weight equivalents to PMMA narrow molecular weight standards. [c] std = standard

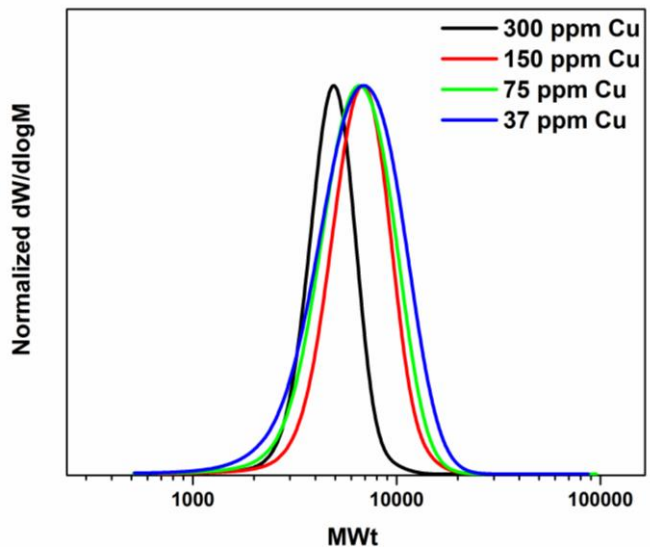

Figure 3-7. THF-SEC traces for the low volume (10 μL) PMA_{50} synthesized with different $Cu(II)Br_2$ concentrations *via* oxygen tolerant photoinduced Cu-RDRP.

To explore the extent of control over higher molar masses, a range of different degrees of polymerization (100-400) were targeted for PMA, on a 60 μL scale. Well-defined PMAs up to DP_n = 400 were obtained with final $M_{n,SEC}$ = 38,500 g mol^{-1} and dispersity of 1.19 at high monomer conversions (>82%) (**Figure 3-8, Table 3-5**). Unfortunately, targeting higher DPs *(e.g.* 600 and 800) resulted in no conversion, even when the reaction was left to proceed overnight. This was expected, since very low initiator and catalyst concentrations are challenging for a non-deoxygenated polymerization. As discussed in section 3.2.3 "*Insights into the oxygen tolerance mechanism*", the initiator participates in oxygen consumption thus, less than the targeted amount of the latter is available for polymerization process.

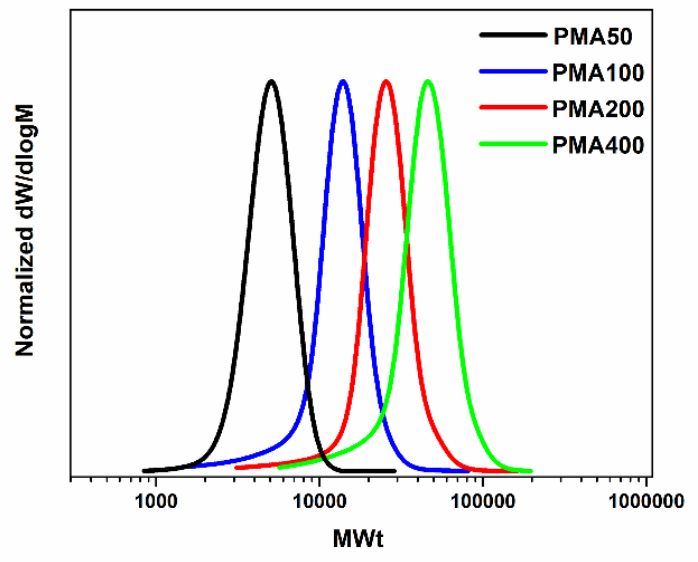

Figure 3-8. THF-SEC traces for low volume PMA with targeted DPs 50-400 synthesized *via* oxygen-tolerant photoinduced Cu-RDRP with [MA]:[EBiB]:[Cu(II)Br_2]:[Me_6Tren] = [DP_n]:[1]:[0.02]:[0.12] under a UV lamp with broad band λ_{max} ~ 360 nm.

Table 3-5. ^{1}H NMR and SEC analysis for low volume PMA with different targeted DPs obtained *via* photoinduced Cu-RDRP in the absence of deoxygenation. [a]

DP_n	**Conversion ^{1}H NMR (%)**	**$M_{n,th.}$ (g mol^{-1})**	**$M_{n,SEC}$[b] (g mol^{-1})**	**$Đ$**
50	98	4,400	5,400	1.08
100	99	8,700	11,000	1.18
200	92	16,000	23,000	1.19
400	82	24,800	38,500	1.19

[a] In all polymerizations the volume ratio of monomer to solvent was maintained 1:1 and conversion was calculated *via* ^{1}H NMR. [b] Determined by THF SEC based on DRI analysis and expressed as molecular weight equivalents to PMMA narrow molecular weight standards.

Subsequently, the applicability of the low volume oxygen tolerant photoinduced Cu-RDRP was examined in a wide range of hydrophobic, hydrophilic and semi-fluorinated monomers. Given the tolerance of the methodology in the

presence of large headspace when DMSO was used as a solvent, ethylene glycol methyl ether acrylate (EGA) was polymerized efficiently at 10 μL scale with $M_{n,SEC}$ = 7,300 g mol^{-1} and $Đ$ ~ 1.17 at 99% conversion (**Figure 3-9a, Figure 3-22, Table 3-6**). Polymerization of the hydrophilic poly(ethylene glycol) methyl ethyl acrylate $(PEGA_{480})_{20}$ also afforded a well-defined polymer at high conversion (>99%) with narrow molecular weight distributions ($Đ$ ~ 1.18) (**Figure 3-9b, Figure 3-23, Table 3-6**). These results further highlight the versatility of DMSO to enable the synthesis of controlled polymers at very high conversions and ultra-low reaction volumes,[69] even in the presence of a headspace.

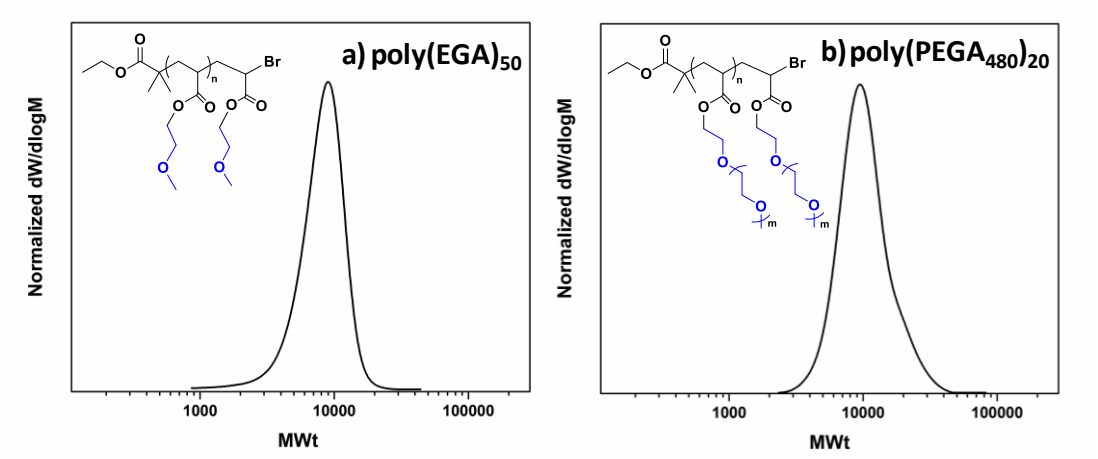

Figure 3-9. THF-SEC traces for **a**) P(EGA) with targeted DP_n = 50 and **b**) P($PEGA_{480}$) with targeted DP_n = 20 synthesized *via* oxygen-tolerant photoinduced Cu-RDRP with 10 μL total reaction volume.

Subsequently, the photoinduced Cu-RDRP of hydrophobic and semi-fluorinated monomers was investigated in the presence of oxygen. In this context, *tert*-butyl (*t*-BA), hexyl (HA, C6), lauryl (LA, C12) and trifluoroethyl (meth)acrylates (TFEA and TFEMA) were used. However, DMSO has been reported as an unsuitable solvent for these materials, leading to insoluble final polymeric materials and subsequent loss of control.[70,71] As an alternative, the polymerization of *t*-BA and LA was attempted in mixtures of toluene/MeOH (4:1), where a small amount of MeOH is

necessary to facilitate the complete solubilization of the catalyst, while toluene is needed to dissolve the monomers and the resulting polymers. Unfortunately, in the presence of a large headspace (10 μL reaction scale in a 200 μL vial insert) no polymerization was observed within 24 h for either *t*-BA or LA. Moreover, when the polymerization of MA was conducted in the same solvent system in a similar way to the other monomers, no monomer conversion occurred. However, when the identical experiments were performed upon elimination of the headspace to almost zero, the polymerization of *t*-BA (**Figure 3-10a**, **Figure 3-24**, **Table 3-6**), LA (**Figure 3-10b**, **Table 3-6**) and MA (**Figure 3-25**, **Table 3-6**) occurred in a controlled manner, exhibiting narrow molecular weight distributions.

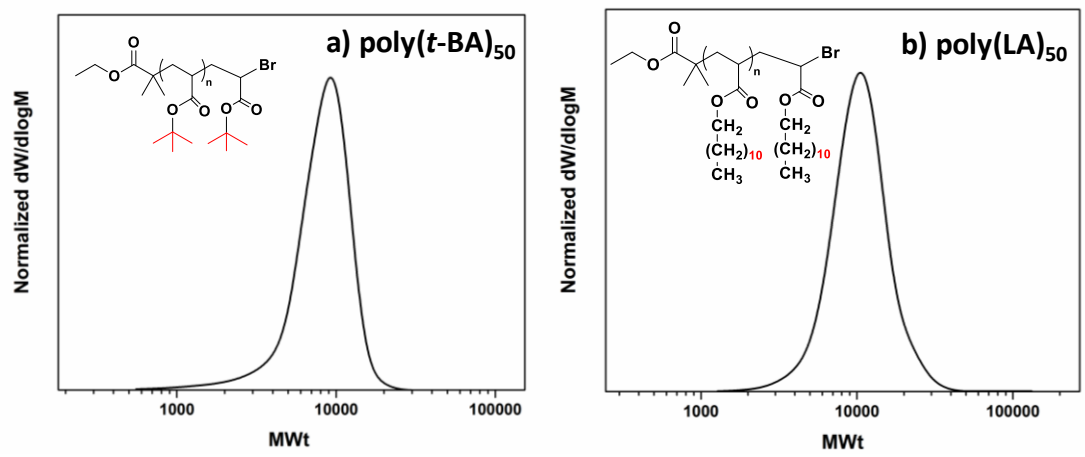

Figure 3-10. THF-SEC traces for **a**) P(*t*-BA) and **b**) PLA with targeted DP_n = 50 synthesized *via* oxygen-tolerant photoinduced Cu-RDRP with 100 μL total reaction volume.

In a similar vein, the polymerization of HA and TFEA, as well as MA in the presence of a large headspace and in trifluoroethanol (TFE) was unsuccessful, and no polymerization was observed. On the contrary, when the low scale polymerizations took place in full vial inserts, control over the polymerization was maintained leading to PHA_{50} (**Figure 3-27**, **Table 3-6**), PMA_{50} **(Figure 3-28**, **Table 3-6**) and $PTFEA_{50}$

(**Figure 3-11b**, **Figure 3-29**, **Table 3-6**) with low dispersity values. Although the polymerization of TFEA was unsuccessful in the presence of a headspace, the methacrylate analogue (TFEMA) was polymerized with ~ 90 μL headspace, yielding a well-defined PTFEMA$_{50}$ with $M_{n,SEC}$ = 8,400 g mol^{-1} and $Đ$ ~ 1.15 (**Figure 3-11a**, **Figure 3-30**, **Table 3-6**). The ability of the semi-fluorinated methacrylate to undergo polymerization even in the presence of significant headspace, was attributed to the higher degree of oxygen tolerance for the methacrylates compared to acrylates.[72]

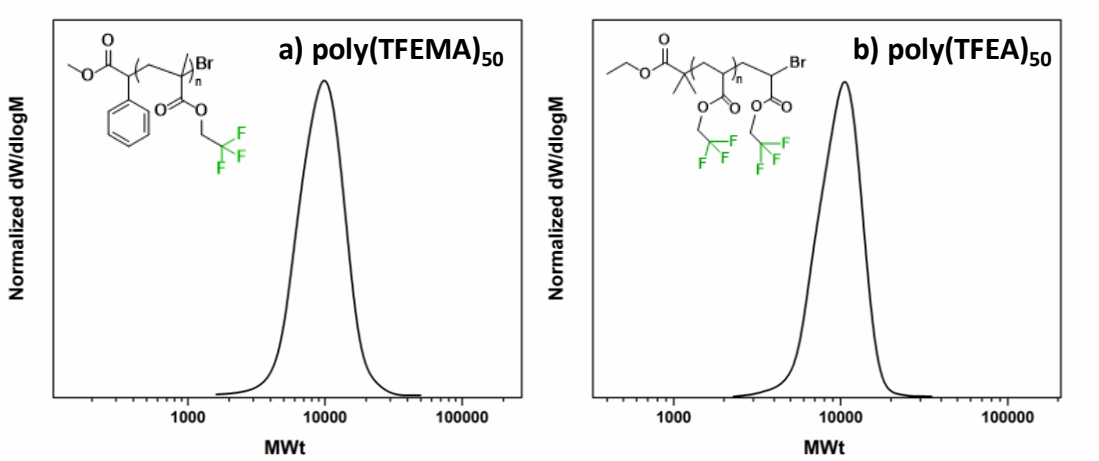

Figure 3-11. THF-SEC traces for **a**) P(TFEMA) and **b**) P(TFEA) with targeted DP$_n$ = 50 synthesized *via* oxygen-tolerant photoinduced Cu-RDRP with 10 μL and 100 μL total reaction volume, respectively.

Overall, these experiments suggest that both toluene/MeOH mixture and TFE have limited headspace tolerance. The limited headspace tolerance of TFE might not be surprising given the capability of fluorinated and semi-fluorinated solvents to act as oxygen carriers.[73] Nevertheless, by eliminating the headspace, the polymerizations proceeded in a controlled manner in all attempted solvents allowing for the low volume polymerization of a wide range of materials at high conversions, as depicted in **Table 3-6**.

Table 3-6. ^{1}H NMR and SEC analysis for all the different polymers obtained through photoinduced Cu-RDRP without any type of deoxygenation and at various solvents and scales. [a]

Polymer	Scale (μL)	Solvent	DP_n	Conversion ^{1}H NMR %	$M_{n,\,th.}$ (g/mol)	$M_{n,SEC}$[b] (g/mol)	$Đ$
PMA	10	DMSO	50	99	4,400	5,000	1.11
PMA	100	TFE	50	99	4,400	5,700	1.13
PMA	100	Tol-MeOH	50	98	4,400	4,400	1.12
P(PEGA$_{480}$)	10	DMSO	20	99	9,500	9,300	1.18
P(EGA)	10	DMSO	50	99	6,700	7,300	1.17
PLA [c,d]	100	Tol-MeOH	50	75	9,200	9,400	1.19
P(*t*-BA) [c,d]	100	Tol-MeOH	50	97	6,400	7,000	1.2
PHA [d]	100	TFE	50	93	7,400	7,600	1.19
PTFEA [d]	100	TFE	50	99	7,900	8,900	1.08
PTFEMA	10	TFE	50	93	8,100	8,400	1.15

[a] In all polymerizations the volume ratio of monomer to solvent was maintained 1:1 and conversion was calculated *via* ^{1}H NMR. [b] Determined by THF SEC analysis based on DRI and expressed as molecular weight equivalents to PMMA narrow molecular weight standards. [c] Solvent ratio toluene : methanol = 4 : 1.
[d] The reaction took place in a custom-made vial insert with total capacity 100 μL.

To investigate the extent of end-group fidelity for the low volume photoinduced Cu-RDRP experiments, matrix-assisted laser desorption/ionization time of flight (MALDI-ToF) mass spectrometry was employed for the mass analysis of PMA with targeted DP_n = 25. A predominant polymer peak distribution was identified corresponding to polymer chains initiated by EBiB and terminated by the desired bromine end-group (**Figure 3-12**). This suggests that active end-groups can be maintained during polymerization, hence allowing for *in-situ* chain extensions.

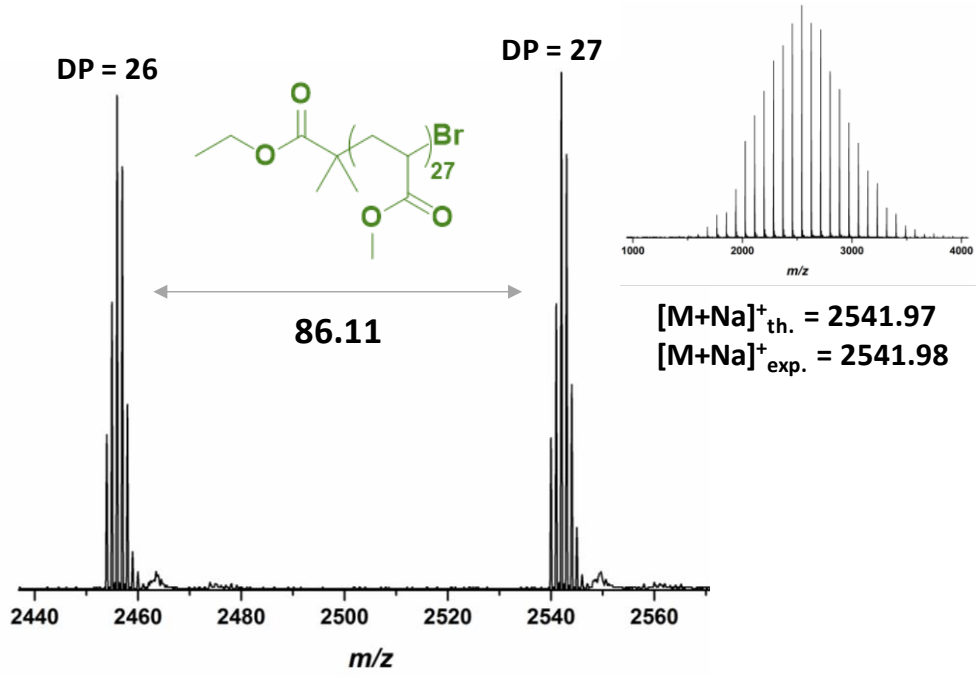

Figure 3-12. MALDI-ToF spectrum for the deoxygenation-free 10 μL PMA_{27} (targeted DP_n = 25) revealing the predominant single peak distribution and confirming MA as the monomer unit.

However, upon chain extending PMA with an aliquot of EGA, inconsistent results were obtained. In particular, the conversion of the second block was either minimal (0-10%), if any, or exhibited a significant tailing to low molecular weights indicating severe termination events. This was rather surprising since MALDI-ToF analysis showed bromine terminated polymer chains prior to chain extension (**Figure**

3-12). It was thus hypothesized that the additional oxygen (either dissolved in the second aliquot of monomer and / or added upon removal of the lid) introduced to the system *via* the addition of the second monomer was detrimental for preserving high end-group fidelity. To confirm whether this is the case, PMA with DP_n = 42 was synthesized and isolated prior to chain extension (**Scheme 3-2**, **Figure 3-31**).

PMA_{42} macroinitiator synthesis

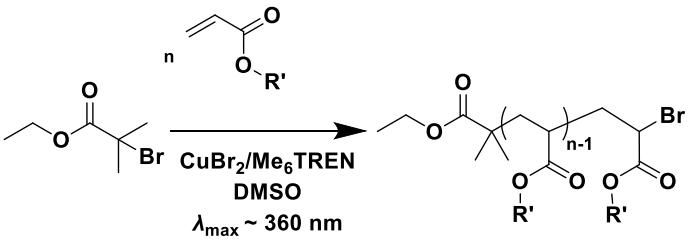

$P(MA)_{42}$–*b*-$P(EGA)_{42}$ synthesis

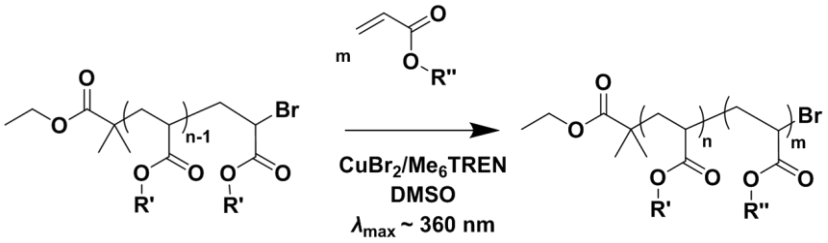

Scheme 3-2. Reaction scheme for the synthesis of **a**) the PMA_{42} macroinitiator and **b**) the PMA_{42}-*b*-$P(EGA)_{42}$ diblock copolymer *via* photoinduced Cu-RDRP in the presence of oxygen, with n = m = 42, R' = $-CH_3$, R'' = $-(CH_2)_2OCH_3$.

Upon re-subjecting the PMA_{42} macroinitiator to irradiation in a fully filled vial insert, in the presence of EGA, well-defined block copolymers of $P(MA)_{42}$-*b*-$P(EGA)_{42}$ could be obtained with the molecular weight distribution shifting to higher molecular weights and negligible tailing observed (**Figure 3-13a**). The final dispersity was ~ 1.15 and the control over the molecular weight distributions was not compromised ($M_{n,SEC}$ = 10,200 g mol^{-1}) even at near quantitative conversions (99%)

(**Figure 3-32)**. An identical chain extension experiment was also performed in the presence of significant headspace (20 μL / 200 μL). Despite the extent of the headspace, a complete shift of the macroinitiator was evident through SEC analysis ($M_{n,SEC}$ = 10,900) yielding diblock copolymers with low dispersity value ($Đ$ ~ 1.12) and high conversion (99%) (**Figure 3-13b**).

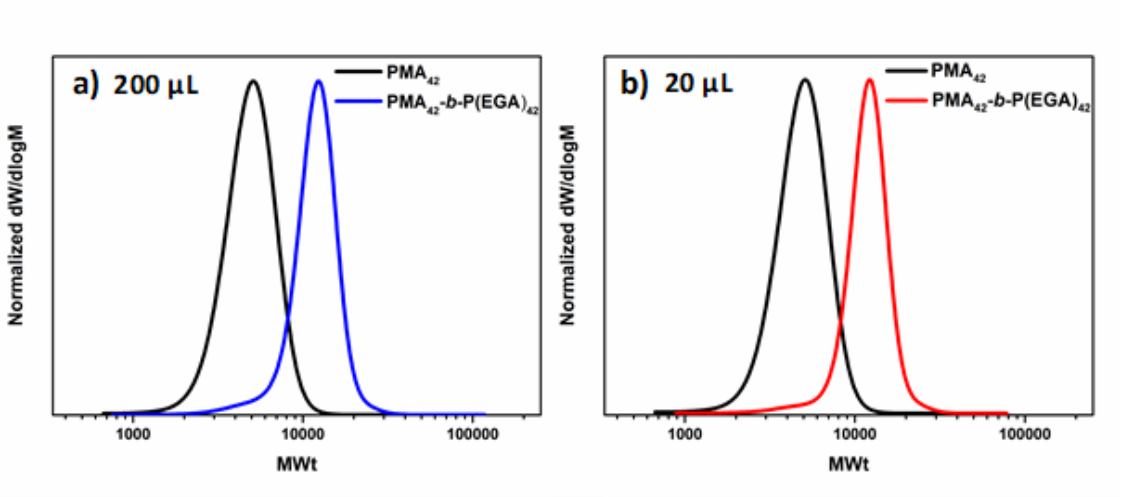

Figure 3-13. THF-SEC traces for the diblock copolymers $P(MA)_{42}$-*b*-$P(EGA)_{42}$ on a **a)** 200 μL scale (absence of headspace) and **b)** 20 μL scale (~ 180 μL of headspace) obtained after chain extension of the isolated PMA_{42} macroinitiator *via* oxygen tolerant photoinduced Cu-RDRP.

Thus, in DMSO, successful chain extensions with or without headspace can be reproducibly achieved by isolating the macroinitiator. These results indicate that, indeed a high proportion of ω-bromo functionality can be maintained and that the unsuccessful *in-situ* chain extensions can be explained by the inclusion of additional oxygen through the addition of the second monomer.

The robustness of oxygen tolerant photoinduced Cu-RDRP over the synthesis of well-defined materials on a high-multigram scale, was investigated through scaling up the polymerization of MA in DMSO (100 ml scale, 50% solids) utilizing a custom made UV box equipped with light bulbs with λ_{max} ~ 360 nm (**Figure 3-33**). However,

in all cases, the septa/lid "popped off" leading to poor monomer conversions and slightly brown colour attributed to the oxidation of the catalyst, as a result of the continuous exposure to oxygen. Due to the exothermic nature of the reaction, which was mainly revealed at higher scales, an exit needle was employed to release the increase in pressure. Although the monomer conversion increased, very high conversions were not achieved, and the dispersity was significantly higher ($Đ$ ~ 1.3) when compared to identical experiments at lower volumes.

As a result, it was envisaged that TFE would be a better alternative given the high-end-group fidelity of polymers synthesized in TFE as well as the significant thermal stability provided by this solvent. As a result, the polymerization was successfully conducted at 100 mL (**Figure 3-14c, Table 3-7**) and 250 mL (**Figure 3-34**) at high conversions (91-94%), exhibiting similar initiator efficiency with the lower volume polymerizations and low dispersity values ($Đ$ ~ 1.12) (**Table 3-7**). Additionally, the polymerization on a 0.5 L scale was successfully performed under the optimized conditions, yielding well-defined PMA with narrow molecular weight distributions ($Đ$ ~ 1.19) and high conversion (91%), thus further highlighting the versatility of the reported approach (**Figure 3-14d, Table 3-7**).

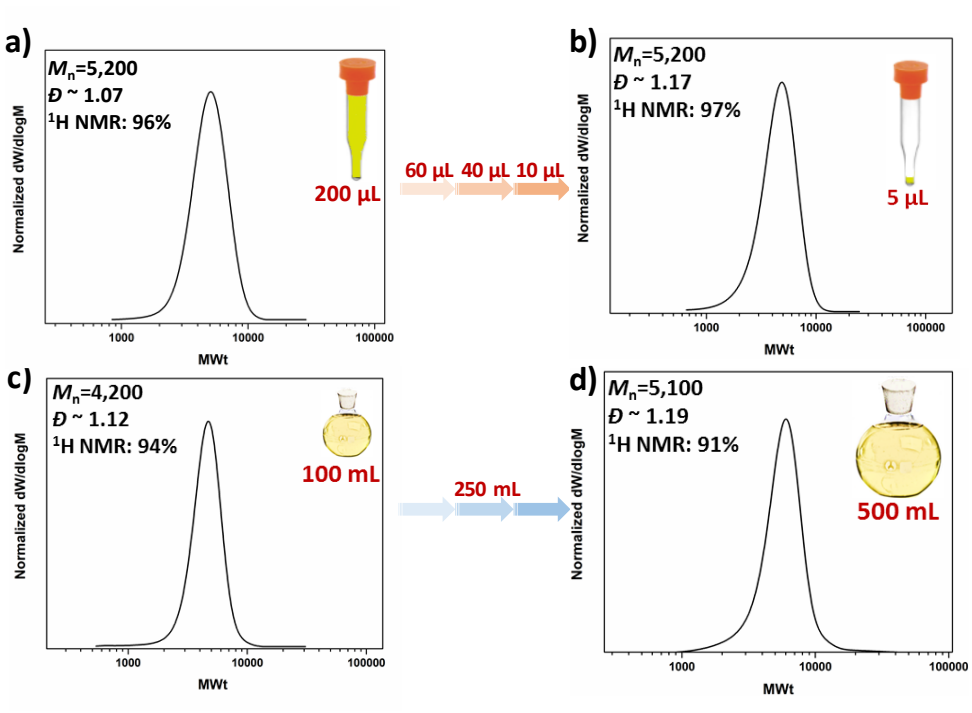

Figure 3-14. SEC traces for **a), b)** the low volume PMA_{50} and **c), d)** the high scale PMA with targeted $DP_n = 50$ synthesized *via* oxygen tolerant photoinduced Cu-RDRP.

Table 3-7. ^{1}H NMR and SEC analysis for the high scale oxygen tolerant photoinduced Cu-RDRP of MA with targeted $DP_n = 50$ [a]

Scale	Conversion (%)	$M_{n,\,th.}$ (g mol^{-1})	$M_{n,\,SEC}$ [b] (g mol^{-1})	Đ
100 mL	94	4200	4200	1.12
250 mL	91	4100	4300	1.10
500 mL	91	4100	5100	1.19

[a] In all polymerizations the volume ratio of monomer to solvent was maintained 1:1 and conversion was calculated *via* ^{1}H NMR. [b] Determined by THF SEC analysis based on DRI and expressed as molecular weight equivalents to PMMA narrow molecular weight standards.

3.3 Insights into the oxygen tolerance mechanism

In order to investigate the fate of the dissolved oxygen in the photoinduced Cu-RDRP system an oxygen probe was employed for the *in-situ* [O_2] monitoring. Under conditions identical to the polymerization solution ([M]:[I]:[Cu(II)Br_2]:[L] = [50]:[1]:[0.02]:[0.12]) and upon UV irradiation (λ_{max} ~ 360 nm), complete oxygen consumption was observed in ~ 5 min (Solution 1) (**Figure 3-15**). This rapid oxygen consumption can be potentially attributed to the reduction of Cu(II)Br_2 (by an excess of free amine) to active species (Cu(I) and/or Cu(0)). The active species can then consume oxygen *via* two different pathways. In particular, the active species can either react directly with oxygen or abstract the bromine from the initiator leading to the generation of initiating radicals which can then react with oxygen.

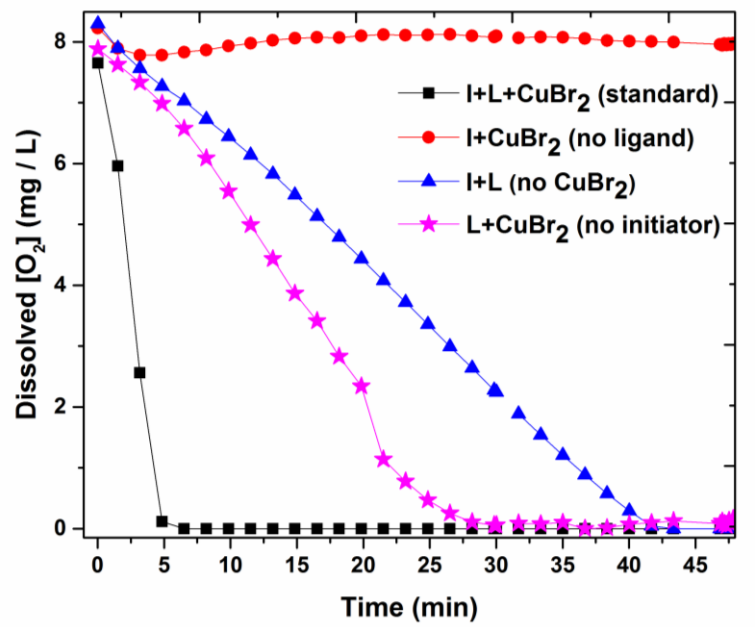

Figure 3-15.Graphical illustration of the dissolved oxygen consumption over time for the standard system (solution 1) and the role of the polymerization components on oxygen consumption.

In order to further investigate, and verify this hypothesis, the contribution of the copper source (Cu(II)Br_2), the ligand (Me_6Tren) and the initiator (EBiB) on the evolution of oxygen consumption was monitored individually. Initially, the same polymerization mixture (Solution 1) was investigated in the absence of Cu(II)Br_2. Interestingly, when only initiator and ligand were present, the oxygen consumption was decelerated to ~ 45 min, thus verifying the importance of Cu(II)Br_2 to enhance the rate of oxygen consumption. In addition, experiments where the concentration of Cu(II)Br_2 was altered were also performed (**Figure 3-16**).

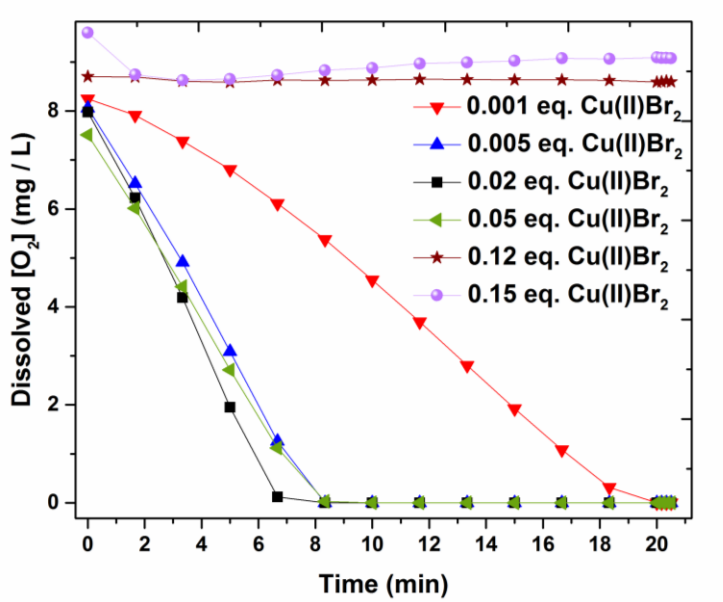

Figure 3-16. Graphical illustration of the dissolved oxygen consumption over time when different Cu(II)Br_2 concentrations were applied.

At very low Cu(II)Br_2 concentration (0.001 equiv. with respect to initiator), the oxygen consumption was completed after ~ 20 min. This was attributed to the slow generation of active species which can then lead to oxygen consumption. However, at higher amounts of Cu(II)Br_2 (0.005-0.05 equiv.) little, if any, differences in the rate of oxygen consumption were observed (~ 6 min). This suggests that upon sufficient generation of active species, the oxygen consumption can proceed at the maximum

rate. It should also be noted that when the concentration of Cu(II)Br_2 either exceeded or equalled the ligand concentration, no oxygen consumption was observed. This is to be expected as according to the literature, excess of free amine is required to mediate the reduction of the copper complex.[74,75]

Subsequently, the role of ligand (Me_6Tren) was examined (**Figure 3-17**). In the absence of ligand, no oxygen consumption was evident within a 60-minute scale, suggesting lack of generated radicals under these conditions. A similar trend was observed when less ligand equivalents than Cu(II)Br_2 (0.01 and 0.02 with respect to initiator) were employed validating previous results, in which an excess of ligand is essential to consume oxygen.

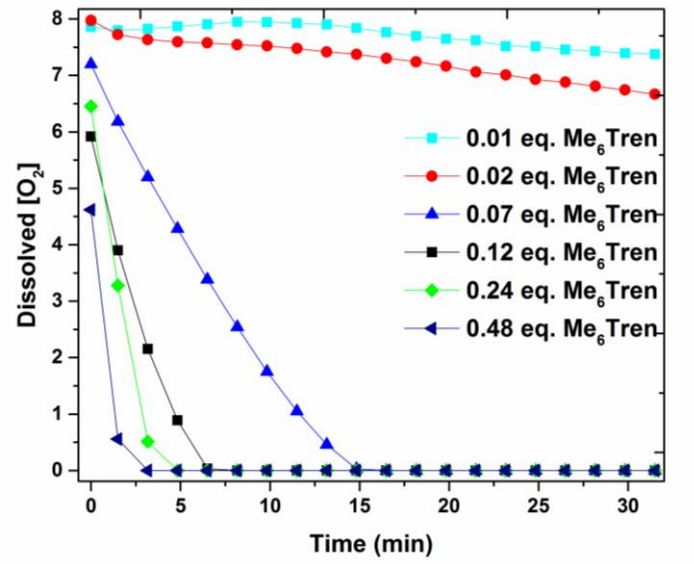

Figure 3-17. Graphical illustration of the dissolved oxygen consumption over time when different ligand concentrations were applied.

However, at higher ligand loadings (0.07 with respect to initiator), oxygen was fully consumed in ~ 15 min. A further gradual increase of the ligand concentration led to even faster oxygen consumption (as fast as ~ 3 min). It can thus be concluded that (i) an excess of ligand is necessary to consume the oxygen and (ii) more ligand leads

to the generation of more active species which can then directly or indirectly consume the oxygen.

Finally, *in-situ* [O_2] monitoring of Solution 1 in the absence of initiator was also conducted. When only Cu(II)Br_2 and ligand were present, the second fastest oxygen consumption rate (with the first one being the Solution 1 with all the components included) was monitored at ~ 27 min (**Figure 3-15**). This observation verifies the initial hypothesis that the copper complex is primarily responsible for the oxygen consumption. Moreover, by altering the initiator equivalents (**Figure 3-18**), it can be concluded that when sufficient amount is present, the oxygen consumption remains equally fast (~ 5 min) regardless of the initiator concentration (0.25, 0.5 and 1 equivalents of initiator). This is a reasonable observation since the complex is the main factor that determines the oxygen consumption and as a result, the same amount of active species generated will only react with a constant amount of initiator, even if further excess of initiator is available. Interestingly, at extremely high initiator loadings (20 equiv. or ~ 25 % *v/v*), slower oxygen consumption was observed (~ 12 min) which is likely due to the change of the reaction medium.

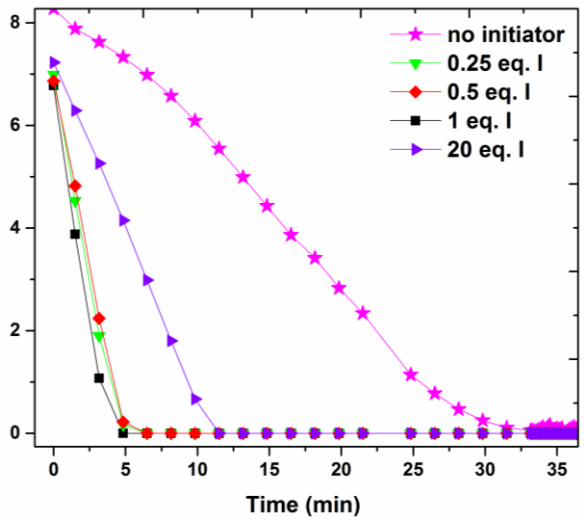

Figure 3-18. Graphical illustration of the dissolved oxygen consumption over time when different initiator concentrations were applied.

In summary, from these experiments it can be inferred that the combination of $Cu(II)Br_2$, ligand and initiator synergistically contribute to the oxygen consumption (~ 5 min). Upon exclusion of initiator, the second fastest oxygen consumption is being monitored (~ 27 min) which can be predominantly attributed to the reduction of the copper complex into active species. Therefore, the presence of initiator is important to accelerate the rate of consumption suggesting that the initiating radicals react with oxygen more rapidly than the active species. At the same time, in the absence of $Cu(II)Br_2$, an even slower oxygen consumption is observed (~ 45 min) which implies that the initiator and the ligand in the absence of copper, are less significant than the complex for the process of oxygen consumption. Although slower, this oxygen consumption can be attributed to either the light-induced C-Br bond scission of the initiator (generating initiating/propagating radicals) or by the formation of a radical cation from the ligand upon irradiation.[63,75] Finally, since no oxygen consumption is evident in the absence of ligand, it is hypothesized that either the C-Br cleavage does not occur at large extent or that the presence of the deactivator is somehow hindering the cleavage even in the absence of ligand (*i.e*. by delivering the bromine back to the initiator).

3.4 Conclusion

In this chapter, the development of photoinduced Cu-RDRP as an *oxygen tolerant* and multi-scale strategy is presented and discussed. Without conventional deoxygenation and in the absence of externally added reducing agents or oxygen scavengers, good control over the polymerization and high-end group fidelity are maintained, yielding well-defined homo- and block co-polymers for a range of monomers with different hydrophobicity. The facile and efficient nature of this approach is applicable to a big range of polymerization scales, from as low as 5 μL, up to 0.5 L. Furthermore, semi-fluorinated (meth)acrylates are polymerized *via* this simplified methodology, providing access to a range of polymer families. Furthermore, the mechanism of oxygen consumption and the role of the polymerization reagents in this system is elucidated *via* the employment of an oxygen probe. The proposed methodology renders the oxygen-tolerant photoinduced Cu-RDRP a multi-applicable strategy for the synthesis of a range of materials, on different scales with undemanding setup.

3.5 Experimental Section

3.5.1 Materials

Methyl acrylate (MA, 99%), *n*-butyl acrylate (*n*-BA, ≥99%), *tert*-butyl acrylate (*t*-BA, 98%), ethylene glycol methyl ether acrylate (EGA, 98%), hexyl acrylate (HA, 98%), lauryl acrylate (LA, 90%) 2,2,2-trifluoroethyl acrylate (TFEA, 99%), ethyl α-bromoisobutyrate (EBiB, 98%), copper(II) bromide (Cu(II)Br_2, 99%) and all the solvents were purchased from Sigma-Aldrich and used as received. 2,2,2-trifluoroethyl methacrylate (TFEMA) was purchased from Cornelius and used as received. Tris-(2-(dimethylamino)ethyl)amine (Me_6Tren) was synthesized and stored in the fridge.

3.5.2 Instrumentation and Characterization techniques

Proton Nuclear Magnetic Resonance (^{1}H NMR)

^{1}H Nuclear Magnetic Resonance. ^{1}H NMR spectra were recorded on Bruker DPX-300 or DPX-400 spectrometers in deuterated chloroform ($CDCl_3$) or deuterium oxide (D_2O) obtained from Sigma-Aldrich. Chemical shifts are given in ppm downfield from the internal standard tetramethylsilane. Monomer conversions were determined *via* ^{1}H NMR spectroscopy by comparing the integrals of monomeric vinyl protons to polymer signals.

Size Exclusion Chromatography (SEC)

THF. SEC measurements were carried out with an Agilent 390-LC MDS instrument equipped with differential refractive index (DRI), viscometry (VS), dual angle light scatter (LS) and dual wavelength UV detectors. The system was equipped

with 2 x PLgel Mixed C columns (300 x 7.5 mm) and a PLgel 5 µm guard column. The eluent was THF with 2 % TEA (triethylamine) and 0.01 % BHT (butylated hydroxytoluene) additives. Samples were run at 1 mL / min at 30 ^{o}C. Poly(methyl methacrylate) and polystyrene standards (Agilent EasyVials) were used to create a third order calibration between 550 g mol^{-1} and 1,568,000 g mol^{-1}. Analyte samples were filtered through a GVHP membrane with 0.22 μm pore size before injection. Respectively, experimental molar mass ($M_{n,SEC}$) and dispersity ($Đ$) values of synthesized polymers were determined by conventional calibration using Agilent GPC/SEC software (version A.02.01).

Matrix assisted laser desorption-ionization time-of-flight mass spectrometry (MALDI-ToF-MS).

MALDI-ToF-MS measurements were conducted using a Bruker Daltonics Ultraflex II MALDI-ToF mass spectrometer, equipped with a nitrogen laser delivering 2 ns laser pulses at 337 nm with positive ion ToF detection performed using an accelerating voltage of 25 kV. Solutions in tetrahydrofuran (THF) (50 µL) of *trans*-2-[3-(4-*tert*-butylphenyl)-2-methyl-2-propyldene] malononitrile (DCTB) as a matrix (saturated solution), sodium iodide as the cationization agent (1.0 mg mL^{-1}) and sample (1.0 mg mL^{-1}) were mixed, and 0.7 µL of the mixture was applied to the target plate. Spectra were recorded in reflectron mode calibrated with poly(ethylene glycol) monomethyl ether (PEG-Me) 1900 kDa.

Oxygen Probe. Pocket Oxygen Meter - FireStingGO2 (Pyro Science)**:** The solvent-resistant oxygen probe OXSOLV measures oxygen partial pressure in most polar and nonpolar solvents. It is based on optical detection principles (REDFLASH

technology) and can be used both in pure and complex organic solvents. The fiber-optic oxygen sensor tip is covered with a stainless-steel tube 1.5 mm in diameter and 150 (or 40) mm in length. The analysis of the data was conducted with the FireStingGO2 Manager software.

UV Source. A UV nail gel curing lamp (λ_{max} ~ 365 nm) with four 9-Watt bulbs was used.

3.5.3 Experimental procedures

Typical 8 mL scale deoxygenation-free photoinduced Cu-RDRP of MA (targeted DP_n = 50) in DMSO

An 8 mL total volume capacity glass vial was charged with Cu(II)Br_2 (4.0 mg, 0.02 eq.) and DMSO (4 mL). Me_6Tren (28.3 μL, 0.12 eq.) was added through a microliter syringe and the solution was vortexed for ~ 1 minute. MA (4 mL, 50 eq.), EBiB (129 μL, 1 eq.) and a stirrer bar were added, and the vial was septum-sealed. The polymerization was allowed to commence for 2 hours under a UV nail lamp (λmax ~ 360 nm). Conversions were measured using ^{1}H NMR in $CDCl_3$ and SEC analysis was conducted in THF after the samples having been passed through neutral alumina for the removal of copper salts.

Typical deoxygenation-free photoinduced Cu-RDRP of MA (targeted DP_n = 50) in DMSO or TFE or toluene-MeOH

A stock solution of Cu(II)Br_2 (1.0 mg, 0.02 eq.), Me_6Tren (9.5 μL, 0.12 eq.) and the solvent (1 mL of DMSO or 1 mL of TFE or toluene (0.8 mL)-MeOH (0.2 mL)) was prepared. The solution was vortexed for ~ 1min (or sonicated for > 10 min when TFE was used) and MA (1 mL, 50 eq.) and EBiB (32 μL, 1 eq.) were added. Aliquots of 200 μL- 5μL were charged in vial inserts and sealed with NMR-tube lids. The

polymerization reactions were placed for 2 hours under a UV nail lamp (λ_{max} ~ 360 nm) and conversions were measured though ^{1}H NMR in $CDCl_3$. SEC analysis was conducted in THF after the samples having been passed through neutral alumina for the removal of copper salts. For targeted DP_n = 100 the reaction was left for 4 hours (99% conversion), 12 hours for DP_n = 200 (92% conversion) and for DP_n = 400 the polymerization was left to commence overnight (82% conversion).

Typical deoxygenation-free photoinduced Cu-mediated RDRP of (*t*-BA) with targeted DP_n = 50 in toluene-MeOH (4 : 1).

A stock solution of Cu(II)Br_2 (0.61 mg, 0.02 eq.), toluene (0.8 mL)-MeOH (0.2 mL) and Me_6Tren (4.4 μL, 0.12 eq.) was prepared and vortexed for ~ 1 minute. *t*-BA (1 mL, 50 eq.) and EBiB (20 μL, 1 eq.) were added and aliquots of 100 μL and 10 μL were charged in vial inserts and sealed with NMR-tube lids. The polymerizations were allowed to commence for 10 hours under a UV lamp (λ_{max} ~ 360 nm). Conversions were measured using ^{1}H NMR in $CDCl_3$ and SEC analysis was conducted in THF after the samples having been passed through neutral alumina for the removal of copper salts.

Typical deoxygenation-free photoinduced Cu-mediated RDRP of (HA) with targeted DP_n = 50 in TFE

A stock solution of Cu(II)Br_2 (0.51 mg, 0.02 eq.), TFE (1 mL) and Me_6Tren (3.7 μL, 0.12 eq.) was prepared and sonicated for >10 minutes. HA (1 mL, 50 eq.) and EBiB (17 μL, 1 eq.) were added in the solution and aliquots of 100 μL and 10 μL were charged in vial inserts and sealed with NMR-tube lids. The polymerizations were allowed to commence overnight under a UV lamp (λ_{max} ~ 360 nm). Conversions were measured using ^{1}H NMR in $CDCl_3$ and SEC analysis was conducted in THF after the samples having been passed through neutral alumina for the removal of copper salts.

Typical deoxygenation-free photoinduced Cu-mediated RDRP of EGA with targeted DP_n = 50 in DMSO

A stock solution of Cu(II)Br_2 (0.675 mg, 0.02 eq.), DMSO (1 mL) and Me_6Tren (5 µL, 0.12 eq.) was prepared and vortexed for ~ 1 min. EGA (1 mL, 50 eq.) and EBiB (22.8 µL, 1 eq.) were added in the solution and aliquots of 100 µL and 10 µL were charged in vial inserts and sealed with NMR-tube lids. The polymerizations were allowed to commence for 2 hours under a UV lamp (λ_{max} ~ 360 nm). Conversions were measured using ^{1}H NMR in $CDCl_3$ and SEC analysis was conducted in THF after the samples having been passed through neutral alumina for the removal of copper salts.

Typical deoxygenation-free photoinduced Cu-mediated RDRP of $PEGA_{480}$ with targeted DP_n = 20 in DMSO

A stock solution of Cu(II)Br_2 (0.5 mg, 0.02 eq.), DMSO (1 mL) and Me_6Tren (3.7 µL, 0.12 eq.) was prepared and vortexed for ~ 1 minute. $PEGA_{480}$ (1 mL, 20 eq.) and EBiB (16.8 µL, 1 eq.) were added in the solution and aliquots of 100 µL and 10 µL were charged in vial inserts and sealed with NMR-tube lids. The polymerizations were allowed to commence for 2 hours under a UV lamp (λ_{max} ~ 360 nm). Conversions were measured using ^{1}H NMR in D_2O and SEC analysis was conducted in THF after the samples having been passed through neutral alumina for the removal of copper salts.

Typical photoinduced Cu-mediated RDRP of TFEA with targeted DP_n = 50 in TFE

A stock solution of Cu(II)Br_2 (0.7 mg, 0.02 eq.), TFE (1 mL) and Me_6Tren (5 µL, 0.12 eq.) was prepared and sonicated for >10 minutes. TFEA (1 mL, 50 eq.) and EBiB (23 µL, 1 eq.) were added in the solution and aliquots of 100 µL and 10 µL were charged in vial inserts and sealed with NMR-tube lids. The polymerizations were allowed to commence for 24 hours under a UV lamp (λ_{max} ~ 360 nm). Conversions were measured

using ^{1}H NMR in $CDCl_3$ and SEC analysis was conducted in THF after the samples having been passed through neutral alumina for the removal of copper salts.

Typical photoinduced Cu-mediated RDRP of TFEMA with targeted DP_n = 50 in TFE

A stock solution of Cu(II)Br_2 (0.63 mg, 0.02 eq.), TFE (1 mL) and Me_6Tren (4.5 μL, 0.12 eq.) was prepared and sonicated for >10 minutes. TFEMA (1 mL, 50 eq.) and MBPA (22 μL, 1 eq.) were added in the solution and aliquots of 100 μL and 10 μL were charged in vial inserts and sealed with NMR-tube lids. The polymerizations were allowed to commence for 19 hours under a UV lamp (λ_{max} ~ 360 nm). Conversions were measured using ^{1}H NMR in $CDCl_3$ and SEC analysis was conducted in THF after the samples having been passed through neutral alumina for the removal of copper salts.

Typical photoinduced Cu-mediated RDRP of PMA macroinitiator with DP_n = 42 in DMSO

MA (12 mL or 11.46 g, 50 eq.), EBiB (0.391 mL, 1 eq.), Cu(II)Br_2 (11.9 mg, 0.02 eq.) and DMSO (12 mL) were added to a septum sealed vial and the mixture was subsequently deoxygenated by bubbling with nitrogen for 15 minutes. Me_6Tren (86 μL, 0.12 eq.) was then introduced in the vial *via* a gas-tight syringe and the polymerization was allowed to commence under UV irradiation for 45 minutes. SEC analysis was conducted in THF after the sample having been passed through neutral alumina for the removal of dissolved copper salts. The polymer was isolated *via* three precipitations in MeOH:H_2O (70% MeOH) and dried under vacuum. The degree of polymerization of the PMA was calculated by ^{1}H NMR in $CDCl_3$.

Typical chain extension of PMA with EGA *via* photoinduced Cu-mediated RDRP

A stock solution of $CuBr_2$ (2.48 mg, 0.02 eq.) and Me_6Tren (17.8 µL, 0.12 eq.) was prepared in DMSO (1 mL). 100 µL of this catalyst solution (0.02 equiv. $CuBr_2$ and 0.12 equiv. Me_6Tren), PMA macroinitiator (0.25 g, DP_n = 42, 1 eq.) dissolved in DMSO (0.5 mL) and EGA (0.357 mL, 42 eq.) were mixed and a 200 µL aliquot of this solution was added to a capped vial insert prior to UV irradiation for 7 hours. Conversions were measured using ^1H NMR in $CDCl_3$ and SEC analysis was conducted in THF after the samples having been passed through neutral alumina for the removal of copper salts.

High-scale deoxygenation-free photoinduced Cu-mediated RDRP of MA with targeted DP_n = 50 in DMSO or TFE

A 0.5 L round bottom flask (RBF) was charged with $Cu(II)Br_2$ (250 mg, 0.02 eq.) and DMSO or TFE (250 mL). Me_6Tren (1.769 mL, 0.12 eq.) was added and the solution was sonicated for ~ 15 minutes. MA (250 mL, 50 eq.), EBiB (8.063 mL, 1 eq.) and stirrer bar were added. The RBF was septum-sealed and an exit needle was added and maintained throughout the whole duration of the polymerization in order to facilitate gas-pressure release. The polymerization was allowed to commence overnight under a custom-made UV box with λ_{max} ~ 360 nm. Conversions were measured using ^1H NMR in $CDCl_3$ and SEC analysis was conducted in THF after the samples having been passed through neutral alumina for the removal of copper salts.

3.5.4 Supplementary Figures & Characterization

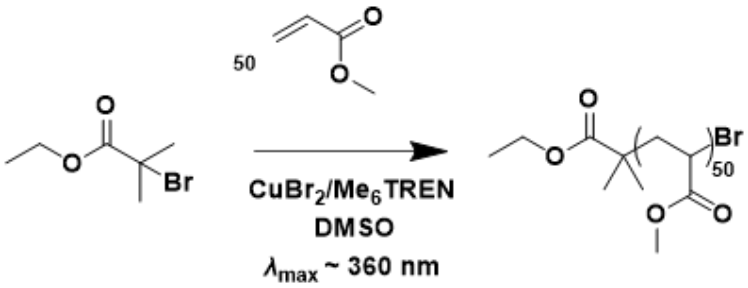

Scheme 3- 3. Reaction scheme for the oxygen tolerant photoinduced Cu-RDRP of MA with targeted DP_n = 50. Conditions: [MA]:[EBiB]:[$CuBr_2$]:[Me_6Tren] = [50]:[1]:[0.02]:[0.12] in 50 % v/v DMSO, under a UV nail lamp with broad band emission and λ_{max} ~ 360 nm.

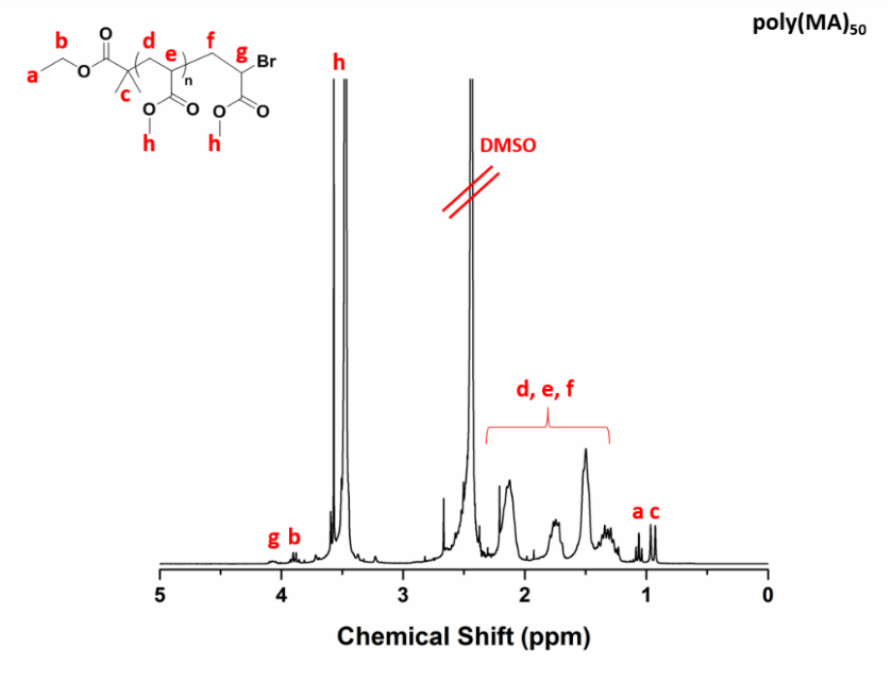

Figure 3- 19. ^{1}H NMR spectrum in $CDCl_3$ for PMA with targeted DP_n = 50 synthesized *via* low volume oxygen tolerant photoinduced Cu-mediated RDRP with [MA]:[EBiB]:[$CuBr_2$]:[Me_6Tren] = [50]:[1]:[0.02]:[0.12] in 50 % *v/v* DMSO under a UV nail lamp with broad band emission and λ_{max} ~ 360 nm.

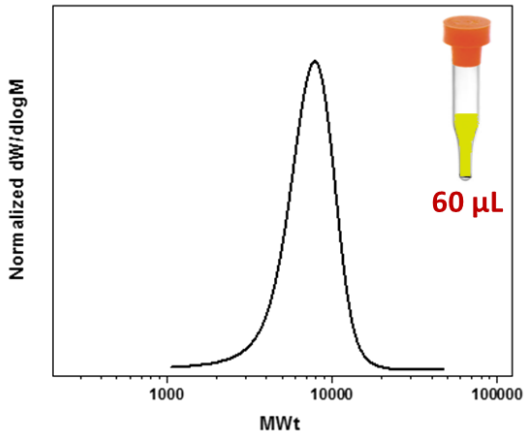

Figure 3-20. THF-SEC trace of PMA with targeted DP_n = 50 synthesized *via* oxygen tolerant photoinduced Cu-mediated RDRP in 60 µL (total reaction volume).

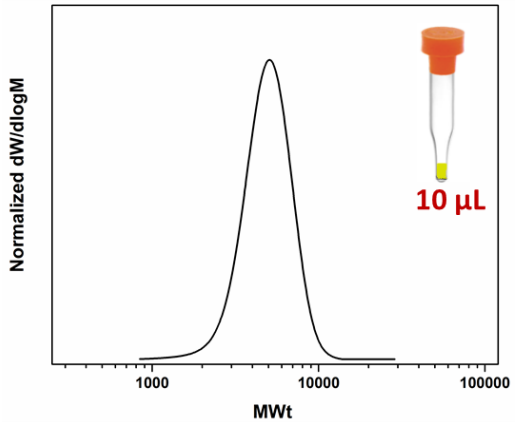

Figure 3-21.THF-SEC trace of PMA with targeted DP_n = 50 synthesized *via* oxygen tolerant photoinduced Cu-mediated RDRP in 10 µL (total reaction volume).

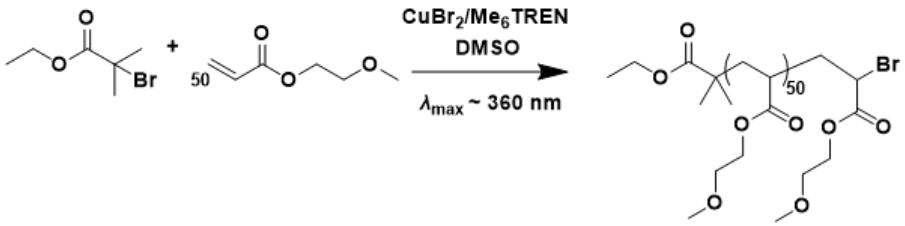

Scheme 3-4. Reaction scheme for the oxygen tolerant photoinduced Cu-RDRP of EGA with targeted DP_n = 50. Conditions: [EGA]:[EBiB]:[$CuBr_2$]:[Me_6Tren] = [50]:[1]:[0.02]:[0.12] in 50 % *v/v* DMSO, under a UV nail lamp with broad band emission and λ_{max} ~ 360 nm.

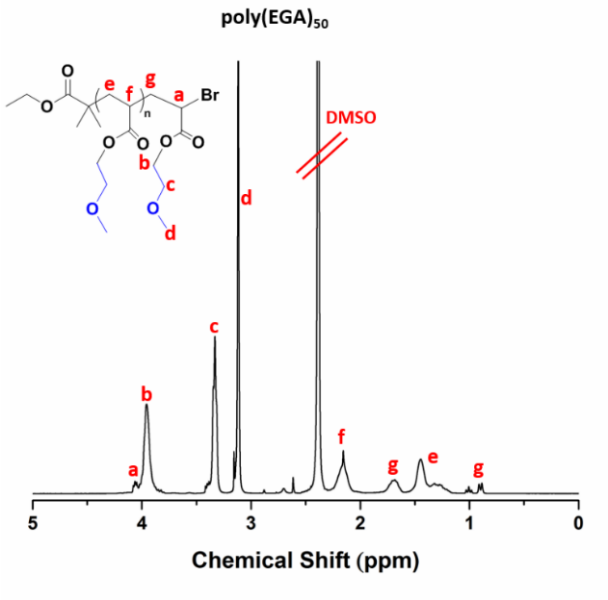

Figure 3-22. ^{1}H NMR spectrum in $CDCl_3$ for P(EGA) with targeted DP_n = 50 synthesized *via* oxygen tolerant photoinduced Cu-mediated RDRP on a 10 µL scale with [EGA]:[EBiB]:[$CuBr_2$]:[Me_6Tren] = [50]:[1]:[0.02]:[0.12] in 50 % *v/v* DMSO.

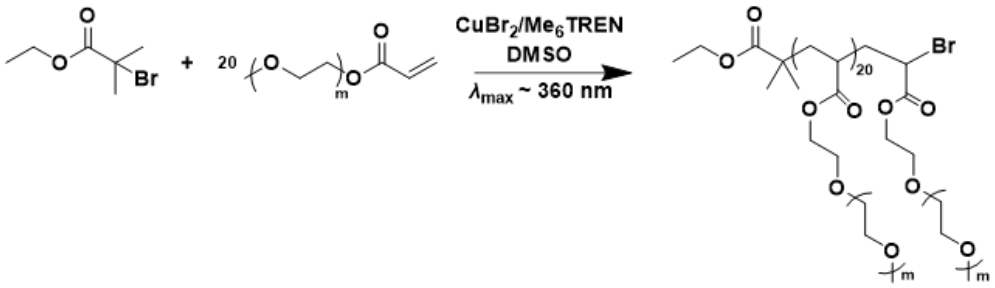

Scheme 3-5. Reaction scheme for the oxygen tolerant photoinduced Cu-RDRP of $PEGA_{480}$ with targeted DP_n = 50. Conditions: [$PEGA_{480}$]:[EBiB]:[$CuBr_2$]:[Me_6Tren] = [20]:[1]:[0.02]:[0.12] in 50 % *v/v* DMSO, under a UV nail lamp with broad band emission and λ_{max} ~ 360 nm.

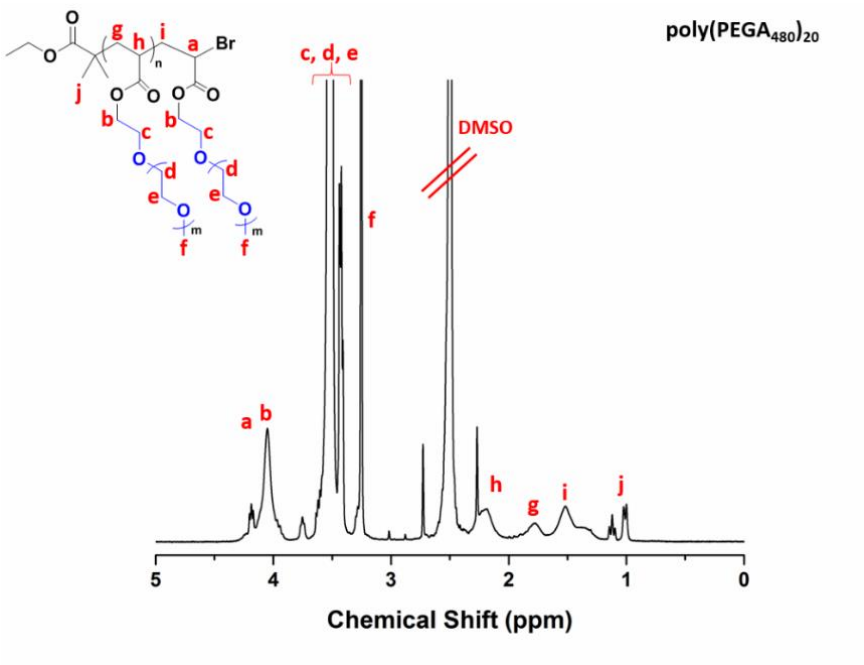

Figure 3-23. ^{1}H NMR spectrum in D_2O for P(PEGA$_{480}$) with targeted DP$_n$ = 20 synthesized *via* oxygen tolerant photoinduced Cu-mediated RDRP of on a 10 µL scale with [PEGA$_{480}$]:[EBiB]:[$CuBr_2$]:[Me_6Tren] = [20]:[1]:[0.02]:[0.12] in 50 % *v/v* DMSO.

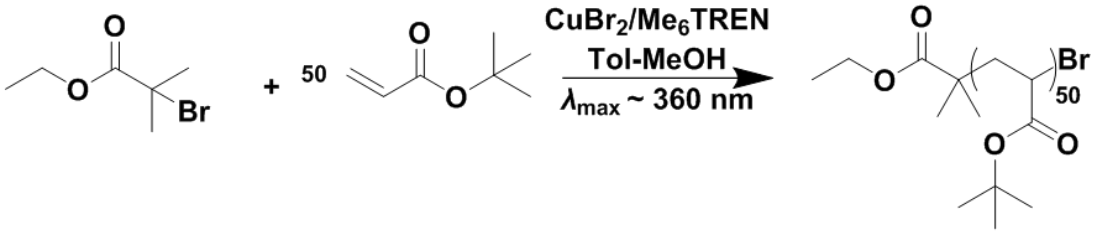

Scheme 3-6. Reaction scheme for the oxygen tolerant photoinduced Cu-RDRP of *t*-BA with targeted DP$_n$ = 50. Conditions: [*t*-BA]:[EBiB]:[$CuBr_2$]:[Me_6Tren] = [50]:[1]:[0.02]:[0.12] in 50 % *v/v* toluene-methanol (4:1) (or DMF, DMSO), under a UV nail lamp with broad band emission and λ_{max} ~ 360 nm.

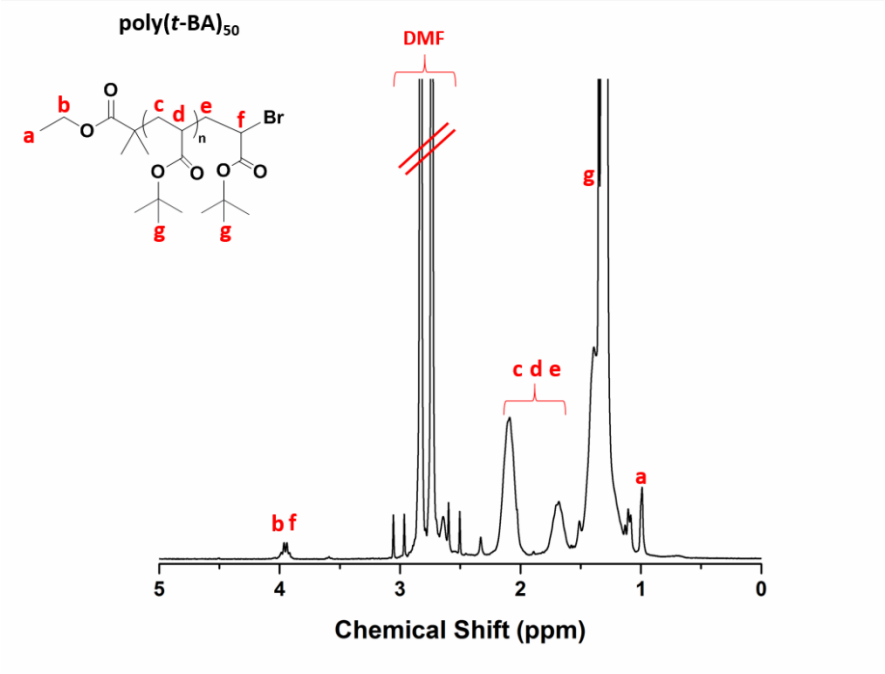

Figure 3-24. ^{1}H NMR spectrum in $CDCl_3$ for P(*t*-BA) with targeted DP_n = 50 synthesized *via* oxygen tolerant photoinduced Cu-mediated RDRP of on a 100 µL scale with [*t*-BA]:[EBiB]:[$CuBr_2$]:[Me_6Tren] = [50]:[1]:[0.02]:[0.12] in 50 % *v/v* DMF.

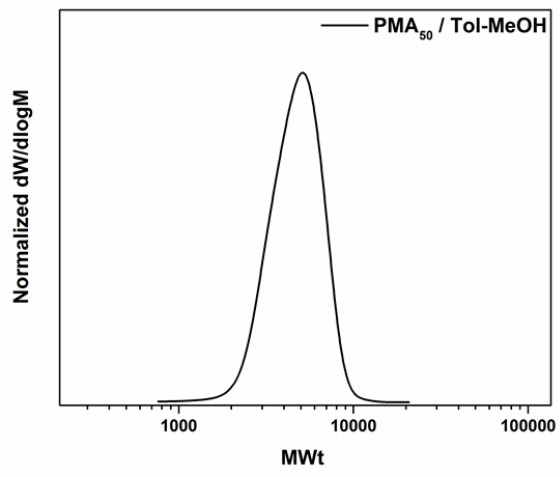

Figure 3-25. SEC trace for PMA_{50} synthesized on a 100 µL scale *via* oxygen tolerant photoinduced Cu-RDRP utilizing MeOH-Toluene (1:4) as solvent system using a UV lamp with broad band emission and λ_{max} ~ 360 nm.

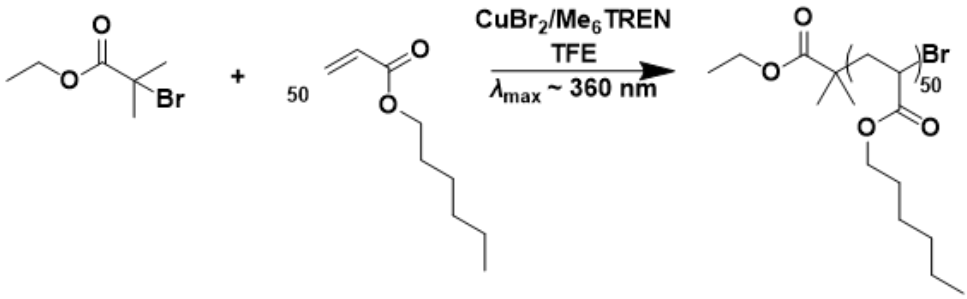

Scheme 3-7. Reaction scheme for the oxygen tolerant photoinduced Cu-RDRP of HA with targeted DP_n = 50. Conditions: [HA]:[EBiB]:[$CuBr_2$]:[Me_6Tren] = [50]:[1]:[0.02]:[0.12] in 50 % *v/v* TFE, under a UV nail lamp with broad band emission and λ_{max} ~ 360 nm.

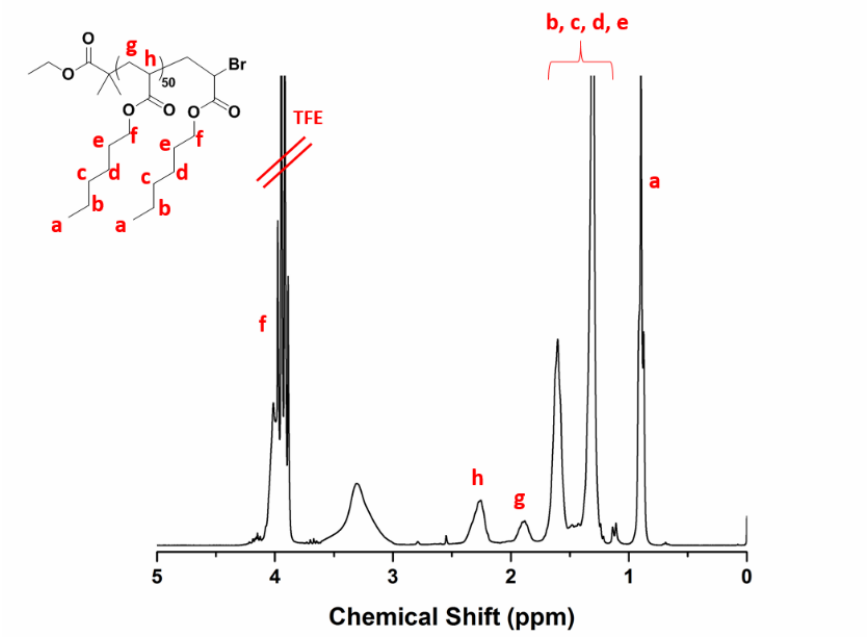

Figure 3-26. ^{1}H NMR spectrum in $CDCl_3$ for PHA with targeted DP_n = 50 synthesized *via* oxygen tolerant photoinduced Cu-RDRP on a 100 µL scale with [HA]:[EBiB]:[$CuBr_2$]:[Me_6Tren] = [50]:[1]:[0.02]:[0.12] in 50 % *v/v* TFE.

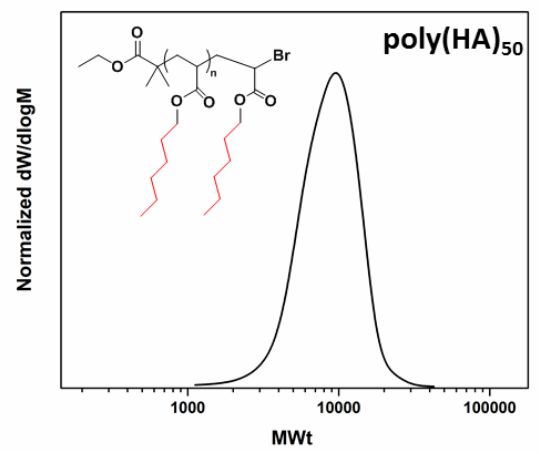

Figure 3-27. THF-SEC trace for PHA with targeted DP_n = 50 synthesized on a 100 µL scale *via* oxygen tolerant photoinduced Cu-RDRP in TFE using a UV lamp with broad band emission and λ_{max} ~ 360 nm.

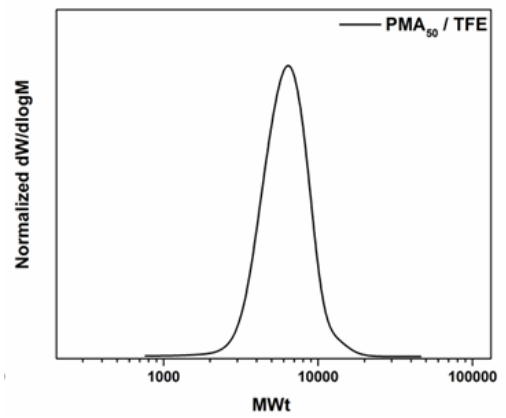

Figure 3-28. SEC trace for PMA with targeted DP_n = 50 synthesized on a 100/100 µL scale *via* oxygen tolerant photoinduced Cu-RDRP in TFE using a UV lamp with broad band emission and λ_{max} ~ 360 nm.

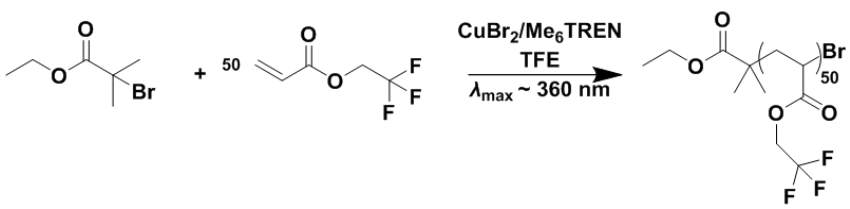

Scheme 3-8. Reaction scheme for the oxygen tolerant photoinduced Cu-mediated RDRP of TFEA on a 100 µL scale with [TFEA]:[EBiB]:[$CuBr_2$]:[Me_6Tren] =

[50]:[1]:[0.02]:[0.12] in 50 % v/v TFE using a UV lamp with broad band emission and λ_{max} ~ 360 nm.

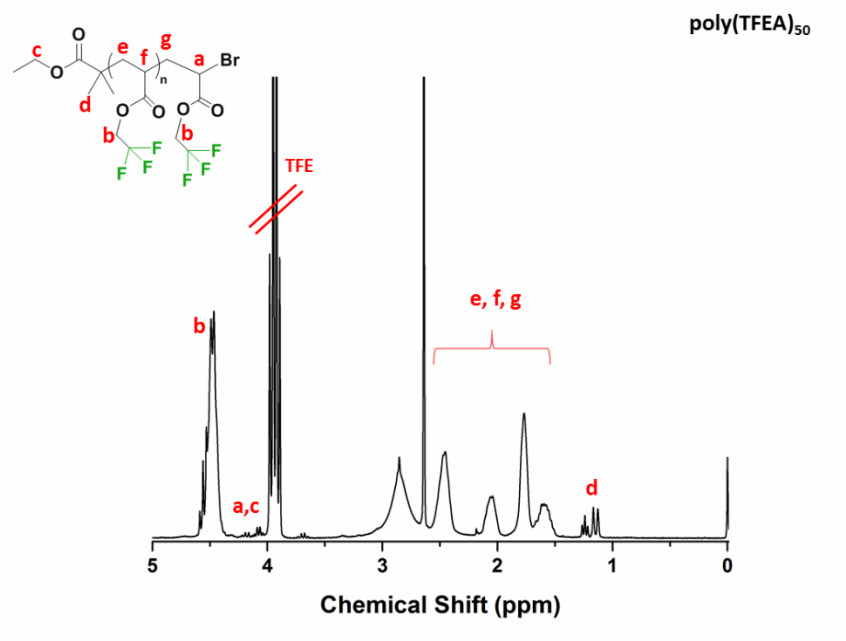

Figure 3-29. ^{1}H NMR spectrum in $CDCl_3$ for PTFEA with targeted DP_n = 50 synthesized *via* oxygen tolerant photoinduced Cu-RDRP on a 100 µL scale with [TFEA]:[EBiB]:[$CuBr_2$]:[Me_6Tren] = [50]:[1]:[0.02]:[0.12] in 50 % *v/v* TFE.

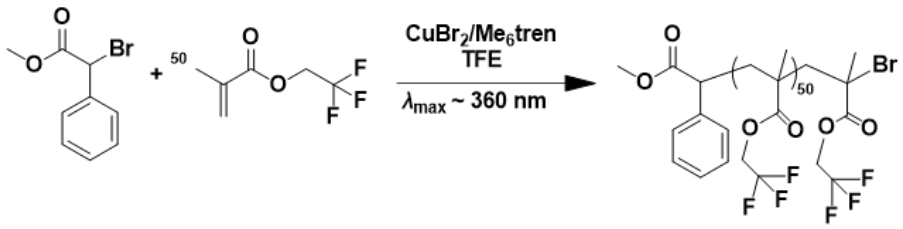

Scheme 3-9. Reaction scheme for the oxygen tolerant photoinduced Cu-mediated RDRP of TFEMA on a 10 µL scale with [TFEA]:[EBiB]:[$CuBr_2$]:[Me_6Tren] = [50]:[1]:[0.02]:[0.12] in 50 % v/v TFE using a UV lamp with broad band emission and λ_{max} ~ 360 nm.

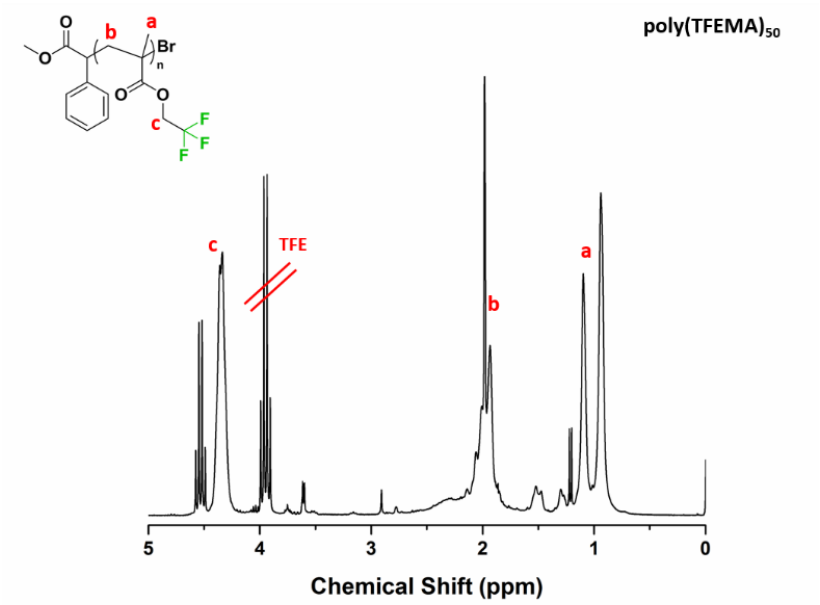

Figure 3-30. ^{1}H NMR spectrum in $CDCl_3$ for PTFEMA with targeted DP_n = 50 synthesized *via* oxygen tolerant photoinduced Cu-RDRP on a 10 µL scale with [TFEMA]:[EBiB]:[$CuBr_2$]:[Me_6Tren] = [50]:[1]:[0.02]:[0.12] in 50 % *v/v* TFE.

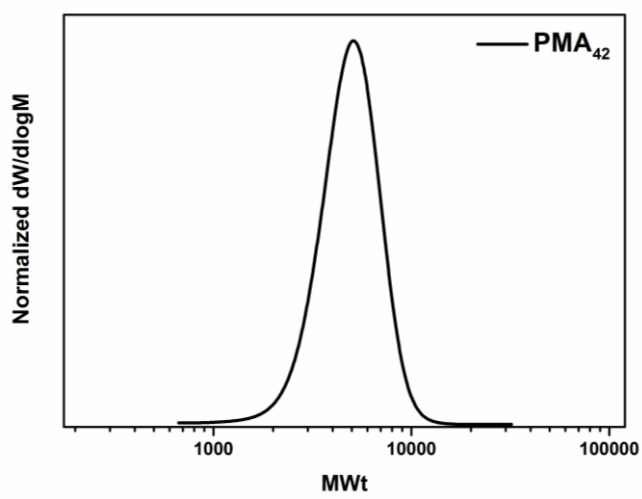

Figure 3-31. THF-SEC trace for the PMA_{42} macroinitiator synthesized *via* photoinduced Cu-RDRP in DMSO using a UV lamp with broad band emission and λ_{max} ~ 360 nm.

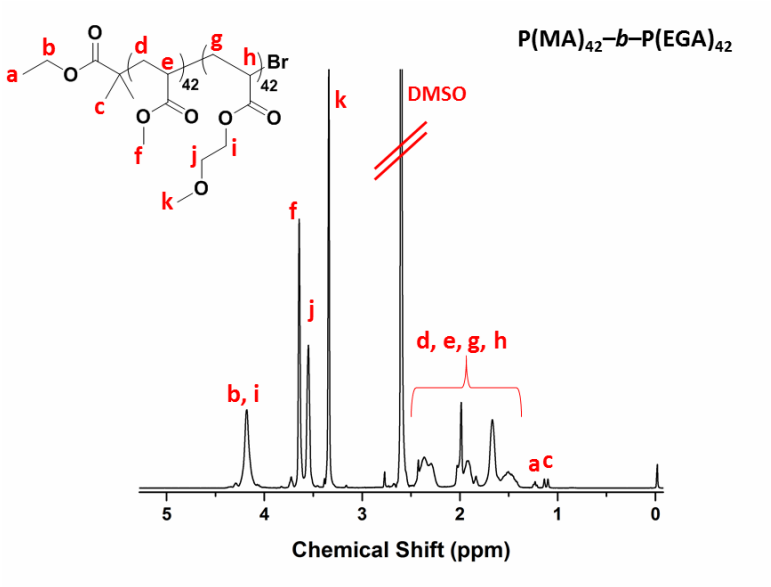

Figure 3-32. ^{1}H NMR spectrum in $CDCl_3$ for the diblock copolymer $P(MA)_{42}$-*b*-$P(EGA)_{42}$ synthesized *via* low-volume oxygen tolerant photoinduced Cu-mediated RDRP. For the macroinitiator [MA]:[EBiB]:[$CuBr_2$]:[Me_6Tren] = [42]:[1]:[0.02]:[0.12] in 50 % v/v DMSO. The block copolymerization was achieved upon re-irradiation of PMA_{42} in the presence of EGA.

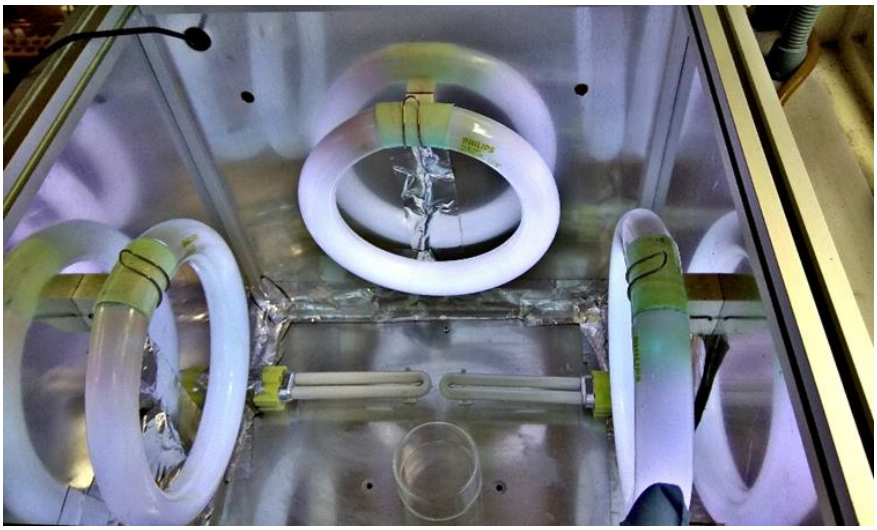

Figure 3-33. Custom-made UV box setup for the high-scale polymerizations with 4 9-W bulbs, broad band emission and λ_{max} ~ 360 nm.

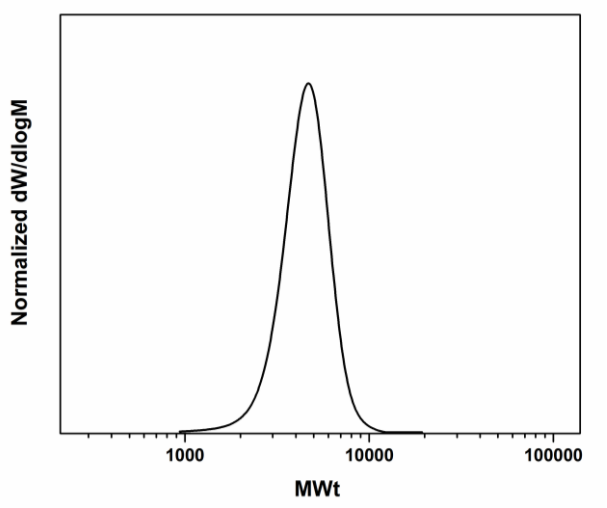

Figure 3-34. THF-SEC trace for PMA with targeted DP_n = 50 synthesized on 250 mL scale *via* oxygen tolerant photoinduced Cu-RDRP in TFE using a UV lamp with broad band emission and λ_{max} ~ 360 nm.

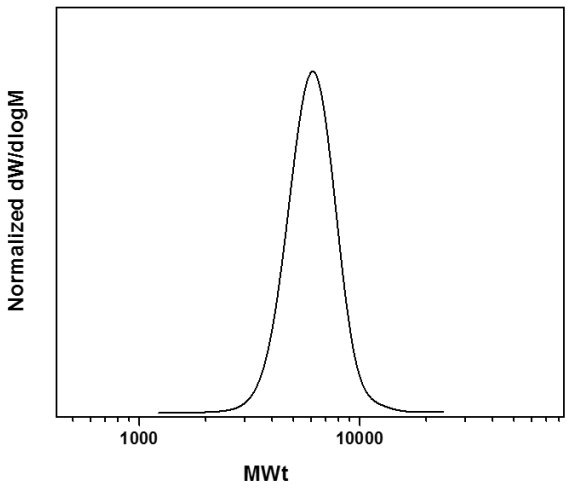

Figure 3-35. THF-SEC trace for PMA with targeted DP_n = 50 synthesized on 5 mL scale (headspace 3 mL) *via* oxygen tolerant photoinduced Cu-RDRP in DMSO using a UV lamp with broad band emission and λ_{max} ~ 360 nm.

3.6 References

1 A. Anastasaki, V. Nikolaou and D. M. Haddleton, *Polym. Chem.*, 2016, 7, 1002–1026.

2 A. Anastasaki, J. Willenbacher, C. Fleischmann, W. R. Gutekunst and C. J. Hawker, *Polym. Chem.*, 2017, **8**, 689–697.

3 G. R. Jones, A. Anastasaki, R. Whitfield, N. Engelis, E. Liarou and D. M. Haddleton, *Angew. Chemie Int. Ed.*, 2018, **57**, 10468–10482.

4 K. Matyjaszewski, *Macromolecules*, 2012, **45**, 4015–4039.

5 K. Matyjaszewski, *Adv. Mater.*, 2018, **30**, 1706441.

6 S. Perrier, *Macromolecules*, 2017, 50, 7433–7447.

7 B. M. Rosen and V. Percec, *Chem. Rev.*, 2009, **109**, 5069–5119.

8 E. Baeten, J. J. Haven and T. Junkers, *Polym. Chem.*, 2017, **8**, 3815–3824.

9 J. De Neve, J. J. Haven, L. Maes and T. Junkers, *Polym. Chem.*, 2018, 9, 4692–4705.

10 R. Aksakal, M. Resmini and C. R. Becer, *Polym. Chem.*, 2016, **7**, 171–175.

11 M. Kato, M. Kamigaito, M. Sawamoto and T. Higashimura, *Macromolecules*, 1995, **28**, 1721–1723.

12 J.-S. Wang and K. Matyjaszewski, *J. Am. Chem. Soc.*, 1995, **117**, 5614–5615.

13 V. Percec, T. Guliashvili, J. S. Ladislaw, A. Wistrand, A. Stjerndahl, M. J. Sienkowska, M. J. Monteiro and S. Sahoo, *J. Am. Chem. Soc.*, 2006, **128**, 14156–14165.

14 M. R. Hill, R. N. Carmean and B. S. Sumerlin, *Macromolecules*, 2015, **48**, 5459–5469.

15 J. Chiefari, Y. K. (Bill) Chong, F. Ercole, J. Krstina, J. Jeffery, T. P. T. Le, R. T. A. Mayadunne, G. F. Meijs, C. L. Moad, G. Moad, E. Rizzardo and S. H. Thang, *Macromolecules*, 1998, **31**, 5559–5562.

16 G. Moad and E. Rizzardo, in *RSC Polymer Chemistry Series*, Royal Society of Chemistry, 2016, 1–44.

17 T. Junkers, C. Barner-Kowollik and J. Lalevée, in *RSC Polymer Chemistry Series*, Royal Society of Chemistry, 2016, 264–304.

18 E. G. Bagryanskaya and S. R. A. Marque, in *RSC Polymer Chemistry Series*, Royal Society of Chemistry, 2016, 45–113.

19 V. A. Bhanu and K. Kishore, *Chem. Rev.*, 1991, **91**, 99–117.

20 S. C. Ligon, B. Husár, H. Wutzel, R. Holman and R. Liska, *Chem. Rev.*, 2014, 114, 577–589.

21 J. Yeow, R. Chapman, A. J. Gormley and C. Boyer, *Chem. Soc. Rev.*, 2018.

22 C. E. Barnes, R. M. Elofson and G. D. Tones, *J. Am. Chem. Soc.*, , DOI:10.1021/ja01157a059.

23 T. Arakawa, S. J. Prestrelski, W. C. Kenney and J. F. Carpenter, *Adv. Drug Deliv. Rev.*, 2001, **46**, 307–326.

24 C. M. Tseng, M. F. Lin, Y. L. Yang, Y. C. Ho, C. K. Ni and J. L. Chang, *Phys. Chem. Chem. Phys.*, 2010, **12**, 4989–4995.

25 M. F. Lin, Y. A. Dyakov, Y. T. Lee, S. H. Lin, A. M. Mebel and C. K. Ni, *J. Chem. Phys.*, 2007, **127**, 064308.

26 Y. Wang, L. Fu and K. Matyjaszewski, *ACS Macro Lett.*, 2018, **7**, 1317–1321.

27 R. Chapman, A. J. Gormley, M. H. Stenzel and M. M. Stevens, *Angew. Chemie - Int. Ed.*, 2016, **128**, 4576–4579.

28 R. Chapman, A. J. Gormley, K.-L. L. Herpoldt and M. M. Stevens, *Macromolecules*, 2014, **47**, 8541–8547.

29 F. Oytun, M. U. Kahveci and Y. Yagci, *J. Polym. Sci. Part A Polym. Chem.*, 2013, **51**, 1685–1689.

30 A. E. Enciso, L. Fu, S. Lathwal, M. Olszewski, Z. Wang, S. R. Das, A. J. Russell and K. Matyjaszewski, *Angew. Chemie Int. Ed.*, 2018, **57**, 16157–16161.

31 A. E. Enciso, L. Fu, A. J. Russell and K. Matyjaszewski, *Angew. Chemie Int. Ed.*, 2018, **57**, 933–936.

32 A. Anastasaki, V. Nikolaou, A. Simula, J. Godfrey, M. Li, G. Nurumbetov, P. Wilson and D. M. Haddleton, *Macromolecules*, 2014, **47**, 3852–3859.

33 A. Anastasaki, V. Nikolaou, Q. Zhang, J. Burns, S. R. Samanta, C. Waldron, A. J. Haddleton, R. McHale, D. Fox, V. Percec, P. Wilson and D. M. Haddleton, *J. Am. Chem. Soc.*, 2014, **136**, 1141–1149.

34 M. Chen, M. Zhong and J. A. Johnson, *Chem. Rev.*, 2016, **116**, 10167–10211.

35 J. Xu, K. Jung, A. Atme, S. Shanmugam and C. Boyer, *J. Am. Chem. Soc.*, 2014, **136**, 5508–5519.

36 N. J. Treat, B. P. Fors, J. W. Kramer, M. Christianson, C. Y. Chiu, J. R. De Alaniz and C. J. Hawker, *ACS Macro Lett.*, 2014, **3**, 580–584.

37 S. Shanmugam and C. Boyer, *J. Am. Chem. Soc.*, 2015, **137**, 9988–9999.

38 J. Yeow, S. Shanmugam, N. Corrigan, R. P. Kuchel, J. Xu and C. Boyer, *Macromolecules*, 2016, **49**, 7277–7285.

39 S. Shanmugam, J. Xu and C. Boyer, *J. Am. Chem. Soc.*, 2015, **137**, 9174–9185.

40 I. H. Lee, E. H. Discekici, A. Anastasaki, J. R. De Alaniz and C. J. Hawker, *Polym. Chem.*, 2017, **8**, 3351–3356.

41 J. Yeow, R. Chapman, J. Xu and C. Boyer, *Polym. Chem.*, 2017, **8**, 5012–5022.

42 J. Xu, S. Shanmugam, H. T. Duong and C. Boyer, *Polym. Chem.*, 2015, **6**, 5615–5624.

43 S. Shanmugam, J. Xu and C. Boyer, *Macromolecules*, 2017, **50**, 1832–1846.

44 G. Ng, J. Yeow, J. Xu and C. Boyer, *Polym. Chem.*, 2017, **8**, 2841–2851.

45 S. Fleischmann, B. M. Rosen and V. Percec, *J. Polym. Sci. Part A Polym. Chem.*, 2010, **48**, 1190–1196.

46 Z. Huang, C. Feng, H. Guo and X. Huang, *Polym. Chem.*, 2016, **7**, 3034–3045.

47 Y. Que, Z. Huang, C. Feng, Y. Yang and X. Huang, *ACS Macro Lett.*, 2016, **5**, 1339–1343.

48 S. Dadashi-Silab, X. Pan and K. Matyjaszewski, *Macromolecules*, 2017, **50**, 7967–7977.

49 K. Borská, D. Moravčíková and J. Mosnáček, *Macromol. Rapid Commun.*, 2017, **38**, 1600639.

50 J. Mosnáček, A. Eckstein-Andicsová and K. Borská, *Polym. Chem.*, 2015, **6**, 2523–2530.

51 Q. Yang, J. Lalevée and J. Poly, *Macromolecules*, 2016, **49**, 7653–7666.

52 Q. Fu, K. Xie, T. G. McKenzie and G. G. Qiao, *Polym. Chem.*, 2017, **8**, 1519–1526.

53 P. Gurnani, T. Floyd, J. Tanaka, C. Stubbs, D. Lester, C. Sanchez-Cano and S. Perrier, *Polym. Chem.*, , DOI:10.1039/c9py01521c.

54 J. Tanaka, P. Gurnani, A. B. Cook, S. Häkkinen, J. Zhang, J. Yang, A. Kerr, D. M. Haddleton, S. Perrier and P. Wilson, *Polym. Chem.*, 2019, **10**, 1186–1191.

55 Z. Li, S. Kosuri, H. Foster, J. Cohen, C. Jumeaux, M. M. Stevens, R. Chapman and A. J. Gormley, *J. Am. Chem. Soc.*, 2019, **141**, 19823–19830.

56 G. Ng, J. Yeow, R. Chapman, N. Isahak, E. Wolvetang, J. J. Cooper-White and C. Boyer, *Macromolecules*, 2018, **51**, 7600–7607.

57 E. Liarou, A. Anastasaki, R. Whitfield, C. E. Iacono, G. Patias, N. G. Engelis, A. Marathianos, G. R. Jones and D. M. Haddleton, *Polym. Chem.*, 2019, **10**, 963–971.

58 V. Beyer, J. Kim and C. R. Becer, *Polym. Chem.*, 2020, **11**, 1271-1291.

59 V. P. Beyer, B. Cattoz, A. Strong, D. J. Phillips, A. Schwarz and C. Remzi Becer, *Polym. Chem.*, 2019, **10**, 4259–4270.

60 S. R. Samanta, M. E. Levere and V. Percec, *Polym. Chem.*, 2013, **4**, 3212–3224.

61 E. Hancox, E. Liarou, J. S. Town, G. R. Jones, S. A. Layton, S. Huband, M. J. Greenall, P. D. Topham and D. M. Haddleton, *Polym. Chem.*, 2019,**10**, 6254-6259.

62 K. A. Davis and K. Matyjaszewski, *Macromolecules*, 2000, **33**, 4039–4047.

63 E. Liarou, M. Staniforth, J. S. Town, A. Marathianos, M. Grypioti, Y. Li, Y. Chang, S. Efstathiou, E. Hancox, A. M. Wemyss, P. Wilson, B. A. Jones, M. Aljuaid, V. G. Stavros and D. M. Haddleton, *Eur. Polym. J.*, 2020, 109388.

64 T. J. Zerk and P. V. Bernhardt, *Dalt. Trans.*, 2013, **42**, 11683–11694.

65 G. Kickelbick, T. Pintauer and K. Matyjaszewski, *New J. Chem.*, 2002, **26**, 462–468.

66 S. R. Samanta, R. Cai and V. Percec, *Polym. Chem.*, 2014, **5**, 5479–5491.

67 A. Plichta, M. Zhong, W. Li, A. M. Elsen and K. Matyjaszewski, *Macromol. Chem. Phys.*, 2012, **213**, 2659–2668.

68 R. Whitfield, K. Parkatzidis, M. Rolland, N. P. Truong and A. Anastasaki, *Angew. Chemie*, 2019, **131**, 13457–13462.

69 G. R. Jones, R. Whitfield, A. Anastasaki, N. Risangud, A. Simula, D. J. Keddie and D. M. Haddleton, *Polym. Chem.*, 2018, **9**, 2382–2388.

70 A. Anastasaki, B. Oschmann, J. Willenbacher, A. Melker, M. H. C. Van Son, N. P. Truong, M. W. Schulze, E. H. Discekici, A. J. McGrath, T. P. Davis, C. M. Bates and C. J. Hawker, *Angew. Chemie Int. Ed.*, 2017, **56**, 14483–14487.

71 V. Nikolaou, A. Anastasaki, F. Brandford-Adams, R. Whitfield, G. R. Jones, G. Nurumbetov and D. M. Haddleton, *Polym. Chem.*, 2016, **7**, 191–197.

72 T. Y. Lee, C. A. Guymon, E. S. Jönsson and C. E. Hoyle, *Polymer*, 2004, **45**, 6155–6162.

73 J. G. Riess, *Tetrahedron*, 2002, **58**, 4113–4131.

74 T. G. Ribelli, D. Konkolewicz, S. Bernhard and K. Matyjaszewski, *J. Am. Chem. Soc.*, 2014, **136**, 13303–13312.

75 E. Frick, A. Anastasaki, D. M. Haddleton and C. Barner-Kowollik, *J. Am. Chem. Soc.*, 2015, **137**, 6889–6896.

Chapter 4.

Rapidly Self-deoxygenating Controlled Radical Polymerization in water via in-situ Disproportionation of Cu(I)

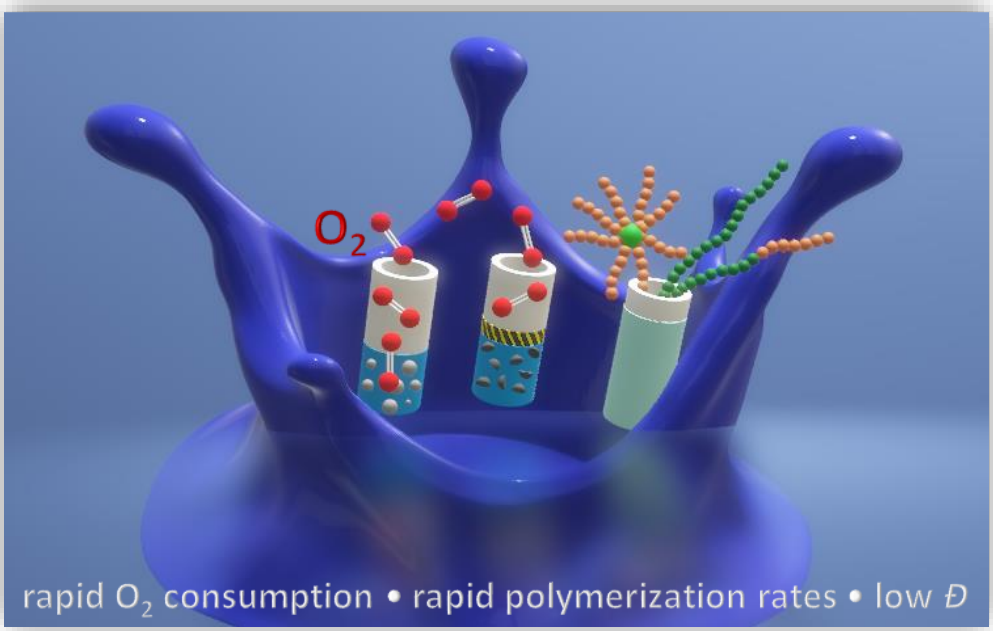

This chapter focuses on the development of a rapidly *self-deoxygenating* Cu-RDRP in aqueous media. The disproportionation of Cu(I)/Me_6Tren in water towards Cu(II) and highly reactive Cu(0) leads to O_2-free reaction environments within the first seconds of the reaction, even when the reaction takes place in the open-air. By leveraging this significantly fast O_2-reducing activity of the disproportionation reaction, a range of well-defined water-soluble polymers with narrow dispersity are attained in a few minutes or less. This

methodology provides the ability to prepare block copolymers *via* sequential monomer addition with little evidence for chain termination over the lifetime of the polymerization and allows for the synthesis of star-shaped polymers with the use of multi-functional initiators. The use of various characterization tools provides insights into this *self-deoxygenating* platform and identifies the species that participate in the oxygen consumption, as well as the species generated upon exposure of the solution to O_2-rich environments.

4.1 Introduction

Reversible Deactivation Radical Polymerization (RDRP) methods, including atom-transfer radical polymerization (ATRP),[1,2] single electron transfer-living radical polymerization (SET-LRP),[3,4] reversible addition–fragmentation chain-transfer polymerization (RAFT)[5,6] and nitroxide-mediated polymerization (NMP)[7,8] have provided access to an increasing range of well-defined materials with sophisticated architectures, various functionalities and controlled (macro)molecular characteristics.[9–11] Until recently, a notable hindrance for development has been intolerance towards oxygen/air. Consequently, controlled radical polymerization processes conducted in the presence of air are inhibited due to the ability of oxygen to react with carbon-centered radicals, leading to the formation of peroxy radicals *via* side reactions. [12–14]

Although the traditionally applied deoxygenation approaches, including freeze-pump-thaw cycles and N_2/Ar sparging are unarguably efficient for O_2 removal, they can be disadvantageous when volatile reagents are deoxygenated leading to their evaporation, and they are often incompatible with new polymerization platforms (*i.e.* high-throughput) approaches were the reaction scales are low.[15–17] In this context, research has been recently

focused on the replacement of these traditional methods either chemically through oxygen scavengers and reducing agents (*i.e.* glucose oxidase (GOx)),[18–21] ascorbic acid,[17,22–25] hydrazine,[26,27] photoredox catalysts[28–30]) or by physically displacing the oxygen through headspace elimination.[16,31,32]

The reaction medium plays an important role on the evolution of an *oxygen tolerant* polymerization, since not only does the concentration of dissolved O_2 vary in different solvents, but also differs with changes in temperature, solution viscosity and pressure.[33–35] Although oxygen tolerance and consumption has been investigated in organic media, *oxygen tolerant* polymerization in aqueous media can be considered as a challenging task since, apart from the high concentration of dissolved O_2 in water (> 8 mg/L at ambient temperature) there is high potential of side reactions including hydrolysis or elimination of the R-X or P-X bond and dissociation of the deactivating Cu(II) species when Cu-RDRP is applied,[36–38] as well as hydrolysis of the (macro-)chain transfer agent (CTA or macro-CTA),[5,39] in the case of RAFT. Consequently, *oxygen tolerant polymerizations* in aqueous media, require the efficient removal of oxygen from the polymerization solution, and also necessitate rapid rates in order to avoid these chain termination events.

In order to avoid conventional deoxygenation in aqueous-mediated RAFT photopolymerization of *N*,*N*-dimethylacrylamide, Boyer and colleagues reported the use of a zinc porphyrin photocatalyst ($ZnTPPS^{4-}$) with ascorbic acid as a singlet oxygen quencher.[40] In a separate study, the same group demonstrated the combination of eosin Y with ascorbic acid as a reducing agent system, for the oxygen tolerant aqueous RAFT photopolymerization at low volumes.[17] The addition of Cu(0) and ascorbic acid as reducing agents, was reported by He and co-workers, for the surface-initiated ATRP of 2-hydroxyethyl methacrylate.[41,42] Matyjaszewski and colleagues have reported the conversion of O_2 to CO_2 through GOx, for the aqueous ATRP of oligo(ethylene oxide)

methyl ether methacrylate ($OEOMA_{500}$) in the presence of pyruvates[21] or horseradish peroxidase.[43] Recently, Bennetti and colleagues reported an oxygen tolerant Fe(0) system for the SI-ATRP of polymer brushes in aqueous media, where the iron acts both as a source of catalyst and as a reducing agent showing excellent cytocompatibility towards mammalian cells for preparation of biomaterials.[44]

Herein, the *instantaneously self-deoxygenating* aqueous Cu-RDRP of various monomers is reported, by avoiding conventional deoxygenation methods and external reducing agents. The disproportionation of Cu(I) in the presence of Me_6Tren as a tertiary amine aliphatic sigma-donor ligand in water towards Cu(0) and Cu(II) is exploited, leading to full oxygen consumption within a few seconds, both in sealed and open-air conditions. Owing to the rapid O_2 reducing activity of the disproportionation reaction, a range of hydrophilic homo- and block co-polymers with controlled molecular weight, low dispersity and high-end group fidelity are synthesized within minutes. The aqueous oxygen consumption profile is elucidated by the *in-situ* online monitoring of the dissolved [O_2] through a fiber-optic oxygen monitoring probe, and the effect of the catalyst and ligand concentration, as well as the effect of different solvents are presented and discussed. A number of analytical methods collectively verify the rapid oxidation of Cu-species and elucidate the nature of the oxidized products.

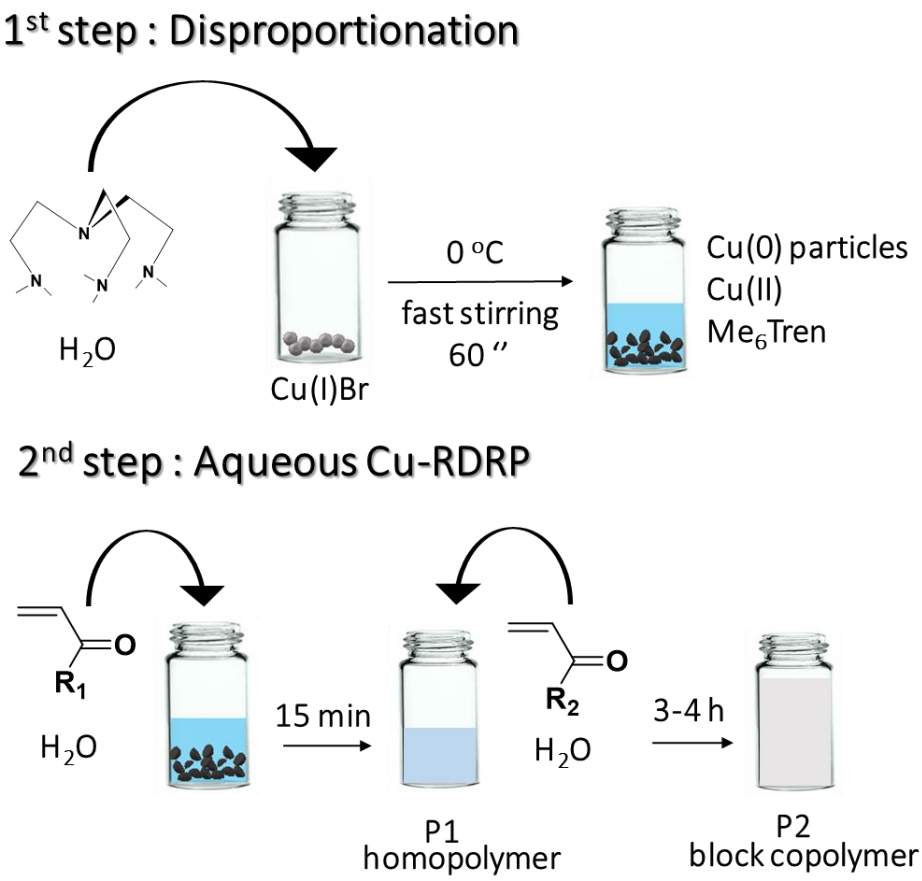

Scheme 4-1. Schematic representation of the self-deoxygenating Cu-RDRP of acrylamides employing the pre-disproportionation of Cu(I)Br/Me_6Tren in water.

4.2 Results and Discussion

4.2.1 Self-deoxygenating aqueous Cu-RDRP

Initially, in order to examine the ability to carry out efficient polymerization reactions in the presence of oxygen/air, the aqueous Cu-RDRP of *N*-isopropylacrylamide (NiPAm) was conducted without any type of external deoxygenation (**Scheme 4-1**), using only headspace elimination, following the conditions [I] : [DP_n] : [Cu(I)Br] : [Me_6Tren] = 1 : 50 : 0.4 : 0.4. For this purpose, a sealed 8 mL glass vial was charged with Cu(I)Br, 1 mL H_2O and Me_6Tren, and was placed in ice-bath with rapid stirring (900 rpm) for 60 seconds. Upon formation of a heterogeneous blue solution (indication of the formation

[Cu(II)(H_2O)$_6$)] with a black-purple Cu(0) precipitate, an aqueous solution of NiPAm and the water-soluble initiator (2, 3-dihydroxypropyl 2-bromo-2-methylpropanoate) were added in the disproportionation solution, and the polymerization left to commence. Kinetic studies were performed to reveal rapid polymerization rates, with >99% monomer conversion after only 12 minutes (**Figure 4-1a&c, Table 4-1**) in accordance with previous results, as well as low dispersity being achieved ($Đ$ = 1.15) and good agreement between experimental and theoretical M_n values ($M_{n,SEC}$ = 6,200 g/mol and $M_{n,th.}$ = 5,900 g/mol) verifying the versatility to carry out the polymerization without prior removal of dissolved oxygen (**Figure 4-1e, Table 4-1**). Furthermore, when the PNiPAm$_{50}$ from this non-deoxygenated reaction was compared with the N_2-sparged deoxygenation, good agreement was observed between both the two $M_{n, SEC}$ values and the dispersities (**Figure 4-23, Table 4-1**).

The aqueous Cu-RDRP of NiPAm with targeted DP_n = 50 was also investigated under "open to air" conditions, performing both the disproportionation of Cu(I) and the polymerization reaction without sealing the vial, whilst applying a fast stirring rate (900 rpm). Although the polymerization reached near-quantitative conversion (> 99%) after 12 minutes (similarly to the sealed reaction) (**Figure 4-1d**), and control over the molecular weight and dispersity was observed (**Figure 4-1f, Table 4-1**), an induction period, ascribed to continuous O_2 diffusion into the reaction, was observed (**Figure 4-1b**), which was further assisted by the rapid stirring rate, as discussed in the mechanistic section below.

Table 4-1. ^{1}H NMR and DMF-SEC analysis for PNiPAm with targeted DP_n = 50 synthesized *via* N_2-deoxygenated, non-deoxygenated (sealed vial) and open-to-air aqueous Cu-RDRP. [a]

Reaction condition	Conversion (%) ^{1}H NMR [b]	$M_{n,\,SEC}$ [c] (g mol^{-1})	$M_{n,\,th.}$ (g mol^{-1})	$Đ$	Reaction Time (min)
N_2 sparging	>99	6,200	5,900	1.10	12
No deoxygenation/sealed	>99	7,200	5,900	1.13	12
No deoxygenation/ open-to-air	>99	6,800	5,900	1.12	12

[a] In all polymerizations, the monomer concentration was 10 *w/v* % and the conditions were [I] : [DP_n] : [Cu(I)Br] : [Me_6Tren] = 1 : 50 : 0.4 : 0.4. [b] Conversion was calculated *via* ^{1}H NMR in D_2O. [c] Determined by DMF-SEC analysis based on DRI and expressed as molecular weight equivalents to PMMA narrow molecular weight standards.

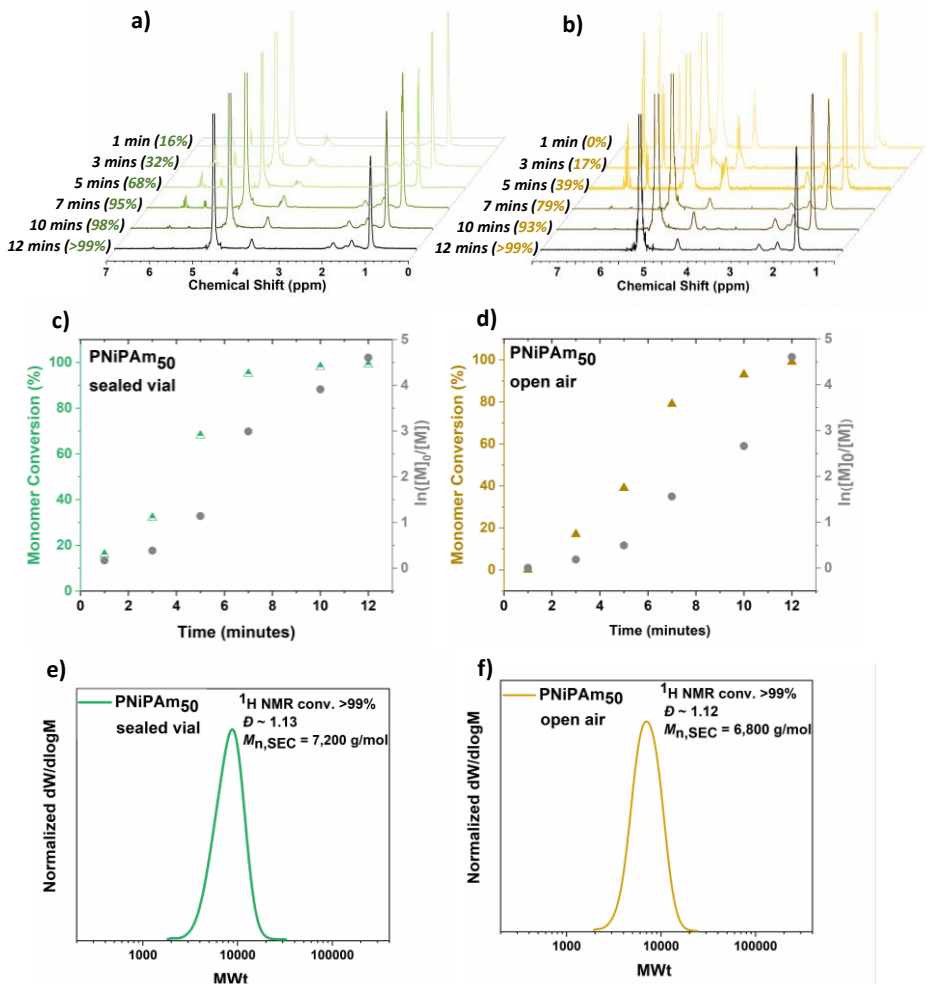

Figure 4-1. Kinetic studies for the *self-deoxygenating* aqueous Cu-RDRP of NiPAm with targeted DP_n = 50 when the polymerization was carried out in (**a, c, e**) sealed vial and (**b, d, f**) "open-to-air" conditions with ^{1}H NMR spectra (top), plots of conversion

and $\ln([M]_0/[M])$ over time (middle) and DMF-SEC derived molecular weight distributions (bottom).

Consequently, in order to further investigate the robustness of this system, higher molecular weights were targeted, applying the same conditions *i.e.* low monomer concentration of 10 w/v % and low temperature without any external deoxygenation. It has previously been reported that when $DP_n \geq 80$ was targeted, the ratio [Cu(I)Br] : [Me_6Tren] = 1 : 1 resulted in inefficient deactivation, which was observed as high dispersity values.[45] Therefore, for PNiPAm with targeted DP_n = 100, 200 and 400 twice as much Cu(I)Br as for DP_n = 50 was used, following the conditions [I] : [M] : [Cu(I)Br] : [Me_6Tren] = 1 : DP_n : 0.8 : 0.4.

It should be noted that, although the polymerization with targeted DP_n = 50 reached >99% conversion after only 12 minutes, for higher molar masses longer reaction times were required with DP_n = 200 taking 60 minutes to reach >99 % conversion and DP_n = 400 taking up to 90 minutes (**Figure 4-2, Table 4-2**). Furthermore, when DP_n = 400 was initially targeted with 10 *w/v* % monomer concentration, the polymerization was not successful while when 20 *w/v* % (thus higher catalyst concentration) was used, high conversion, low dispersity and controlled molecular weight of products were obtained.

Table 4-2. ^{1}H NMR and DMF-SEC analysis of PNiPAm with targeted DPs = 100-400 synthesized *via self-deoxygenating* aqueous Cu-RDRP with the pre-disproportionation of Cu(I)/Me_6Tren in H_2O at 0 °C. [a]

DP_n	Conv. (%) ^{1}H NMR	$M_{n,\ SEC}$ (g mol^{-1})	$M_{n,\ th.}$ (g mol^{-1})	$Đ$	[CuBr] : [Me_6Tren]	Time (minutes)
50	>99	6,200	5,900	1.15	0.4 : 0.4	12
100	>99	14,800	11,600	1.08	0.8 : 0.4	60
200	>99	25,100	22,900	1.15	0.8 : 0.4	60
400	92	39,600	41,900	1.18	0.8 : 0.4	90

[a] In all polymerizations the monomer concentration was 10 *w/v* %. [b] Conversion was calculated *via* ^{1}H NMR in D_2O. [c] Determined by DMF-SEC analysis based on DRI and expressed as molecular weight equivalents to PMMA narrow molecular weight standards.

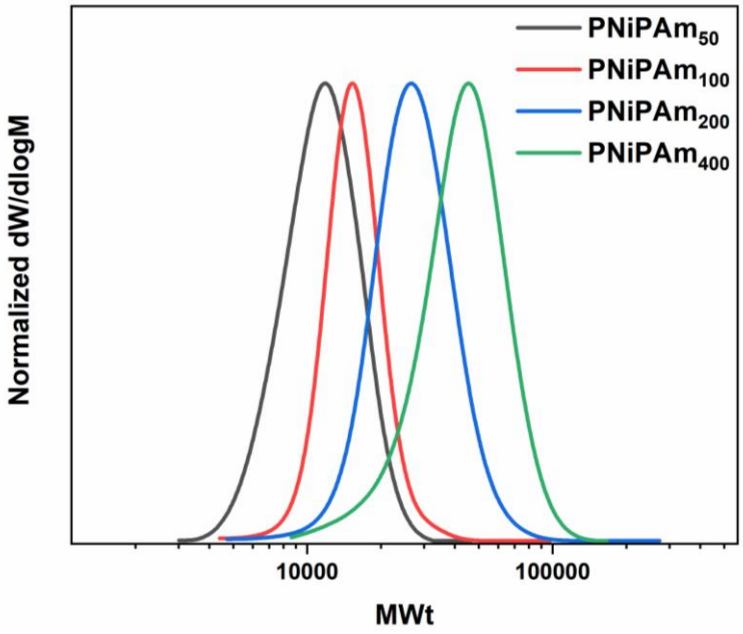

Figure 4-2. DMF-SEC derived molecular weight distributions of PNiPAm with targeted DPs = 50-400 synthesized *via self-deoxygenated* aqueous Cu-RDRP with the pre-disproportionation of Cu(I)/Me_6Tren in H_2O at 0 °C.

In order to expand the versatility of this methodology, we investigated the implementation of the aqueous self-deoxygenated system for both acrylates and acrylamides, as well as more complex polymer architectures including star-shaped polymers. NiPAm, *N*-hydroxyethyl acrylamide (HEAm) (**Table 4-3**, **Figure 4-3a**, **Figure 4-25**), *N*, *N* dimethylacrylamide (DMA) (**Table 4-3**, **Figure 4-3d**), poly(ethylene glycol) methyl ethyl acrylate ($PEGA_{480}$) (**Table 4-3**, **Figure 4-3b, Figure 4-26**) and *N*-acryloylmorpholine (NAM) (**Table 4-3**, **Figure 4-3c, Figure 4-27**) were polymerized through aqueous Cu-RDRP, without applying any type of external deoxygenation, resulting in excellent control over the obtained $M_{n,SEC}$ values, with low dispersity and at near-quantitative conversions in short reaction times.

Table 4-3. Macromolecular characteristics and reaction time of the various linear polymers synthesized *via self-deoxygenating* Cu-RDRP in aqueous media.[a]

Polymer	**DP_n**	**Conv. (%) ^{1}H NMR** [d]	**$M_{n,SEC}$ (g mol^{-1})** [e]	**$M_{n,th.}$ (g mol^{-1})**	**$Đ$**	**Time (minutes)**
PNiPAm [b]	100	> 99	16,200	11,600	1.14	15
PHEAm [b]	100	> 99	26,200	11,800	1.17	15
$P(PEGA_{480})$ [c]	20	98	9,300	9,600	1.17	30
PNAM [b]	40	98	7,100	5,800	1.09	240
PDMA [b]	80	> 99	11,300	8,200	1.15	20

[a] In all polymerizations the monomer concentration was 10 *w/v* %. [b] [Cu(I)Br] : [Me_6Tren] = [0.8] : [0.4]. [c] [Cu(I)Br] : [Me_6Tren] = [0.4] : [0.4]. [d] Conversion was calculated *via* ^{1}H NMR in D_2O. [e] Determined by DMF-SEC analysis based on DRI and expressed as molecular weight equivalents to PMMA narrow molecular weight standards.

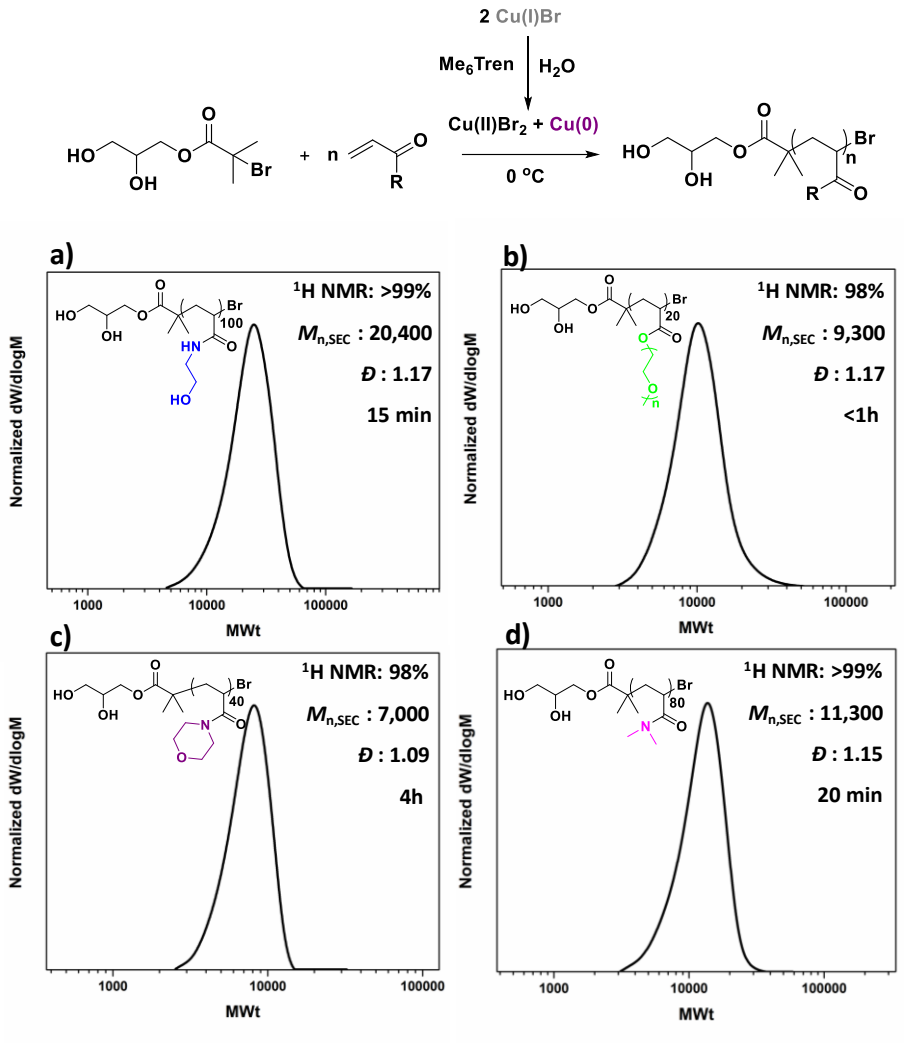

Figure 4-3. Reaction scheme (top) and DMF-SEC derived molecular weight distributions of **a**) PHEAm with targeted DP_n = 100, **b**) P($PEGA_{480}$) with targeted DP_n = 20, **c**) PNAM with targeted DP_n = 40 and **d**) PDMA with targeted DP_n = 80 synthesized *via self-deoxygenated* aqueous Cu-RDRP with the pre-disproportionation of Cu(I)/Me_6Tren in H_2O at 0 °C.

Subsequently, since star-shaped polymers have gained much academic interest due to their diverse properties,[9,46,47] the *self-deoxygenating* approach was applied for the synthesis of star-shaped PHEAm polymers with overall targeted DP_n = 60, 80 and 120. For this purpose, 3-, 4- and 8-arm multifunctional initiators (**Scheme 4-2**) were utilized for the synthesis of PHEAm star-shaped polymers with each arm having a targeted DP_n = 20. As the multi-arm star initiators were relatively hydrophobic, polymerizations were conducted

in water – organic solvent mixtures (either methanol or DMSO), with the pre-disproportionation of Cu(I) carried out in pure water in each case.[48] As a result, PHEAm star-shaped polymers were obtained at near-quantitative conversions (>99%) and narrow molecular weight distributions ($Đ$ = 1.11-1.2) in less than 2 hours (**Table 4-4, Figure 4-4**). It should be noted that the higher than the theoretical $M_{n,SEC}$ values for both linear and star-shaped PHEAm are attributed to interactions of the two -OH groups with the SEC-column and such deviations are observed for all the HEAm-derived polymers.

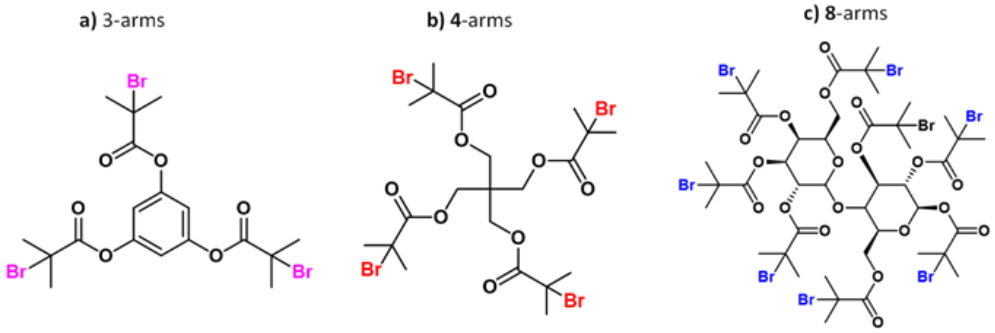

Scheme 4-2. Chemical structures for the different multi-functional initiators used for the synthesis of star-shaped polymers.

Table 4-4. Macromolecular characteristics and reaction time of the various star-shaped polymers synthesized *via self-deoxygenating* Cu-RDRP in aqueous/organic mixtures.[a]

Polymer	Conv. (%) ^{1}H NMR[b]	$M_{n,\ SEC}$ [c] (g mol^{-1})	$Đ$	Time (minutes)	[Cu(I)Br] : [Me_6Tren]
3-arm $PHEAm_{60}$	>99	17,200	1.20	60	1.2 : 1.2 [d]
4-arm $PHEAm_{80}$	>99	18,600	1.20	90	3.2 : 2.4 [e]
8-arm $PHEAm_{160}$	>99	26,500	1.12	120	6.4 : 4.8 [f]

[a] In all polymerizations the monomer concentration was 10 *w/v* %. [b] Conversion was calculated *via* ^{1}H NMR in D_2O. [c] Determined by DMF-SEC analysis and expressed as molecular weight equivalents to PMMA narrow molecular weight standards. [d] for each initiator -Br site : [Cu(I)Br] : [Me_6Tren] = 0.4 : 0.4, [e] for each initiator -Br site : [Cu(I)Br] : [Me_6Tren] = 0.8 : 0.6, [f] for each initiator -Br site : [Cu(I)Br] : [Me_6Tren] = 0.8 : 0.6.

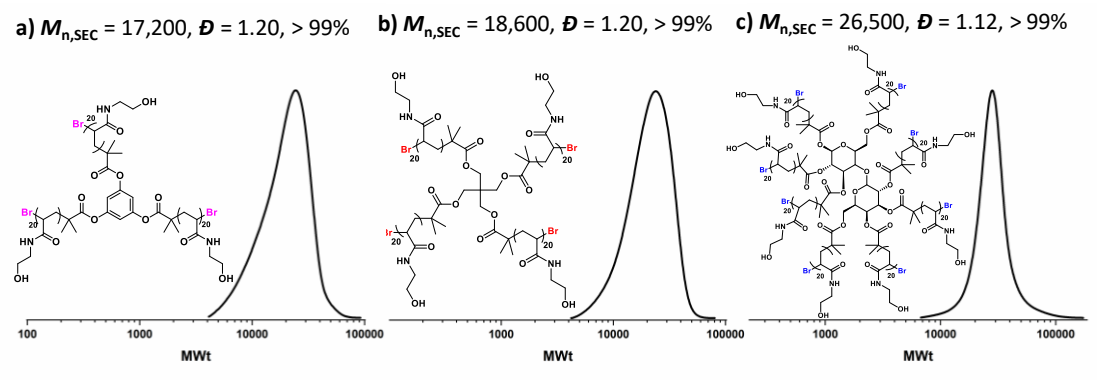

Figure 4-4. DMF-SEC derived molecular weight distributions for the star-shaped PHEAm utilizing **a**) 3-arm initiator and targeted overall DP_n = 60, **b**) 4-arm initiator and targeted overall DP_n = 80 and **c**) 8-arm initiator and targeted overall DP_n = 160, synthesized *via self-deoxygenating* Cu-RDRP in water – organic solvent mixtures.

The extent of end group fidelity was investigated in this approach, given the non-deoxygenated environment as well as the side reactions which are well-known to occur in aqueous media. For this purpose, MALDI-ToF-MS was employed for the mass characterization of PNiPAm with targeted DP_n = 50, synthesized in a sealed vial. MALDI-ToF analysis revealed that there are peak distributions corresponding to polymer chains that had undergone both elimination and hydrolysis of the alkyl halide, whilst bromine capped chains were also observed (**Figure 4-5**).

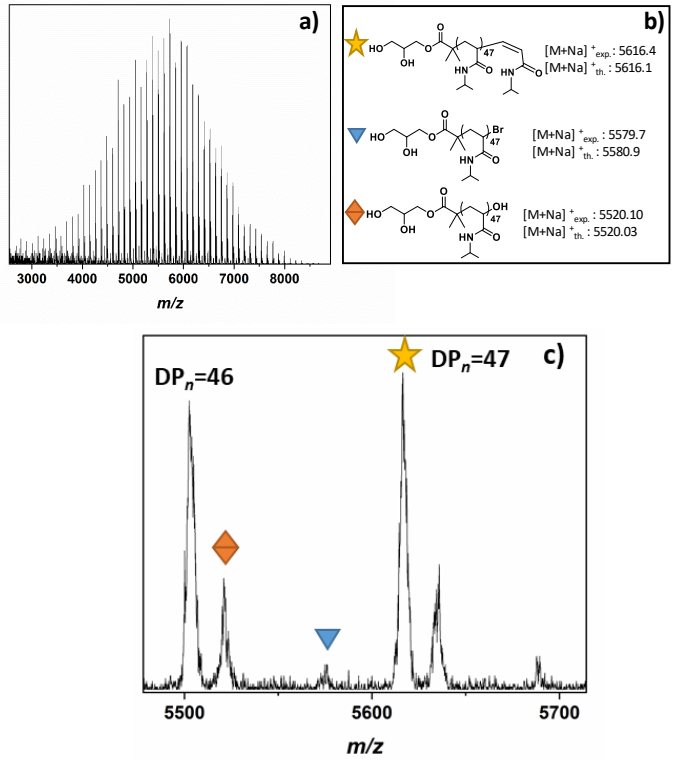

Figure 4-5. a, c) MALDI-ToF spectrum of PNiPAm with targeted DP_n = 50 and actual DP_n = 47 revealing that he predominant single peak distribution corresponds to Br-eliminated chains ($[M+Na]^+$ = 5616.4), **b)** the presence of –OH terminated chains ($[M+Na]^+$ = 5520.10) and –Br terminated ($[M+Na]^+$ = 5579.7) chains is evident.

These chain termination events are also observed under conventionally deoxygenated systems[45] originating from the excess of water where the rate of hydrolysis is lower than the rate of chain propagation, thus they cannot be correlated with the presence or absence of oxygen. The extent of end group fidelity was further verified by *in-situ* block copolymerizations *via* sequential monomer addition which resulted in polyacrylamide diblock copolymers with well-defined molecular characteristics at high conversions (**Table 4-5**, **Figures 4-6a&b**). Although this rapid polymerization without loss of end group fidelity *via* radical-radical termination is not in accordance with classical free radical polymerization kinetics which have previously been applied, Ballard and Asua have shown that when the probability density functions of the termination reactions are altered to allow

for radical diffusion, the reduced rate of termination can explain "*the ability for a seemingly impossible level of control of radical reactions*".[49]

Table 4-5. ^{1}H NMR and DMF-SEC analysis for the diblock copolymers synthesized *in-situ via self-deoxygenating* aqueous Cu-RDRP. [a]

Polymer	Conv. (%) ^{1}H NMR [b]	$M_{n,\,SEC}$ (g mol^{-1}) [c]	$Đ$	Time (minutes)
PHEAm$_{50}$	> 99	11,700	1.18	15
PHEAm$_{50}$-*b*-PNiPAm$_{50}$	> 99	18,100	1.20	240
PHEAm$_{50}$	97	12,600	1.18	15
PHEAm$_{50}$-*b*-P(PEGA$_{480}$)$_{20}$	> 99	20,500	1.19	240

[a] In all polymerizations the monomer concentration was 10 *w/v* % and the macroinitiators were synthesized in the presence of headspace. [b] Conversion was calculated *via* ^{1}H NMR in D_2O. [c] Determined by DMF-SEC analysis based on DRI and expressed as molecular weight equivalents to PMMA narrow molecular weight standards.

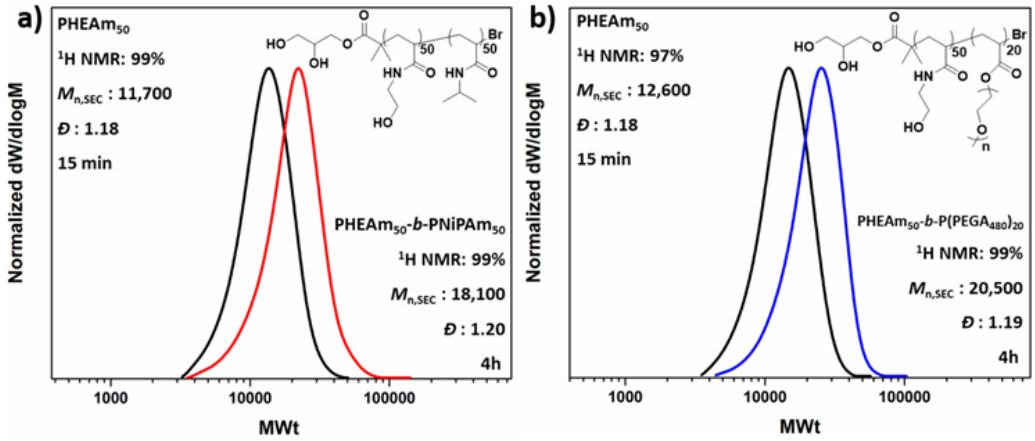

Figure 4-6. DMF-SEC derived molecular weight distributions for the *in-situ* sequential monomer addition diblock copolymers **a**) PHEAm$_{50}$-*b*-PNiPAm$_{50}$ and **b**) PHEAm$_{50}$-*b*-P(PEGA$_{480}$)$_{20}$.

The versatility of the methodology was further verified through low volume reactions carried out in 96-well plates which were sealed with a plate-lid. Both PNiPAm and HEAm

were polymerized in 300 μL total reaction volume, exhibiting good control over the molecular weights and the dispersity at high conversion (**Figure 4-7**).

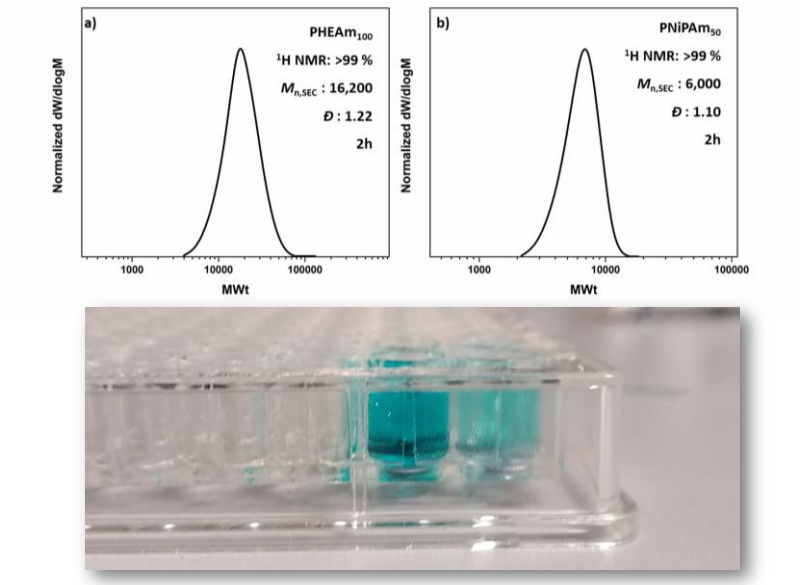

Figure 4-7. DMF-SEC derived molecular weight distributions for the low-volume **a**) PHEAm with targeted DP_n = 100 and **b**) PNiPAm with targeted DP_n = 50.

4.2.2 Rate of oxygen consumption during Cu(I) disproportionation to Cu(II) and Cu(0).

The rate of the oxygen reducing activity of the disproportioning Cu(I)/Me_6Tren aqueous solution was investigated *via* the online monitoring of the dissolved O_2 concentration with the use of an oxygen probe. Initially, the $[O_2]_{dissolved}$ in the disproportionation solution used for the polymerization of NiPAm with targeted DP_n = 50 (with [Cu(I)] : [Me_6Tren] = 1 : 1) was monitored resulting rapid (a few seconds) oxygen consumption (**Figure 4-8, gray**). Subsequently, since the concentration of the components able to consume oxygen affect the rate of oxygen consumption, different concentrations were examined, using 1-7 mL of H_2O (**Figure 4-8**).

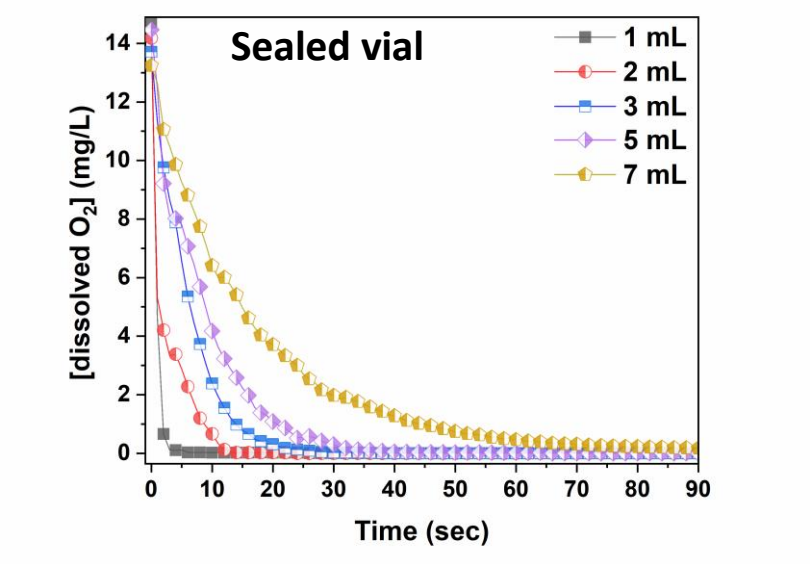

Figure 4-8. Line graphs illustrating the oxygen consumption over time with different concentrations of the Cu(I)Br/Me_6Tren complex in a sealed environment.

As expected, the rate of oxygen consumption exhibited differences depending on the concentration, with the fastest oxygen consumption (~ 3 sec.) observed for the most concentrated solution (1 mL of H_2O), and the slowest rate observed for 7 mL of H_2O (~ 1 min). It should be noted that when 1 mL of the solution was used prior to monomer (HEAm in this case) and initiator addition, the polymerization exhibited the highest control over the molecular weights (**Figure 4-9**, **Table 4-6**), suggesting that the fate of an aqueous non-deoxygenated polymerization is dependent on the concentration of the disproportionation reagents (Cu(I)Br/Me_6Tren) and/or their products (Cu(0), Cu(II)), and sufficient amount of these species is important in order to facilitate the O_2 consumption process.

Table 4-6. ^{1}H NMR and DMF-SEC analysis of PNiPAm with targeted DP_n = 50 synthesized *via self-deoxygenating* aqueous Cu-RDRP with different concentrations of the disproportionation solution. [a]

Disproportionation Volume (mL)	Conv. (%) [b] ^{1}H NMR	$M_{n,SEC}$ [c] g mol^{-1}	$M_{n,th.}$ g mol^{-1}	$Đ$
1	>99	16,200	11,800	1.08
2	97	16,700	11,800	1.15
3	15	16,900	11,800	1.18
5	0	N/A	N/A	N/A

[a] In all polymerizations the monomer concentration was 10 *w/v* %. [b] Conversion was calculated *via* ^{1}H NMR in D_2O. [c] Determined by DMF-SEC analysis based on DRI and expressed as molecular weight equivalents to PMMA narrow molecular weight standards.

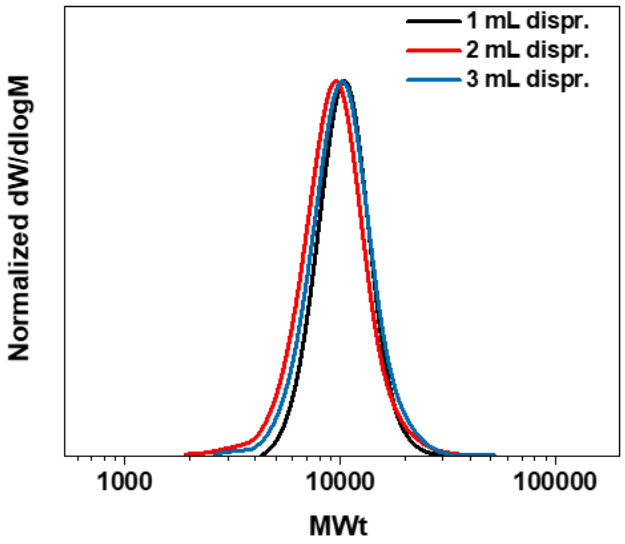

Figure 4-9. DMF-SEC derived molecular weight distributions of PHEAm with targeted DP_n = 50 synthesized *via self-deoxygenated* aqueous Cu-RDRP with different concentrations of the disproportionation solution.

In order to provide an insight into the open-to-air polymerization where almost perfect control over the macromolecular characteristics was observed, the [O_2] monitoring was performed in an open vial. In this case, the oxygen consumption was again rapid (~ 10-60

sec) (**Figure 4-10**), with the 1 mL solution being *self-deoxygenated* within the first 10 seconds. The trend of consumption exhibited the same profile as in the sealed vial, again depending on the concentration of the disproportionation solution with the main difference between the sealed and the open-to-air experiments being that the latter required slightly longer reaction times for total deoxygenation to occur, which could be attributed to the constant diffusion of O_2 into the solution from the air during high stirring rates. It should be noted that at ~ 0 °C (temperature applied at the disproportionation and polymerization reactions), the solubility of oxygen is higher than at ambient (*i.e.* 25 °C) temperature (~ 14 mg/L and ~ 8 mg/L respectively), while the diffusion rate of oxygen is lower.[50–52] Hence, although there is a constant exposure of the reaction solution to air/oxygen, the reducing ability of Cu(0) (as well as Cu(I)), combined with the low-temperature conditions could further facilitate the *oxygen tolerant* nature of this aqueous Cu-RDRP.

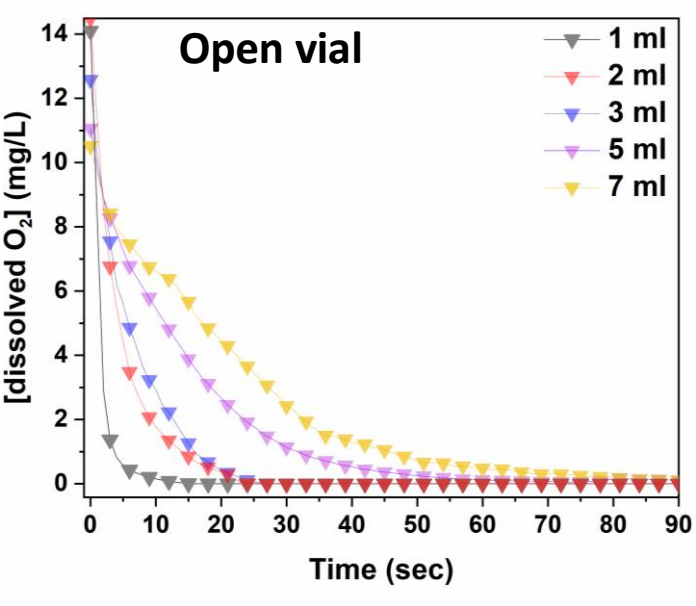

Figure 4-10. Line graphs illustrating the oxygen consumption over time with different concentrations of the Cu(I)Br/Me_6Tren complex in open air conditions.

The effect of the different reagents was also examined individually, with the monitoring of solutions with different loadings of Cu(I)Br and consistent [Me_6Tren], and *vice versa*. In each case, 3 mL of H_2O were used for the solubilization of the complex in order to reasonably decelerate the rate of the reaction, and thus be able to monitor any changes. Initially, in order to investigate role of the Cu(I)Br, a solution containing only H_2O/Me_6Tren (without any Cu(I)Br) was monitored and no oxygen consumption was observed. When low loadings of Cu(I)Br ([Cu(I)Br] : [Me_6Tren] = 0.125 : 1) were added into 3 mL H_2O/Me_6Tren solution, the oxygen consumption rate was slow, reaching an oxygen concentration of 6 mg/L after 1 minute (**Figure 4-11, green**), while with a slight increase of [Cu(I)] to 0.25 eq. (with respect to Me_6Tren), the rate of O_2 consumption accelerated, resulting in a deoxygenated solution only after 1 minute (**Figure 4-11, pink**). Further increases in [Cu(I)] showed faster rates of O_2 consumption, with the fastest full O_2 consumption (~ 5 sec) being evidenced when excess of Cu(I) was used ([Cu(I)Br] : [Me_6Tren] = 2.5 : 1) (**Figure 4-11, dark cyan**).

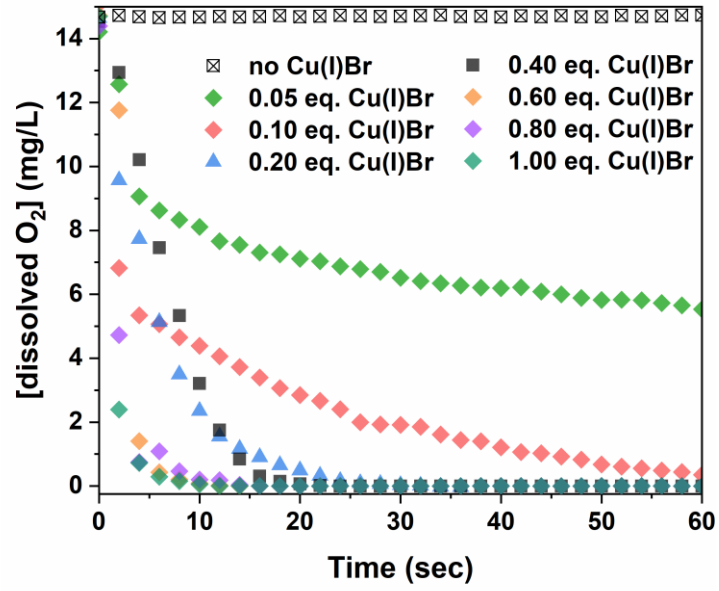

Figure 4-11. Line graphs illustrating the oxygen consumption over time with different concentrations of Cu(I)Br when the concentration of Me_6Tren was kept constant.

Subsequently, the role of the ligand was investigated by using different amounts of Me_6Tren with respect to Cu(I)Br. Initially, a solution containing only Cu(I)Br and 3 mL H_2O was examined which, although being heterogeneous (due to the insolubility of Cu(I)Br in water), a very slow O_2 consumption was observed (from 14 mg/L to ~ 13 mg/L after 1 min). However, with the addition of low loadings of Me_6Tren ([Cu(I)Br] : [Me_6Tren] = 1 : 0.125) full O_2 consumption was observed after ~ 40 sec (**Figure 4-12, green and pink**). Following this, higher concentrations of Me_6Tren resulted in accelerated consumption rates (**Figure 4-12**), with the fastest O_2 consumption being observed when excess of Me_6Tren was applied ([Cu(I)Br] : [Me_6Tren] = 1 : 2.5, **Figure 4-12, dark cyan**), as in the case of Cu(I)Br. This indicates that, upon formation of the Cu-complex with the amine ligand in water, the rapid disproportionation of Cu(I) is followed by rapid O_2 consumption, even when low loadings of Cu(I)Br or ligand are employed. In this context, it is hypothesized that even small amounts of the *in-situ* generated Cu(0) particles can "consume" oxygen. However, since the "nascent" Cu(0) particles are highly reactive, we hypothesized that their generation is followed by their oxidation in the presence of O_2 (*vide infra* electron microscopy and XPS).

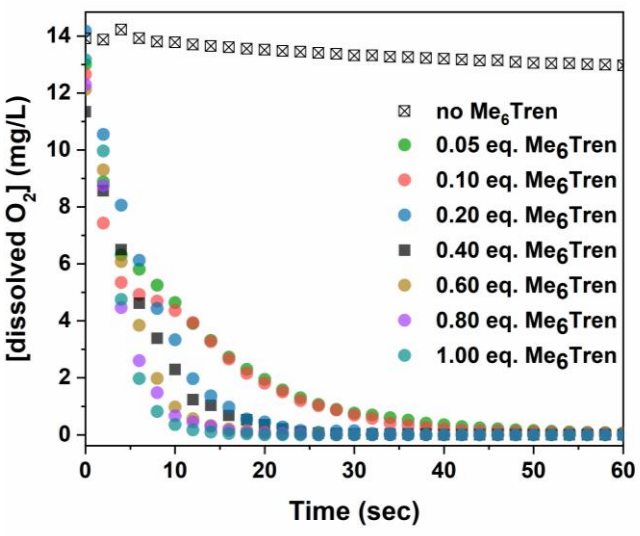

Figure 4-12. Line graphs illustrating the oxygen consumption over time with different concentrations of Me_6Tren when the concentration of Cu(I)Br was kept constant.

In order to examine which of the Cu-species following disproportionation participate in the O_2 consumption, the [O_2] evolution was also monitored in different solvents including ethanol, methanol and dimethylformamide (DMF) which promote disproportionation of Cu(I),[51] as well as solvents that stabilize Cu(I)[52] and thus, disproportionation is not favored (*i.e.* acetone, acetonitrile, toluene) (**Figure 4-13**). Specifically, when EtOH and MeOH were used, the oxygen consumption was similar to when H_2O was used as a solvent, an observation that is expected since alcohols promote the disproportionation of Cu(I).

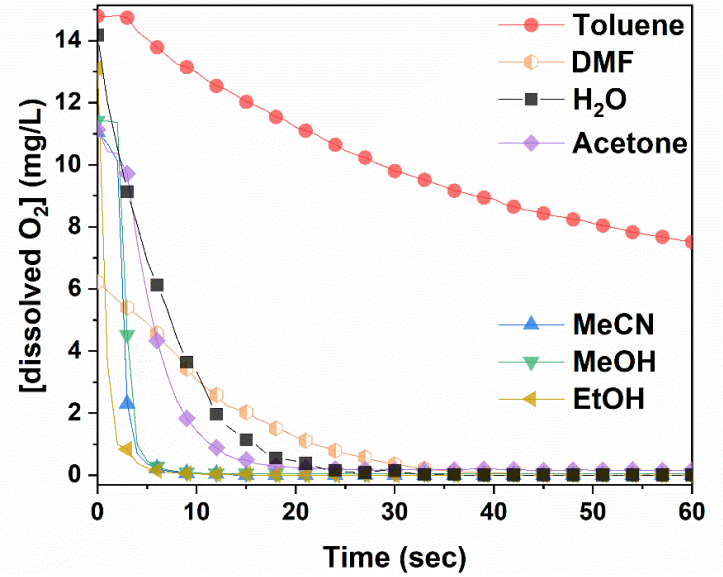

Figure 4-13. Line graphs illustrating the oxygen consumption of the disproportionation reaction over time in different solvents.

In the case of the polar aprotic DMF and acetone, the consumption of O_2 was similar to pure H_2O, while when acetonitrile (MeCN) which stabilizes Cu(I) was employed, the O_2 consumption was similar to alcohols. Acetonitrile stabilizes Cu(I) and does not promote disproportionation, thus we ascribe that O_2 consumption occurs from the oxidation of Cu(I). Based on this, it is possible that O_2 consumption is assisted by the oxidation of

both Cu(I) and the "nascent" Cu(0), and depending on the solvent choice, the oxidation of Cu(0) and Cu(I) are competing reactions which can both lead to rapid deoxygenation.

The continuous deoxygenation profile (even after the addition of monomer and initiator solutions the [O_2] has been reduced) (**Figure 4-14**) might be attributed to the regeneration of Cu(I) upon oxidation of Cu(0), which can *re*-disproportionate and thus "perpetuate" the reduction of O_2 until the reagents are fully consumed. As a result, it is hypothesized that Cu(I), originating either from the initially added Cu(I)Br or from the oxidation of Cu(0), and "nascent" Cu(0) participate in the consumption of both dissolved and in gas phase O_2, and due to the long-lasting paucity of these Cu-species, the reaction solutions remain deoxygenated even open-to-air.

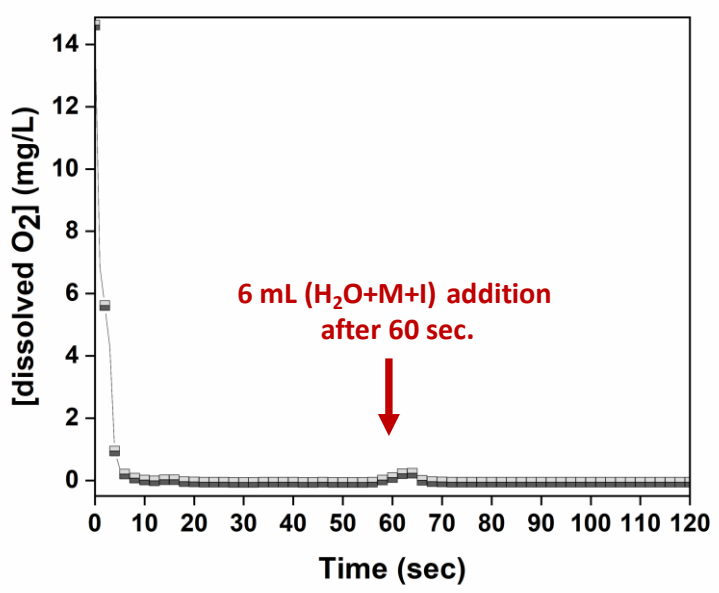

Figure 4-14. Line graph illustrating the oxygen consumption profile of the disproportionation reaction over time which after 60 seconds undergoes addition of 6 mL aqueous solution of monomer and initiator. Although a small increase is observed for ~ 5 seconds upon addition of M+I, the reaction rapidly re-establishes the O_2-free environment

In order to better understand the effect of O_2 on the catalyst species and in an attempt to identify the oxidation products, XPS and EM (TEM, SEM, ADF-STEM and EELS) were employed. Initially, the solution following disproportionation in the presence of O_2 was examined through SEM (**Figure 4-16**). The Cu(I)Br sample in water consists of > 1 μm size well-shaped aggregates (**Figure 4-16a**). Upon addition of Me_6Tren and after the ~ 1st second of the reaction, where there is an instantaneous observation of black/purple Cu(0) precipitate with fast stirring, the sample mainly includes three different structures, namely dendrite-like shaped aggregates which consist of particles >100 nm, small multi-sized particles, as well as faceted crystal structures (**Figure 4-16b**). It is notable that the crystal-shaped morphologies are mainly present for the sample taken immediately after the addition of Me_6Tren (" ~ 1-sec " sample), and considering the loss of the larger Cu(I)Br aggregates, it can be hypothesized that the crystals are formed upon instant consumption of Cu(I)Br, following a clusterization process (**Figure 4-15**) which can be correlated with the formation of the dendrite-like shaped aggregates.

After ~ 3 seconds of the reaction, the observed crystal structures are significantly less, whilst the dendritic-like aggregates, which we hypothesize that follow a nucleation and growth process become more evident (**Figure 4-16c-e**). It is notable that this morphology is still observed after 60 seconds of the reaction, while after 5 minutes this dendritic pattern becomes "softer", with the dendritic-like branches becoming less evident and more uniform (**Figure 4-16f**).

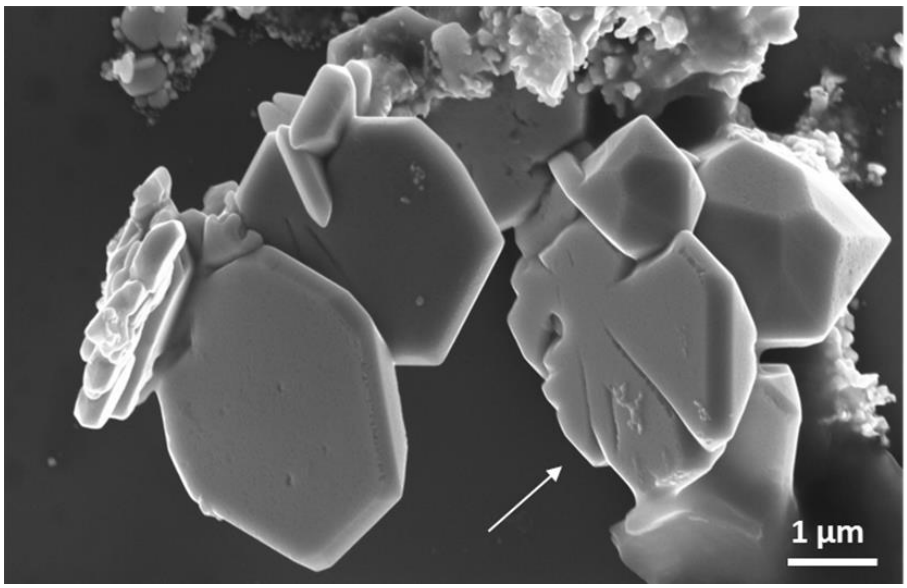

Figure 4-15. SEM image illustrating the morphological alterations of the faceted crystal-like Cu-particles.

Finally, after 30 minutes, small particle-like aggregates are observed which are covered by more uniform larger aggregates (**Figure 4-16g**) and finally, after 24 hours of the reaction, large aggregates that consist of smaller particles are observed (**Figure 4-16h**). Apart from the different species of copper that participate in the disproportionation reaction, which are challenging to monitor due to the rapid chemical processes that take place, these observations might be related to the oxidation of the copper species since, as previously described, the disproportionation reaction is a self-deoxygenation mechanism. In order to gain a better understanding, Energy-Dispersive X-ray spectroscopy (EDX) was employed.

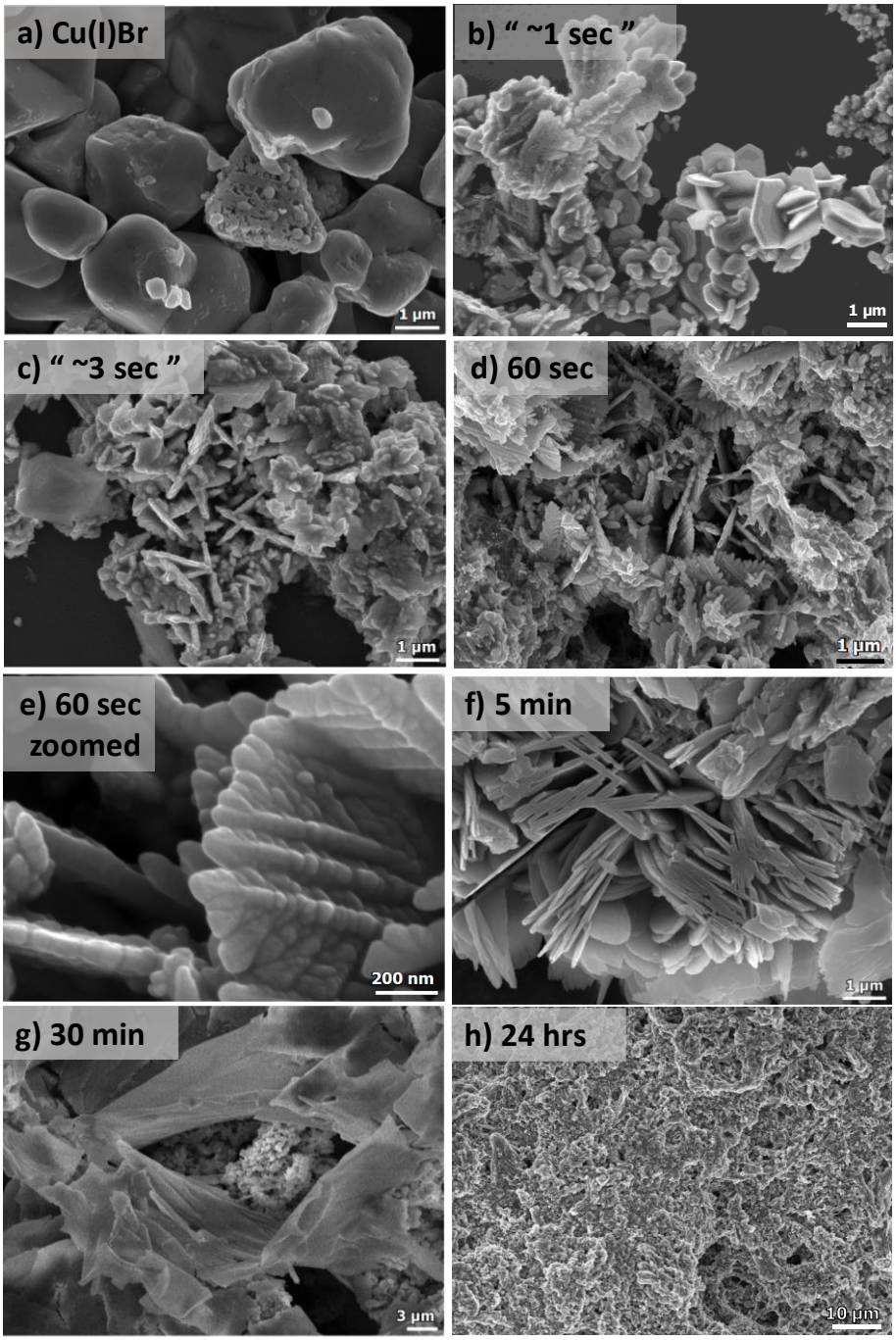

Figure 4-16. SEM images of **a**) Cu(I)Br dispersed in H_2O and (**b-h**) the *self-deoxygenating* disproportionation reaction precipitate collected at different times. The "~ 1-sec" was taken immediately after the addition of Me_6Tren.

It was hypothesized that the consumption of O_2 would lead to the possible formation of different copper oxides and thus, the EDX studies were focused on the presence of oxygen with respect to copper. Initially, Cu(I)Br was measured as blank

sample, showing a distinctive peak at 0.9 keV corresponding to Cu, as well as a very small peak assigned to oxygen at 0.5 keV and could be attributed to the oxidation of the Cu(I)Br powder from air over time (**Figure 4-17, black**). When the precipitate from the disproportionation was examined immediately after the addition of Me_6Tren (the sample was taken after ~ 1 second), the peak at 0.5 keV, assigned to oxygen increased slightly (**Figure 4-17, blue**) (as well as after ~ 3 seconds, **Figure 4-17, green**) and became even more evident after 60 seconds of the reaction (**Figure 4-17, red**). This observation might be related to the formation of oxides as the reaction takes place in the presence of oxygen, a hypothesis that is corroborated by the full O_2 consumption within the first 60 seconds. After 30 minutes, the oxygen peak was further increased (**Figure 4-17, yellow**), with the highest intensity being observed after 24 hours (**Figure 4-17, white**).

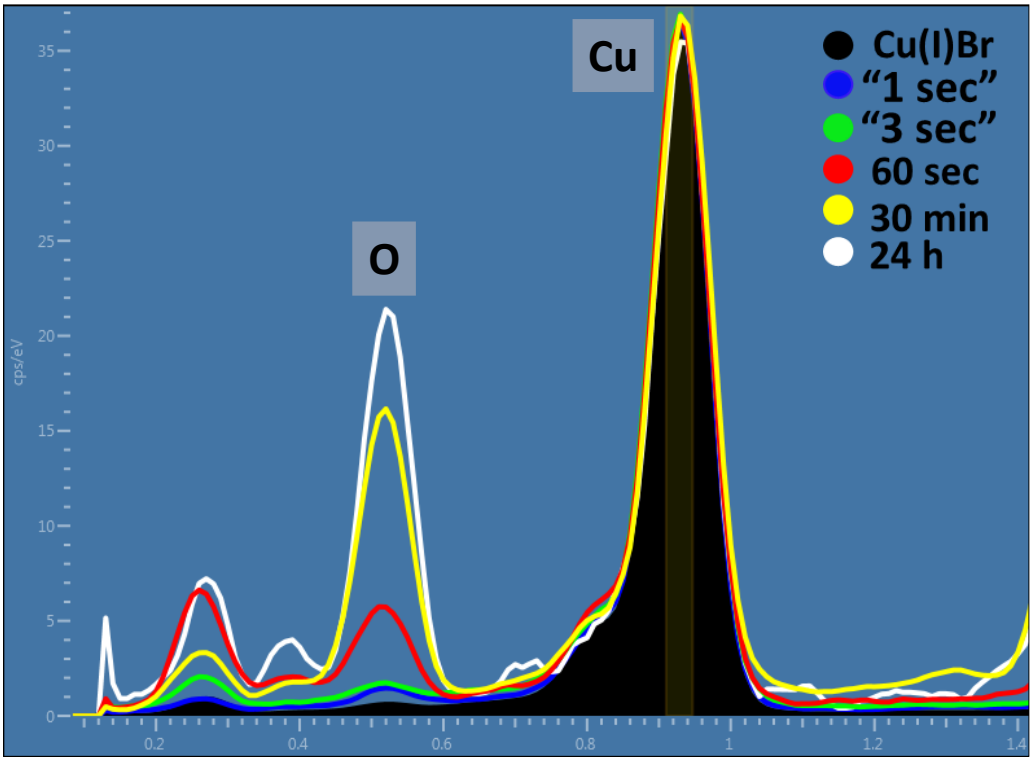

Figure 4-17. EDX spectra showing the distinctive copper peak (0.9 keV) and the increase of the oxygen peak (0.5 keV) for the disproportionation precipitate at different times.

The presence of copper oxides and hydroxide was also verified through X-ray photoelectron spectroscopy (XPS) for both the black precipitate and the supernatant after 60 sec. Examination of the Cu $2p_{3/2}$ region revealed the presence of Cu(II) states in the precipitate (**Figure S19**), as evidenced by the shake-up features observed between 940 eV and 945 eV. Detailed fitting of this region and the peak around 934 eV showed evidence for $Cu(OH)_2$, CuO and $Cu(II)Br_2$. Turning to the peak at 932.3 eV, it is not possible to distinguish between Cu(0) and Cu(I) states so one must look at alternative regions in order to understand the chemistry of the system. **Figure 4-28** presents the data from the Br 3*d* region, where two doublets were required to fit the data corresponding to Cu(I)Br and $Cu(II)Br_2$. Next the Cu LMM Auger emission region was analysed (**Figure 4-29**) and required the addition of the Cu(0) components to replicate the data. Comparing the Auger spectra of the precipitate and the supernatant, a downward shift of around 2 eV in the kinetic energy of the peak intensity is observed when moving from the precipitate to the supernatant, suggesting a higher Cu(II) concentration in the supernatant. This hypothesis is corroborated by the Cu $2p_{3/2}$ spectrum acquired from the supernatant (**Figure 4-20a)**, where the intensity of the shake-up features and the peak at 934.2 eV have both increased relative to the precipitate (**Figure 4-18**). The O 1*s* data acquired also suggest the existence of both $Cu(OH)_2$ and Cu oxides in both the supernatant (**Figure 4-20b**) and the precipitate (**Figure 4-19**). Overall, based on the elemental analysis of both the precipitate and supernatant, copper and oxygen are mainly predominant in the precipitate, while nitrogen originating from the ligand, as well as bromine (originating from Cu(I)Br) are mainly present in the supernatant (**Figure 4-20a&b**).

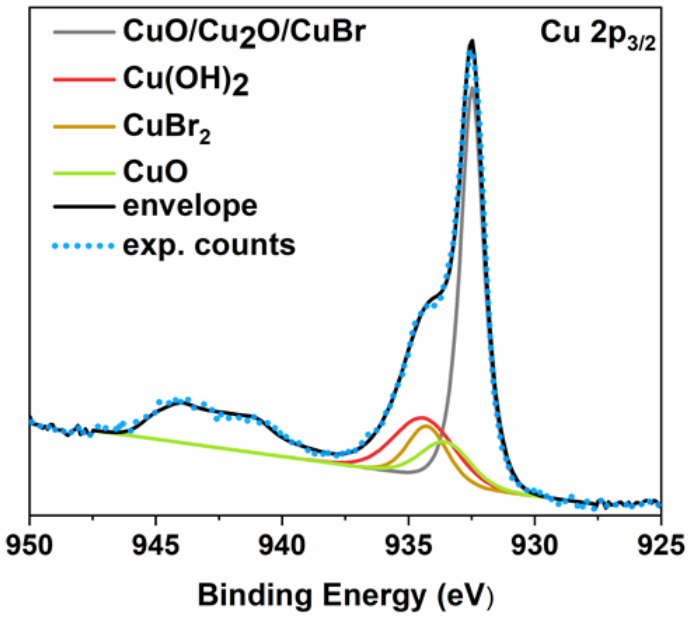

Figure 4-18. XPS core level Cu $2p_{3/2}$ spectra of the disproportionation precipitate after 60 seconds of the reaction. The features between 940 eV and 945 eV are due to shake-up peaks from Cu^{2+} states.

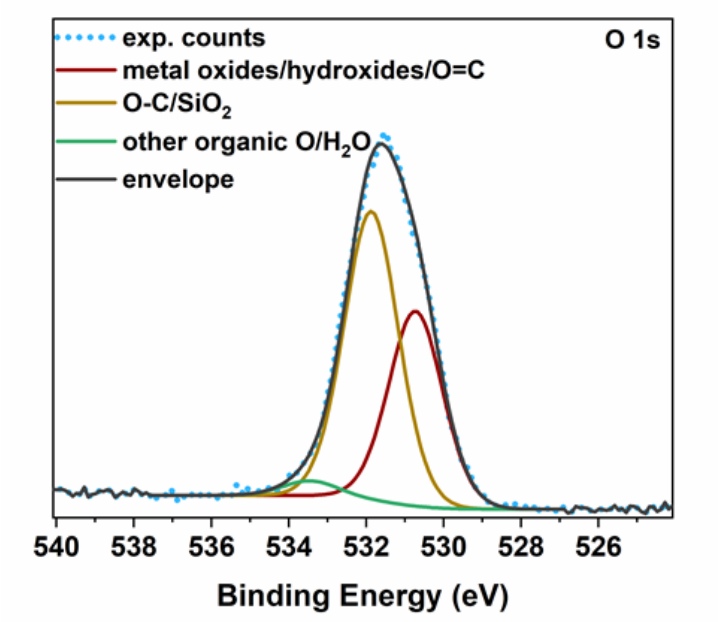

Figure 4-19. XPS core level O 1*s* spectra of the disproportionation precipitate after 60 seconds of the reaction.

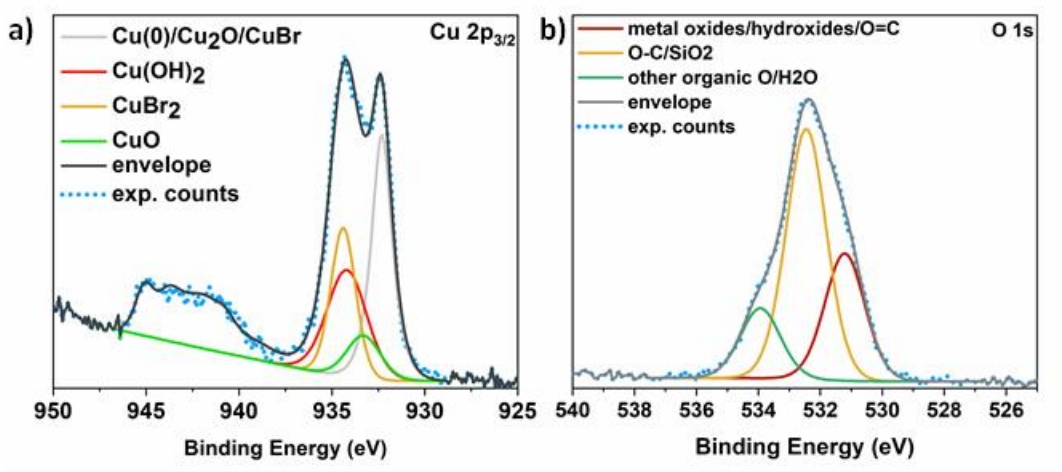

Figure 4-20. XPS core level **a**) Cu $2p_{3/2}$ and **b**) O 1*s* spectra of the disproportionation supernatant solution after 60 seconds of the reaction. The features between 940 eV and 945 eV are due to shake-up peaks from Cu^{2+} states.

The use of high-resolution transmission electron microscopy (HR-TEM) and annular dark field-scanning transmission electron microscopy (ADF-STEM) in combination with electron energy loss spectroscopy (EELS) provided more details on the chemical state of the Cu-species generated upon reaction with oxygen. The ADF-STEM and HR-TEM of the disproportionation precipitate (60 seconds aliquot) verified the presence of copper species with different morphology in the nanoscale, showing dendrite-like shaped patterns (**Figure 4-21 e&f**), as well as multi-sized particles consisting of both well-defined faceted (**Figure 4-21 g & h**) and smaller particles (**Figures 4-21 a-d**). Based on the EELS analysis, the faceted particles exhibited a Cu-L_3 edge located at 935.9 eV (**Figure 4-22 ii, blue**), whilst no O-K edge was evident suggesting assignment as Cu(0) which, based on the lack of oxygen signal, has remained unaffected from the presence of oxygen within the first 60 seconds of the reaction. Contrary to the faceted particles, the dendrite-like patterns exhibited a strong O-K edge indicative of oxygen presence (**Figure 4-22 i**), as well as a Cu-L_2 edge at 936.2 eV which is assigned as Cu(I) (**Figure 4-22 ii, red)**.

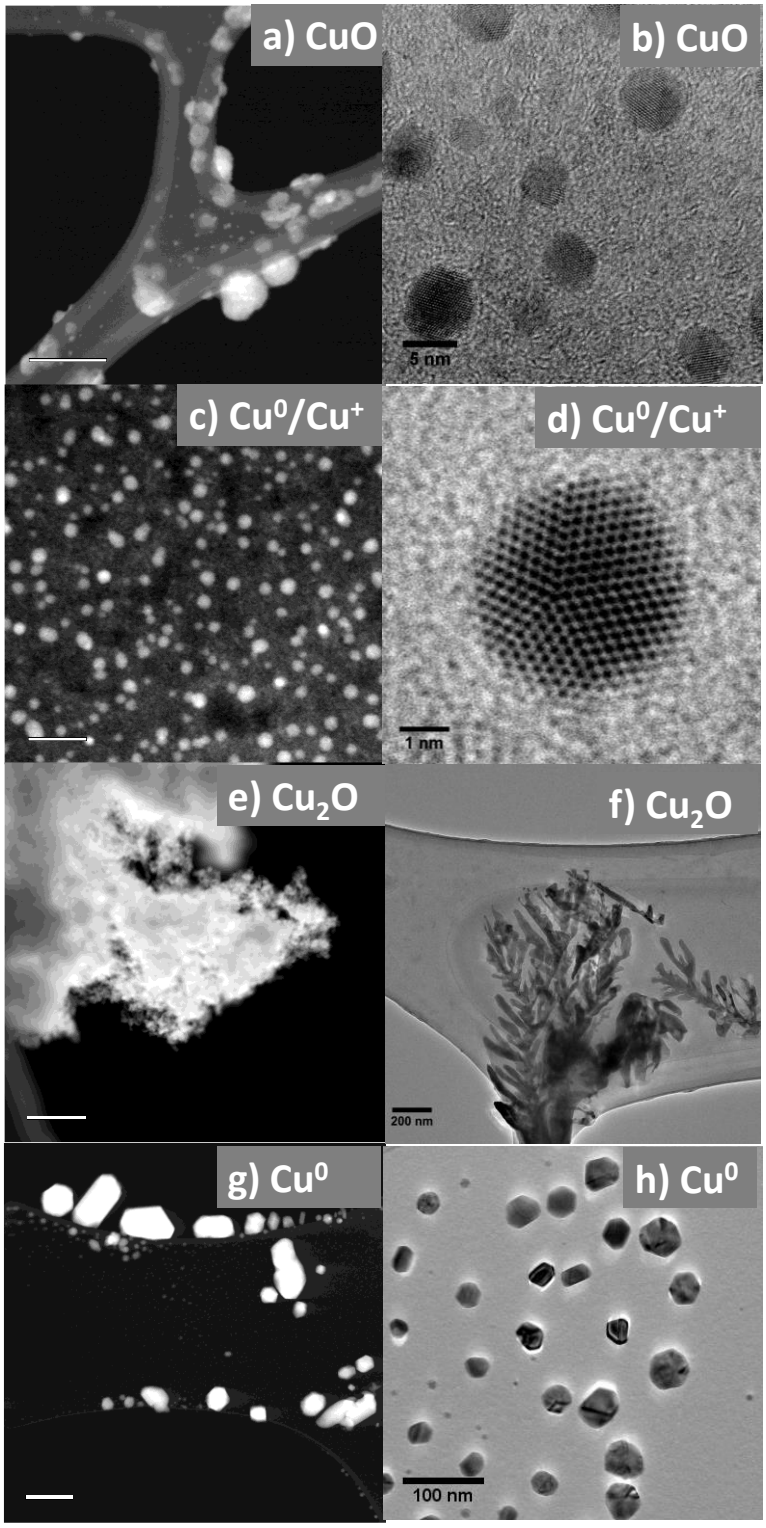

Figure 4-21. ADF-STEM images (**a, c, e, g**) and the corresponding TEM images (**b, d, f, h**) showing the existence of different Cu-species after 60 seconds of the reaction.

Thus, based on the EELS analysis it is hypothesized that these dendritic patterns are representative of Cu_2O which, based on their immediate presence upon addition of the ligand (after ~ 1 second) are rapidly formed. The EELS of the smaller (<80 nm) particles revealed a distinctive Cu-L_3 edge peak at 933.5 eV which compared to the literature values[53,54] and the symmetric L_2 and L_3 peaks (**Figure 4-22 ii, yellow)** lead to the hypothesis that these particles correspond to Cu(II) which, upon analysis of the Cu/O atomic ratio is possibly found as CuO. Apart from the aforementioned species, the presence of even smaller (2-10 nm) particles was observed (**Figure 4-21 c&d**) which, although exhibiting unclear O-K edge, can be considered as a mixture of Cu(I) and Cu(0) based on the characteristics of their steep Cu-L edge (**Figure 4-22 ii, grey**).

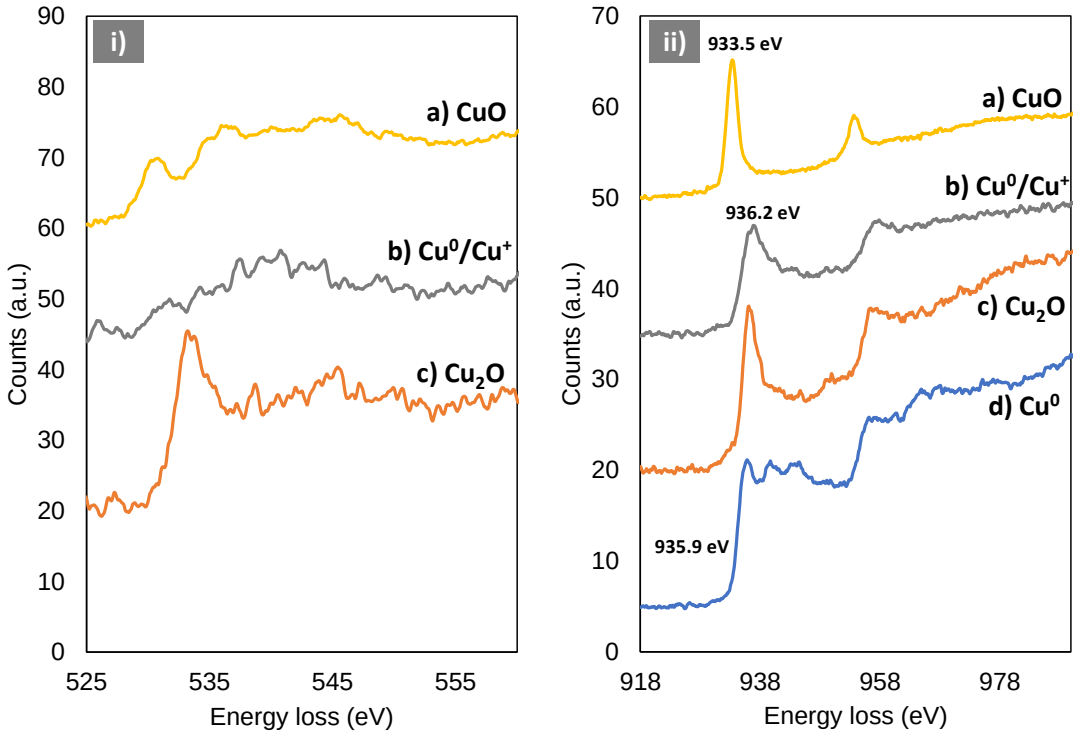

Figure 4-22. EELS spectra of **i**) O-*K* edge and **ii**) Cu-*L* edge from different regions of the 60-sec sample. In view of the fine structures exhibited in the EELS spectra, it is confirmed that **a**) is CuO, **c**) is Cu_2O and **d**) is Cu(0). In **d**), the Cu/O atomic ratio is estimated to be <2, indicating a mixture of Cu(0) and Cu_2O.

4.3 Conclusion

In this chapter, the rapidly *self-deoxygenating* Cu-RDRP in aqueous media of various linear and non-linear, homo- and block-copolymers is presented and discussed. The disproportionation of Cu(I)/Me_6Tren in water towards Cu(II) and highly reactive Cu(0), leads to O_2-free reaction environments within the first seconds of the reaction, even when the reaction takes place in the open-air. By leveraging this significantly fast O_2-reducing activity of the disproportionation reaction, well-defined water-soluble polymers with very narrow dispersity are attained in just a few minutes. This methodology provides the ability to prepare block copolymers *via* sequential monomer addition with little evidence for chain termination over the lifetime of the polymerization and allows for the synthesis of star-shaped polymers with the use of multi-functional initiators. The use of a range of characterization tools provides insights into this *self-deoxygenating* platform and identifies the species that participate in the oxygen consumption, as well as the species generated upon exposure of the solution to O_2-rich environments. The unprecedentedly fast reducing ability of the Cu(I) disproportionation can be an advantageous and mild platform for applications that require instantaneous O_2-free environments for long periods.

4.4 Experimental Section

4.4.1 Materials

The monomers *N*-isopropyl acrylamide (NiPAm, ≥ 99%), *N*-hydroxyethyl acrylamide (HEAm, 97%), *N, N* dimethylacrylamide (DMA, 99%), poly(ethylene glycol) methyl ethyl acrylate ($PEGA_{480}$, 97%), *N*-acryloylmorpholine (NAM, 97%) and the solvents were purchased from Sigma Aldrich / Merck and used as received. For all the disproportionation reactions and the polymerizations distilled water was used. *Tris*(2-(dimethylamino)ethyl)amine (Me_6Tren) was synthesized according to the literature[55] and stored under N_2 atmosphere prior to use. The water-soluble initiator 2, 3-dihydroxypropyl 2-bromo-2-methylpropanoate was synthesized according to the literature.[56] Copper (I) bromide (CuBr, 98%, Sigma-Aldrich) was washed with acetic acid and ethanol, dried under vacuum and stored under N_2 atmosphere.

4.4.2 Instrumentation and Characterization techniques

Proton Nuclear Magnetic Resonance (^{1}H NMR)

^{1}H NMR spectra were recorded on Bruker DPX-300 or DPX-400 spectrometers in deuterium oxide (D_2O) obtained from Sigma-Aldrich. Chemical shifts are given in ppm downfield from the internal standard tetramethylsilane. Monomer conversions were determined *via* ^{1}H NMR spectroscopy by comparing the integrals of monomeric vinyl protons to polymer signals.

Size Exclusion Chromatography (SEC)

DMF. Agilent Infinity II MDS instrument equipped with differential refractive index (DRI), viscometry (VS), dual angle light scatter (LS) and variable wavelength

UV detectors. The system was equipped with 2 x PLgel Mixed D columns (300 x 7.5 mm) and a PLgel 5 µm guard column. The eluent was DMF with 5 mmol NH_4BF_4 additive. Samples were run at 1 ml/min at 50 ^oC. Poly(methyl methacrylate) standards (Agilent EasyVials) were used for calibration between 955,000 – 550 g mol^{-1}. Analyte samples were filtered through a nylon membrane with 0.22 µm pore size before injection. Respectively, experimental molar mass ($M_{n,SEC}$) and dispersity ($Đ$) values of synthesized polymers were determined by conventional calibration and universal calibration using Agilent GPC/SEC software.

PL50 DMF. Agilent PL50 instrument equipped with differential refractive index (DRI) and UV detectors. The system was equipped with 2 x PolarGel M columns (300 x 7.5 mm) and a PolarGel 5 µm guard column. The eluent is DMF with 0.1 % LiBr additive. Samples were run at 1ml/min at 50 ^oC. Poly(methyl methacrylate) standards (Agilent EasyVials) were used for calibration. Analyte samples were filtered through a nylon membrane with 0.22 µm pore size before injection. Respectively, experimental molar mass ($M_{n,SEC}$) and dispersity ($Đ$) values of synthesized polymers were determined by conventional calibration using Agilent GPC/SEC software.

Matrix assisted laser desorption-ionization time-of-flight mass spectrometry (MALDI-ToF-MS).

MALDI-ToF-MS measurements were conducted using a Bruker Daltonics Ultraflex II MALDI-ToF mass spectrometer, equipped with a nitrogen laser delivering 2 ns laser pulses at 337 nm with positive ion ToF detection performed using an accelerating voltage of 25 kV. Solutions in tetrahydrofuran (THF) (50 µL) of *trans*-2-[3-(4-*tert*-butylphenyl)-2-methyl-2-propyldene] malononitrile (DCTB) or α-cyano-4-hydroxycinnamic acid (CHCA) as a matrix (saturated solution), sodium iodide as the

cationization agent (1.0 mg mL^{-1}) and sample (1.0 mg mL^{-1}) were mixed, and 0.7 μL of the mixture was applied to the target plate. Spectra were recorded in reflectron mode calibrated with Poly(ethylene glycol) monomethyl ether (PEG-Me) 1900 kDa.

Oxygen Probe. Pocket Oxygen Meter - FireStingGO2 (Pyro Science)**:** The solvent-resistant oxygen probe OXSOLV measures oxygen partial pressure in most polar and nonpolar solvents. It is based on optical detection principles (REDFLASH technology) and can be used both in pure and complex organic solvents. The fibre-optic oxygen sensor tip is covered with a stainless-steel tube 1.5 mm in diameter and 150 (or 40) mm in length. The analysis of the data was conducted with the FireStingGO2 Manager software.

Scanning Electron Microscopy (SEM) and energy-dispersive X-ray (EDX) spectroscopy

Scanning electron microscopy was performed using a ZEISS Gemini SEM - Field Emission Scanning Electron Microscope and a ZEISS Supra. Best results were obtained when using the InLens detector with ~ 3.5 mm working distance, 20 (Gemini) or 30 (Supra) μm aperture and 5-15 kV acceleration voltage, with respect to sample tolerance. EDX spectroscopy and elemental analysis were performed *via* the Gemini instrument through its SDD EDX detector.

Sample Preparation: A 3mL total capacity glass vial placed in an ice bath was charged with 7.2 mg (1 eq.) Cu(I)Br and 1 mL DI-H_2O and was septum-sealed. Upon fast stirring (900 rpm), Me_6Tren (14 μL, 1 eq.) was added in the Cu(I)Br solution and aliquots from the heterogeneous solution were drop-cast on silicon wafer chips (5 mm x 7 mm) which were attached to aluminum specimen stubs. The drop-cast samples were instantly being placed under N_2 blanket and left to dry.

Transmission Electron Microscopy (TEM) imaging and Electron Energy Loss Spectroscopy (EELS)

TEM imaging was carried out using a JEOL 2100 electron microscope. Annular dark-field STEM imaging and EELS spectrum imaging were performed in a double-corrected JEOL ARM200f microscope, equipped with a Gatan Quantum spectrometer, operated at 200 kV. A probe convergence semi-angle of 32 mrad and a spectrometer semi-collection angle of 25 mrad were used for the collection of the EELS signals. The energy resolution of the EELS measurements was 1.2 eV, as estimated from the full-width-half-maximum of the zero-loss peaks. A Dual EELS mode was used at a dispersion of 0.1 eV per channel, where the core loss spectra from either Cu or O were calibrated using the zero loss peaks in the low loss spectra. The samples for TEM were prepared by drop-casting aliquots of the disproportionation solution onto lacey carbon grids supplied by EM Resolutions and were left to dry under N_2 blanket.

X-ray photoelectron spectroscopy (XPS)

XPS measurements were performed using a Kratos Axis Ultra DLD spectrometer. The samples were illuminated using X-rays from a monochromated Al Kα source ($h\nu$ = 1486 eV) and detected at a take-off angle of 90°. The resolution, binding energy referencing, and transmission function of the analyzer were determined using a clean polycrystalline Ag foil. XPS peak fitting was carried out using the CasaXPS software (Voigt -mixed Gaussian−Lorentzian line shapes and a Shirley background). The peaks were corrected with respect to C1*s* at 284.7 eV due to the use of the charge neutralizer to avoid surface charging.

4.4.3 Experimental procedures

Typical procedure for the self-deoxygenating aqueous Cu-RDRP of NiPAm with targeted DP_n = 50.

Conditions*:* [I] : [NiPAm] : [Cu(I)Br] : [Me_6Tren] = 1 : 50 : 0.4 : 0.4.

A vial (***solution A***) was charged with 0.7 g NiPAm (50 eq., 6.186 mmol), 28.8 mg (1 eq., 0.124 mmol) water-soluble initiator (2,3-dihydroxypropyl 2-bromo-2-methylpropanoate) and **5.3 mL DI-H_2O**. The solution was sonicated until total dissolution of NiPAm. In parallel, a second glass vial (***solution B - disproportionation***) was charged with a stirrer bar, Cu(I)Br (0.4 eq., 0.0495 mmol, 7.1 mg), **1 mL** of DI-H_2O and Me_6Tren (0.4 eq., 0.0495 mmol, 13.3 μL). The vial was septum-sealed, and the disproportionation reaction was left to commence in ice-bath (0-1 ^oC) with **900 rpm stirring** applied for **60 seconds**. Instantly, ***solution B*** became blue (indicating Cu(II)) and black/purple particles (Cu(0) particles) were formed, indicating the successful disproportionation of Cu(I) towards Cu(II) and Cu(0). After 60 seconds, the solution containing the monomer and the initiator (***solution A***) was transferred in the disproportionation solution (***solution B***) through a plastic syringe and the polymerization was left to commence for 12 minutes. It should be noted that while ***solution A*** was being was transferred in ***solution B*** (disproportionation solution), an exit needle was used to facilitate the solution transfer. After 12 minutes, 0.6 mL of the polymerization solution were taken; 0.2 mL were diluted in D_2O for ^1H NMR analysis, while 0.4 mL were diluted in DMF, passed through a neutral alumina column for the removal of copper traces and were filtered prior to DMF-SEC characterization.

Typical procedure for the self-deoxygenating aqueous Cu-RDRP of NiPAm with targeted DP_n = 50 (open-to-air)

Conditions*: [I] : [NiPAm] : [Cu(I)Br] : [Me_6Tren] = 1 : 50 : 0.4 : 0.4.*

A vial (***solution A***) was charged with 0.7 g NiPAm (50 eq., 6.186 mmol), 28.8 mg (1 eq., 0.124 mmol) water-soluble initiator (2,3-dihydroxypropyl 2-bromo-2-methylpropanoate) and **5.3 mL DI-H_2O**. The solution was sonicated until total dissolution of NiPAm. In parallel, a second glass vial (***solution B - disproportionation***) was charged with a stirrer bar, Cu(I)Br (0.4 eq., 0.0495 mmol, 7.1 mg), **1 mL** of DI-H_2O and Me_6Tren (0.4 eq., 0.0495 mmol, 13.3 μL) and the disproportionation reaction was left to commence in ice-bath (0-1 ^oC) with **900 rpm stirring** applied for **60 seconds**. Instantly, ***solution B*** became blue (indicating Cu(II)) and black/purple particles (Cu(0) particles) were formed. After 60 seconds, the solution containing the monomer and the initiator (***solution A***) was transferred in the disproportionation solution (***solution B***) through a plastic syringe and the polymerization was left to commence for 12 minutes. After 12 minutes, 0.6 mL of the polymerization solution were taken; 0.2 mL were diluted in D_2O for ^1H NMR analysis, while 0.4 mL were diluted in DMF, passed through a neutral alumina column for the removal of copper traces and were filtered prior to DMF-SEC characterization.

Typical procedure for the self-deoxygenating aqueous Cu-RDRP of $PEGA_{480}$ with targeted DP_n = 20

Conditions*: [I] : [$PEGA_{480}$] : [Cu(I)Br] : [Me_6Tren] = 1 : 20 : 0.4 : 0.4.*

A vial (***solution A***) was charged with 0.7 mL $PEGA_{480}$ (20 eq., 1.59 mmol), 19.2 mg (1 eq., 0.08 mmol) water-soluble initiator (2,3-dihydroxypropyl 2-bromo-2-methylpropanoate) and **5.3 mL DI-H_2O**. In parallel, a second glass vial (***solution B - disproportionation***) was charged with a stirrer bar, Cu(I)Br (0.4 eq., 0.0318 mmol, 4.6

mg), **1 mL** of DI-H_2O and Me_6Tren (0.4 eq., 0.0318 mmol, 8.5 μL). The vial was septum-sealed, and the disproportionation reaction was left to commence in ice-bath (0-1 ^oC) with **900 rpm stirring** applied for **60 seconds**. Instantly, ***solution B*** becomes blue (indicating Cu(II)) and black/purple particles (Cu(0) particles) are formed, indicating the successful disproportionation of Cu(I) towards Cu(II) and Cu(0). After 60 seconds, the solution containing the monomer and the initiator (***solution A***) was transferred in the disproportionation solution (***solution B***) through a plastic syringe and the polymerization was left to commence for 30 minutes. It should be noted that while ***solution A*** was being was transferred in ***solution B*** (disproportionation solution), an exit needle was used to facilitate the solution transfer. After 30 minutes, 0.6 mL of the polymerization solution were taken; 0.2 mL were diluted in D_2O for ^1H NMR analysis, while 0.4 mL were diluted in DMF, passed through a neutral alumina column for the removal of copper traces and were filtered prior to DMF-SEC characterization.

Typical procedure for the self-deoxygenating aqueous Cu-RDRP of NAM with targeted DP_n = 40

Conditions*: [I] : [NAM] : [Cu(I)Br] : [Me_6Tren] = 1 : 40 : 0.8 : 0.4.*

A vial (***solution A***) was charged with 0.7 mL NAM (40 eq., 5.56 mmol), 33.5 mg (1 eq., 0.14 mmol) water-soluble initiator (2,3-dihydroxypropyl 2-bromo-2-methylpropanoate) and **5.3 mL DI-H_2O**. In parallel, a second glass vial (***solution B - disproportionation***) was charged with a stirrer bar, Cu(I)Br (0.8 eq., 0.112 mmol, 16 mg), **1 mL** of DI-H_2O and Me_6Tren (0.4 eq., 0.084 mmol, 22.5 μL). The vial was septum-sealed, and the disproportionation reaction was left to commence in ice-bath (0-1 ^oC) with **900 rpm stirring** applied for **60 seconds**. Instantly, ***solution B*** becomes blue (indicating Cu(II)) and black/purple particles (Cu(0) particles) are formed,

indicating the successful disproportionation of Cu(I) towards Cu(II) and Cu(0). After 60 seconds, the solution containing the monomer and the initiator (***solution A***) was transferred in the disproportionation solution (***solution B***) through a plastic syringe and the polymerization was left to commence for 4 hours. It should be noted that while ***solution A*** was being was transferred in ***solution B*** (disproportionation solution), an exit needle was used to facilitate the solution transfer. After 4 hours, 0.6 mL of the polymerization solution were taken; 0.2 mL were diluted in D_2O for ^1H NMR analysis, while 0.4 mL were diluted in DMF, passed through a neutral alumina column for the removal of copper traces and were filtered prior to DMF-SEC characterization.

Typical procedure for the self-deoxygenating aqueous Cu-RDRP of HEAm with targeted DP_n = 100

Conditions*: [I] : [HEAm] : [Cu(I)Br] : [Me_6Tren] = 1 : 100 : 0.8 : 0.4.*

A vial (***solution A***) was charged with 0.7 mL HEAm (100 eq., 6.75 mmol), 14.6 mg (1 eq., 0.067 mmol) water-soluble initiator (2,3-dihydroxypropyl 2-bromo-2-methylpropanoate) and **5.3 mL DI-H_2O**. In parallel, a second glass vial (***solution B - disproportionation***) was charged with a stirrer bar, Cu(I)Br (0.8 eq., 0.054 mmol, 7.75 mg), **1 mL** of DI-H_2O and Me_6Tren (0.4 eq., 0.027 mmol, 7.2 μL). The vial was septum-sealed, and the disproportionation reaction was left to commence in ice-bath (0-1 ^oC) with **900 rpm stirring** applied for **60 seconds**. Instantly, ***solution B*** becomes blue (indicating Cu(II)) and black/purple particles (Cu(0) particles) are formed, indicating the successful disproportionation of Cu(I) towards Cu(II) and Cu(0). After 60 seconds, the solution containing the monomer and the initiator (***solution A***) was transferred in the disproportionation solution (***solution B***) through a plastic syringe and the polymerization was left to commence for 15 minutes. It should be noted that while ***solution A*** was being was transferred in ***solution B*** (disproportionation

solution), an exit needle was used to facilitate the solution transfer. After 15 minutes, 0.6 mL of the polymerization solution were taken; 0.2 mL were diluted in D_2O for ^1H NMR analysis, while 0.4 mL were diluted in DMF, passed through a neutral alumina column for the removal of copper traces and were filtered prior to DMF-SEC characterization.

Typical procedure for the self-deoxygenating aqueous Cu-RDRP of DMA with targeted DP_n = 80

Conditions*:* [I] : [DMA] : [Cu(I)Br] : [Me_6Tren] = 1 : 80 : 0.8 : 0.4.

A vial (***solution A***) was charged with 0.7 mL DMA (80 eq., 6.79 mmol), 12.2 mg (1 eq., 0.085 mmol) water-soluble initiator (2,3-dihydroxypropyl 2-bromo-2-methylpropanoate) and **5.3 mL DI-H_2O**. In parallel, a second glass vial (***solution B - disproportionation***) was charged with a stirrer bar, Cu(I)Br (0.8 eq., 0.068 mmol, 9.75 mg), **1 mL** of DI-H_2O and Me_6Tren (0.4 eq., 0.034 mmol, 9 μL). The vial was septum-sealed, and the disproportionation reaction was left to commence in ice-bath (0-1 ^oC) with **900 rpm stirring** applied for **60 seconds**. Instantly, ***solution B*** becomes blue (indicating Cu(II)) and black/purple particles (Cu(0) particles) are formed, indicating the successful disproportionation of Cu(I) towards Cu(II) and Cu(0). After 60 seconds, the solution containing the monomer and the initiator (***solution A***) was transferred in the disproportionation solution (***solution B***) through a plastic syringe and the polymerization was left to commence for 20 minutes. It should be noted that while ***solution A*** was being was transferred in ***solution B*** (disproportionation solution), an exit needle was used to facilitate the solution transfer. After 20 minutes, 0.6 mL of the polymerization solution were taken; 0.2 mL were diluted in D_2O for ^1H NMR analysis, while 0.4 mL were diluted in DMF, passed through a neutral alumina column for the removal of copper traces and were filtered prior to DMF-SEC characterization.

Typical procedure for the self-deoxygenating aqueous Cu-RDRP of PHEAm (8-arm) star-shaped polymers with overall targeted DP_n = 160

Conditions*: [I] : [HEAm] : [Cu(I)Br] : [Me_6Tren] = 1 : 160 : 6.4 : 4.2.*

The multi-functional (8-arms) initiator (64.7 mg, 1 eq., 0.042mmol) was dissolved in 4 mL DMSO and in the same vial, 0.7 mL HEAm (160 eq., 6.75 mmol) which were dissolved in 1.3 mL DI-H_2O were added (***solution A***). In parallel, a second glass vial (***solution B - disproportionation***) was charged with a stirrer bar, Cu(I)Br (6.4 eq., 38.7 mg), **1 mL** of DI-H_2O and Me_6Tren (4.2 eq., 48.5 μL). The vial was septum-sealed, and the disproportionation reaction was left to commence in ice-bath (0-1 ^oC) with **900 rpm stirring** applied for **60 seconds**. Instantly, ***solution B*** becomes blue (indicating Cu(II)) and black/purple particles (Cu(0) particles) are formed, indicating the successful disproportionation of Cu(I) towards Cu(II) and Cu(0). After 60 seconds, the solution containing the monomer and the initiator (***solution A***) was transferred in the disproportionation solution (***solution B***) through a plastic syringe and the polymerization was left to commence for 90 minutes. It should be noted that while ***solution A*** was being was transferred in ***solution B*** (disproportionation solution), an exit needle was used to facilitate the solution transfer. After 90 minutes, 0.6 mL of the polymerization solution were taken; 0.2 mL were diluted in D_2O for ^1H NMR analysis, while 0.4 mL were diluted in DMF, passed through a neutral alumina column for the removal of copper traces and were filtered prior to DMF-SEC characterization. The same process was followed for the other star-shaped polymers with different concentrations of Cu(I)Br and Me_6Tren, as described in the analogous section and **Table 4-4**.

4.4.4 Supplementary Figures & Characterization

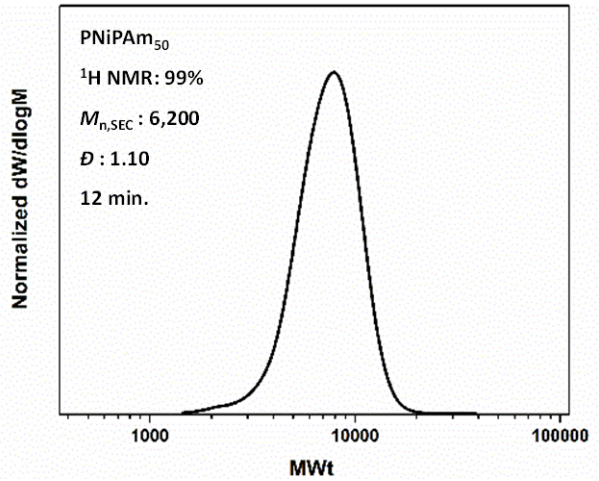

Figure 4-23. DMF-SEC derived molecular weight distribution of PNiPAm with targeted DP_n = 50 synthesized *via* N_2-deoxygenated aqueous Cu-RDRP with the pre-disproportionation of Cu(I)/Me_6Tren in H_2O at 0 °C.

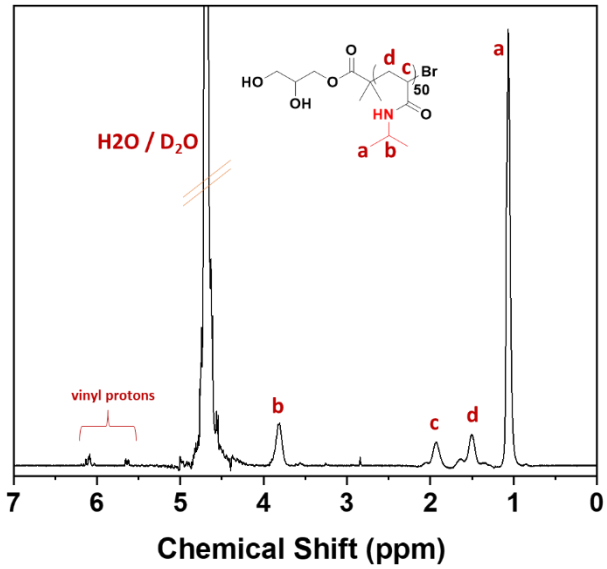

Figure 4-24. ^{1}H NMR spectrum in D_2O for the PNiPAm with targeted DP_n = 50 synthesized *via self-deoxygenating* aqueous Cu-RDRP with the pre-disproportionation of Cu(I)/Me_6Tren in H_2O at 0 °C. Conversion was determined by comparing the integrals of monomeric vinyl protons (~ 5.5-6.5 ppm) to polymer signal.

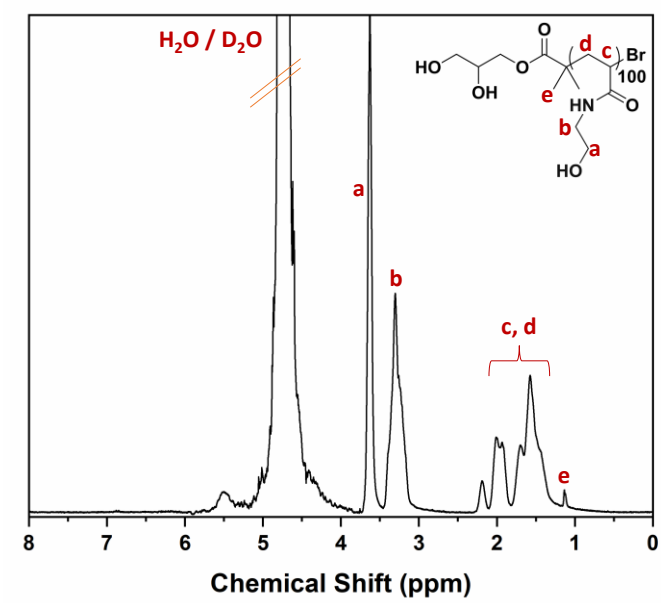

Figure 4-25. ^{1}H NMR spectrum in D_2O for the PHEAm with targeted DP_n = 100 synthesized *via self-deoxygenating* aqueous Cu-RDRP with the pre-disproportionation of Cu(I)/Me_6Tren in H_2O at 0 °C. Conversion was determined by comparing the integrals of monomeric vinyl protons to polymer signal.

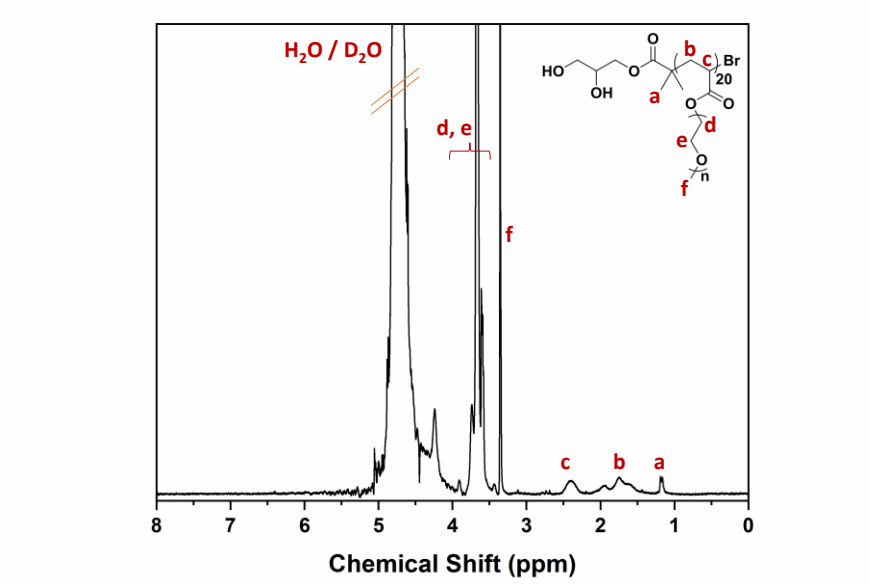

Figure 4-26. ^{1}H NMR spectrum in D_2O for the P($PEGA_{480}$) with targeted DP_n = 20 synthesized *via self-deoxygenating* aqueous Cu-RDRP with the pre-disproportionation of Cu(I)/Me_6Tren in H_2O at 0 °C. Conversion was determined by comparing the integrals of monomeric vinyl protons to polymer signal.

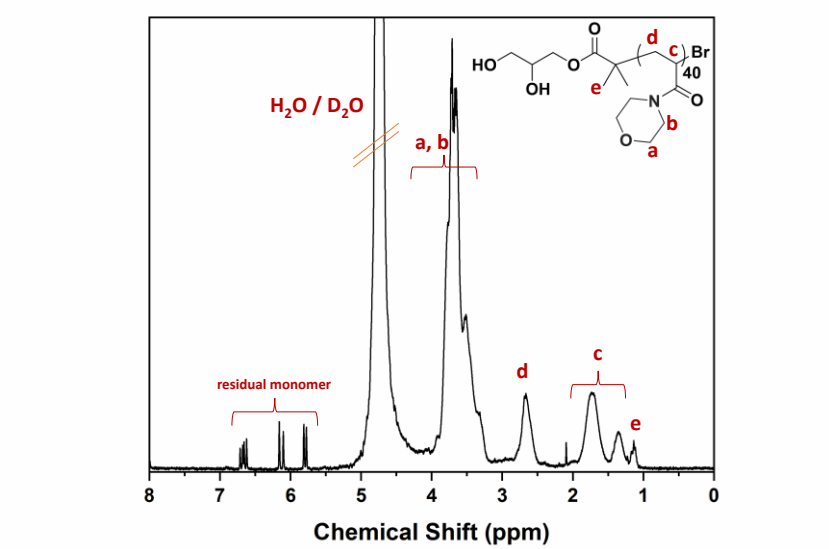

Figure 4-27. ^{1}H NMR spectrum in D_2O for the PNAM with targeted DP_n = 40 synthesized *via self-deoxygenating* aqueous Cu-RDRP with the pre-disproportionation of Cu(I)/Me_6Tren in H_2O at 0 °C. Conversion was determined by comparing the integrals of monomeric vinyl protons (~ 5.5 – 6.8 ppm) from the residual monomer to polymer signal.

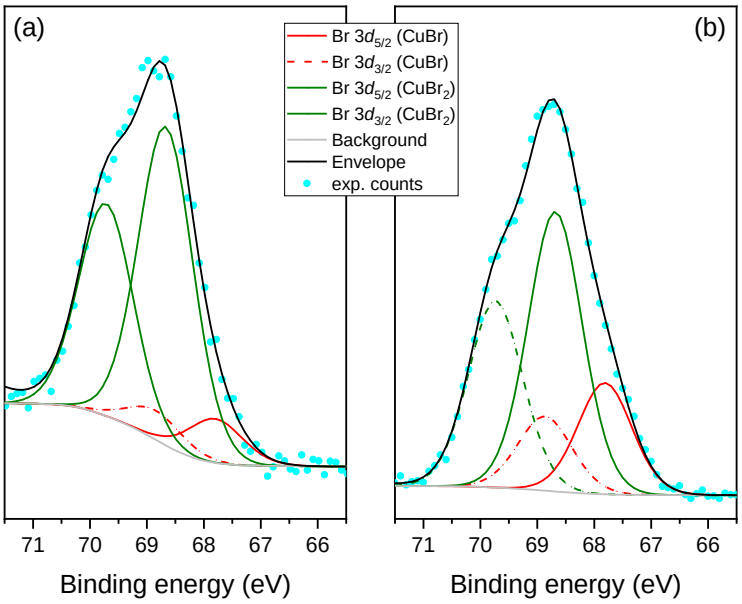

Figure 4-28. High resolution XPS of the Br 3*d* region revealing the presence of CuBr and $CuBr_2$ in both **a)** the disproportionation precipitate and **b)** the supernatant.

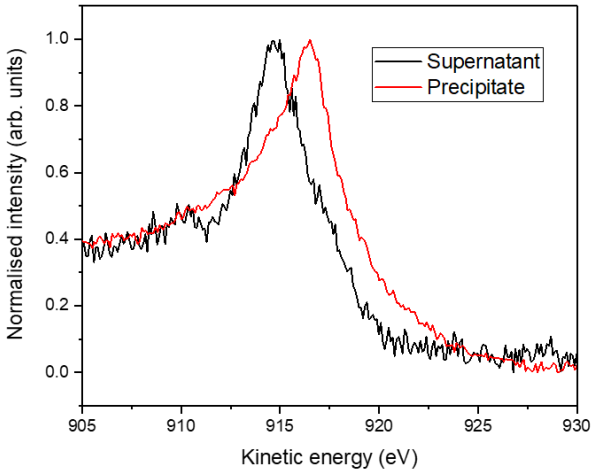

Figure 4-29. Cu LMM Auger spectra of the disproportionation precipitate and the supernatant after 60 seconds of the reaction. The shift in the position of the maximum intensity reflects a decrease in the relative amount of Cu(II) states ($CuBr_2$, CuO, $Cu(OH)_2$) in the supernatant to a higher proportion of Cu(0) or Cu(I) in the precipitate.

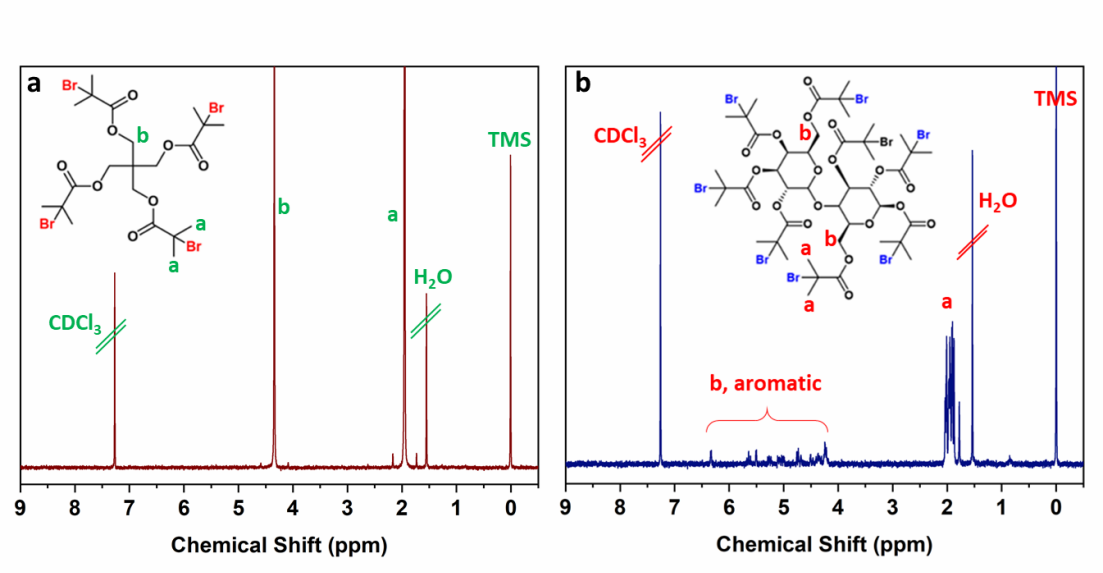

Figure 4-30. ^1H NMR spectrum in D_2O for a) the 4-arm initiator and b) the 8-arm initiator which were *in-house* synthesized and used for the synthesis of the star-shaped PHEAm polymers.

4.5 References

1 M. Kato, M. Kamigaito, M. Sawamoto and T. Higashimura, *Macromolecules*, 1995, **28**, 1721–1723.
2 J.-S. Wang and K. Matyjaszewski, *J. Am. Chem. Soc.*, 1995, **117**, 5614–5615.
3 V. Percec, T. Guliashvili, J. S. Ladislaw, A. Wistrand, A. Stjerndahl, M. J. Sienkowska, M. J. Monteiro and S. Sahoo, *J. Am. Chem. Soc.*, 2006, **128**, 14156–14165.
4 B. M. Rosen and V. Percec, *Chem. Rev.*, 2009, **109**, 5069–5119.
5 G. Moad, E. Rizzardo and S. H. Thang, *Aust. J. Chem.*, 2009, **62**, 1402–1472.
6 S. Perrier, *Macromolecules*, 2017, 50, 7433–7447.
7 C. J. Hawker, A. W. Bosman and E. Harth, *Chem. Rev.*, 2001, **101**, 3661–3688.
8 G. Moad and E. Rizzardo, in *RSC Polymer Chemistry Series*, Royal Society of Chemistry, 2016, 1–44..
9 R. Aksakal, M. Resmini and C. R. Becer, *Polym. Chem.*, 2016, **7**, 171–175.
10 J. De Neve, J. J. Haven, L. Maes and T. Junkers, *Polym. Chem.*, 2018, **9**, 4692–4705.
11 L. Tao, J. Liu and T. P. Davis, *Biomacromolecules*, 2009, **10**, 2847–2851.
12 V. A. Bhanu and K. Kishore, *Chem. Rev.*, 1991, **91**, 99–117.
13 J. Yeow, R. Chapman, A. J. Gormley and C. Boyer, *Chem. Soc. Rev.*, 2018.
14 J. G. Riess, *Tetrahedron*, 2002, **58**, 4113–4131.
15 P. Gurnani, T. Floyd, J. Tanaka, C. Stubbs, D. Lester, C. Sanchez-Cano and S. Perrier, *Polym. Chem.*, , DOI:10.1039/c9py01521c.
16 E. Liarou, A. Anastasaki, R. Whitfield, C. E. Iacono, G. Patias, N. G. Engelis, A. Marathianos, G. R. Jones and D. M. Haddleton, *Polym. Chem.*, 2019, **10**, 963–971.
17 J. Yeow, R. Chapman, J. Xu and C. Boyer, *Polym. Chem.*, 2017, **8**, 5012–5022.
18 F. Oytun, M. U. Kahveci and Y. Yagci, *J. Polym. Sci. Part A Polym. Chem.*, 2013, **51**, 1685–1689.
19 R. Chapman, A. J. Gormley, K.-L. L. Herpoldt and M. M. Stevens, *Macromolecules*, 2014, **47**, 8541–8547.
20 Y. Wang, L. Fu and K. Matyjaszewski, *ACS Macro Lett.*, 2018, **7**, 1317–1321.
21 A. E. Enciso, L. Fu, A. J. Russell and K. Matyjaszewski, *Angew. Chemie Int. Ed.*, 2018, **57**, 933–936.
22 T. Zhang, J. Yeow and C. Boyer, *Polym. Chem.*, 2019, **10**, 4643–4654.
23 G. Ng, J. Yeow, J. Xu and C. Boyer, *Polym. Chem.*, 2017, **8**, 2841–2851.
24 G. Ng, J. Yeow, J. Xu and C. Boyer, *Polym. Chem.*, 2017, **8**, 2841–2851.
25 K. Min, H. Gao and K. Matyjaszewski, *Macromolecules*, 2007, **40**, 1789–1791.
26 S. Fleischmann, B. M. Rosen and V. Percec, *J. Polym. Sci. Part A Polym. Chem.*, 2010, **48**, 1190–1196.
27 S. Fleischmann and V. Percec, *J. Polym. Sci. Part A Polym. Chem.*, 2010, **48**, 2243–2250.

28 J. Yeow, S. Joshi, R. Chapman and C. Boyer, *Angew. Chemie Int. Ed.*, 2018, **57**, 10102–10106.

29 N. Corrigan, D. Rosli, J. W. J. Jones, J. Xu and C. Boyer, *Macromolecules*, , DOI:10.1021/acs.macromol.6b01306.

30 S. Shanmugam, J. Xu and C. Boyer, *J. Am. Chem. Soc.*, 2015, **137**, 9174–9185.

31 E. Liarou, R. Whitfield, A. Anastasaki, N. G. Engelis, G. R. Jones, K. Velonia and D. M. Haddleton, *Angew. Chemie*, 2018, **57**, 8998–9002.

32 A. Marathianos, E. Liarou, A. Anastasaki, R. Whitfield, M. Laurel, A. M. Wemyss and D. M. Haddleton, *Polym. Chem.*, 2019, **10**, 4402-4406.

33 T. Sato, Y. Hamada, M. Sumikawa, S. Araki and H. Yamamoto, *Ind. Eng. Chem. Res.*, 2014, **53**, 19331–19337.

34 H. Ramesh, T. Mayr, M. Hobisch, S. Borisov, I. Klimant, U. Krühne and J. M. Woodley, *J. Chem. Technol. Biotechnol.*, 2016, **91**, 832–836.

35 C. B. Kretschmer, J. Nowakowska and R. Wiebe, *Ind. Eng. Chem.*, 1946, **38**, 506–509.

36 G. R. Jones, A. Anastasaki, R. Whitfield, N. Engelis, E. Liarou and D. M. Haddleton, *Angew. Chemie Int. Ed.*, 2018, **57**, 10468–10482.

37 F. Alsubaie, E. Liarou, V. Nikolaou, P. Wilson and D. M. Haddleton, *Eur. Polym. J.*, 2019, **114**, 326-331.

38 G. R. Jones, Z. Li, A. Anastasaki, D. J. Lloyd, P. Wilson, Q. Zhang and D. M. Haddleton, *Macromolecules*, 2016, **49**, 483–489.

39 M. R. Hill, R. N. Carmean and B. S. Sumerlin, *Macromolecules*, 2015, **48**, 5459–5469.

40 S. Shanmugam, J. Xu and C. Boyer, *Macromolecules*, 2016, **49**, 9345–9357.

41 H. Qian and L. He, *Anal. Chem.*, 2009, **81**, 9824–9827.

42 G. O. Okelo and L. He, *Biosens. Bioelectron.*, 2007, **23**, 588–592.

43 A. E. Enciso, L. Fu, S. Lathwal, M. Olszewski, Z. Wang, S. R. Das, A. J. Russell and K. Matyjaszewski, *Angew. Chemie Int. Ed.*, 2018, **57**, 16157–16161.

44 A. Layadi, B. Kessel, W. Yan, M. Romio, N. D. Spencer, M. Zenobi-Wong, K. Matyjaszewski and E. M. Benetti, *J. Am. Chem. Soc.*, 2020, jacs.9b12974.

45 Q. Zhang, P. Wilson, Z. Li, R. McHale, J. Godfrey, A. Anastasaki, C. Waldron and D. M. Haddleton, *J. Am. Chem. Soc.*, 2013, **135**, 7355–7363.

46 S. Aksakal, R. Aksakal and C. R. Becer, *Macromol. Rapid Commun.*, 2019, **40**, 1900247.

47 R. Whitfield, A. Anastasaki, N. P. Truong, P. Wilson, K. Kempe, J. A. Burns, T. P. Davis and D. M. Haddleton, *Macromolecules*, 2016, **49**, 8914–8924.

48 X. Jiang, S. Fleischmann, N. H. Nguyen, B. M. Rosen and V. Percec, *J. Polym. Sci. Part A Polym. Chem.*, 2009, **47**, 5591–5605.

49 N. Ballard and J. M. Asua, *ACS Macro Lett.*, 2020, 190–196.

50 J. C. T. Vogelaar, A. Klapwijk, J. B. Van Lier and W. H. Rulkens, *Water Res.*, 2000, **34**, 1037–1041.

51 P. Han and D. M. Bartels, *J. Phys. Chem.*, 1996, **100**, 5597–5602.

52 R. T. Ferrell and D. M. Himmelblau, *J. Chem. Eng. Data*, 1967, **12**, 111–115.

53 L. Laffont, M. Y. Wu, F. Chevallier, P. Poizot, M. Morcrette and J. M. Tarascon, *Micron*, 2006, **37**, 459–464.

54 Y. Wang, S. Lany, J. Ghanbaja, Y. Fagot-Revurat, Y. P. Chen, F. Soldera, D. Horwat, F. Mücklich and J. F. Pierson, *Phys. Rev. B*, 2016, **94**, 245418.

55 M. Ciampolini and N. Nardi, *Inorg. Chem.*, 1966, **5**, 41–44.

56 S. Perrier, S. P. Armes, X. S. Wang, F. Malet and D. M. Haddleton, *J. Polym. Sci. Part A Polym. Chem.*, 2001, **39**, 1696–1707.

Chapter 5.

UV irradiation of Cu-based complexes with aliphatic amine ligands as used in living radical polymerization

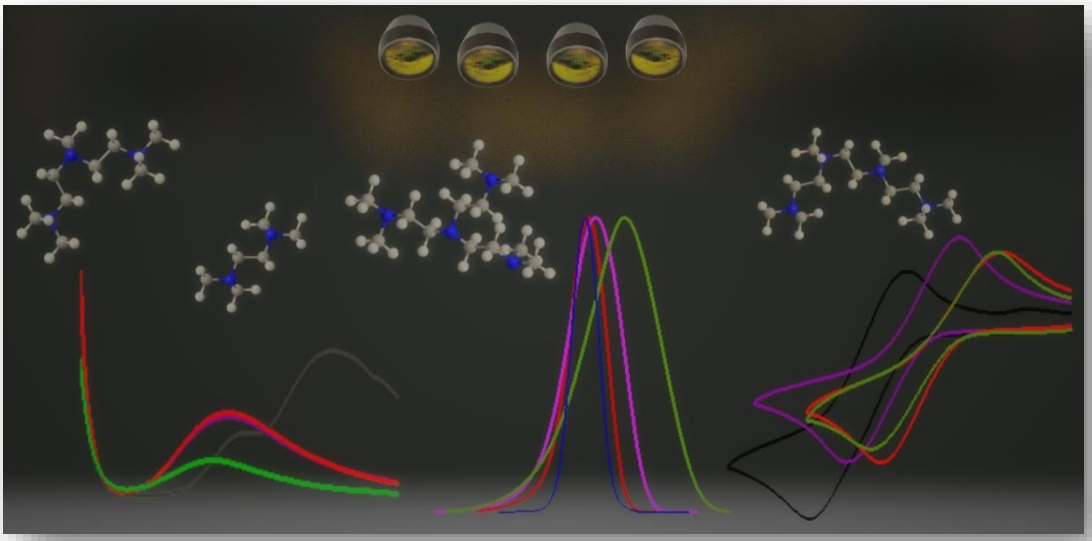

In this chapter, the effect UV of irradiation on Cu(II)-based complexes with aliphatic amine ligands is investigated and discussed. Four aliphatic amines are used as ligands and Cu(II)Br_2 as the metal source for the formation of catalyst complexes that can be used for the photoinduced copper mediated-Reversible Deactivation Radical Polymerization (Cu-RDRP) of methyl acrylate. Different characterization techniques such as transient electronic absorption spectroscopy (TEAS), ultraviolet-

visible (UV-Vis) spectroscopy, electrospray ionization time of flight mass spectrometry (ESI-ToF-MS) and cyclic voltammetry (CV) are applied in order to provide insight into the catalyst behaviour upon photo-irradiation. The excited-state dynamics, the electrochemical behaviour of the Cu(II)/Cu(I) redox couples and the detection of different species upon complexation of the ligand to the metal centre (before and after UV irradiation) are further depicted in the quality of the obtained polymers.

5.1 Introduction

The controlled/living radical polymerization of vinyl monomers (methacrylates, acrylates, acrylamides, styrene) has revolutionized the field of polymer science. Transition metal mediated/catalyzed methodologies were introduced in 1995 using low valent Ru(II)[1] and Cu(I)[2] complexes in conjunction with alkyl halides. Up until this point, ionic and ionic-related polymerization were most successful requiring the use of anhydrous conditions and pure reagents and solvents. The transition metal-based radical techniques such as Atom Transfer Radical Polymerization (ATRP)[1, 2] and Single Electron Transfer Living Radical Polymerization (SET-LRP),[3-6] emerged as powerful tools for the synthesis of numerous materials, with different architectures and functionalities, in a variety of media and under different conditions without the requirement of rigorously removing water and other protic impurities or the need for protecting groups for monomers containing such functionality.[7-14]

These methods depend on an activation-deactivation equilibrium between active and dormant species, related to the transition metal complex (M^n X/L) which activates an alkyl halide (P_n-X) leading to M^{n+1} X_2/L and a P_n radical leading to chain growth.[15-17] As in other living polymerizations, the chain length is determined by the

[monomer]/[R-X] with the α-terminus derived from the initiator (R-X) and the ω-group of the halide. Initiation and propagation occur *via* reversible homolytic bond cleavage of the R-X bond and the low concentration of resulting radicals means chain termination *via* second order radical/radical reaction is minimised. This allows for the design and control of the transition metal complex through external stimuli such as electrochemical[18] and photochemical methods.[17, 19, 20]

The application of photochemistry in these systems offers numerous advantages such as mild reaction conditions, spatial and temporal control, is environmentally friendly and non-invasive and as a result it has been proved to be an excellent candidate for triggering organic reactions and polymerizations.[21-31] Hawker and colleagues, utilizing visible light and a photoactive iridium complex (*fac*-[Ir(ppy)$_3$] (ppy = 2-pyridylphenyl), reported the synthesis of well-defined poly(methyl methacrylate) (PMMA) with spatiotemporal control.[32, 33] Yagci and co-workers reported the synthesis of PMMA applying different conditions, such as in the presence and absence of photoinitiators and photosensitizers, as well as different applied wavelengths.[34-37] Matyjaszewski and colleagues have reported the synthesis of acrylates and methacrylates by employing low loadings (parts per million) of copper catalyst under visible light, as well as in different media.[22, 38] Haddleton and colleagues have investigated the photoinduced Cu-mediated Reversible Deactivation Radical Polymerization (Cu-RDRP) of various acrylates utilizing excess of an aliphatic tertiary amine under UV irradiation reaching near-quantitative conversions at different molar masses.[17]

The versatility of these photo-regulated systems has led researchers to understand the mechanism of photoRDRP in an attempt to provide insights into the transition metal complex behaviour. The catalyst mainly consists of the transition metal (copper

(Cu) in this current study) and the ligand(s) (herein aliphatic amines). Consequently, as the catalyst has a determining role on transferring the halogen and regulating the equilibrium between active and dormant species, the impact of photo-irradiation is important. Haddleton and co-workers reported that an excess of the aliphatic amine ligand (relative to $Cu(II)Br_2$) is required so as to maintain excellent control over the polymerization by varying the composition of the catalyst ($Cu(II)Br_2$ and tris[2-(dimethylamino)ethyl]amine (Me_6TREN) as ligand) for the polymerization of acrylates.[17] UV-vis spectroscopy was applied to follow the polymerization and monitor the effect of UV irradiation on the components of the polymerization over time. They proposed that the photoexcitation of free Me_6Tren is responsible for the C-Br bond homolysis, which occurs through an outer-sphere single-electron transfer (OSET) when the alkyl halide initiator is present, with the occurring radical initiating the polymerization. Moreover, this OSET process results in Me_6Tren radical cations and Br anions that participate in the oxidation of the generated active species, into $Cu(II)Br_2/Me_6$Tren. Matyjaszewski's group investigated the mechanism of activation and radical regeneration in photoATRP by performing a series of experiments with several reaction conditions, and experimental and kinetic simulation techniques.[39] Based on their findings, the (re)generation of the activator occurs from the photochemical reduction of Cu(II) complexes when excess of the amine ligand is employed, with the latter being oxidized to form a ligand-based radical cation, capable of initiating a new chain. Barner-Kowollik and colleagues investigated the initiation mechanism of photoRDRP utilizing pulsed-laser polymerization (PLP) and high resolution mass spectrometry, highlighting the role of the ligand which acts as a reducing agent.[40] They demonstrated that upon UV irradiation, scission of the initiator's C-Br bond occurs which subsequently provides radicals that can propagate

and also react with Cu(II) species. Upon UV irradiation, an electron transfer reaction takes place between the photoexcited ligand and Cu(II) moieties leading to the generation of Cu(I) species, and apart from that, it was proposed that the Cu(II) complex gets excited and subsequently quenched by the free ligand, generating the analogous Cu(I) complex and the ligand radical cation. All the aforementioned approaches highlight the importance of the excess ligand on photoinduced-RDRP and by utilizing different analytical (*i.e.* spectroscopic) techniques, interesting insights on the mechanism have been reported. However, a limited number of different ligands have been employed for these investigations, with Me_6Tren having been the most extensively studied ligand for photo-induced Cu-RDRP.

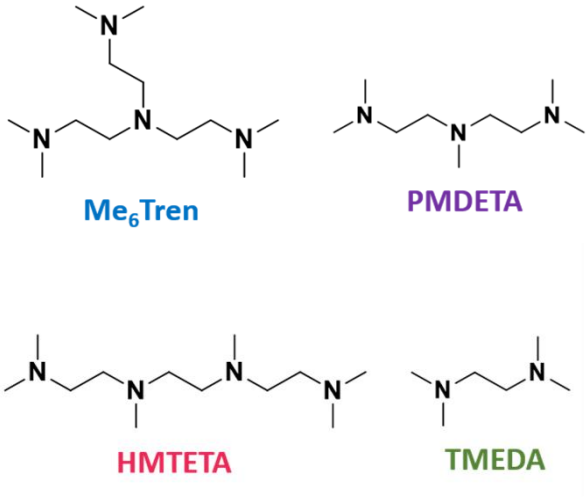

Scheme 5-1. Chemical structures of the aliphatic amines used as ligands in this investigation.

In this chapter, the application of different characterization methods and analytical techniques including UV-Vis spectroscopy, ESI-ToF-MS and CV give insights into the effect of UV irradiation (broad band λ_{max} ~ 360 nm) on the transition metal complex, when different aliphatic amines are employed as ligands (**Scheme 1**) and Cu(II)Br_2 as the metal source. In order to investigate the excited-state behaviour of these complexes in depth, the [Cu(II)(Me_6Tren)Br_2] and the [Cu(II)(PMDETA)Br_2]

complexes are studied through TEAS. Furthermore, the different catalytic complexes are employed for the photoinduced Cu-RDRP of methyl acrylate in organic media, leading to differences in the molecular characteristics of the obtained PMAs.

5.2 Results and Discussion

Initially, different Cu-based complexes with aliphatic amine ligands (L) were prepared *in-situ* in dimethyl sulfoxide (DMSO), including tris[2-(dimethylamino)ethyl]amine (Me_6Tren) (tripodal, 4N), 1,1,4,7,10,10-Hexamethyltriethylenetetramine (HMTETA) (linear tetradentate, 4N), N,N,N′,N″,N″-Pentamethyldiethylenetriamine (PMDETA) (tridentate, 3N) and tetramethylethylenediamine (bidentate, 2N) (TMEDA) as ligands and Cu(II)Br_2 as the metal source. Subsequently, the different complexes were employed for the photoinduced Cu-RDRP of methyl acrylate (MA) with ethyl α-bromoisobutyrate (EBiB) as the initiator, following the ratio [MA]:[EBiB]:[L]:[Cu(II)Br_2] = [50]:[1]:[0.02]:[0.12], in 50 % v/v DMSO, under a UV "nail lamp" with broad band emission and λ_{max} ~ 360 nm. As previously reported, the use of Me_6Tren (in excess with respect to Cu(II)Br_2) leads to control over the polymerization with well-defined polyacrylates and low dispersities. Kinetic experiments showed that, as expected, the rate of the polymerization was very fast (**Table 5-1**) and the semi-logarithmic plot of $\ln[M_0/M_t]$ versus time follows linear trend, indicating that the reaction is first order with respect to [monomer] and the generation of the radicals is constant (**Figure 5-1A**). Moreover, the experimental M_n values ($M_{n,SEC}$) exhibited very good agreement with the theoretical values ($M_{n,th.}$) which was depicted by the linear evolution of $M_{n,SEC}$ with respect to monomer conversion.

When HMTETA, a linear tetradentate aliphatic amine similar to Me_6Tren was employed as ligand, although the $M_{n,SEC}$ showed linear behaviour with conversion and there was agreement between $M_{n,SEC}$ and $M_{n,th}$., the $\ln[M_0/M_t]$ versus time plot exhibited deviations from first order behaviour with respect to monomer. This indicates that the [propagating chains] was not constant throughout the polymerization and possibly there was an increase at high conversions (**Figure 5-1B**). Moreover, slower polymerization rates were observed compared to Me_6Tren (quantitative conversion after 2.5 hours) with the monomer conversion reaching 97% after 8 hours (**Table 5-1**). The dispersity of the polymers was higher than in the case of Me_6Tren with $Đ$ = 1.4 at 97% conversion.

When PMDETA (tridentate aliphatic amine) was used as ligand, good control over the molecular weights was observed as previously (**Table 5-1, Figure 5-1C**), although the dispersity values for PMA were slightly higher in comparison to the results obtained when Me_6Tren was used, reaching $Đ$ ~ 1.18 at 95% monomer conversion (after 8 hours). Although the $\ln[M_0/M_t]$ versus time slightly deviated from the first order trend, there was not clear curvature of the plot that would indicate inconsistency on the radical generation. When the bidentate TMEDA was utilized, the $M_{n,SEC}$ values deviated from the theoretical and the dispersity was higher than in the previous cases, reaching $Đ$ ~ 1.90 (**Table 5-1**). Moreover, the rate of polymerization was slightly slower than when tetradentate and tridentate ligands were used, reaching 90% monomer conversion after 8 hours (**Figure 5-1D**) and the $\ln[M_0/M_t]$ did not increase linearly with time.

Table 5-1. ^{1}H NMR and THF-SEC analysis for the photoinduced Cu-RDRP of MA (targeted DP_n = 50) with different aliphatic amines as ligands. [a]

Aliphatic amine	Time (hrs)	Conv. (%) [b]	$M_{n,SEC}$ [c] (g/mol)	$M_{n,th.}$ (g/mol)	$Đ$
Me$_6$Tren (tripodal, 4N)	0.5	45	1,400	2,100	1.17
	1	78	3,100	3,500	1.10
	1.5	89	3,900	4,000	1.09
	2	95	4,200	4,300	1.08
	2.5	98	4,400	4,400	1.08
HMTETA (linear, 4N)	1	3	-	-	-
	2	9	-	-	-
	3	25	900	1,200	1.80
	4	40	1,700	1,900	1.80
	6	92	4,100	4,200	1.50
	8	97	4,600	4,400	1.45
PMDETA (3N)	1	17	-	-	-
	2	30	1,100	1,500	1.40
	3	54	2,410	2,500	1.35
	4	72	3,400	3,300	1.30
	6	90	4,000	4,100	1.22
	8	95	4,500	4,300	1.18
TMEDA (2N)	1	1	-	-	-
	2	7	-	-	-
	3	18	3,100	970	1.60
	4	51	5,200	2,400	2.20
	6	72	5,800	3,300	2.00
	8	93	7,400	4,200	1.90

[a] For all the polymerizations the conditions were [MA]:[EBiB]:[L]:[Cu(II)Br$_2$] = [50]:[1]:[0.02]:[0.12], in 50 % *v/v* DMSO, under a UV lamp with broad band emission and λ_{max} ~ 360 nm. [b] Monomer conversion obtained through ^{1}H NMR in $CDCl_3$. [c] Determined by THF SEC analysis based on DRI and expressed as molecular weight equivalents to PMMA narrow molecular weight standards.

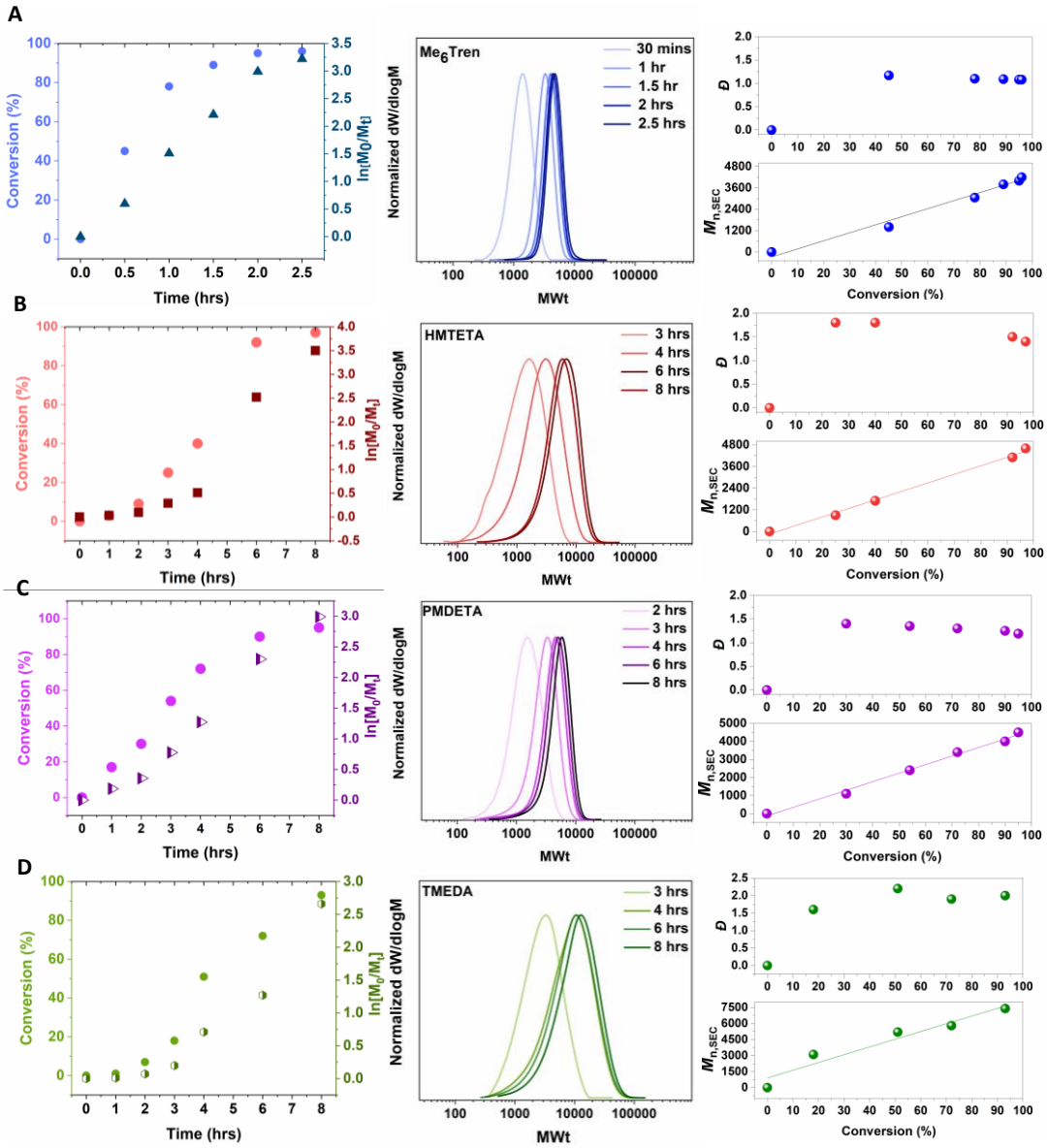

Figure 5-1. Kinetic plots of conversion and ln[M_0/M_t] over time, THF-SEC derived molecular weight distributions, and $M_{n,SEC}$ and dispersity ($Đ$) versus monomer conversion for PMA with targeted DP_n = 50 with **A)** Me_6Tren, **B)** HMTETA, **C)** PMDETA and **D)** TMEDA as ligands under UV lamp with broad band λ_{max} ~ 360 nm and [MA]:[EBiB]:[L]:[Cu(II)Br_2] = [50]:[1]:[0.02]:[0.12].

Since the evolution of the photoinduced Cu-RDRP of MA exhibited differences when different ligands where used (**Figure 5-8**), the behaviour of the different catalysts upon UV irradiation was subsequently investigated. Initially, deoxygenated solutions of the complexes in DMSO and [Cu(II)Br_2]:[L] = 1:6

(conditions also applied for polymerization) were prepared and studied through UV-Vis spectroscopy, upon exposure to UV irradiation. As has been extensively reported, the maximum absorbance at ~ 700 nm is attributed to the d-d transitions of the d^9 Cu(II) complex. It should be noted that deviations from the literature can be attributed to the different solvents used, since the solvent can play an important role on the coordination of Cu-complexes.[41] For the [Cu(II)(Me_6Tren)Br_2] complex, the characteristic maximum absorbance is found at 950 nm, with a second absorbance feature at 750 nm (**Figure 5-3A**). The reduction of these maxima, indicative of the reduction of Cu(II) to Cu(I) and attributed to a ligand-to-metal charge transfer (LMCT), was highly evident even after a short period of exposure at UV irradiation (**Figures 5-3 A&E**). Noteworthy is that apart from a consistent reduction in [Cu(II)(Me_6Tren)Br_2] during the first 5 hours of UV irradiation, after 24 hours a scattering slope is evident, indicating that changes in the physical properties of the complex take place without excluding the hypothesis of Cu(0) particle generation and accumulation. When the [Cu(II)(HMTETA)Br_2] complex was monitored, a reduction of the characteristic band at 725 nm was also evident, indicating the generation of Cu(I) from Cu(II) (**Figures 5-3 B&F**). In comparison to [Cu(II)(Me_6Tren)Br_2], the reduction of the [Cu(II)(HMTETA)Br_2] complex was slower and at lower degree, an observation that can potentially corroborate the slower rate of polymerization when HMTETA is used as ligand (**Table 5-1, Figure 5-1B**).

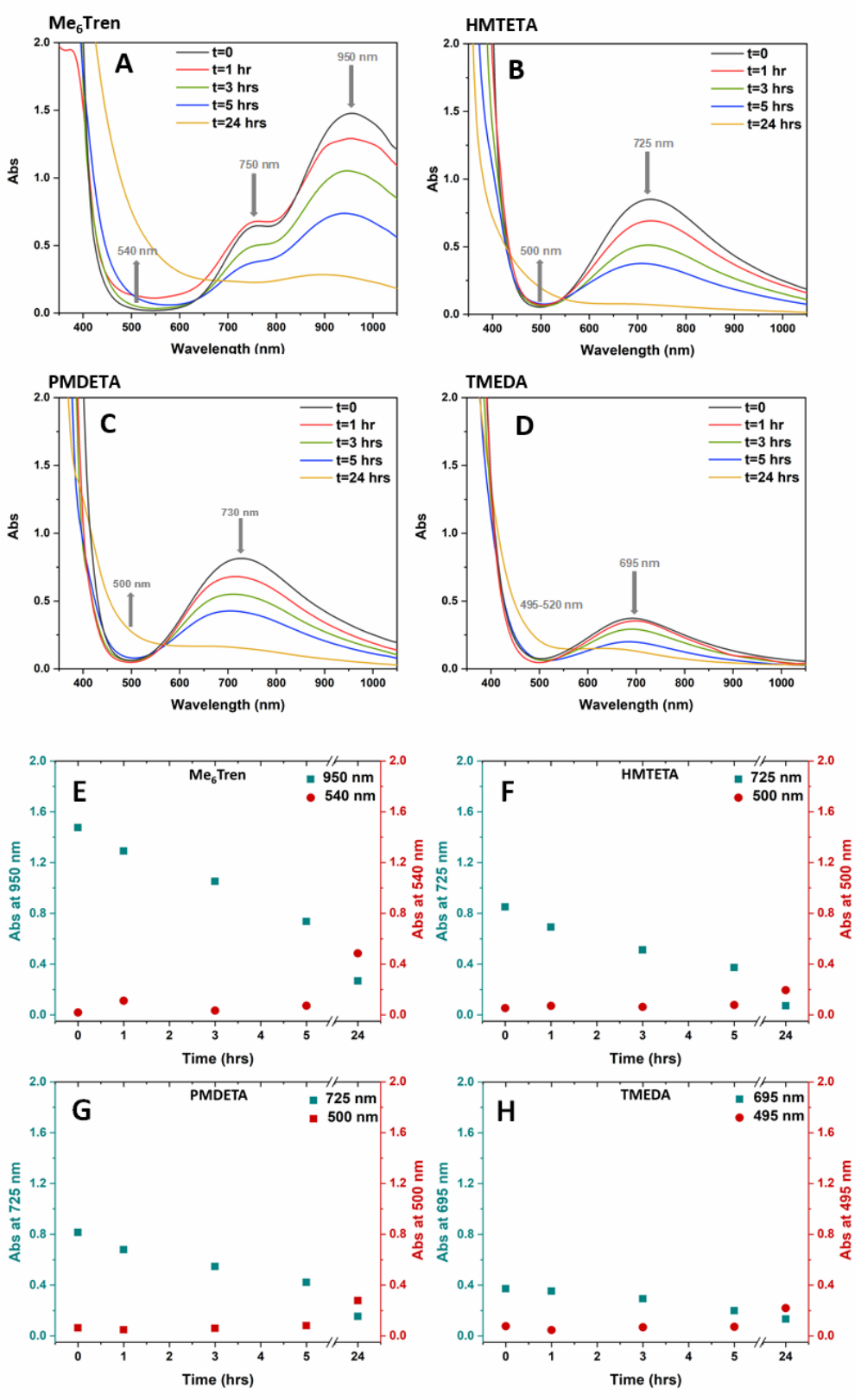

Figure 5-2. Time-dependent UV-Vis spectra and kinetic profile of the Cu-based complexes with **A**), **E**) Me_6Tren, **B**), **F**) HMTETA, **C**), **G**) PMDETA and **D**), **H**) TMEDA following broadband irradiation with λ_{max} ~ 360 nm.

In the case of PMDETA used as ligand, the absorbance reduction at 730 nm was similar to the [Cu(II)(HMTETA)Br_2], indicating a slower rate of Cu(II) reduction to Cu(I), and again conformed with the slower rates of polymerization (**Figures 5-3 C&G**). The [Cu(II)(TMEDA)Br_2] characteristic band at 695 nm exhibited the lowest degree of reduction (**Figures 5- D&H**) compared to the other complexes. This observation might be correlated with the polymerization results when TMEDA was used as ligand and give insight into the generation of Cu(I) when the bidentate TMEDA is employed for the formation of [Cu(II)(TMEDA)Br_2].

Consequently, the dynamics of the catalyst upon UV irradiation were explored with the use of TEAS, which was applied for the comparison of the complexes that exhibited the greatest control over the polymerization. As such, the [Cu(II)(Me_6Tren)Br_2] complex was compared with the [Cu(II)(PMDETA)Br_2] complex, as well as with Cu(II)Br_2 in the absence of ligand. These results are illustrated in the false-colour heat maps following excitation with 0.5 mW 365 nm radiation (**Figures 5-3A-C**). Each of the false-colour heat maps starts with a large (10s of mΔOD) absorption feature centred at ~ 400 nm, which persists on the timescale of the instrument response (~ 80 fs, see Supporting Information). This feature likely includes mostly contributions from the solvent/glass of the flow cell and has not been included in **Figures 5-3 A-C**, for ease of visualisation on the relevant signal from the sample. As shown, a broad, but much weaker absorption feature which spans from 400 to 700 nm is also present, with a corresponding ground state bleach (negative feature) around the excitation wavelength.

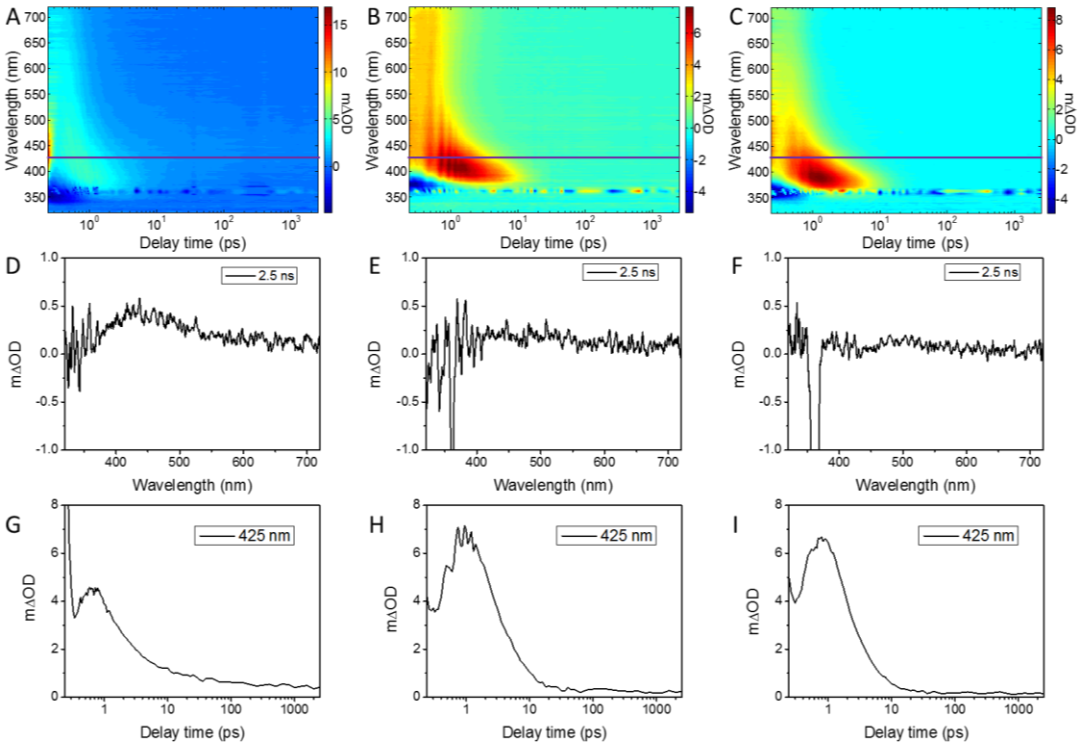

Figure 5-3. TEAS generated false-colour heat maps of **A**) Cu(II)Br_2, **B**) [Cu(II)(Me_6Tren)Br_2] and **C**) [Cu(II)(PMDETA)Br_2], transient absorption spectra taken 2.5 ns after photoexcitation for **D**) Cu(II)Br_2, **E**) [Cu(II)(Me_6Tren)Br_2] and **F**) [Cu(II)(PMDETA)Br_2] and lineouts taken at 425 nm probe wavelength (purple line in **A-C**) for **G**) Cu(II)Br_2, **H**) [Cu(II)(Me_6Tren)Br_2] and **I**) [Cu(II)(PMDETA)Br_2].

This feature blue shifts, narrows, and grows in intensity, within the first 1 ps after photoexcitation, eventually becoming centred again on ~ 400 nm. Subsequently, this decays within ~ 5-10 ps, and a very small positive absorption offset persists throughout the temporal window of the experiment, suggesting that a small amount of photoproduct is created. This long lived state is evident in the non-zero transient absorption spectrum taken at 2.5 ns delay time, shown in **Figures 5-3D-F**, as well in the non-zero offset at long delay times in lineouts of the TEAS, taken at 425 nm probe wavelength (purple lines **Figures 5-3 A-C**), and shown in **Figures 5-3 G-I**. It is hypothesised that the differences in the UV-Vis absorption upon irradiation are caused by transitioning from Cu(II) to Cu(I) (with some contribution growing possibly from

Cu(0) over time). As such, it is suggested that the long-lived state observed is due to the creation of small amounts of Cu(I) complexes. The large amount of noise in all three TEAS (and the large negative feature observed in **Figure 5-3F**) around 365 nm is caused by scatter from the pump pulse which could not be thoroughly removed.

All three false-colour heat maps are qualitatively similar, with the exception of an oscillating signal, with a peak to peak separation of ~ 220 fs, which is clearly present in the [Cu(II)(Me_6Tren)Br_2] complex (**Figures 5-3 B&H**) and persists for at least 1 ps. This is also present but much weaker in the [Cu(II)(PMDETA)Br_2] (**Figures 5-3 C& I**) complex, and while an accurate peak to peak separation cannot be extracted, the frequency appears identical to that observed in [Cu(II)(Me_6Tren)Br_2]. Such an oscillatory signal is not observed in the Cu(II)Br_2 alone (**Figures 5-3 A&G**). Similar TEAS were recorded when changing the halogen to chlorine, but no beat was observed (**Figure 5-4**). This suggest that both the ligand and the halogen are playing a role in the oscillatory signal observed in [Cu(II)(Me_6Tren)Br_2] and [Cu(II)(PMDETA)Br_2]. As such, it was postulated here that the beat observed in the transient absorption spectra is caused by the system oscillating between two different oxidation states of Cu, possibly caused by motion of the bromine between the copper and the ligand.

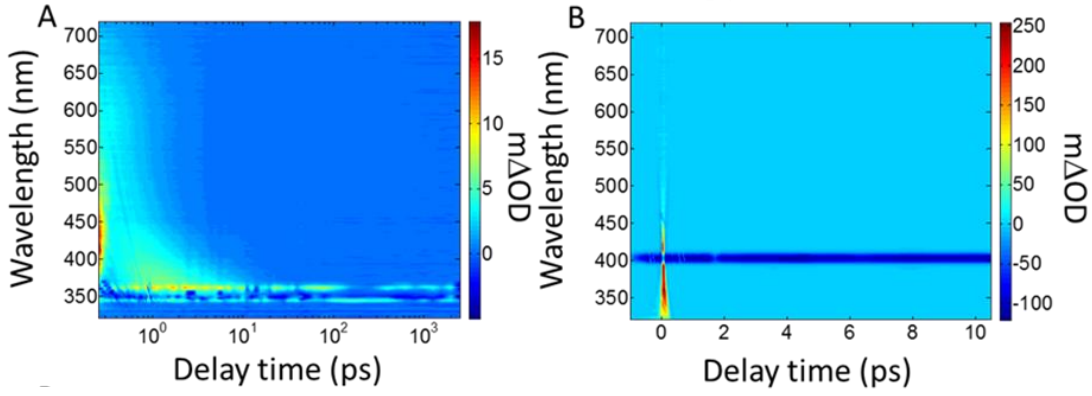

Figure 5-4. Transient Electronic Absorption Spectra of **A**) [Cu(II)(Me_6Tren)Cl_2], and **B**) DMSO alone, excited with 0.5 mW 365 nm pulses.

Subsequently, CV studies were carried out in order to provide information about changes in the redox properties of the complexes upon UV irradiation. For the CV measurements, solutions of different complexes were prepared in DMSO and CV measurements were performed under a N_2 atmosphere on a glassy carbon electrode. The voltammogram of [Cu(II)(Me_6Tren)Br_2] shows reduction (Cu(II) to Cu(I)) during the cathodic trace and corresponding oxidation peak during the anodic trace, as has been previously reported.[43] Although before UV irradiation the redox couple does not exhibit "perfect" quasi-reversible behavior, upon UV irradiation the quasi-reversible behavior was clear, possibly due to stabilization of the complex (**Figure 5-5A**). The half-wave potential ($E_{1/2}$) in both cases was negative, and after UV irradiation an increase from -0.200 V (before UV) to -0.130 V (after UV) was observed.

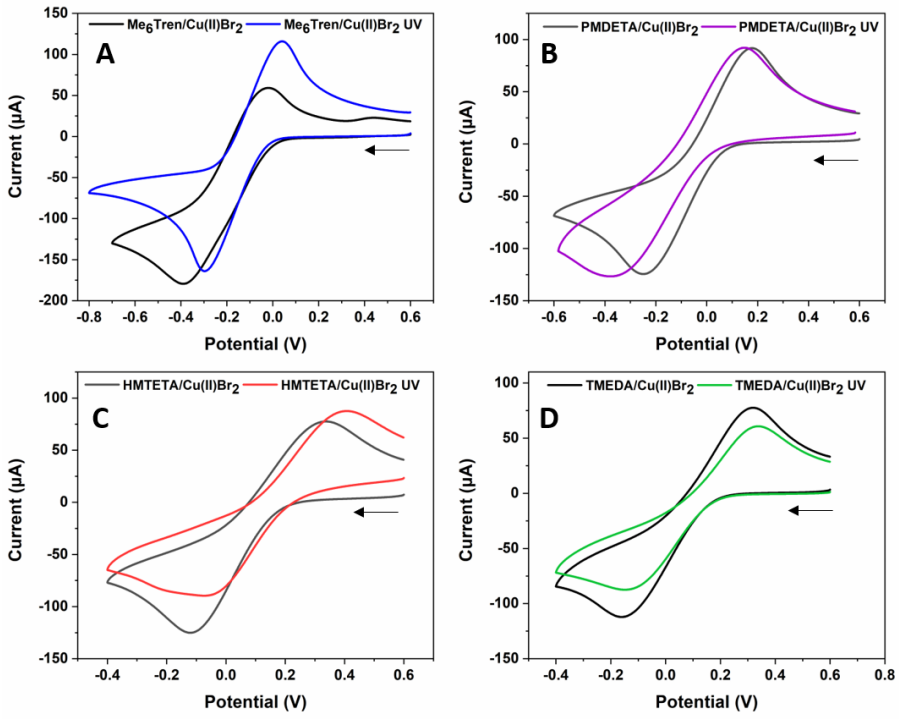

Figure 5-5. Cyclic voltammograms of **A**) [Cu(II)(Me_6Tren)Br_2], **B**) [Cu(II)(PMDETA)Br_2], **C**) [Cu(II)(HMTETA)Br_2] and **D**) [Cu(II)(TMEDA)Br_2] complexes with 0.01 M concentration, in a 0.1 M tetrabutylammonium hexafluorophosphate (NBu_4PF_6) solution in DMSO with scan rate 0.5 V/s *vs.* Ag/AgCl on a glassy carbon electrode.

When the tridentate [Cu(II)(PMDETA)Br_2] complex was measured before irradiation, reduction and oxidation were clearly observed during the cathodic and anodic trace (**Figure 5-5B**), exhibiting a quasi-reversible behavior (ΔE_p = 470 mV>>60 mV, **Table 5-2**). After UV irradiation, although the anodic peak does not show significant changes, the cathodic sweep exhibits alterations, shifting to more negative values indicative of deviation from a reversible redox reaction. The peak-to-peak separation exhibits differences before and after UV irradiation, 470 mV and 320 mV respectively, showing that more energy is needed for the reduction of the complex after UV irradiation, an observation that can probably be attributed to the amount of species available for reduction.

The [Cu(II)(HMTETA)Br_2] complex exhibited changes on the cathodic sweep after UV irradiation, showing a notable decrease (**Figure 5-5C**). Apart from the shift in potential, a second peak in the cathodic sweep was observed, probably attributed to a second population available for reduction. This might be attributed to changes in the coordination sphere of the metal complex upon exposure to UV light. It should be noted that due to the significant decrease of the cathodic peak, the peak-to-peak separation values could not be identified precisely after UV irradiation.

In the case of [Cu(II)(TMEDA)Br_2] both the anodic and cathodic traces were decreased upon UV irradiation (**Figure 5-5D**), an observation that led us to hypothesize that electrochemically the effect of UV irradiation on the catalyst complex is not as significant as in the other complexes examined. This information might provide an explanation on the behavior of the TMEDA ligand (and the analogous TMEDA/Cu(II)Br_2 complex) on the polymerization results which exhibited significant differences from the other cases. In all cases, the ΔE_p values exhibited values much higher that 60 mV. These trends, although qualitatively examined, provide some

information on the effect of UV light on the behavior of redox couples that govern photoinduced Cu-RDRP and are reflected in the quality of the obtained polymers when the different ligands are used.

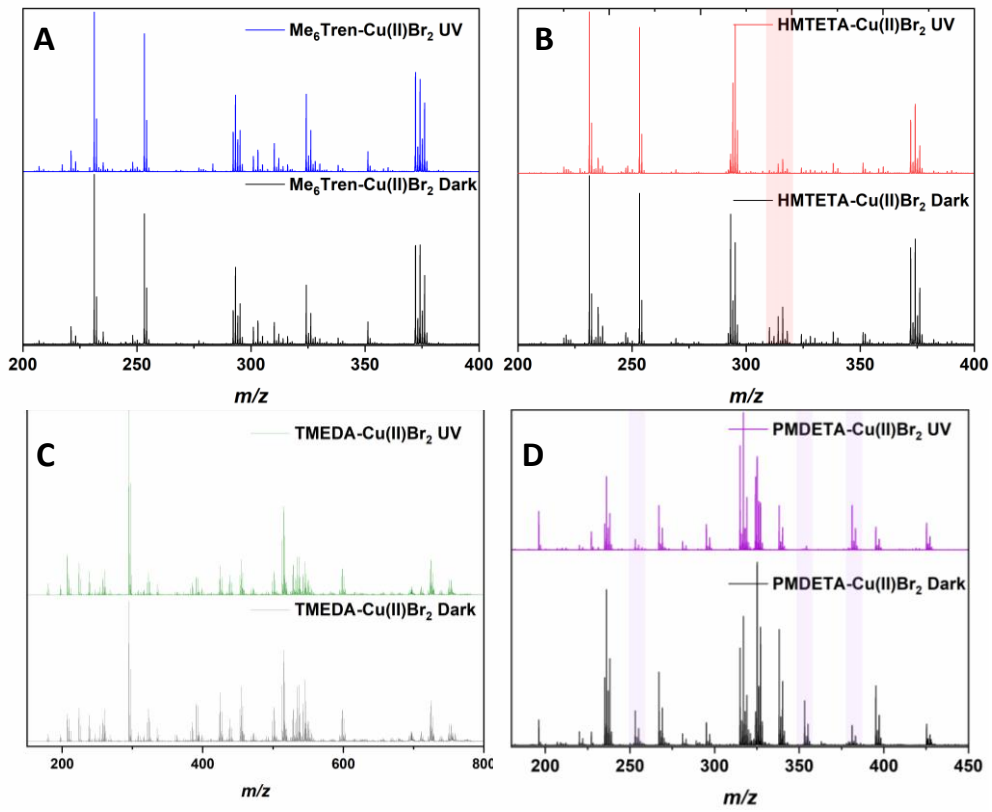

Figure 5-6. ESI-MS spectra of **A**) [Cu(II)(Me_6Tren)Br_2], **B**) [Cu(II)(HMTETA)Br_2], **C**) [Cu(II)(TMEDA)Br_2] and **D**) [Cu(II)(PMDETA)Br_2] before and after UV irradiation in MeOH.

Finally, ESI-ToF-MS was employed to investigate potential photoproducts that occur after photo-irradiation of the complexes and can be detected through ESI as positively charged species in the gas phase. Apart from the individual complexes, a solution of [Cu(II)(Me_6Tren)Br_2] combined with a chlorine-based initiator (**Figure 5-7, Figure 5-9**) was examined before and after exposure to UV light, to investigate the possibility of halogen exchange between the metal complex and the initiator. In all complexes, peaks corresponding to $[L + H]^+$, $[L\text{-}CuBr + H]^+$ and $[L\text{-}CuBr_2 + H]^+$ were detected in the positive ion mode. Apart from H^+ charged species, all of the samples

included Na^+ charged species. For the [Cu(II)(Me_6Tren)Br_2] complex the main species detected were the [Cu(Me_6Tren) + H]$^+$, [Cu(Me_6Tren)Br]$^+$ and the [Cu(Me_6Tren)(OCH_3)]$^+$ (**Figure 5-6A**) both before and after UV irradiation. Apart from these intact complex species, free ligand [Me_6Tren + H] $^+$ and [Me_6Tren + Na] $^+$ were detected and only after UV irradiation a small peak corresponding to [(Me_6Tren)(OCH_3) + Na]$^+$ was found. Based on the TEAS results, it should be noted that when Me_6Tren is used, any changes in the complexation of the metal are significantly fast and would be difficult to monitor. For the [Cu(II)(HMTETA)Br_2] complex, the main species detected, apart from [L + H]$^+$, were the [Cu(HMTETA)Br]$^+$, [Cu(HMTETA)Br_2]$^+$ and [Cu(HMTETA)$_2$(OH)$_2$ + Na]$^+$. Furthermore, although before UV irradiation a peak attributed to [Cu_2(HMTETA)$_2$Br(OCH_3)$_2$]$^+$ was detected, it was absent after UV irradiation (**Figure 5-6B**).

For the TMEDA-based complex the assignment of the peaks was a challenging task since many species were detected including [Cu(TMEDA)]$^+$ and [Cu(TMEDA)$_2$]$^+$, [Cu(TMEDA)$_2$Br(OH)]$^+$, [Cu(TMEDA)$_2$$Br_2$]$^+$ and [Cu_2(TMEDA)$_2$$Br_2$]$^+$ as well as [Cu_2(TMEDA)$_2$$Br_4$ + Na]$^+$. The species detected only after UV irradiation were the [Cu(TMEDA)$_2$Br]$^+$, [Cu_2(TMEDA)$_2$(OCH_3)$_2$]$^+$ and [Cu_2(TMEDA)$_2$$O_4$]$^+$ (**Figure 5-6C**). The existence of many species in the solution of the TMEDA-based complex might also be a factor that affects the polymerization and, thus the obtained polymers exhibit high dispersity and molecular weights.

For the [Cu(II)(PMDETA)Br_2] complex the main species assigned were the [Cu(PMDETA)]$^+$, [Cu(PMDETA) (OCH_3)]$^+$, [Cu(PMDETA)$_2$(OH)$_2$ + H]$^+$ and [Cu(PMDETA)Br_2]$^+$ both before and after UV exposure (**Figure 5-6D**). However, peaks that correspond to intact [Cu(PMDETA)(OH)]$^+$ (as well as [CuO(PMDETA)]$^+$) and [CuO(PMDETA)Br + Na^+]) were observed only after UV irradiation. For the

solution in which, apart from the [Cu(II)(Me_6Tren)Br_2] complex a chlorine initiator was added, a main peak at 328.16 *m/z* was detected corresponding to [Cu(Me_6Tren)Cl]$^+$ as well as at 372.11 *m/z* the [Cu(Me_6Tren)Br]$^+$ showing that exchange of the halogen between the complex and the initiator takes place (**Figure 5-7**). Noteworthy is the peak at 414.20 *m/z* attributed to reactions taking place between the complex and the initiator, with the latter complexing with the ligand and corresponding to [Cu(Me_6Tren)(-C_3H_6)Cl]$^+$ (**Figure 5-7, e&e'**). As a result, many different charged species were detected through ESI-MS for each complex, with all of them including not only the complexation of the Cu-metal center with the ligand and the halogen, but also the occupation of vacant coordination sites with solvent. The determination of the oxidation state of copper was avoided since the several species could have a positive charge due to the imbalance of copper and the counterion or due to a radical formed by the ligand.

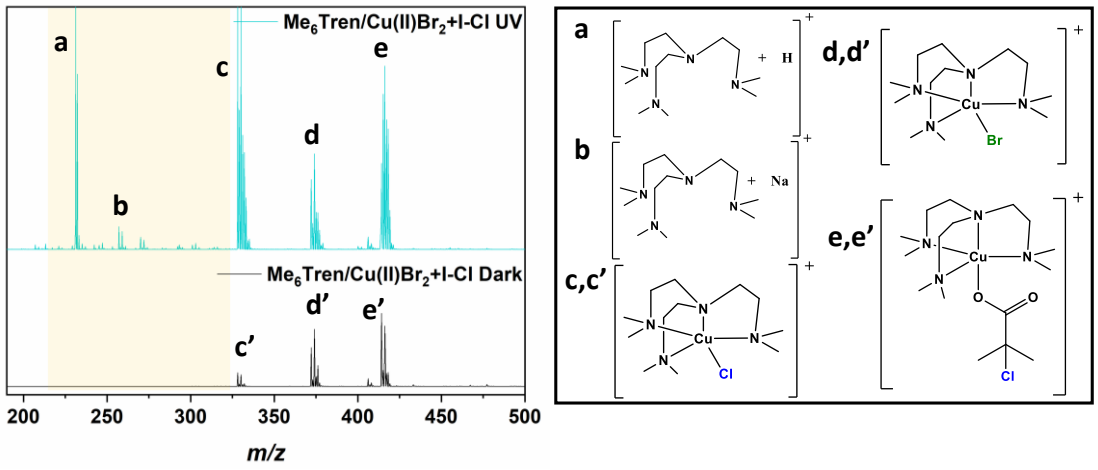

Figure 5-7. ESI-MS spectra of [Cu(II)(Me_6Tren)Br_2] in the presence of a Cl-initiator before and after UV irradiation in MeOH (top) and chemical structures corresponding to the ESI-MS peaks (bottom).

5.3 Conclusion

In this chapter, the effect of UV irradiation on Cu-based complexes including different aliphatic amine ligands has been investigated. Various state-of-the-art characterization tools such as UV-Vis spectroscopy, CV and ESI-MS, collectively provided information about the behaviour of [Cu(II)(Me_6Tren)Br_2], [Cu(II)(PMDETA)Br_2], [Cu(II)(HMTETA)Br_2] and [Cu(II)(TMEDA)Br_2] upon exposure to UV light. Based on the UV-Vis results, all the complexes showed reduction of Cu(II) to Cu(I) (and even Cu(0)), with the most prominent one being observed for the [Cu(II)(Me_6Tren)Br_2] complex. The [Cu(II)(PMDETA)Br_2] and [Cu(II)(HMTETA)Br_2] complexes exhibited slower and at lower degree reduction of Cu(II) to Cu(I), and this was depicted in the rate of the polymerization (*vide infra* "Results and Discussion" section). Importantly, the excited-state dynamics of the two most commonly used complexes (*i.e.* [Cu(II)(Me_6Tren)Br_2], [Cu(II)(PMDETA)Br_2]) were investigated through TEAS, indicating that the copper is found between two oxidation states, and this is due to the bromine moving between the copper and the ligand. The investigation of the excited-state dynamics, the redox behaviour and the different species generated upon complexation of the ligand to the metal centre, before and after UV irradiation are further depicted in the quality of the polymers obtained after utilization of these transition metal complexes for the photoinduced Cu-RDRP of MA.

5.4 Experimental Section

5.4.1 Materials

Methyl acrylate (MA, 99%), ethyl α-bromoisobutyrate (EBiB, 98%), copper(II) bromide (Cu(II)Br_2, 99%) and all the solvents were purchased from Sigma-Aldrich and used as received. Tris-(2-(dimethylamino)ethyl)amine (Me_6Tren) was synthesized according to the literature and stored in the fridge.[44] The ligands *N,N,N′,N″,N″*-Pentamethyldiethylenetriamine (PMDETA), tetramethylethylenediamine (TMEDA), 1,1,4,7,10,10-Hexamethyltriethylenetetramine (HMTETA) were purchased from Sigma-Aldrich and were distilled before use.

5.4.2 Instrumentation and Characterization techniques

Proton Nuclear Magnetic Resonance (^{1}H NMR)

^{1}H NMR spectra were recorded on Bruker DPX-300 or DPX-400 spectrometers in deuterium oxide (D2O) obtained from Sigma-Aldrich. Chemical shifts are given in ppm downfield from the internal standard tetramethylsilane. Monomer conversions were determined *via* ^{1}H NMR spectroscopy by comparing the integrals of monomeric vinyl protons to polymer signals.

Size Exclusion Chromatography (SEC)

SEC measurements were carried out using THF as the eluent with an Agilent 390-LC MDS instrument equipped with differential refractive index (DRI), viscometry (VS), dual angle light scatter (LS) and dual wavelength UV detectors. The system was equipped with 2 x PLgel Mixed C columns (300 x 7.5 mm) and a PLgel 5 µm guard column. The eluent was THF with 2 % TEA (triethylamine) and 0.01 % BHT (butylated hydroxytoluene) additives. Samples were run at 1 mL / min at 30 ^{o}C.

Poly(methyl methacrylate) standards (Agilent EasyVials) were used to create a third order calibration between 550 $gmol^{-1}$ and 1,568,000 $gmol^{-1}$. Analytical samples were filtered through a GVHP membrane with 0.22 μm pore size before injection. Experimental molar mass ($M_{n,SEC}$) and dispersity (Đ) values of synthesized polymers were determined by conventional calibration using Agilent GPC/SEC software (version A.02.01).

Electrospray Ionization Time-of-Flight Mass Spectrometry (ESI-ToF-MS)

ESI-ToF MS measurements were performed using a Bruker MicroToF in positive mode. The ion source voltage was set to 3.5 kV with a dry gas flow of 4.0 l/min and a dry temp of 195 degrees Celsius. Samples were diluted in methanol [1 eq. Cu(II)Br2 (4 mg) and 6 eq. ligand in 10 mL MeOH) and directly injected into the ESI-ToF mass spectrometer with a flow rate of 10 microlitres per minute. Spectra were accumulated over 1 minute; the average spectra then being reported here. When using a UV light source, the syringe containing the sample mixture was irradiated before direct injection.

UV-Vis spectroscopy (UV-Vis)

UV-Vis spectra were recorded on an Agilent Technologies Cary 60 UV-Vis spectrometer in the range of 200-1100 nm using a quartz cuvette (purchased from Starna) with 10 mm optical length. All the samples were prepared using Cu(II)Br2 (4 mg, 1 eq.) and ligand (6 eq.) in 8 mL DMSO and subsequently degassed for 15 min before getting placed under a UV lamp with broad band λ_{max} ~ 360 nm. Stirring (900 rpm) was applied for the whole duration of the kinetics.

Transient Electronic Absorption Spectroscopy (TEAS)

The TEAS setup has been previously described in detail.[45] A commercially available Ti:Sapphire oscillator and amplifier (Newport Spectra Physics Spitfire Ace PA) generates 800 nm, 40 fs duration laser pulses at a repetition rate of 1 kHz with 15 W average power. This is split four ways into roughly equally powered beams. Only one of these beams is used in the current experiments. One of these 3.5 W beams is split again to 2.5 W and 1 W. The 2.5 W beam pumps an optical parametric amplifier system (TOPAS, Light Conversion) which generates the pump beam centred at 365 nm and 0.5 mW average power. This beam is chopped at a frequency of 500 Hz to facilitate pump on and pump off measurements (see below). The remaining 1 W is reduced to 5% power and focused onto a translated calcium fluoride window to generate a white light continuum probe beam spanning the spectral range 320 to 720 nm. A hollow gold retroreflector is used to delay the probe beam with respect to the pump beam. The two beams interact with the sample ($Cu(II)Br_2$, 20 mg, 1 eq. and ligand (6 eq.) in 40 mL DMSO) which is circulated through a flow cell (Harrick Scientific) such that each laser pulse interrogates a fresh sample. Transient absorption spectra are taken at various delay times, Δt. Difference spectra are obtained by taking the log difference between the unpumped and pumped spectra. Data is globally fit using the fitting program Glotaran.[46]

Cyclic Voltammetry (CV)

Cyclic voltammetry was performed using a CH-Instruments 600 E potentiostat. A standard three-electrode cell equipped with a 3 mm glassy carbon disc working electrode, a Ag/Ag+ reference electrode, and a platinum counter electrode was established. The glassy carbon working electrode was polished with 0.05 μm alumina powder, rinsed sequentially with acetone, isopropanol and MilliQ water prior to each

use. The platinum wire counter electrode was annealed in a blue flame before use. The silver wire reference electrode was polished before every use. All experiments were carried out in a 0.1 M tetrabutylammonium hexafluorophosphate (NBu_4PF_6) solution in DMSO under a nitrogen atmosphere. A concentration of 0.01 M copper complexes was used (1 eq. Cu(II)Br_2 and 6 eq. ligand) for all CV measurements. The ferrocene/ferrocenium redox couple (Fc/Fc+) was used for internal calibration.

5.4.3 Experimental Procedures

Typical 4 mL scale photoinduced Cu-RDRP of MA (targeted DP_n = 50) in DMSO

A glass vial was charged with Cu(II)Br_2 (2.0 mg, 0.02 eq.) and DMSO (2 mL). Ligand (0.12 eq.) was added through a microliter syringe and the solution was vortexed for ~ 1 minute. MA (2 mL, 50 eq.), EBiB (65 µL, 1 eq.) and a stirrer bar were added, the vial was septum-sealed, and the solution was deoxygenated through N_2 sparging for 15 min. The polymerization was allowed to commence under a UV nail lamp (λ_{max} ~ 360 nm). Conversions were measured using ^{1}H NMR in $CDCl_3$ and SEC analysis was conducted in THF after the samples having been passed through neutral alumina for the removal of copper salts.

5.4.4 Supplementary Figures & Characterization

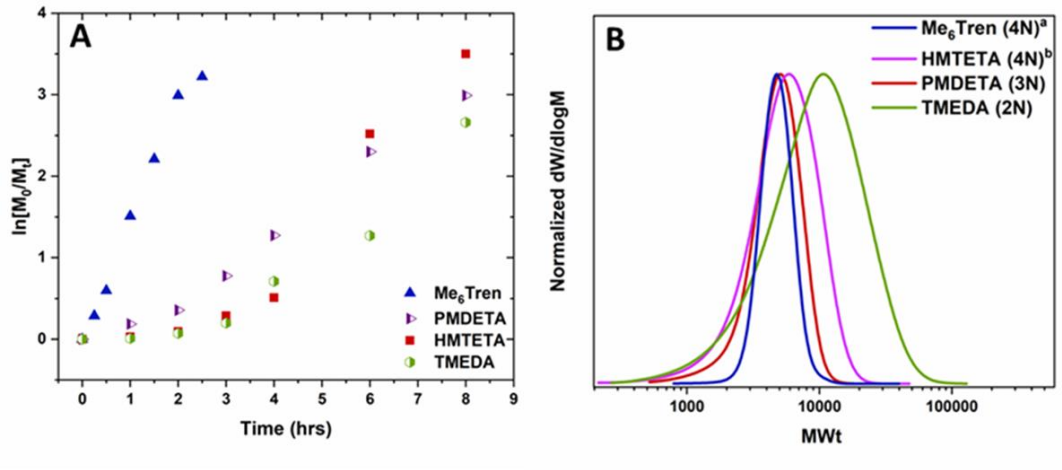

Figure 5-8. A) Kinetic plots of $\ln[M_0/M_t]$ over time and **B**) THF-SEC derived molecular weight distributions for all the PMAs with targeted DP = 50 when different ligands were used. The THF-SEC traces of the PMAs belong to samples with Me_6Tren (2.5 hrs of polymerization), TMEDA (8 hrs), PMDETA (8 hrs) and HMTETA (8 hrs).

[a] branched tripodal.

[b] linear.

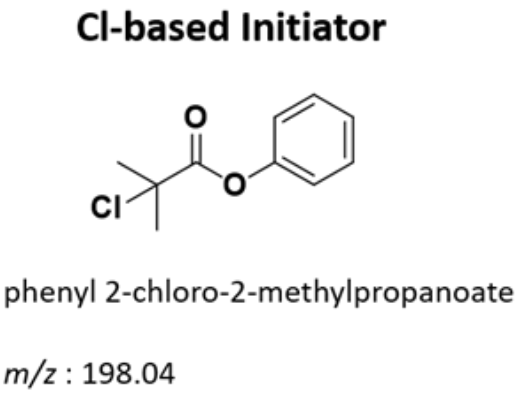

Figure 5-9. Chemical structure of the chlorine initiator used for the monitoring of halogen exchange between initiator and Cu(II)Br_2 through ESI-ToF-MS.

Table 5-2. Potentials of anodic (E_{pa}) and cathodic (E_{pc}) peaks and peak-to-peak separation values (ΔE_p) for the different complexes, obtained by cyclic voltammetry before and after UV irradiation.

	Complex	**$E_{p,a}$ (V)**	**$E_{p,c}$ (V)**	**ΔE_p (mV)**	**$E_{1/2}$ (V)**
Before UV	[Cu(II)(Me_6Tren)Br_2]	-0.020	-0.400	380	-0.200
	[Cu(II)(PMDETA)Br_2]	0.250	-0.220	470	0.015
	[Cu(II)(HMTETA)Br_2]	0.330	-0.120	210	0.105
	[Cu(II)(TMEDA)Br_2]	0.320	-0.160	480	0.080
After UV	[Cu(II)(Me_6Tren)Br_2]	0.040	-0.300	340	-0.130
	[Cu(II)(PMDETA)Br_2]	0.220	-0.100	320	0.060
	[Cu(II)(HMTETA)Br_2]	0.400	N/A	N/A	N/A
	[Cu(II)(TMEDA)Br_2]	0.330	-0.140	470	0.095

5.5 References

1. M. Kato, M. Kamigaito, M. Sawamoto and T. Higashimura, *Macromolecules*, 1995, **28**, 1721-1723.
2. J.-S. Wang and K. Matyjaszewski, *J. Am. Chem. Soc.*, 1995, **117**, 5614-5615.
3. B. M. Rosen and V. Percec, *Chem. Rev.*, 2009, **109**, 5069-5119.
4. V. Percec, T. Guliashvili, J. S. Ladislaw, A. Wistrand, A. Stjerndahl, M. J. Sienkowska, M. J. Monteiro and S. Sahoo, *J. Am. Chem. Soc.*, 2006, **128**, 14156-14165.
5. A. Moreno, S. Grama, T. Liu, M. Galià, G. Lligadas and V. Percec, *Polym. Chem.*, 2017, **8**, 7559-7574.
6. A. Moreno, J. Lejnieks, M. Galià, G. Lligadas and V. Percec, *Polym. Chem.*, 2018, **9**, 5411-5417.
7. K. Matyjaszewski, *Macromolecules*, 2012, **45**, 4015-4039.
8. E. Liarou, R. Whitfield, A. Anastasaki, N. G. Engelis, G. R. Jones, K. Velonia and D. M. Haddleton, *Angew. Chem. Int. Ed.*, 2018, **57**, 8998-9002.
9. G. R. Jones, A. Anastasaki, R. Whitfield, N. Engelis, E. Liarou and D. M. Haddleton, *Angew. Chem. Int. Ed.*, 2018, **57**, 10468-10482.
10. A. Anastasaki, V. Nikolaou and D. M. Haddleton, *Polym. Chem.*, 2016, **7**, 1002-1026.
11. A. Anastasaki, V. Nikolaou, G. Nurumbetov, P. Wilson, K. Kempe, J. F. Quinn, T. P. Davis, M. R. Whittaker and D. M. Haddleton, *Chem. Rev.*, 2016, **116**, 835-877.
12. F. Alsubaie, E. Liarou, V. Nikolaou, P. Wilson and D. M. Haddleton, *Eur. Polym. J.*, 2019, **114**, 326-331.
13. R. Whitfield, N. P. Truong, D. Messmer, K. Parkatzidis, M. Rolland and A. Anastasaki, *Chemical Science*, 2019, **10**, 8724-8734.
14. E. Daskalaki, B. Le Droumaguet, D. Gérard and K. Velonia, *Chem. Commun.*, 2012, **48**, 1586-1588.
15. W. Tang, Y. Kwak, W. Braunecker, N. V. Tsarevsky, M. L. Coote and K. Matyjaszewski, *J. Am. Chem. Soc.*, 2008, **130**, 10702-10713.

16. H. Tang, N. Arulsamy, M. Radosz, Y. Shen, N. V. Tsarevsky, W. A. Braunecker, W. Tang and K. Matyjaszewski, *J. Am. Chem. Soc.*, 2006, **128**, 16277-16285.
17. A. Anastasaki, V. Nikolaou, Q. Zhang, J. Burns, S. R. Samanta, C. Waldron, A. J. Haddleton, R. McHale, D. Fox, V. Percec, P. Wilson and D. M. Haddleton, *J. Am. Chem. Soc.*, 2014, **136**, 1141-1149.
18. M. Fantin, S. Park, Y. Wang and K. Matyjaszewski, *Macromolecules*, 2016, **49**, 8838-8847.
19. M. Chen, M. Zhong and J. A. Johnson, *Chem. Rev.*, 2016, **116**, 10167-10211.
20. K. J. Arrington and J. B. Matson, *Polym. Chem.*, 2017, **8**, 7452-7456.
21. E. Liarou, A. Anastasaki, R. Whitfield, C. E. Iacono, G. Patias, N. G. Engelis, A. Marathianos, G. R. Jones and D. M. Haddleton, *Polym. Chem.*, 2019, **10**, 963-971.
22. X. Pan, N. Malhotra, A. Simakova, Z. Wang, D. Konkolewicz and K. Matyjaszewski, *J. Am. Chem. Soc.*, 2015, **137**, 15430-15433.
23. A. A. Alzahrani, A. H. Erbse and C. N. Bowman, *Polym. Chem.*, 2014, **5**, 1874-1882.
24. G. R. Jones, R. Whitfield, A. Anastasaki and D. M. Haddleton, *J. Am. Chem. Soc.*, 2016, **138**, 7346-7352.
25. R. Whitfield, K. Parkatzidis, M. Rolland, N. P. Truong and A. Anastasaki, *Angew. Chem. Int. Ed.*, 2019, **0**.
26. V. Nikolaou, A. Anastasaki, F. Brandford-Adams, R. Whitfield, G. R. Jones, G. Nurumbetov and D. M. Haddleton, *Polym. Chem.*, 2016, **7**, 191-197.
27. C. Bian, Y.-N. Zhou, J.-K. Guo and Z.-H. Luo, *Polym. Chem.*, 2017, **8**, 7360-7368.
28. P. Garra, C. Dietlin, F. Morlet-Savary, F. Dumur, D. Gigmes, J.-P. Fouassier and J. Lalevée, *Polym. Chem.*, 2017, **8**, 7088-7101.
29. K. Kaya, M. Seba, T. Fujita, S. Yamago and Y. Yagci, *Polym. Chem.*, 2018, **9**, 5639-5643.
30. T.-G. Zhan, M.-D. Lin, J. Wei, L.-J. Liu, M.-Y. Yun, L. Wu, S.-T. Zheng, H.-H. Yin, L.-C. Kong and K.-D. Zhang, *Polym. Chem.*, 2017, **8**, 7384-7389.
31. A. Marathianos, E. Liarou, A. Anastasaki, R. Whitfield, M. Laurel, A. M. Wemyss and D. M. Haddleton, *Polym. Chem.*, 2019, **10**, 4402-4406.

32. B. P. Fors and C. J. Hawker, *Angew. Chem. Int. Ed.*, 2012, **51**, 8850-8853.
33. J. E. Poelma, B. P. Fors, G. F. Meyers, J. W. Kramer and C. J. Hawker, *Angew. Chem. Int. Ed.*, 2013, **52**, 6844-6848.
34. M. A. Tasdelen, M. Uygun and Y. Yagci, *Macromol. Rapid Commun.*, 2011, **32**, 58-62.
35. M. A. Tasdelen, M. Uygun and Y. Yagci, *Macromol. Chem. Phys.*, 2010, **211**, 2271-2275.
36. M. A. Tasdelen, M. Uygun and Y. Yagci, *Macromol. Chem. Phys.*, 2011, **212**, 2036-2042.
37. M. A. Tasdelen, M. Ciftci and Y. Yagci, *Macromol. Chem. Phys.*, 2012, **213**, 1391-1396.
38. D. Konkolewicz, K. Schröder, J. Buback, S. Bernhard and K. Matyjaszewski, *ACS Macro Lett.*, 2012, **1**, 1219-1223.
39. T. G. Ribelli, D. Konkolewicz, S. Bernhard and K. Matyjaszewski, *J. Am. Chem. Soc.*, 2014, **136**, 13303-13312.
40. E. Frick, A. Anastasaki, D. M. Haddleton and C. Barner-Kowollik, *J. Am. Chem. Soc.*, 2015, **137**, 6889-6896.
41. T. J. Zerk and P. V. Bernhardt, *Dalton Trans.*, 2013, **42**, 11683-11694.
42. J. Xia and K. Matyjaszewski, *Macromolecules*, 1997, **30**, 7697-7700.
43. J. Qiu, K. Matyjaszewski, L. Thouin and C. Amatore, *Macromol. Chem. Phys.*, 2000, **201**, 1625-1631.
44. M. Ciampolini, N. Nardi, *Inorg. Chem.*, 1966, **5**, 41–44
45. J. M. Woolley, M. Staniforth, M. D. Horbury, G. W. Richings, M. Wills and V. G. Stavros, *J. Phys. Chem. Lett.*, 2018, **9**, 3043-3048.
46. M., *J. Stat. Softw.* 2012, *49*, 1– 22

Chapter 6.

Conclusion: Limitations, applications & perspectives

6.1 Limitations

The development of less sophisticated controlled radical polymerization strategies is a significantly important requirement for the expansion of these methodologies, not only from an academic perspective but also from an industrial point of view. The traditional deoxygenation platforms (*i.e.* gas sparging, freeze-pump-thaw, glove box equipment) require personnel training, are time-demanding and often uneconomic and can exhibit scalability limitations. Hence, the replacement / circumvention of these conventional approaches and the development of oxygen tolerant methodologies, entail with the higher simplicity, reliability and application scope for CRPs.

Nevertheless, apart from the advantages of oxygen tolerance, not all the CRP systems can proceed successfully in the presence of oxygen, or more importantly, some oxygen tolerant approaches can be more complex in their implementation compared to conventional deoxygenation. For instance, in some Cu-RDRP and RAFT polymerizations, sacrificial reducing agents (*e.g.* ascorbic acid, hydrazine, phenols) are used in order to quench molecular oxygen, leading to the formation of side

products. On the other hand, the "polymerizing through" oxygen approach can be incompatible when low k_p monomers are used, or when there is no rapid radical generation.[1]

Furthermore, it should be noted that since oxygen acts as radical scavenger, its presence might affect the rate of the polymerization and the macromolecular characteristics of the obtained polymers.[2,3] In other words, long induction periods related to oxygen consumption might be seen, followed in many cases by prolonged polymerization times.[4] Additionally, since carbon-centred radicals react with (singlet) oxygen, loss of initiator efficiency might be observed, leading to high molecular weights.[1,5] In the case of transition metal-catalyzed reactions, oxygen can react with the metal catalyst-complex, leading to the formation of metal-peroxo analogues and thus, altering the polymerization evolution.[3]

Table 6-1. Advantages and disadvantages of conventional deoxygenation and oxygen tolerant methods based on selected criteria.

Characteristics	Oxygen tolerance strategies	Conventional Deoxygenation
Setup simplicity		
Time-saving		
Compatibility with reagents		
Multi-scale		
Cost-effective		
Efficiency		
Compatibility with various CRPs		
Potential of side reactions		

positive medium negative

Consequently, judicious optimization is needed in order to exploit an oxygen tolerant approach and render it beneficial and in parallel more facile than conventional deoxygenation. In any case, the main purpose for applying a deoxygenation-free

platform, is the simplification of the already existent polymerization protocols, in parallel with the retention of control over the polymerization.

6.2 Applications

As has been discussed in this thesis, the main purpose of developing oxygen tolerant CRP platforms is the simplification and expansion of the already existing methodologies. In this context, some of the most promising, current and prospective, applications of oxygen tolerant CRPs can be found in diverse fields including high-throughput syntheses,[6,7] continuous-flow polymerizations[8,9] and education.

High-throughput syntheses

The development of high-throughput systems has attracted significant interest the last years due to the fast-track synthesis of polymer libraries.[6,10–12] A basic characteristic of these approaches is the low volume of the reactions (normally μL) which renders the conventional deoxygenation approaches inefficient and difficult to apply. For instance, gas sparging and freeze-pump-thaw are practically challenging and glove boxes are costly. Thus, research has been focused on the replacement of conventional deoxygenation, either *via* "enzyme degassing",[13] or with the "*polymerizing through*" oxygen approach.[14] As a result, well-defined diverse materials are being synthesized, in a facile and economical manner.

Polymerizations in continuous flow

Continuous flow chemistry has been proved as an efficient alternative of batch reactions, providing high reproducibility, consistency, low-cost and multi-scale polymerizations.[15–17] However, the implementation of flow-setup for CRPs can be a

challenging task when stringent anaerobic conditions are required. This is due to the fact that a flow-setup consists of various parts including connections and tubing. In particular, the choice of tubing is highly important since, depending on the material, the latter can be oxygen permeable. For instance, tubing made of perfluoroalkoxy alkane (PFA) or fluorinated ethylene propylene (FEP) has high oxygen permeability, while Halar and Tefzel (tetrafluoroethylene) exhibit higher oxygen barrier properties.[16] In order to provide simplicity in the flow-setup, researchers have introduced oxygen tolerant approaches for continuous flow polymerizations, especially when light is used as external stimulus (*i.e.* PET-RAFT, photoinduced Cu-RDRP).[8,9,18] Thus, the combination of oxygen tolerance and flow-chemistry has been considered as an important platform for multi-scale polymerizations in a facile and consistent manner.

Educational purposes

In 2019, Lewin introduced the term "*pedagogical reduction*" to describe, examine and clarify the approaches that need to be made in order to achieve the simple and understandable transfer of knowledge to students.[19] In this context, simpler yet efficient processes need to be introduced in the field of polymer chemistry, especially since this field has been an essential subject of chemical education the last 50 years.[20,21]

Apart from the practical difficulty of conventional deoxygenation methods (*i.e.* Schlenk lines), it should also be considered that not all the existing chemical laboratories have sufficient resources to provide expensive gas supplies in wide experimental range. Hence, it is highly possible that oxygen tolerance would enable universities with low financial status to include CRPs in their educational programs, thus providing more knowledge to young developing polymer scientists.

As a result, although oxygen tolerance in CRPs might be considered as a controversial field of research due to current limitations, the continuous progress and the increasing interest in this objective, could significantly broaden the scope of CRP techniques into user-friendly platforms for a range of applications.

6.3 Conclusions

The focus of this Ph.D. thesis was to develop Cu-RDRP and render it a more user-friendly and versatile platform. For this purpose, three different Cu-RDRP methodologies, Cu(0)-wire mediated RDRP (*Chapter 2*), photoinduced Cu-RDRP (*Chapter 3*) and aqueous Cu-RDRP with the pre-disproportionation of Cu(I) (*Chapter 4*), were studied in the absence of conventional deoxygenation or extrinsic oxygen scavengers. Apart from the oxygen tolerant nature of these platforms, the effect of UV-irradiation on Cu-based complexes was investigated (*Chapter 5*), providing insights into the excited state dynamics and the photo-redox behaviour Cu(II)-based complexes, and the effect of different aliphatic amines on photoinduced Cu-RDRP.

In *Chapter 2*, the application of Cu(0)-wire RDRP in the absence of deoxygenation was investigated. By simply adjusting the headspace of the reaction vessel, a wide range of monomers, namely acrylates, methacrylates, acrylamides, and styrene, were polymerized in a controlled manner, yielding polymers with low dispersities, near-quantitative conversions (>99%), and high end-group fidelity, which was verified with *in-situ* chain extensions and block copolymerizations. This approach was tolerant to elevated temperatures (up to 90 ^{o}C), compatible with both organic and aqueous media, as well as with conventional ATRP. Furthermore, by eliminating the

headspace, higher reaction scales were achieved (*ca*. 125 g), further verifying the robustness of this simple approach.

In Chapter 3, a fully oxygen tolerant photoinduced Cu-RDRP system, independent of any externally added oxygen quenchers, reducing agents or deoxygenation methods was developed and discussed. By eliminating the headspace of the reaction vessels (8 mL scale), a range of monomer families, including hydrophobic, hydrophilic and semi-fluorinated (meth)acrylates were polymerized with the utilization of various solvents. The versatility of the proposed oxygen-tolerance methodology was verified by achieving high control over the molecular weights and end-group fidelity in near-quantitative polymerizations, enabling *in-situ* chain extensions and block copolymerizations. That approach was efficiently scalable from extremely low volumes such as 5 μL, to high scale reactions of 0.5 L. The oxygen consumption in the photoinduced polymerization was monitored with the use of an oxygen probe, and the role of the different components that comprise a deoxygenation-free polymerization was investigated.

The rapidly self-deoxygenating Cu-RDRP of various acrylamides in aqueous media was discussed in *Chapter 4*. The disproportionation of Cu(I) in the presence of Me_6Tren as a tertiary amine aliphatic sigma-donor ligand in water towards Cu(0) and Cu(II) was exploited, leading to full oxygen consumption within seconds, both in sealed and open-air conditions. In the absence of any type of external deoxygenation, a range of hydrophilic homo- and block co-polymers with controlled molecular weight, low dispersity and high-end group fidelity were synthesized within minutes. The aqueous oxygen consumption profile was elucidated by the *in-situ* online monitoring of the dissolved [O_2] through a fiber-optic oxygen monitoring probe, and the effect of the catalyst and ligand concentration, as well as the effect of different solvents were examined. A number of analytical methods

including EM, EELS and XPS collectively verified the rapid oxidation of Cu-species and elucidated the nature of the oxidized products.

Finally, in *Chapter 5*, the effect of UV irradiation of Cu(II)-derived complexes with different alphatic amines as ligands, was investigated and discussed. For this purpose, four aliphatic amines were used as ligands and $Cu(II)Br_2$ as the metal source for the formation of catalyst complexes that can be used for the photoinduced Cu-RDRP of methyl acrylate. Different characterization techniques such as transient electronic absorption spectroscopy (TEAS), ultraviolet-visible (UV-Vis) spectroscopy, electrospray ionization time of flight mass spectrometry (ESI-ToF-MS) and cyclic voltammetry (CV) were applied in order to provide insight into the catalyst behaviour upon photo-irradiation. The motion of the bromine between the copper and the ligand was investigated *via* TEAS, while the electrochemical behaviour of the Cu(II)/Cu(I) redox couples was examined through CV. Finally, the detection of different species upon complexation of the ligand to the metal centre (before and after UV irradiation) provided further information about the effect of photoirradiation on the different complexes, and consequently on the polymerization.

6.4 Outlook & Future Work

The development of oxygen tolerant Cu-RDRP has simplified the synthesis of well-defined poly(acrylates), poly(styrene) and poly(acrylamides), providing access to high molar masses and one-pot chain extensions and block copolymerizations. The oxygen tolerant approaches discussed in this thesis are compatible with many conditions including various temperatures, reaction media and polymerization scales. However, apart from poly(acrylates), poly(styrene) and poly(acrylamides), more monomer families need to be investigated including poly(methacrylates) and

poly(methacrylamides) in organic and aqueous media, respectively. Furthermore, although the chain-end fidelity of the thus far synthesized polymers is high and allows for *in-situ* chain extensions, further studies are needed in order to examine the extent of this characteristic, and the ability to synthesize multi-block copolymers in the presence of oxygen. This will render the oxygen tolerant Cu-RDRP methodology more robust. Finally, although low volume polymerizations have been reported, the expansion to larger scales or industrially relevant conditions, would facilitate the "commercialization" of RDRPs.

6.5 References

1 J. Yeow, R. Chapman, A. J. Gormley and C. Boyer, *Chem. Soc. Rev.*, 2018.

2 S. C. Ligon, B. Husár, H. Wutzel, R. Holman and R. Liska, *Chem. Rev.*, 2014, 114, 577–589.

3 V. A. Bhanu and K. Kishore, *Chem. Rev.*, 1991, **91**, 99–117.

4 F. A. Bovey and I. M. Kolthoff, *Chem. Rev.*, 1948, **42**, 491–525.

5 E. Liarou, R. Whitfield, A. Anastasaki, N. G. Engelis, G. R. Jones, K. Velonia and D. M. Haddleton, *Angew. Chemie*, 2018, **57**, 8998–9002.

6 R. Chapman, A. J. Gormley, M. H. Stenzel and M. M. Stevens, *Angew. Chemie - Int. Ed.*, 2016, **128**, 4576–4579.

7 P. Gurnani, T. Floyd, J. Tanaka, C. Stubbs, D. Lester, C. Sanchez-Cano and S. Perrier, *Polym. Chem.*, 2020, **11**, 1230–1236.

8 N. Corrigan, D. Rosli, J. W. J. Jones, J. Xu and C. Boyer, *Macromolecules*, 2016, **49**, 6779–6789.

9 A. Marathianos, E. Liarou, A. Anastasaki, R. Whitfield, M. Laurel, A. M. Wemyss and D. M. Haddleton, *Polym. Chem.*, 2019, **10**, 4402–4406.

10 R. Hoogenboom, M. A. R. Meier and U. S. Schubert, *Macromol. Rapid Commun.*, 2003, **24**, 15–32.

11 Y. Mei, K. Saha, S. R. Bogatyrev, J. Yang, A. L. Hook, Z. I. Kalcioglu, S. W. Cho, M. Mitalipova, N. Pyzocha, F. Rojas, K. J. Van Vliet, M. C. Davies, M. R. Alexander, R. Langer, R. Jaenisch and D. G. Anderson, *Nat. Mater.*, 2010,

9, 768–778.

12 S. Cosson, M. Danial, J. R. Saint-Amans and J. J. Cooper-White, *Macromol. Rapid Commun.*, 2017, **38**, 1600780.

13 R. Chapman, A. J. Gormley, K.-L. L. Herpoldt and M. M. Stevens, *Macromolecules*, 2014, **47**, 8541–8547.

14 J. R. Lamb, K. P. Qin and J. A. Johnson, *Polym. Chem.*, 2019, **10**, 1585–1590.

15 E. Baeten, J. J. Haven and T. Junkers, *Polym. Chem.*, 2017, **8**, 3815–3824.

16 A. Melker, B. P. Fors, C. J. Hawker and J. E. Poelma, *J. Polym. Sci. Part A Polym. Chem.*, 2015, **53**, 2693–2698.

17 A. Kermagoret, B. Wenn, A. Debuigne, C. Jérôme, T. Junkers and C. Detrembleur, *Polym. Chem.*, 2015, **6**, 3847–3857.

18 N. Zaquen, W. A. A. W. Azizi, J. Yeow, R. P. Kuchel, T. Junkers, P. B. Zetterlund and C. Boyer, *Polym. Chem.*, 2019, **10**, 2406–2414.

19 D. Lewin, *Educ. Theory*, 2018, **68**, 495–512.

20 C. S. Marvel, *J. Chem. Educ.*, 1965, **42**, 3.

21 L. J. Mathias, *J. Chem. Educ.*, 1983, **60**, 990.

Publication List

The following list includes publications relevant to the work of this Ph.D. thesis, or relevant to work that was conducted in parallel.

(* indicates corresponding author, ¥ indicates equal contribution)

1. Marathianos, A.;[¥] **Liarou, E.**;[¥] Hancox, E.; Grace, J. L.; Lester, D. W.; Haddleton, D. M.[*], Dihydrolevoglucosenone (CyreneTM) as a bio-renewable solvent for Cu(0)-mediated RDRP without external deoxygenation, *Green Chem.*, 2020, DOI: 10.1039/D0GC02184A, (Peer reviewed, Impact Factor (JCR 2019): 9.48, Rank in category: 20 of 177 / 2 of 41)

2. Aljuaid, M.; **Liarou, E.**; Town, J.; Baker, J.; Haddleton, D. M.; Wilson, P.[*], Synthesis and [2+2]-photodimerisation of monothiomaleimide functionalised linear and brush-like polymers, *Chem. Commun.*, 2020, 56, 9545-9548, (Peer reviewed, Impact Factor (JCR 2019): 5.996, Rank in category: 34 of 177)

3. Zhang, J.; **Liarou, E**.; Town, J.; Li, Y.; Wemyss, A. M.; Haddleton, D. M.[*], Aqueous copper-mediated reversible deactivation radical polymerization (RDRP) utilizing polyetheramine derived initiators, *Polym. Chem.*, 2020, DOI: 10.1039/D0PY00555J, (Peer reviewed, Impact Factor (JCR 2019): 5.342, Rank in category: 8 of 89)

4. **Liarou, E.**; Han, Y.; Sanchez, A. M.; Walker, M.; Haddleton, D. M.[*], Rapidly Self-deoxygenating Controlled Radical Polymerization in water *via in-situ* Disproportionation of Cu(I), *Chem. Sci.*, 2020, 11, 5257-5266, (Peer reviewed, Impact Factor (JCR 2019): 9.346, Rank in category: 21 of 177)

5. Ma, C.; Han, T.; Kang, M.; **Liarou, E.**; Wemyss, A. M.; Efstathiou, S.; Tang, B. Z.; Haddleton, D. M. [*], Aggregation-Induced Emission Active Polyacrylates via Cu-Mediated Reversible Deactivation Radical Polymerization with Bioimaging Applications, *ACS Macro Lett.*, 9, 5, 769-775, (Peer reviewed, Impact Factor (JCR 2019): 6.042, Rank in category: 6 of 89)

6. Theodorou, A.; **Liarou, E.**; Haddleton, D. M.; Stavrakaki, I.; Skordalidis, P.; Whitfield, R.; Anastasaki, A.[*]; Velonia, K.[*], Protein-Polymer Bioconjugates via a Versatile Oxygen Tolerant Photoinduced Controlled Radical Polymerization Approach, *Nat Commun.*, 11, 1486 (2020), (Peer reviewed, Impact Factor (JCR 2019): 12.121, Rank in category: 6 of 71)

7. **Liarou, E.***; Staniforth, M.; Town, J. S.; Marathianos, A.; Grypioti, M.; Li, Y.; Chang, Y.; Efstathiou, S.; Hancox, E.; Wemyss, A. M.; Wilson, P.; Jones, B. A.; Aljuaid, M., Stavros, V. G.; Haddleton, D. M.*, UV irradiation of Cu-based complexes with aliphatic amine ligands as used in living radical polymerization, *Eur. Polym. J.*, 2020, 109388. (**Invited**, Peer reviewed, Impact Factor (JCR 2019): 3.862, Rank in category: 14 of 89)

8. Shegiwal, A.; Wemyss, A. M.; **Liarou, E.**; Town, J; Patias, G.; Atkins, C. J.; Marathianos, A.; Lester, D. W.; Efstathiou, S. and Haddleton, D. M.*, Polymerisable surfactants for polymethacrylates using catalytic chain transfer polymerisation (CCTP) combined with sulfur free-RAFT in emulsion polymerization, *Eur. Polym. J.*, 2020, 125, 109491. (Peer reviewed, Impact Factor (JCR 2019): 3.862, Rank in category: 14 of 89)

9. Hancox, E.; **Liarou, E.**; Town, J. S.; Jones, G. R.; Huband, S.; Topham, P. D. and Haddleton D. M.*, Microphase separation of highly amphiphilic, low N polymers by photoinduced copper-mediated polymerization, achieving sub-2 nm domains at half-pitch, *Polym. Chem.*, 2019, 10 (46), 6254-6259. (Peer reviewed, Impact Factor (JCR 2019): 5.342, Rank in category: 8 of 89)

10. Town, J. S.*; Gao, Y.; Hancox, E.; **Liarou, E.**; Shegiwal, A.; Atkins, C. J. and Haddleton, D. M.*, Automatic peak assignment and visualisation of copolymer mass spectrometry data using the 'genetic algorithm', *Rapid Commun Mass Spectrom.*, 2020;e8654. (**Invited**, Peer reviewed, Impact Factor (JCR 2018): 2.045, Rank in category: 47 of 84)

11. Marathianos A.; **Liarou E.**; Anastasaki A.; Whitfield R.; Laurel M.; Wemyss A. M. and Haddleton D. M.*, Photo-induced copper-RDRP in continuous flow without external deoxygenation, *Polym. Chem.*, 2019, 10, 4402-4406. (Peer reviewed, Impact Factor (JCR 2019): 5.342, Rank in category: 8 of 89)

12. Alsubaie, F.; Liarou, E.; Nikolaou, V.; Wilson, P.; Haddleton, D. M.*, Thermoresponsive viscosity of polyacrylamide block copolymers synthesised *via* aqueous Cu-RDRP, *Eur. Polym. J.*, 2019, 114, 326-331. (Peer reviewed, Impact Factor (JCR 2019): 3.862, Rank in category: 14 of 89)

13. Shegiwal, A.; Wemyss, A. M.; Schellekens, M. A. J.; de Bont, J.; Town, J.; **Liarou, E.**; Patias, G.; Atkins, C. J.; Haddleton, D. M.*, Exploiting catalytic chain transfer polymerization for the synthesis of carboxylated latexes *via* sulfur-free RAFT, *J. Polym. Sci. A: Polym. Chem.*, 2019, 57 (3), E1-E9. (**Invited**, Peer reviewed, Impact Factor (JCR 2019): 2.93, Rank in category: 26 of 89)

14. **Liarou, E.**; Anastasaki, A.; Whitfield, R.; Iacono, C. E.; Patias, G.; Engelis, N. G.; Marathianos, A.; Jones, G. R.; Haddleton, D. M.*, Ultra-low volume oxygen tolerant photoinduced Cu-RDRP, *Polym. Chem.*, 2019, 10 (8), 963-971. (Peer reviewed, Impact Factor (JCR 2019): 5.342, Rank in category: 8 of 89)

15. Jones, G. R.; Anastasaki, A.; Whitfield, R.; Engelis, N.; **Liarou, E.**; Haddleton, D. M.*, Copper-Mediated Reversible Deactivation Radical Polymerization in Aqueous Media, *Angew. Chemie Int. Ed.*, 2018, 57, 10468–10482. (Peer reviewed, Impact Factor (JCR 2018): 12.257, Rank in category: 17 of 172)

16. **Liarou, E.**¥; Whitfield, R.¥; Anastasaki, A.*; Engelis, N. G.; Jones, G. R.; Velonia, K.; Haddleton, D. M.*, Copper-Mediated Polymerization without External Deoxygenation or Oxygen Scavengers, *Angew. Chemie Int. Ed.*, 2018, 57 (29), 8998-9002. (Peer reviewed, Impact Factor (JCR 2018): 12.257, Rank in category: 17 of 172)

17. **Liarou, E.**; Varlas, S.; Skoulas, D.; Tsimblouli, C.; Sereti, E.; Dimas, K.; Iatrou, H.*, Smart polymersomes and hydrogels from polypeptide-based polymer systems through α-amino acid N-carboxyanhydride ring-opening polymerization. From chemistry to biomedical applications, *Prog. Polym. Sci.*, 2018, 83, 28-78. (Review Article, Peer reviewed, Impact Factor (JCR 2018): 24.505, Rank in category: 1 of 87)

18. Engelis, N. G.; Anastasaki, A.*; Whitfield, R.; Jones, G. R.; **Liarou, E.**; Nikolaou, V.; Nurumbetov, G.; Haddleton, D. M.*, Sequence-Controlled Methacrylic Multiblock Copolymers: Expanding the Scope of Sulfur-Free RAFT, *Macromolecules*, 2018, 51 (2), 336-342. (Peer reviewed, Impact Factor (JCR 2018): 5.997, Rank in category: 5 of 87)

19. Anastasaki, A.; Whitfield, R.; Nikolaou, V.; Truong, N. P.; Jones, G. R.; Engelis, N. G.; **Liarou, E.**; Whittaker, M. R; and Haddleton, D. M., One-Pot Sequence-Controlled (SC) Multiblock Copolymers *via* Copper-Mediated Polymerization, Sequence-Controlled Polymers, John Wiley & Sons, 2018, 417-434. (**book chapter**)